



# **Anoctamins in Volume Regulation, Proliferation and Apoptotic Cell Death**



DISSERTATION ZUR ERLANGUNG DES DOKTORGRADES  
DER NATURWISSENSCHAFTEN (DR.RER.NAT.)  
DER FAKULTÄT FÜR BIOLOGIE UND VORKLINISCHE MEDIZIN  
DER UNIVERSITÄT REGENSBURG

Vorgelet von  
Wanitchakool Podchanart  
Aus Nonthaburi, Thailand  
im Oktober 2016

**Das Promotionsgesuch wurde eingereicht am:  
14-10-2016**

**Die Arbeit wurde angeleitet von:  
Prof. Dr. Karl Kunzelmann**

**Unterschrift:**

Promotionsgesuch eingereicht am: Oktober 2016

Die Arbeit wurde angeleitet von: Prof. Dr. med. Karl Kunzelmann

Prüfungsausschuss:

Vorsitzender: Prof. Dr. Gernot Längst

1.Gutachter: Prof. Dr. med. Karl Kunzelmann

2.Gutachter: Prof. Dr. Bernhard weber

3.Prüfer: Prof. Dr. med. Ernst R. Tamm

Ersatzperson: Prof. Dr. Rainer Schreiber

## SUMMARY

The family of anoctamins consists of ten different proteins (called ANO1-10 or TMEM16A-K). A variety of functions have been attributed to anoctamins such as that of  $\text{Ca}^{2+}$  activated  $\text{Cl}^-$  channels controlling  $\text{Cl}^-$  secretion, cell volume, cell migration and proliferation, and that of phospholipid scramblases contributing to apoptotic cell death. Some anoctamin members are overexpressed in tumors and have been linked to developmental defects. Mutations in anoctamins can cause genetic diseases and cancer. However, it is unknown how anoctamins fulfill these various functions.

Before ANO1 was identified as a protein forming a chloride channel, it was known as the cancer marker DOG1. DOG1/ANO1 is expressed in gastrointestinal stromal tumors (GIST) and particularly in head and neck squamous cell carcinoma (HNSCC), and is not detected at very high levels in other tissues. We found that ANO1 strongly augments cell proliferation, cell migration and metastasis. We also found that ANO1 expression is controlled by histone deacetylases (HDAC), corresponding well to the known role of HDAC in HNSCC. As ANO1 did not enhance proliferation in every cell type, its function is perhaps modulated by cell-specific factors. In contrast to ANO1, we found that ANO6, by operating as a  $\text{Ca}^{2+}$  activated membrane phospholipid scramblase, supports cellular apoptosis and necroptosis rather than promoting proliferation.

Earlier findings from our laboratory and other groups indicated that ANO6 is a  $\text{Cl}^-$  channel, a phospholipid scramblase and a nonselective cation channel activated by intracellular  $\text{Ca}^{2+}$  and pro-apoptotic stimuli. Moreover, previous studies characterized ANO6 as an outwardly rectifying  $\text{Cl}^-$  channel (ORCC) and volume-regulated anion channel (VRAC) that is activated during apoptotic cell death. In the experiments presented here I found a major role of ANO6 for both regulatory volume decrease (RVD) as well as apoptotic volume decrease (AVD). RVD and AVD were examined in four different cell types under physiological conditions, i.e. in the presence of physiological intracellular and extracellular bath solutions and at 37 °C. Moreover swelling activated whole cell currents and volume regulation was assessed in

freshly isolated intestinal epithelial cells from wild type and anoctamin 6 knockout mice. The data indicate that ANO6 generates a VRAC and is activated during RVD by membrane stretch,  $\text{Ca}^{2+}$  influx through TRP channels and activation of phospholipase A2 (PLA<sub>2</sub>), which generates membrane lysophospholipids (LPL). Accumulation of LPL in the plasma membrane enhances membrane tension, which possibly induces a conformational change of ANO6, thereby opening the  $\text{Cl}^-$  conductive pore and causing RVD. Remarkably, RVD was largely reduced in intestinal epithelial cells from ANO6 knockout mice. The results also demonstrate that ANO6 is activated by low intracellular  $\text{Cl}^-$ , which suggests that ANO6 operates as an osmosensor.

ANO6 was further demonstrated to participate in the innate immune response in macrophages. We could demonstrate that in macrophages  $\text{Ca}^{2+}$  influx through P2X<sub>7</sub> channels leads to initial cell shrinkage, phospholipid scrambling, cell membrane blebbing and ultimately cell death. Cell migration and phagocytic activity was found to be largely reduced in *Ano6*<sup>-/-</sup> macrophages. We proposed that ANO6 plays a central role for the immune defense realized by macrophages. The data also indicate that P2X<sub>7</sub>-induced cell death in macrophages is due to activation of apoptosis as well as necrosis.

Another member of the anoctamin family, ANO10, was also demonstrated to be expressed in macrophages and to participate in innate immune response. In collaboration with the Max Planck institute of experimental Medicine in Göttingen we showed that the genomic ANO10 mutation R263H increases serum titers of antibodies directed against Lyme disease causing *Borrelia*. We suggest that ANO10-R263H enhances susceptibility towards *Borrelia* infection and attenuates clearance of spirochetes after tick bites. ANO10-R263H caused a reduced VRAC activity and RVD. Loss of ANO10 expression in macrophages compromised phagocytosis and clearance of *Borrelia*, attenuated volume regulation and reduced apoptotic cell death. Taken together the results demonstrate that anoctamins participate in the regulation of proliferation and cell death and play important roles in cancer and innate immune defense.

## Zusammenfassung

Die Anoctamin-Familie besteht aus zehn verschiedenen Proteinen (ANO1-10 oder TMEM16A-K). Inzwischen wurde den Anoctaminen eine Vielzahl von Funktionen zugeordnet. So bilden Anoctamine  $\text{Ca}^{2+}$ -aktivierte Chloridkanäle, nehmen Einfluß auf das Zellvolumen, die Zellmigration und Zellproliferation und bilden Membranphospholipid-Scramblasen, womit sie einen Beitrag zum apoptotischen Zelltod leisten. Einige Anoctamine sind in Tumoren überexprimiert und werden mit Entwicklungsstörungen in Verbindung gebracht. Anoctamin-Mutationen können genetisch bedingte Krankheiten und Krebs verursachen. Es ist jedoch weitgehend unbekannt, wie Anoctamine diese verschiedenen Funktionen erfüllen.

Bevor Anoctamin 1 (ANO1) als Chloridionenkanal identifiziert wurde, war es als der Krebsmarker DOG1 bekannt. DOG1/ ANO1 ist in gastrointestinalen Stromatumoren (GIST) und vor allem in Weichteiltumoren des Kopfbereichs (HNSCC) derart hoch exprimiert, wie man dies in gesunden Geweben nie vorfindet. Wir fanden heraus, dass ANO1 die Zellproliferation, Zellmigration und Tumormetastasierung fördert. Wir fanden ebenfalls, dass die ANO1-Expression durch Histon-Deacetylasen (HDAC) kontrolliert wird. Dies korreliert sehr gut mit der bekannten Rolle von HDAC in Kopftumoren. Da ANO1 nicht in jedem Zelltyp die Proliferation stimuliert, ist anzunehmen, dass seine Funktion durch zellspezifische Faktoren moduliert wird. Im Gegensatz zu ANO1 fanden wir, dass ANO6 als  $\text{Ca}^{2+}$ -aktivierte Plasmamembran-Phospholipidscramblase die zelluläre Apoptose und Nekroptose unterstützt, anstatt Proliferation zu fördern.

Ergebnisse aus unserem Labor und von anderen Arbeitsgruppen zeigen, dass ANO6 offensichtlich gleichzeitig ein Chloridionenkanal, eine Phospholipidscramblase und einen nichtselektiven Kationenkanal bildet und durch intrazelluläre Calciumionen und proapoptische Stimuli aktiviert wird. Weiterhin kennzeichnen frühere Studien ANO6 als auswärts-gleichrichtenden Chloridionenkanal (ORCC) und als volumenregulierten

Anionenkanal (VRAC). Diese Ionenkanalströme werden während des apoptotischen Zelltods aktiviert. In den hier vorgestellten Experimenten fand ich eine dominante Rolle von ANO6 sowohl für regulatorische Volumenabnahme (RVD), als auch für den apoptotischen Volumenverlust (AVD). RVD und AVD wurden in vier verschiedenen Zellarten unter physiologischen Bedingungen, d.h. in Gegenwart von physiologischen intra- und extrazellulären Ionenkonzentrationen und bei 37 ° C, untersucht. Darüber hinaus wurden Chloridionenströme und Volumenregulation in frisch isolierten Darmepithelzellen von Wildtyp-Mäusen und ANO6-Knockoutmäusen untersucht. Die Ergebnisse zeigen, dass ANO6 einen VRAC generiert und während RVD durch Dehnung der Plasmamembran,  $\text{Ca}^{2+}$  Einstrom durch Transient Receptor Potential (TRP)- Kanälen und Aktivierung von Phospholipase A2 (PLA<sub>2</sub>) aktiviert wird. PLA<sub>2</sub> führt zur Bildung und Akkumulation von Lysophospholipiden (LPL) in der Plasmamembran, was zu einer Spannungsänderung innerhalb der Plasmamembran bewirkt und eine Konformationsänderung von ANO6 zur Folge hat. Diese Konformationsänderung induziert die Öffnung des ANO6-Kanals und die Aktivierung von RVD. Bemerkenswerterweise war die Kanalaktivierung und RVD in intestinalen Epithelzellen von ANO6-Knockoutmäusen deutlich reduziert. Weitere Ergebnisse zeigen, dass ANO6 durch eine niedrige intrazelluläre Chloridionenkonzentration aktiviert wird, was darauf hindeutet, dass ANO6 als Osmosensor funktioniert.

Weiterhin konnte eine Beteiligung von ANO6 bei der Immunreaktion in Makrophagen demonstriert werden. Wir konnten zeigen, dass in Makrophagen der  $\text{Ca}^{2+}$  Einstrom durch P2X<sub>7</sub> Kanäle zur initialen Zellschrumpfung führt und danach Phospholipidscrambling, Zellmembran-Blebbing und schließlich Zelltod induziert wird. Die Zellmigration und Phagozytose-Aktivität war deutlich reduziert in Ano6-Knockout-Makrophagen. Hieraus schlossen wir, dass ANO6 eine zentrale Rolle bei der Immunabwehr durch Makrophagen spielt. Die Daten zeigen ebenfalls, dass der P2X<sub>7</sub>-induzierte Zelltod in Makrophagen durch gleichzeitige Aktivierung von Apoptose und Nekrose zustande kommt.

Ein weiteres Mitglied der Anoctaminfamilie, ANO10, wird ebenfalls in Makrophagen exprimiert. In Zusammenarbeit mit dem Max-Planck-Institut für experimentelle Medizin in Göttingen konnten wir zeigen, dass die genomische ANO10 Variante R263H zu erhöhten Serum-Titern von Antikörpern gegen *Borrelia* führt, welche die Lyme-Krankheit verursachen. Wir vermuten, dass ANO10-R263H die Anfälligkeit für *Borrelia*-Infektionen erhöht und deren Elimination nach Übertragung durch Zeckenbisse reduziert. ANO10-R263H inhibiert die VRAC-Aktivität und vermindert RVD. Ein Verlust der ANO10-Expression in Makrophagen hemmt die Phagozytose und Elimination von Spirochäten, beeinträchtigt RVD und hemmt Apoptose. Zusammengefasst zeigen die Ergebnisse, dass Anoctamine Proliferation und Zelltod kontrollieren und eine wichtige Rolle bei Krebs und angeborener Immunabwehr spielen.

**CONTENTS**

SUMMARY.....	i
ZUSAMMENFASSUNG.....	iii
CONTENTS.....	iv
CHAPTER 1 Introduction.....	1
CHAPTER 2 Role of anoctamins in cancer and apoptosis.....	12
CHAPTER 3 Cellular volume regulation by anoctamin 6: Ca <sup>2+</sup> , phospholipase A2 and osmosensing .....	26
CHAPTER 4 Anoctamin 6 mediates effects essential for innate immunity downstream of P2X <sub>7</sub> -Receptors in macrophages .....	48
CHAPTER 5 A coding variant of <i>ANO10</i> , affecting volume regulation of macrophages, is associated with <i>Borrelia</i> seropositivity.....	78
CHAPTER 6 Discussion.....	106
CONCLUSION.....	116
REFERENCES.....	117
ACKNOWLEDGEMENTS.....	146
ERKLÄRUNGEN.....	147
CURRICULUM VITAE.....	148

## CHAPTER 1

### Introduction

**Ion channels** form transmembrane pores, which have mechanisms for gating to control the movement of particular ions species. Ions are driven by their concentration gradient to move from one side of plasma membrane to the other (1). Membrane ion channels are in charge of numerous physiological functions. In fact mutations in ion channels cause either a loss or a gain of channel function, which may lead to very different cellular problems, the so called ion channel diseases (1).

### Chloride channels

Chloride ( $\text{Cl}^-$ ) channels consist of a large family of functionally and structurally different anion-selective channels in plasma membranes or intracellular organelles (2). Some  $\text{Cl}^-$  channels are not only permeable for chloride, but also for other anions such as bicarbonate, bromide, and iodide, as well as small organic osmolytes like taurine (3). Their functions involve membrane excitability in neurons, skeletal muscle, cardiac muscle, and smooth muscle cells. In addition  $\text{Cl}^-$  channels are necessary to counterbalance the electrogenic transport by the  $\text{H}^+$ -ATPase, which is required for acidification of internal and extracellular compartments (2).  $\text{Cl}^-$  currents are also essential for transepithelial salt transport, as well as for the regulation of the cell volume. Moreover,  $\text{Cl}^-$  channels are in charge of cellular homeostasis during cell proliferation and differentiation (4).  $\text{Cl}^-$  channels can be classified into five functional groups (4): **i) Ligand-gated  $\text{Cl}^-$  channels** are made as pentameric structures and are excitatory in embryonic neurons and inhibitory in the differentiated neuronal tissues of the central nervous system (1). For example GlyR and  $\text{GABA}_A\text{R}$  respond to the inhibitory neurotransmitters, glycine (Gly) and  $\gamma$ -aminobutyric acid (GABA) (3). **ii) The cAMP/PKA activated channel** which is the well-known cystic fibrosis transmembrane conductance regulator (CFTR), a member of the ATP-binding cassette (ABC) transporter superfamily. CFTR is most prominently expressed in the apical surface of various epithelial cells and is regulated by cyclic AMP-dependent protein kinase A (PKA) and ATP-binding.

CFTR is demonstrated to regulate volume-regulated anion channels (VRAC), as well as other  $\text{Cl}^-$  channels, such as outwardly rectifying chloride channel (ORCC), and calcium-activated  $\text{Cl}^-$  channels (CaCC). CFTR also functions as a regulator of other ion channels and transporters, such as amiloride-sensitive epithelial  $\text{Na}^+$  channels (ENaC), inwardly rectifying potassium channels like the renal outer medullary potassium channel (ROMK) and various ion exchangers (5;6). The mutation  $\Delta\text{F508}$  (deletion of phenylalanine at position 508) is the most common mutation causing cystic fibrosis due to misfolding of the protein and consequently targeting for degradation within endoplasmic reticulum (ER) (2;6). **iii) Voltage-gated  $\text{Cl}^-$  channels** are found either in the plasma membrane or in intracellular compartments of several cell types. The so called CLC channels form an important group of voltage-gated  $\text{Cl}^-$  channels (3;5). This family has been demonstrated to play a role in a variety of physiological processes, including maintenance of resting membrane potentials, pH regulation, cell volume regulation, ion transport, cell migration, cell proliferation and differentiation (1;7;8). **iv) Calcium-activated  $\text{Cl}^-$  channels (CaCCs)** exhibit slow activation, subsequent membrane depolarization, outward rectification of the steady-state current voltage relationship and an anion permeability sequence of  $\Gamma > \text{Cl}^-$ . Various stimuli (such as cholinergic agonists) directly activate CaCCs by rising intracellular  $\text{Ca}^{2+}$  ( $[\text{Ca}^{2+}]_i$ ) via inositol 1,4,5-triphosphate ( $\text{IP}_3$ ) signaling and  $\text{Ca}^{2+}$  influx through plasma membrane voltage-gated  $\text{Ca}^{2+}$  channels (6). CaCCs are abundantly expressed in most eukaryotic cells and are associated with a large number of physiological functions, such as epithelial fluid secretion, sensory transduction, neuronal and cardiac excitability, regulation of smooth muscle contraction and nociception, cell proliferation, phospholipid scrambling and regulation of cell death (5). **v) Volume-regulated  $\text{Cl}^-$  channels** are activated by cell swelling in response to hypotonic shock. Regulation of the cell volume always involves activation of volume-regulated  $\text{K}^+$  and  $\text{Cl}^-$  channels, resulting in a release intracellular ions and water efflux to re-shrink the cells. This is called the regulatory volume decrease (RVD) (2). These channels, called  $I_{\text{Cl,swell}}$ , are generally produce outwardly-rectifying  $\text{Cl}^-$  currents and show time-dependent inactivation at positive membrane potentials (9). Various mediators and signaling

pathways have been reported to activate these channels, such as extracellular-regulated kinase ERK1/2, the cytoskeleton, phospholipase A2-dependent pathways and intracellular ATP or  $\text{Ca}^{2+}$  (10-13). In mammalian cells, volume-regulated  $\text{Cl}^-$  channels are important for cell volume regulation, immunological responses, cell proliferation, cell differentiation and cell death (9;14-16). Cells have mechanisms to control their volume during cell cycle progression. It has been reported that volume-regulated  $\text{Cl}^-$  channels are involved in survival signaling to control downstream target proteins in G0/G1 and S phases of cell cycle (14;17). Additionally, changes of cell volume are related to cell death, particularly apoptosis (14;18). Cell shrinkage has been shown to be the hallmark of the initial step in apoptosis termed apoptotic volume decrease (AVD) which is induced by several apoptotic compounds and pathological situations (16;19;20).

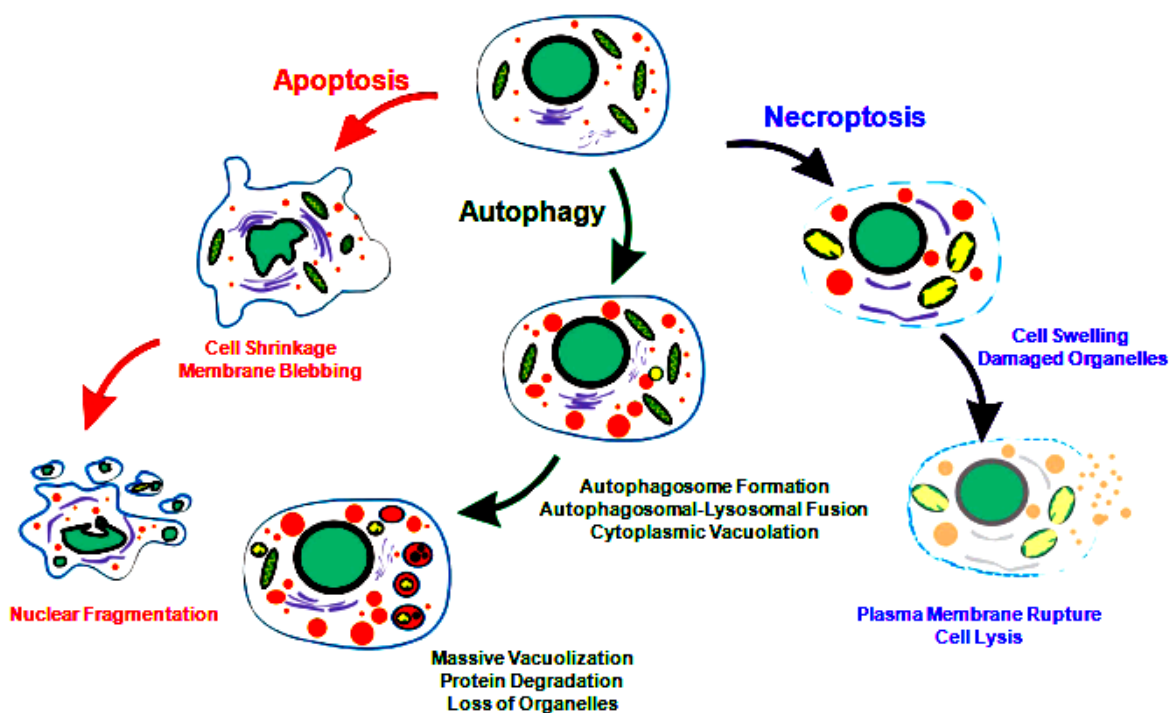


**Fig. 1: Apoptosis, Autophagy and Necroptosis.** Morphological features of distinct programmed cell death (PCD) (21).

## Cell death

Programmed cell death (PCD) is an essential biological process during development,

homeostasis and immunity of multicellular organisms. The type of PCD is depended on stimuli and background of individual cells. PCD is required for elimination of individual cells during homeostasis of adult organisms, tissue remodeling and organ development. However, PCD is also involved in various diseases, such as cancers, autoimmune and immunodeficiency disorders. To date, PCD is described by morphological criteria into three types. PCD type I is called apoptosis (Fig. 1). Apoptosis is described by unique morphological and biochemical changes consisting of cell shrinkage (pyknosis), DNA fragmentation (karyorrhexis), nuclear condensation, activation of proteolytic enzymes caspases and blebbing of the plasma membrane. The internal cell components are tightly packed in apoptotic bodies and then rapidly engulfed by phagocytes (22;23). PCD type II is named autophagy (Fig. 1). Autophagy is typically triggered by nutrient starvation. Autophagy is initiated by formation of unique organelles termed 'autophagosome'. After fusion with lysosomes cell organelles and proteins are degraded in vacuoles by lysosomal or vascular hydrolases after (25). PCD type III is called necrosis or necroptosis (Fig. 1). After stimulation of the TNF receptor (TNFR) by TNF $\alpha$  the recruitment of the TNF receptor-associated death domain (TRADD) and receptor-interacting protein kinase 1 (RIPK1) is initiated. In the absence of active caspase 8, RIPK1 and RIPK3 forms a complex called necrosome, which activates the pro-necroptotic protein mixed lineage kinase domain-like (MLKL) (26). Active MLKL is translocated to the plasma membrane and into the membranes of intracellular organelles (such as ER, mitochondria and lysosome), forms nonspecific pores and Na<sup>+</sup> and Ca<sup>2+</sup> influxes which is required for necroptosis induced cell death (27).

### **Apoptosis**

Apoptosis is a well-organized sequence of morphological events and energy dependent processes. Apoptotic cells are recognized by phagocytes and rapidly engulfed without inflammatory responses. Apoptosis has been considered as an irreversible process. Because activation of caspases (caspase-3, -6 and -7) commit cells to a 'point-of-no-return' (28;29). Caspases-dependent apoptosis pathways are mediated by extrinsic (receptor-mediated) or intrinsic (mitochondria-mediated) signaling pathways (30).

## The extrinsic or receptor-mediated pathway

Two mechanisms of the direct initiation of apoptosis have been suggested: the TNF-induced signal pathway and the Fas-Fas ligand-mediated signal pathway. Both pathways involve receptors of the TNF receptor (TNFR) family (Fig. 2, 30;31). Activation of these receptors leads to the formation of two different death-inducible signaling complexes (DISC). Complex I is associated with TNFR1, TNFR-associated death domain (TRADD), TRAF2, RIP1, cIAP1 and cIAP2 in the plasma membrane. Complex II requires Fas-associated death domain (FADD), TRADD and caspase-8 (30). Autoproteolytic of caspase-8 causes activation of executioner caspases cascade (32).

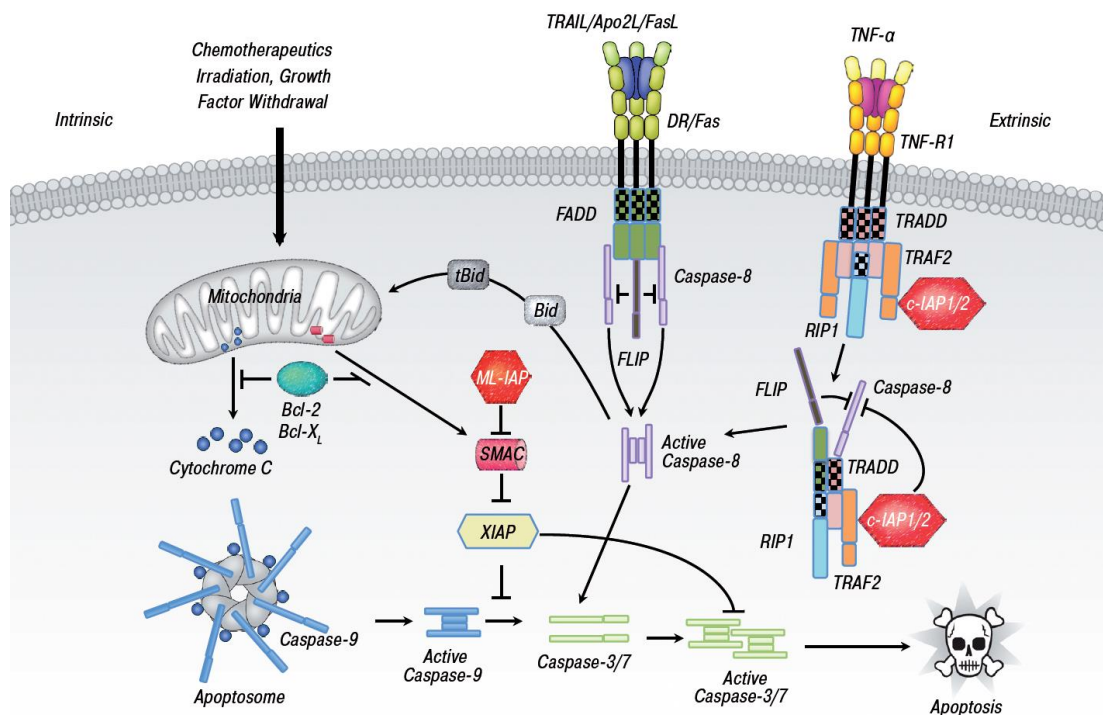


**Fig. 2 Major distinct pathways of apoptosis.** The extrinsic (receptor-mediated) pathway acts via death receptors while the intrinsic pathway acts via release of mitochondrial proteins. Activation of both pathways leads to cell death by activation of caspases. Crosstalk between the pathways occurs via the Bcl-2 family member, Bid (33).

## The intrinsic or mitochondria-mediated pathway

The intrinsic or mitochondria-mediated pathway (Fig. 2) is activated by various stimuli, such as DNA damage, irradiation, cytotoxic agents, growth deprivation, endoplasmic reticulum (ER) stress, intracellular Ca<sup>2+</sup> overload and oxidative stress (29). The central role of this

pathway is dysfunction of mitochondrial, including the opening of a permeability transition pore (PTP), mitochondrial matrix swelling and outer mitochondrial membrane (OMM) rupture (34). Generally, mitochondria integrity is maintained by Bcl-2 family proteins, including anti-apoptotic (Bcl-2, Bcl-xL and Bcl-w) and pro-apoptotic (Bax, Bak, Bad, Bid and Bim) members (31). In the presence of apoptotic stimuli, oligomerization of Bax and Bak translocate and form pore into OMM, leading to release of mitochondrial components, such as cytochrome C, Smac/Diablo and apoptosis-inducing factor (AIF). Consequently, cytochrome C forms the complex with protease-activating factor-1 (Apaf-1) and caspase-9, called 'apoptosome' complex (29). Activated caspase-9 induces downstream executioner caspases-3, -6 and -7. However, there is crosstalk between extrinsic and intrinsic pathway in certain cell types. Subsequent activation of caspase-8 results in cleavage of pro-apoptotic protein 'Bid'. Truncated Bid then translocate to mitochondria, causing the release of cytochrome C (32).

### **Clearance of death cells**

After cell death processes, phagocytosis is a crucial termination process for death cells to prevent surrounding tissue from the release of intracellular immunogenic contents (36). Bever *et al.* reported the present of phosphatidylserine (PS) on the outer cell surface is one major signal "eat me" to attract phagocytes (Fig, 3, 37-39). Consistent with apoptosis and tumorigenic cells, large amount of PS exposure triggers the recognition of macrophages and phagocytosis. However, asymmetrical distribution of phospholipids is composed of phosphatidylcholine (PC) and sphingomyelin (SM) in the outer leaflet, while PS, phosphatidylinositol (PI) and phosphatidylethanolamine (PE) in the inner leaflet of plasma membrane. This lipid asymmetry is maintained by the action of three distinct activities, including two of ATP-dependent and one of  $\text{Ca}^{2+}$ -dependent manner. ATP-dependent enzymes have been known as flippases and floppases to translocate phospholipids in and out of cell surface, respectively (39). The transiently and rapidly translocation of PS and PE into the outer leaflet of plasma membrane is regulated by  $\text{Ca}^{2+}$ -dependent manner, called scramblase (39;40).

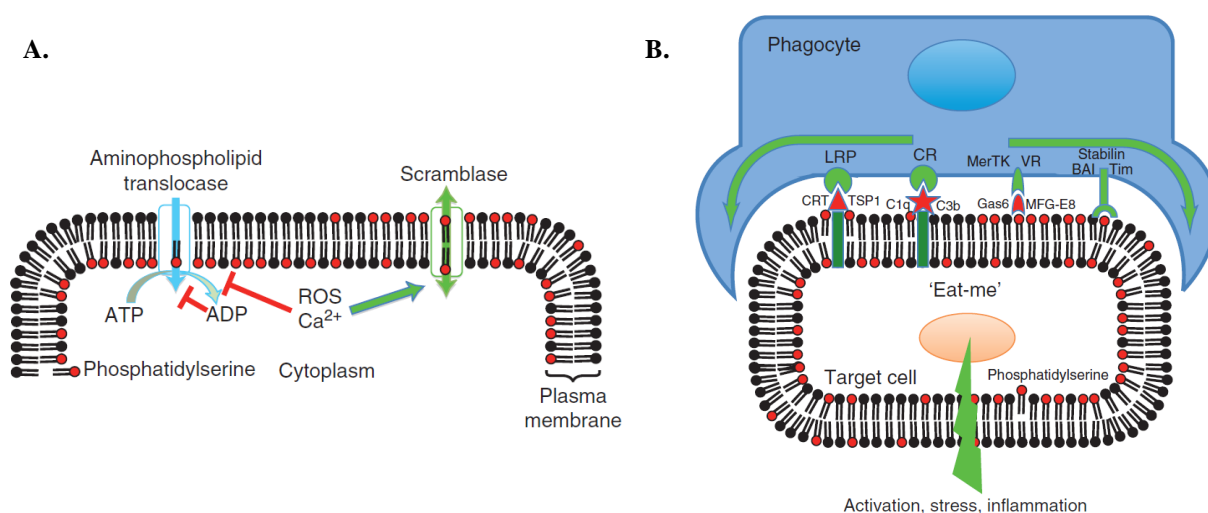


**Fig. 3 The regulation and physiology of membrane phospholipid asymmetry. A.)** The aminophospholipid translocase uses ATP to pump phosphatidylserine (PS) from the outer to inner leaflet of the plasma membrane, whereas the calcium-activated phospholipid scramblase can cause PS exposure by randomizing of phospholipid distribution. **B.)** ‘Eat-me’ signaling. PS activates phagocytosis via lipoprotein receptor-related protein (LRP) and other receptors on the phagocyte (35).

For example, the impairment of scramblase activity is found in Scott syndrome, an inherited bleeding disorder (41;42). According to PS-recognized by macrophages, PS exposure on apoptotic cells can bind to lipoprotein receptor-related protein (LRP) and other receptors on surface of macrophages (39). After clearance process, phagocytes produce anti-inflammatory cytokines or immune suppressor proteins (36;43;44). Interestingly, it has been shown in earlier finding that Cl<sup>-</sup> channels strongly regulate several cellular functions of macrophages (45;46).

### Role of anoctamins in cell death

Anoctamins are homologous plasma membrane protein family consists of ten different members (TMEM16A to K, excluding I or ANO1-ANO10) with several splice variants. They are composed of ten putative transmembrane-spanning domains and the NH<sub>2</sub> and COOH termini protruding into cytosol (46-50). Anoctamins reveal tissue-specific expression. ANO1, 6, 7, 8, 9 and 10 are expressed in various tissues, whereas ANO2, 3, 4 and 5 are specifically expressed in neuronal and musculoskeletal tissues (51-53). Anoctamins are involved in ion

transport, cell proliferation, phospholipid scrambling and cell death (50;51;53-55).

**ANO1** is frequently amplified on chromosomal region 11q13 which is associated with growth, proliferation, metastasis and poor prognosis in cancer cells, including head, and neck squamous cell carcinomas (HNSCC), pancreatic cancer, gastric cancer, prostate cancer and breast cancer (56-60). This region has been found to harbor several genes that have potential to drive oncogenes (55;58). ANO1 has been defined in multiple names depended on different cancer cells, such as gastrointestinal stromal tumors protein1 (DOG1) and tumor-amplified and over expressed sequence2 (TAOS2) (60). ANO1 plays a role in several tissues, including smooth muscles, secretory epithelia (in airway, exocrine glands and intestine) and sensory neurons (57;61-68). Knockout of ANO1 is embryonically lethal because it is an important in disease states, such as pulmonary diseases, hypertension and diarrhea (53;69). There are evidences showed that overexpression of ANO1 contributed tumorigenesis through the activation of EGF receptor (FGFR), CAMK, AKT (70;71) and MAPK signaling pathways (58;72;73). Consistent with previous studies, ANO1 is pro-proliferative protein which controls G1/S transition of cell cycle and cancer progression (74). It has been demonstrated that ANO1 interacts with signaling/scaffold actin-binding regulatory proteins, such as ezrin, radixin, moesin and RhoA, accompanied with localized cell shrinkage at the rear part in migrating cells (75-79). Moreover, it has been reported that ANO1 is an important for both RVD and AVD (79).

**ANO6** has been shown to be expressed in various tissues, such as the respiratory system, the gastrointestinal tract, kidney, ovary, skeleton, and skin (51;54;80). ANO6 plays a role in skeletal development in embryonic tissues, cell migration, metastasis, cell volume regulation and phosphatidylserine (PS) exposure during early phase of apoptosis (70;78;81-83). It has been reported to act as  $\text{Ca}^{2+}$ -activated nonselective cation channel,  $\text{Ca}^{2+}$ -activated  $\text{Cl}^-$  channel,  $\text{Ca}^{2+}$ -dependent phospholipid scrambling (70;83-85). Additionally, ANO6 is identified to be a volume-regulated  $\text{Cl}^-$  channel, which generates an outwardly rectifying  $\text{Cl}^-$  current (ORCC) to contribute RVD and AVD (86;87). Our previous studies showed knockdown of ANO6 significantly inhibited Fas- and staurosporine-induced ORCC but not  $\text{Ca}^{2+}$  dependent chloride

channels in lung epithelial cells (87). Nevertheless, Shumilina *et al.* showed  $\text{Ca}^{2+}$ -dependent ORCC, which is an important for migration in dendritic cells. The authors suggested ANO6 may form variation of oligomeric complexes caused different ORCC functions in specific cell types. Interestingly, Suzuki *et al.* demonstrated PS scrambling in Ba/F3 lymphocytes that is induced by overexpression of ANO6. Patients with Scott syndrome have a loss-of-function mutation in ANO6 characterized by a deficiency in platelet pro-coagulant activity, causing the congenital bleeding disorder (56;60). There is intriguing evidence that ANO6 mutation in Scott patients impairs not only PS exposure but also decrease cell blebbing and shedding of microparticles from membrane in platelets, red blood cells and lymphocytes (44;83;88-91). Moreover, recently finding has reported that a deficiency of PS scrambling in ANO6 knock-out mice reduce the production of calcified bone matrix during bone mineralization (82;92).

**ANO10** comprises like other anoctamins a DUF590 domain of unknown function. In mouse tissues, ANO10 is frequently expressed in the same tissues with ANO1 and Ano6, especially in neuronal and muscle tissues (53;80;93;94). In adult human, ANO10 is predominantly expressed in frontal and cerebellum in contrast to fetal brain. It has been reported that ANO10 certainly encodes a subunit of  $\text{Ca}^{2+}$ -regulated  $\text{Cl}^-$  channel and plays a role in Purkinje cells of cerebellum (93). The results from the combination of homozygosity mapping together with targeted array-based sequencing showed mutations in ANO10 are associated with autosomal-recessive cerebellar ataxia (93). Cerebellar degeneration has been suggested to involve mitochondrial- and DNA-repair dysfunction. Previously, it has reported ANO10 is probable role in cerebellar ataxia and schizophrenia (95). Furthermore, *Drosophila* ortholog of ANO10 has been also found to play a role in spindle formation and cell cycle progression, termed 'Axs' gene. This gene is proposed to be a mediator of meiotic spindle assembly and chromosome segregation (53).

Apart from ANO1, ANO6 and ANO10, there is less available evidence for other anoctamins. Interestingly, several independent groups have reported that other anoctamins (ANO2, ANO3, ANO8 and ANO9) exhibited their function as  $\text{Ca}^{2+}$ -activated  $\text{Cl}^-$  channels which are associated with murine embryogenesis on several organs (52;53;80). ANO8 and

ANO9 were also implicated in the cell volume regulation (94). ANO3, 4, 7 and 9 also play a role in phospholipid scramblases (28). High levels of other anoctamins expression are also related to cancers and diseases. For example, ANO5 (GDD1) is associated with the proliferation and differentiation of skeletal muscle. Mutation of ANO5 effects the repairment of muscle, causing muscular dystrophy (97). ANO7 (NGEP gene) is highly expressed at cell:cell contact regions in prostate cancer cells (98). ANO9 is located in chromosome 11 p15 which plays a role in  $\text{Ca}^{2+}$ -mediated phospholipid scrambling. In recent study, it found ANO9 acts as a metastasis-related gene which exhibit the inhibiting colorectal cancer progression (99). Because of deeply mechanism of anoctamins with diseases is remaining to be puzzled, it is therefore an intriguing issue to be investigated.

## **Intention and outline of the present thesis**

According to physiological evidences, RVD plays a role in cell proliferation, cell death, migration, immune response and cancer. Although, several  $\text{Cl}^-$  channels have been proposed as candidates for RVD, ANO1, 6 and 10 are shown to correlate to cellular volume regulation but the underlying mechanisms is still unclear. Therefore, this thesis will investigate the role of ANO1, 6 and 10 for RVD under physiological and under pathological conditions.

In chapter 2, experiments were aimed to understand the function of ANO1 for RVD in cancer. Therefore, the role of ANO1 in development of human head and neck stromal cell carcinoma (HNSCC) and colonic cancer will be investigated.

In chapter 3 and 5, we investigated several signal pathways which induce RVD and activation of ANO6 and ANO10 using the *Xenopus* oocytes expression system and primary cells from ANO6 and ANO10 knock-out mice.

In chapter 4, we ask the question, whether ANO6 and RVD could play a role in innate immune system in macrophages in response to bacterial infection.

In chapter 5, we investigated an ANO10-R263H mutation found in patients with neuroborreliosis and ask for the role of ANO10 during *Borrelia* infection.

## CHAPTER 2

### Role of anoctamins in cancer and apoptosis

#### Abstract

Anoctamin 1 (TMEM16A, ANO1) is a recently identified  $\text{Ca}^{2+}$ -activated chloride channel and a member of a large protein family comprising 10 paralogues. Before ANO1 was identified as a chloride channel protein, it was known as the cancer marker DOG1. DOG1/ANO1 is expressed in gastrointestinal stromal tumours (GIST) and particularly in head and neck squamous cell carcinoma, at very high levels never detected in other tissues. It is now emerging that ANO1 is part of the 11q13 locus, amplified in several types of tumour, where it is thought to augment cell proliferation, cell migration and metastasis. Notably, ANO1 is upregulated through histone deacetylase (HDAC), corresponding to the known role of HDAC in HNSCC. As ANO1 does not enhance proliferation in every cell type, its function is perhaps modulated by cell-specific factors, or by the abundance of other anoctamins. Thus ANO6, by regulating  $\text{Ca}^{2+}$ -induced membrane phospholipid scrambling and annexin V binding, supports cellular apoptosis rather than proliferation. Current findings implicate other cellular functions of anoctamins, apart from their role as  $\text{Ca}^{2+}$ -activated  $\text{Cl}^-$  channels.

**Key words:** anoctamin 1, anoctamin 6, TMEM16A, TMEM16F, cancer, head and neck stromal cell carcinoma

**Published in:** Podchanart Wanitchakool<sup>1</sup>, Luisa Wolf<sup>1</sup>, Gudrun E. Koehl<sup>2</sup>, Lalida Sirianant<sup>1</sup>, Rainer Schreiber<sup>1</sup>, Sucheta Kulkarni<sup>3</sup>, Umamaheswar Duvvuri<sup>3</sup> and Karl Kunzelmann<sup>1</sup> Role of anoctamins in cancer and apoptosis. *Philosophical transactions of the royal society*: 3;369(1638):20130096 (2014).

**Own experimental contribution:** Most western blot, cell proliferation and migration experiment performed in cell lines.

**Own written contribution:** Methods, Results, Parts of Introduction and Discussion.

**Other contributions:** Designed experiments and analyzed data.

## Introduction

Anoctamin 1 (ANO1, TMEM16A) is a novel  $\text{Ca}^{2+}$ -activated chloride channel (CaCC) with important physiological functions in epithelial cells and other cell types (1-4). It was also shown to be activated during cell swelling, probably secondary to an increase in intracellular  $\text{Ca}^{2+}$  (5). While some detected a role of  $\text{Ca}^{2+}$ -dependent anoctamins, such as ANO1 or ANO6, to volume regulation, others did not (5;6). Upregulation of endogenous  $\text{Ca}^{2+}$ -activated  $\text{Cl}^-$  channels in proliferating cells has been observed recently, but the role of these channels for proliferation has remained unclear (7,8). Before ANO1 was identified as CaCC, it was already known as a protein that is coexpressed with the morphogen sonic hedgehog during embryonic development (9). ANO1 was also known as DOG1, a protein strongly expressed in gastrointestinal stromal tumours and head and neck squamous cell carcinoma (HNSCC). Expression of DOG1 correlates with poor outcome in oesophageal squamous cell cancer (10-12). Interstitial cells of Cajal (ICC) are another predominant site for ANO1 expression (13-15). It has been reported that mice lacking ANO1 had fewer proliferating ICC (16). Moreover, additional data suggested that ANO1 regulates proliferation at the G1/S transition of the cell cycle. Assuming such a pro-proliferative role, targeting of ANO1 has been proposed as a novel method for the treatment of malignant tumours (7;17;18).

## Materials and Methods

**Animals:** Heterozygous  $APC^{Min+/-}$  pups (Fodde R et al, (1994) Proc Natl Acad Sci U S A 91:8969–8973) (Jackson Laboratory, USA) were weaned at 4–5 weeks of age and genotyped by PCR. Animals were fed with complete chow with 15% corn oil (Sniff, Soest, Germany), which has an adverse effect on polyp numbers in these animals (Wasan *et al* (1997) Proc Natl Acad Sci U S A 94:3308–3313).  $APC^{Min+/-}$  were sacrificed after a weight loss of 10%. Wildtype (wt) animals of the same age served as controls. Crypt cell isolation and expression analysis of ion channels in colonic epithelial cells. Colonic crypts were isolated from an inverted colon in  $\text{Ca}^{2+}$  free buffer solution. Animal studies were conducted according to the guidelines of the National Institute of Health and the German laws on protection of animals.

**Cell Culture, siRNA and Transfection:** BHY, CAL-33, T84 and HT<sub>29</sub> cell lines were grown in Opti-MEM or DMEM (Gibco) supplemented with 10% (v/v) heat inactivated fetal bovine serum (FBS, Gibco, Karlsruhe, Germany) at 5% CO<sub>2</sub> and 37°C. Lipofectamine<sup>TM</sup>2000 Transfection Reagent (Invitrogen, Karlsruhe, Germany) was used for transfection of hANO siRNA (Stealth siRNA, Invitrogen, 59-GGUUCCCAGCCUACCUC ACUAACUU-39, 59-AGUUAGUGAGGUAGGCUGGGAACC-39) or Negative Control High GC (Invitrogen) according to the manufacture's guidelines. Experiments were performed 48 h-72 h after transfection.

**Reverse Transcriptase PCR:** Total RNA was isolated from T84 cells using RNeasy Mini-Kit Qiagen; Hilden, Germany). 2 mg of total RNA was reverse-transcribed in 50 ml for 1 h at 40°C using random primer and RT. 30 cycles of RT-PCR was performed using standard procedures (GoTaq DNA Polymerase, Promega), 1 ml RT and primers for anoctamis (Ruiz et al (2012) 7: e43265, PLoS one). For semi-quantitative comparison,  $\beta$ -actin was co-amplified (primer 0.05 mM). Products were analyzed on ethidium bromide-stained 2% agarose gels using densitometry. Densitometric ratios for ANO1 and  $\beta$ -actin were calculated as a measure for relative expression of ANO1.

**Patch Clamp:** Cells were grown on glass cover slips and mounted on a perfused bath on the stage of an inverted microscope (IM35, Zeiss) and kept at 37 °C. The bath was perfused continuously with Ringer solution (mM: NaCl 145, KH<sub>2</sub>PO<sub>4</sub>, K<sub>2</sub>HPO<sub>4</sub> 1.6, D-glucose 6, MgCl<sub>2</sub> 1, Ca<sup>2+</sup>-gluconate 1.3, pH 7.4) at about 5 ml/min. For fast whole-cell patch clamping pipettes were filled with intracellular like solution containing (mM: KCl 30, potassium gluconate 95, NaH<sub>2</sub>PO<sub>4</sub> 1.2, Na<sub>2</sub>HPO<sub>4</sub> 4.8, EGTA 1, calcium gluconate 0.758, MgCl<sub>2</sub> 1.034, D-glucose 5, ATP 3, pH was 7.2). For all solutions Ca<sup>2+</sup> concentrations were adjusted to 0.1  $\mu$ M (pipette) and 1.3 mM (bath). During experiments cells were current clamped and membrane voltages were measured. At intervals cells were voltage clamped to  $\pm$  50 mV in steps of 10 mV for 1 s. The applied clamp voltages were corrected for liquid junction potentials. Because current voltage relationships were rather linear within the clamp voltage range, membrane conductances were calculated according to Ohm's law.

**Impedance based xCELLigence Attachment / Proliferation / Migration assay:** The xCELLigence invasion assay (Roche, Germany) is based on changes in electrical impedance

at the interphase between cell and electrode as migrating cells move through a barrier (Rahim S, Uren A (2011). A real-time electrical impedance based technique to measure invasion of endothelial cell monolayer by cancer cells. *J Vis Exp.* 2011 Apr 1;(50). pii: 2792). These changes were directly correlated with the migrative capacity of BHY and CAL33 cells. The technique provides an advantage over existing methods such as boyden chamber and matrigel assays, and standard proliferation assays, respectively, since the data is obtained continuously in real-time, when compared to endpoint analysis in other methods. For migration assays cells were seeded at a density of 10,000 cells/well on CIM-plates-16 migration plates. The xCELLigence attachment/proliferation assay is based on assessment of impedance during attachment (early phase) and proliferation (late phase) as detected by real-time electrical impedance measurement. For attachment and proliferation assays cells were seeded at a density of 5,000 cells/well on E16 plates (Roche, Germany).

**Western Blot:** Freshly isolated mouse intestinal cells or cultured HT<sub>29</sub>, T84, BHY, and UMSCC cells were lysed with an appropriate buffer (150 mM NaCl, 50 mM Tris-HCl, 1 mM EDTA, 1% NP-40, protease inhibitor, 100 mM DTT; pH 7.4) and DNA was sheared by sonication. Samples were quantified using a Bio-rad protein assay (Biorad) and the same amount of protein (50 mg). Bands were analyzed using densitometry. Densitometric ratios for ANO1 and  $\beta$ -actin were calculated as a measure for relative expression of ANO1.

**Apoptosis assay:** Apoptosis was assessed by NucView<sup>TM</sup> 488 Caspase-3 assay kit (Biotum, Germany). Briefly, cells were incubated with DEVD-NucView488 substrate and apoptotic cells were analyzed using the plate reader NOVOstar.

**Proliferation assay:** For proliferation assays, cells were plated at a density of 2,000 cells/0.35 cm<sup>2</sup> and incubated 2 days later with various concentrations of rapamycin or TSA as indicated. Cell proliferation was assessed by 5-bromo-2-deoxyuridine (BrdUrd) incorporation using an enzyme-linked immunosorbent assay kit (Roche Diagnostics, Penzberg, Germany) and by cell counting. The cell number was assessed after fixation in 3.7% formaldehyde and 0.5% Triton X-100 for 30 min at room temperature and after staining with Mayer's hemalaun (Merck, Darmstadt, Germany) for 5 min. Digitized microscopic images were taken (Fluovert FS, Leitz), and nuclei were counted using imaging software (TINA).

**Immunohistochemistry of ANO1-expression:** Primary tissue samples were collected after obtaining informed consent and approval from the Institutional Review Board. Normal adjacent mucosa is defined as histologically benign appearing mucosa (as judged by an experienced pathologist) acquired from the margins of the tumor resection. Staining was conducted with anti-TMEM16A antisera and scored using a semiquantitative system (IHC index). The index was defined as the relative intensity, scored on a 0 to 3 scale, multiplied by the percentage of positively stained cells. High and low expressors were categorized as having H-scores above or below the median.

## Results and Discussion

### ANO1 is located on the 11q13 amplicon

The coding sequence of ANO1 is located within the 11q13 region, a chromosomal locus that is frequently amplified in a number of different human cancers, such as urinary bladder cancer, breast cancer and HNSCC (100). The 11q13 amplicon contains a stretch of proteins related to cell cycle, proliferation and apoptosis (cyclin D1, ORAOV1, FGF19, FGF4, TMEM16A, Fas-associated via death domain, PPFIA1, cortactin (101). The complex structure of this amplicon has mostly been studied in breast cancer, where multiple genes have been suggested as driver genes (102;103). These findings implied a link between ANO1 expression, cell-cycle regulation and proliferation, which has recently been demonstrated in HNSCC and other cancer cells (55;72-74;104). Surprisingly, downregulation of ANO1 contributes to cerebrovascular remodeling by promoting basilar smooth muscle cell proliferation, which is through inhibition of expression of cyclin D1 and cyclin E (68). We performed additional experiments and compared proliferation of two HNSCC (CAL33, BHY) and one colonic epithelial cell line (HT<sub>29</sub>) using an online impedance-based xCELLigence proliferation assay system (79) (figure 1a). Proliferation was clearly higher in the HNSCC cell lines, which express much higher levels of ANO1, when compared with HT<sub>29</sub> cells (figure 3a) (79). In a previous study, we did not detect inhibition of proliferation of BHY cells by siRNA (79). Using improved Stealth siRNA, these experiments were repeated. Proliferation was suppressed by siRNA-knockdown of ANO1 expression in HNSCC but not in HT<sub>29</sub> cells.

These results suggest that very effective suppression of ANO1 expression is necessary to eliminate the pro-proliferative effects of ANO1, suggesting that low expression of ANO1 is sufficient to induce this effect. While siRNA had no effect in HT<sub>29</sub> cells, 1 mM staurosporine (figure 1a black arrow, dashed lines) inhibited proliferation and induced cell apoptosis in colonic carcinoma cells, as demonstrated in an earlier publication (105). Thus, enhanced expression of ANO1 does not seem to enhance proliferation in every cell type (58;79).

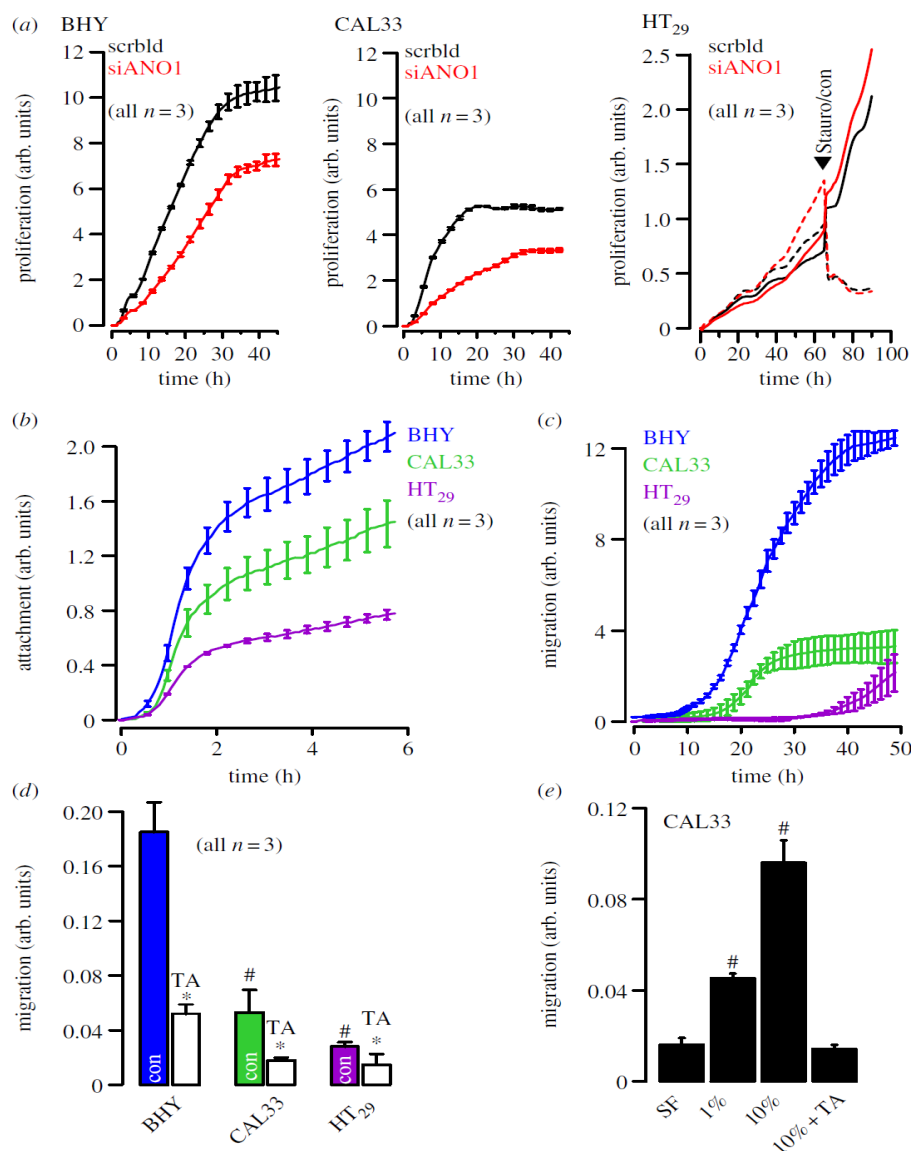


**Fig. 1** ANO1 controls proliferation: (a) Cell proliferation measured online by impedance-based xCELLigence proliferation assay system in HNSCC (BHY, CAL33) and colonic epithelial (HT<sub>29</sub>) cells (see electronic supplementary material). siRNA-knockdown of ANO1 expression reduced proliferation in both BHY and CAL33 cells, but slightly augmented proliferation in HT<sub>29</sub> cells. Staurosporine ( $1 \mu\text{g ml}^{-1}$ ) strongly inhibited proliferation. (b) Attachment of BHY, CAL33 and H<sub>29</sub> cells after seeding in xCELLigence chambers (see electronic supplementary material). (c) Migration of BHY, CAL33 and H<sub>29</sub> cells after seeding

in the xCELLigence migration chamber (see electronic supplementary material). (d) Summary of the rate of cell migration between 10 and 30 h after seeding and inhibition of migration by TA(10 mM). (e) Migration of CAL33 cells and effect of fetal calf serum and TA. Mean $\pm$ s.e.m. (number of cells). Symbol # denotes significant difference when compared with BHY and serum free, respectively ( $p < 0.05$ ; ANOVA). Asterisks (\*) denote significant inhibition by TA ( $p < 0.05$ ; paired t-test).

However, there is increasing consent that high levels of ANO1 lead to enhanced cell motility, distal metastasis and poor prognosis (55;58;72;79). Also in this study, cell attachment and migration was enhanced with increasing expression of ANO1 (BHY, CAL33, HT<sub>29</sub>). It is further demonstrated that migration could be significantly inhibited by tannic acid, a blocker of ANO1 and other anoctamins (figure 1c,d). Moreover, migration was strongly dependent on the presence of serum in the migration chamber and was inhibited by the ANO1 inhibitor tannic acid (TA, figure 1e). Although proliferation, attachment and migration were positively correlated with expression of ANO1, this does not prove that ANO1 is directly responsible for the change of these properties.

### Role of ANO1 for metastasis

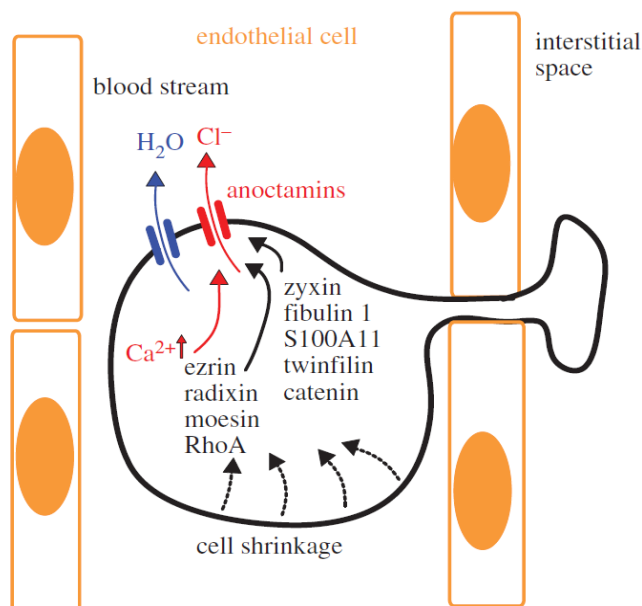


**Fig. 2** Anoctamins facilitate cell volume decrease and support diapedesis and cell migration: model for diapedesis and migration of a tumour cell expressing anoctamin  $\text{Cl}^-$  channels, which allow  $\text{Cl}^-$  release and osmotic cell shrinkage. Anol is regulated by actin and possibly by a number of proteins related to signalling/scaffolding, such as ezrin, radixin, moesin and proteins related to cell attachment and migration, such as zyxin, fibulin 1, S100A11, twinfilin and catenin.

How does ANO1 control the ability of tumour cells to migrate and form distal metastasis? The relationship between ion channel currents, cell volume regulation, migration and metastasis is well established (106-109). Previous findings indicate that ANO1 is activated during hypotonic cell swelling and contributes to regulatory volume decrease (RVD), which certainly requires a rise in intracellular  $\text{Ca}^{2+}$  (51;79;96).

A rise in intracellular  $\text{Ca}^{2+}$  may activate ANO1 together with  $\text{K}^+$  channels to release intracellular  $\text{K}^+$  and  $\text{Cl}^-$  ions. Resulting osmotic loss of intracellular water will cause rapid cell shrinkage and allow passage through narrow gaps like those formed by endothelial cells (109;110) (figure 2).  $\text{Ca}^{2+}$ -dependent activation of ANO1 would support cell shrinkage at the rear end of migrating cells, thereby further reducing cell volume and facilitating diapedesis. Inhibition of  $\text{Cl}^-$  channels impedes cell volume changes and thereby compromises tumour cell invasion. This has been demonstrated for ANO1 (79) as well as other  $\text{Cl}^-$  channels (110). Importantly, cell migration requires constant depolymerization and repolymerization of the actin cytoskeleton, which permanently changes cell-matrix adhesions (76;111). Our earlier findings suggested that ANO1  $\text{Cl}^-$  currents are controlled by the actin cytoskeleton (75). This was supported by a subsequent report indicating that ANO1 associates with the signaling/scaffolding proteins ezrin, radixin, moesin and RhoA, which are known to connect plasma membrane proteins to the cytoskeleton (112). Moreover, results from a two hybrid split ubiquitin screening suggested interaction of ANO1 with a number of proteins related to cell attachment and migration, such as zyxin, fibulin 1, S100A11, twinfilin and catenin (unpublished results from the Kunzelmann laboratory, K. Kunzelman 2012, figure 2).

It was shown that members of the Rho GTPase family exert effects on cell shape and motility by regulating actin cytoskeleton; the activation of Rac1 organizes cortical actin cytoskeleton and promotes formation of lamellipodia at the leading edge, a hallmark of a motile cell, while the activation of RhoA at the rear influences acto-myosin complexes to allow retraction of the trailing end. Spatial and temporal regulation of the activity at each end create an unequal distribution of membranous, cytoskeletal and cytoplasmic contents to induce a highly polarized, motile shape that is suitable for movement and metastasis (108). Thus, the presence of ANO1 at the plasma membrane, its ability to regulate cell shape and volume, and its connections to cytoplasmic/cytoskeletal elements is likely to contribute to cell movement and metastasis.

### **Regulation of expression of ANO1 by histone deacetylase and clinical implications**

Recruitment of histone acetyltransferases and histone deacetylases (HDACs) is a key element in the dynamic regulation of genes controlling cellular proliferation and differentiation during normal development as well as carcinogenesis (113;114). A number of

anti-cancer treatments are based on the inhibition of HDAC. HDAC inhibitors promote expression of p21 in breast cancer cells, which inhibits the action of cyclin D1. HDAC inhibitors may therefore also be useful for the treatment of those HNSCC that show overexpression of ANO1 and concomitant activation of cyclin D1 (55).

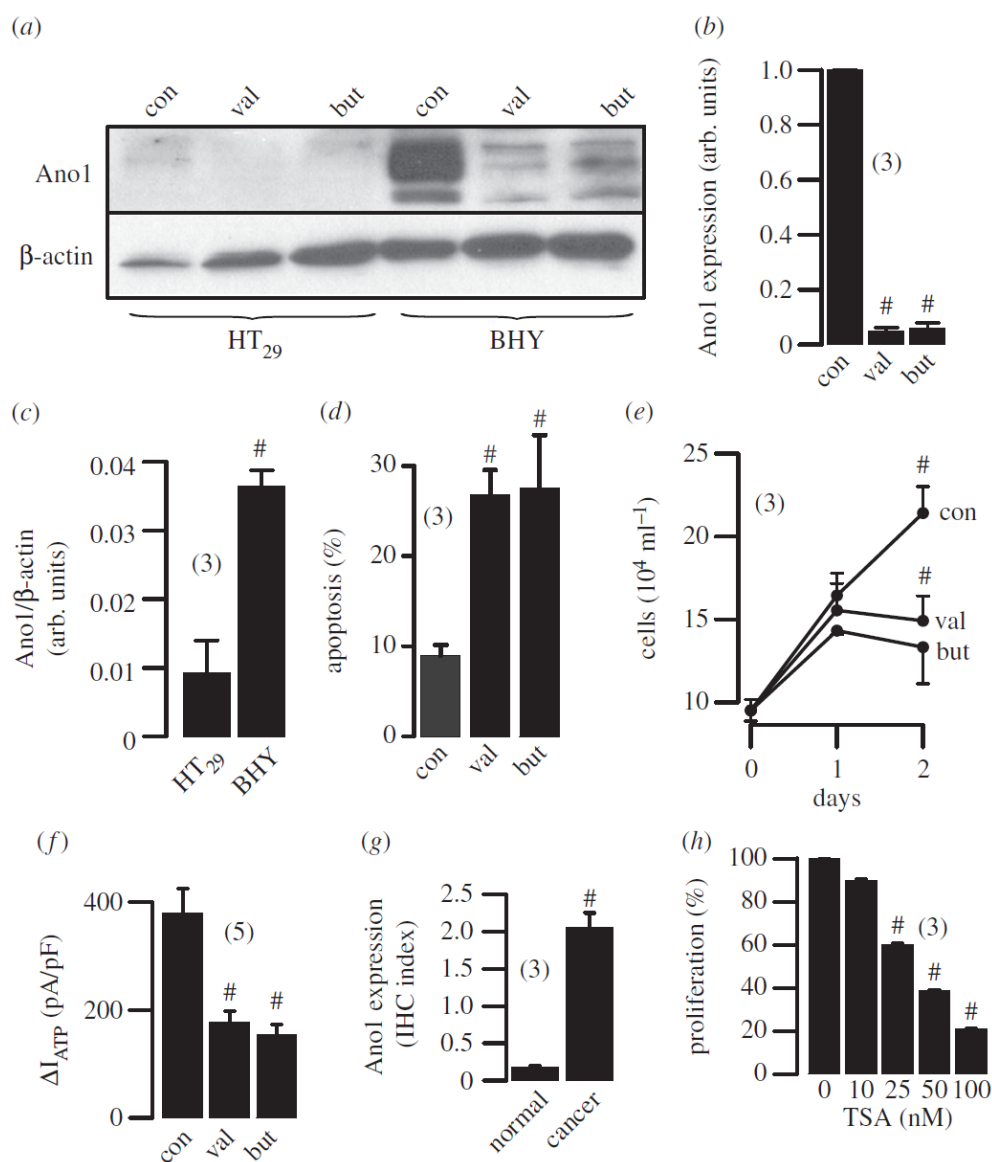


**Fig. 3** HDAC regulates expression of ANO1: (a,b) western blots and densitometric analysis indicating expression of ANO1 in HT<sub>29</sub> colonic epithelial and BHY HNSCC cells, and inhibition by HDAC inhibitors valproic acid (3 mM) and butyrate (4 mM).  $\beta$ -actin was used as a loading control. (c) Real-time PCR analysis of ANO1-mRNA expression in HT<sub>29</sub> and BHY cells. (d,e) Induction of apoptosis and inhibition of proliferation of BHY cells by valproic acid and butyric acid, as measured by apoptosis assays (see electronic supplementary material) and cell counting. (f) Whole cell ANO1  $Cl^-$  currents ( $V_c = +100$  mV) activated by an increase in intracellular  $Ca^{2+}$  owing to stimulation with the purinergic agonist ATP (100 mM). (g) Expression of ANO1 in human HNSCC samples and normal tissue as measured by

immunohistochemistry (cf. electronic supplementary material). (h) Inhibition of proliferation of UM-SCC cancer cells by various concentrations of TSA. Mean $\pm$ s.e.m. (number of cells). Symbol # denotes significant difference when compared with control, normal tissue, HT<sub>29</sub> cells or absence of HDAC inhibitors, respectively ( $p < 0.05$ ; unpaired t-test).

In fact, HDAC inhibitors have already entered preclinical evaluation (115;116). In recent experiments, we found that pronounced expression of ANO1 in the HNSCC cell line BHY was largely inhibited by treatment with the HDCA inhibitors valproic acid or butyric acid, along with inhibition of cell survival and ANO1-dependent whole cell currents (figure 3a-f). Although this does not prove that HDAC inhibitors act through downregulation of ANO, these novel results again demonstrate a correlation between ANO1 expression and proliferation. Corresponding to the data discussed in figure 1, which did not identify a role ANO1 expression for proliferation of HT<sub>29</sub> colonic epithelial cells, expression levels for ANO1 were much lower and were not affected by HDCA inhibitors. As pointed out, expression levels for ANO1 are much higher in HNSCC compared with normal tissues (figure 3g). We also found a dose-dependent inhibition of proliferation of another HNSCC cell line, UM-SCC cancer cells, by a third type of HDAC-inhibitor, trichostatin (TSA) (figure 3h). UM-SCC cells contain amplification of the ANO1 gene locus similar to BHY cells. The results confirm that the inhibitory effect of HDAC inhibitors on ANO1 expression is independent of the HNSCC cell line used. While valproic acid and butyric acid are rather broad, non-selective inhibitors of HDAC, TSA selectively suppresses class I/II, suggesting that ANO1 expression is regulated by these HDACs. Although the mechanisms by which TSA promotes loss of cell survival/growth in these cells is incompletely understood, the present results support the use of HDAC inhibitors for the treatment of HNSCC, which may act in part through inhibition of ANO1 expression.

### **ANO1 and sonic hedgehog**

Interesting links exist between ANO1 and the sonic hedgehog (Hh) signaling pathway. Hh is coexpressed with ANO1 in the zone of polarizing activity in mouse limb buds during E10.5 and E11.5 (117). Hh signaling controls many aspects of development and also regulates cell growth and differentiation in adult tissues. It is activated in a number of human malignancies. Hh and Wnt signaling frequently act together in controlling cell growth and

tissue morphogenesis. Hh is also active in ‘embryonic cancers’ such as basal cell carcinoma of the skin, stromal cancer (118;119) and also during epithelial to mesenchymal transition. Hh expression has been shown to be upregulated in the neoplastic or inflammatory intestine when stem cells compensate for epithelial damage, while suppression of hedgehog signaling by cyclopamine has been shown to induce apoptosis (120;121). It will be interesting to learn more about the correlations between Hh signaling, ANO1 expression and cancer.

### ANO1 required for terminal differentiation

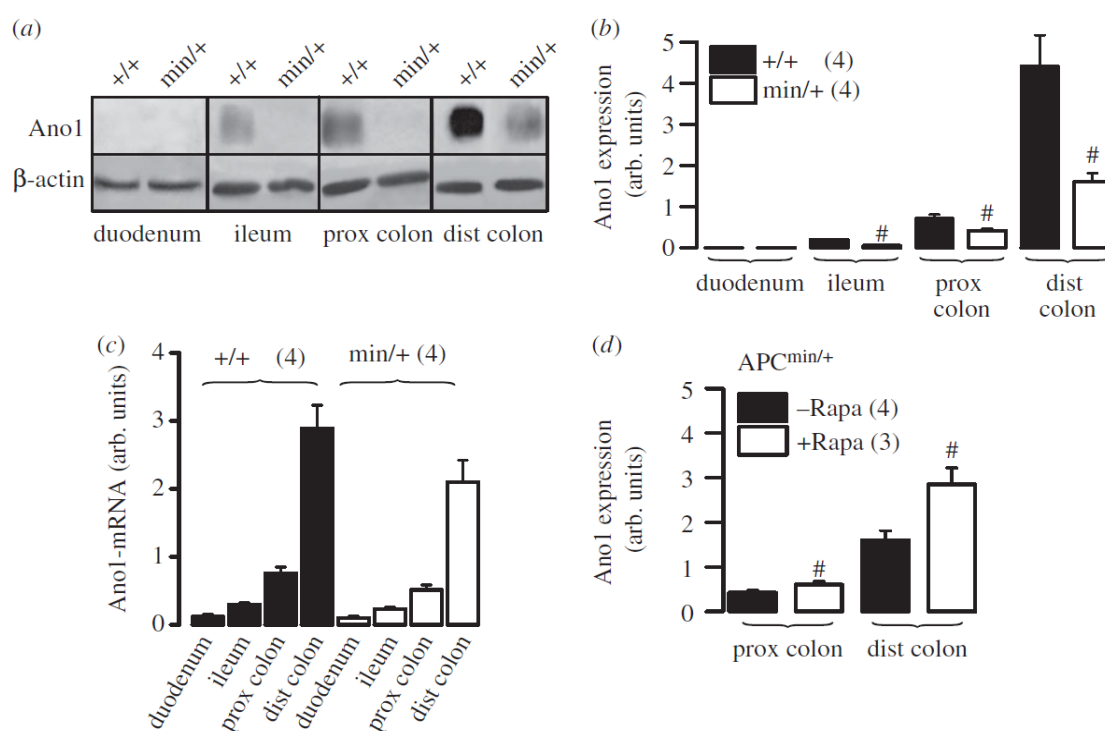


**Figure 4.** APC/mTOR controls expression of ANO1 in mouse intestine: (a,b) western blot analysis of expression of ANO1 in duodenum, ileum and colon of  $APC^{min/+}$  and wild-type mice. (c) Semiquantitative analysis (see electronic supplementary material) of ANO1-mRNA expression in duodenum, ileum and colon of  $APC^{min/+}$  and wild-type mice. (d) Treatment with the mTOR-inhibitor rapamycin increased expression of ANO1 in the intestine of  $APC^{min/+}$  mice. Mice were fed  $40 \text{ mg kg}^{-1}$  Sirolimus (Wyeth Pharmaceuticals, Collegeville, PA, USA) in their chow to reach blood levels of  $12 \pm 2 \text{ ng ml}^{-1}$  rapamycin ( $n = 1/4 \ 66$ ). Mean  $\pm$  s.e.m. (number of cells). Symbol # denotes significant difference when compared with  $+/+$  or -Rapa, respectively ( $p < 0.05$ ; unpaired t-test).

In cell types others than GIST, ANO1 has been reported to be inhibitory on cell proliferation and expression of ANO1 was related to cellular differentiation (68;122). These somewhat surprising results were supported by our own results indicating inhibition of cell proliferation by ANO1 in colonic epithelial cells (figure 1a). Interestingly, one study

identified ANO1 by expression cloning in oocytes from axolotl, a salamander that does not undergo terminal differentiation and metamorphosis, and therefore maintains an amazing ability to regenerate limbs and other parts of the body (123). Terminal differentiation is missing in these animals because of a complete lack of thyroid hormones. Maybe more than a coincidence, plasma thyronine levels were found to be abnormally low in patients with advanced colon carcinoma (124). It might be worth examining whether expression of ANO1 is regulated by these hormones.

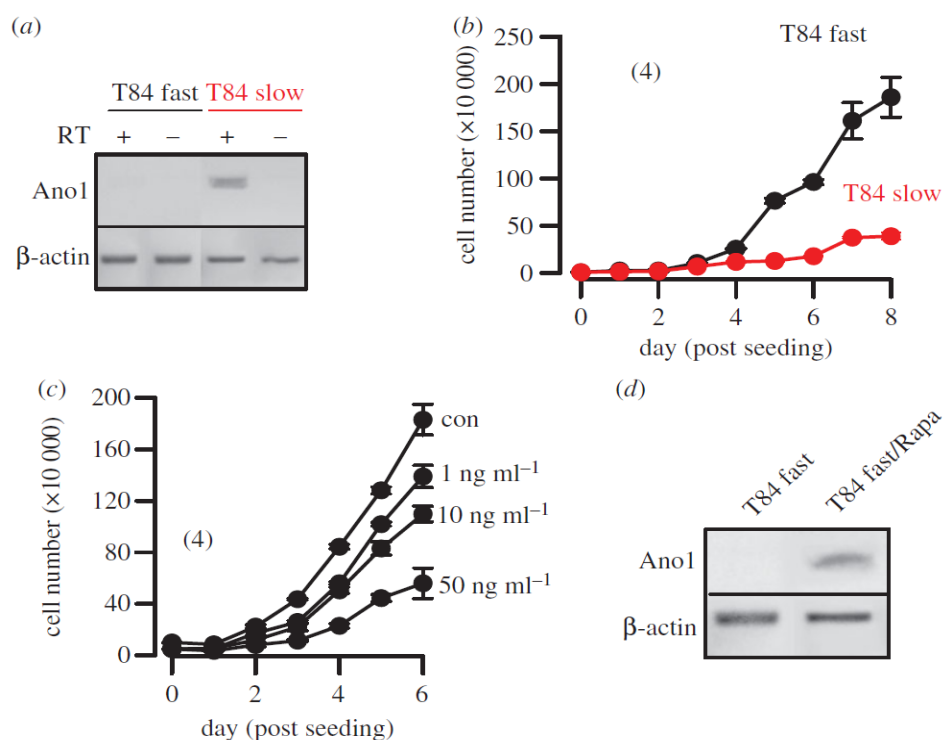


**Fig. 5** APC/mTOR controls expression of ANO1 and proliferation of T84 cells: (a) RT-PCR analysis of ANO1-mRNA expression in fast growing and slowly growing T84 colonic carcinoma cells. +/- RT indicates the presence of or the absence of reverse transcriptase in the react growing T84 cells. (c) Effect of treatment with rapamycin on proliferation of T84 fast cells. (d) RT-PCR analysis of ANO1-mRNA expression in fast growing T84 cells in the absence and the presence of rapamycin. The rapamycin concentration used was 50 ng ml<sup>-1</sup>. Mean  $\pm$  s.e.m. (number of cells)

We found evidence for regulation of ANO1 expression by the tumour suppressor adenomatous polyposis coli (APC) in mouse colon. ANO1 is expressed in mouse ileum, proximal and particularly distal colon, but its expression is largely attenuated in *APC*<sup>min/+</sup> mice. *APC*<sup>min/+</sup> mice demonstrate reduced tumour suppressive activity by APC, resulting in upregulation of mTOR, thus leading to numerous large intestinal polyps and ultimately cancer

(figure 4a,b) (122). *APC<sup>min/+</sup>* mice develop particularly large polyps in the distal colon, where we detected a pronounced decrease in ANO1 expression. Notably, the mTOR-inhibitor rapamycin increased ANO1 expression in both proximal and distal colon (figure 4d). This inverse correlation between low ANO1 levels and upregulation of mTOR (122) suggests that ANO1 may be inhibitory on proliferation of mouse intestinal epithelial cells, similar to HT<sub>29</sub> cells. Interestingly, a fast growing subclone of T84 colonic epithelial cells (T84 fast) is lacking expression of ANO1, when compared with the slowly growing parental cells (T84 slow) (102) (figure 5a,b). Notably, treatment of fast growing T84 cells with the mTOR-inhibitor rapamycin reduced proliferation and induced expression of ANO1 (figure 5c,d). These data support the concept that effects of ANO1 on cell survival are cell-type dependent (55;65).

#### **Other anoctamins correlated to cancer**

Apart from ANO1 and ANO2, much less information is available for other anoctamins. Although a deeper understanding is currently lacking, it should be mentioned that various anoctamins have a role during murine embryogenesis (125). ANO7 (TMEM17G, NGEF) has been detected in prostate cancer (98;126). Studies indicate that the long version of NGEF is present on the plasma membrane of overexpressing LNCaP cells and is highly concentrated at cell-cell contact regions (98). A splice form of ANO6 was identified that was associated with metastatic capability of mammary cancers in mouse and was related to poor prognosis of patients with breast cancer (127). Notably, ANO6 has recently been associated with membrane phospholipid scrambling and cell shrinkage and therefore seems to be correlated to apoptosis rather than proliferation and cancer (70;83;84;87;128).

#### **Role of ANO6 in phospholipid scrambling and apoptosis**

The distribution of lipids in the outer and inner leaflets of plasma membranes is asymmetrical: while phosphatidylcholine is mainly found in the outer leaflet, phosphatidylserine is present in the inner surface. During signaling events such as activation of platelets or cellular apoptosis, the distribution is rapidly altered leading to exposure of phosphatidylserine at the outer surface. A lipid transporter with phospholipid scrambling activity was proposed to be responsible for this process; however, a convincing candidate protein with such ability was not identified until recently. Surprisingly, a member of the TMEM16 family, TMEM16F

(ANO6) was shown to contain phospholipid scrambling activity, when activated by a large increase in intracellular  $\text{Ca}^{2+}$  (70). Moreover, reconstitution experiments in ANO6-deficient thymocytes suggested that other anoctamins such as ANO3, ANO4, ANO7 and ANO9 retain the ability to function as calcium-dependent phospholipid scramblase (129). These results came as a surprise, since ANO6 has been characterized as a  $\text{Ca}^{2+}$ -activated  $\text{Cl}^-$  channel. Moreover,  $\text{Ca}^{2+}$ -activated  $\text{Cl}^-$  currents were also observed after overexpression of An4, 7 and 9 (50;84;87;130;131). However,  $\text{Cl}^-$  channel and scramblase activity were shown to be independent (84). Moreover, we demonstrated recently that An6 is activated during cell swelling and by pro-apoptotic stimuli and therefore contributes to both RVD as well as apoptotic volume decrease (84;87;96). Notably, the amplicon 11q13 that contains the ANO1 gene, not only carries genes that control proliferation but also FADD, a gene associated with apoptosis. Thus, anoctamins can also be regarded as a novel family of regulators of cell proliferation and apoptosis, which may be of particular relevance during development, activation of immune cells such as lymphocytes, dendritic cells (81) and macrophages, and in particular types of cancer.

### **Acknowledgments**

Supported by by Deutsche Krebshilfe, Sander Stiftung Fo'nderprojekt no. 2013.031.1 and DFG SFB699/A7. U.D. was supported in part by a Career Development Award from the Department of Veterans Affairs, and funds from the PNC foundation. We thank Prof. L. Bubendorf (Department of Pathology, University of Basel/Switzerland for supplying the HNSCC cell lines.

## CHAPTER 3

### Cellular volume regulation by anoctamin 6: Ca<sup>2+</sup>, phospholipase A2 and osmosensing

#### Abstract

During cell swelling, Cl<sup>-</sup> channels are activated to lower intracellular Cl<sup>-</sup> concentrations and to reduce cell volume, a process termed regulatory volume decrease (RVD). We show that anoctamin 6 (ANO6; TMEM16F) produces volume-regulated anion currents and controls cell volume in four unrelated cell types. Volume regulation is compromised in freshly isolated intestinal epithelial cells from *Ano6*<sup>-/-</sup> mice and also in lymphocytes from a patient lacking expression of ANO6. Ca<sup>2+</sup> influx is activated and thus ANO6 is stimulated during cell swelling by local Ca<sup>2+</sup> increase probably in functional nanodomains near the plasma membrane. This leads to stimulation of phospholipase A2 (PLA<sub>2</sub>) and generation of plasma membrane lysophospholipids, which activates ANO6. Direct application of lysophospholipids also activates an anion current that is inhibited by typical ANO6 blocker. An increase in intracellular Ca<sup>2+</sup> supports activation of AnO6, but is not required when PLA<sub>2</sub> is fully activated, while re-addition of arachidonic acid completely blocked ANO6. Moreover, ANO6 is activated by low intracellular Cl<sup>-</sup> concentrations and may therefore operate as a cellular osmosensor. High intracellular Cl<sup>-</sup> concentration inhibits ANO6 and activation by PLA<sub>2</sub>. Taken together, ANO6 supports volume regulation and volume activation of anion currents by action as a Cl<sup>-</sup> channel or by scrambling membrane phospholipids. Thereby, it may support the function of LRRC8 proteins.

**Key words:** TMEM16F, Anoctamin 6, Volume regulation, Regulatory volume decrease, RVD, Volume-regulated anion channel, VRAC, Apoptosis

**Published in:** Lalida Sirianant<sup>1</sup>, Jiraporn Ousingsawat<sup>1</sup>, Podchanart Wanitchakool<sup>1</sup>, Rainer Schreiber<sup>1</sup>, Karl Kunzelmann<sup>1</sup> Cellular volume regulation by anoctamin 6: Ca<sup>2+</sup>, phospholipase A2 and osmosensing Pflügers Archiv - European Journal of Physiology:2015 Oct 6.

**Own experimental contribution:** Most western blot, COIP, Flow cytometry experiment performed in cell lines and animals.

**Own written contribution:** Methods, Results, Parts of Introduction and Discussion.

**Other contributions:** Designed experiments and analyzed data.

## Introduction

Volume regulation is an intrinsic property of any living cell. Cell swelling due to increase in intracellular osmolytes or by decrease in extracellular osmolarity is counteracted by volume regulated ion channels, releasing KCl to the extracellular space (132). Volume regulated anion channels (VRAC) have been studied and reviewed extensively, but the contribution of intracellular Ca<sup>2+</sup> remained controversial (9;132;133). Very recently, LRRC8A has been described as an essential component of VRAC. Surprisingly, overexpression of LRRC8A rather suppressed than augmented VRAC (134;135). It was therefore concluded that other essential components are still missing to fully reproduce VRAC.

Anoctamins, a family of Ca<sup>2+</sup> activated Cl<sup>-</sup> channels and phospholipid scramblases (for review see (136), have been proposed to support volume regulation (86;96). Also ANO6 (anoctamin 6, TMEM16F) has pleiotropic functions, since it scrambles plasma membrane phospholipids (70;84;137) and produces Cl<sup>-</sup> and nonselective cation currents (50;83;85;130), triggered by intracellular Ca<sup>2+</sup> and during apoptotic cell death (87). A recent X-ray analysis of a fungal TMEM16 protein provided ideas how TMEM16 proteins may operate as phospholipid scramblases and ion channels (138). Activation of ANO6 induced cell shrinkage and subsequent swelling, and was shown to be a component of the ubiquitous outwardly rectifying Cl<sup>-</sup> channel (86;87;139). Despite the evidence for a role in volume regulation and cell migration, the findings remained controversial (81;86;96;130).

Although studied extensively (for review see (15;132;140), no general concept exists for the activation of Cl<sup>-</sup> currents ( $I_{Cl-swel}$ ) during cell swelling. Also studies on LRRC8A do not provide a molecular mechanism for the regulation of this VRAC-component (134;135). In the present report we identify ANO6 as a volume regulated Cl<sup>-</sup> channel and unravel the molecular mechanism of activation. Volume regulation and current measurements were done at 37 °C and in the presence of physiological extra- and intracellular ion concentrations. We found that volume regulation and proper activation of  $I_{Cl-swel}$ /ANO6 requires i) lowering of the intracellular Cl<sup>-</sup> concentration, ii) Ca<sup>2+</sup> influx through transient receptor potential (TRP) channels, and iii) generation of membrane lysophospholipids through phospholipase A2

(PLA<sub>2</sub>). The data suggest that ANO6 operates as an osmosensor and a Cl<sup>-</sup> release channel during RVD, or may affect volume regulation by scrambling membrane phospholipids.

## Material and Methods

**Animals, cells, cDNA, RT-PCR:** Generation of *Ano6*<sup>-/-</sup> animals and isolation of intestinal epithelial cells has been described earlier (69;82). All animal experiments were approved by the local ethics commission of the University of Regensburg and were conducted according to the guidelines of the American Physiological Society and the German law for welfare of animals. The HEK293 cells were grown as described earlier (50). The culture of EBV-transformed B lymphoblast cell lines from control subjects and Scott-UK or Scott-USA patients has been described in another report (84). Lymphocytes were grown in RPMI 1640 medium (GIBCO, 52140; Darmstadt, Germany) supplemented with 10% fetal calf serum (GIBCO) and penicillin/ streptomycin (GIBCO). LRRC8A cDNA was cloned from HEK293 cells using standard PCR techniques. Generation of cDNA for ANO6 and transfection/expression of ANO6 has been report earlier (50). RT-PCR analyses were performed using standard conditions and appropriate primers.

**siRNA, solutions, materials and statistical analysis:** Knockdown of ANO6 by siRNA was reported in our previous study (96). All experiments were performed 48 h after the transfection. For most experiments cells were kept initially in Ringer solution (mM): NaCl 145, KH<sub>2</sub>PO<sub>4</sub> 0.4, K<sub>2</sub>HPO<sub>4</sub> 1.6, D-glucose 5, MgCl<sub>2</sub> 1, calcium gluconate 1.3, pH 7.4. Ringer solution was then replaced by an isotonic solution (Iso) containing (mmol/l) NaCl 72.5, KH<sub>2</sub>PO<sub>4</sub> 0.4, K<sub>2</sub>HPO<sub>4</sub> 1.6, D-glucose 5, MgCl<sub>2</sub>1, Ca-gluconate 1.3, mannitol 145, pH 7.4. To induce cell swelling a hypotonic solution (150 mosmol/l; 50% Hypo) was produced by removal of mannitol. Alternatively 50 or 100 mmol/l NaCl were removed to produce 17 % and 33% hypotonicity, respectively. Osmolarity was measured using an osmometer.

**Western Blotting of ANO6 and COIP:** Protein was isolated from wt and Scott B-lymphocytes using a sample buffer containing 50 mM Tris-HCl, 150 mM NaCl, 50 mM Tris, 100 mM dithiothreitol, 1% Nonidet P-40, 0.5% deoxycholate sodium, and 1% protease inhibitor mixture (Sigma). Proteins were separated by 8.5 % SDS-PAGE and transferred to a

polyvinyl membrane (GE Healthcare, Munich, Germany). Membranes were incubated with primary anti-ANO6 rabbit polyclonal AB (Ano6 AB P78; Davids Biotech, Regensburg, Germany) at a dilution of 1:1000 overnight at 4 °C. Proteins were visualized using horseradish peroxidase-conjugated secondary antibody and ECL detection.

**For co-immunoprecipitation** Cells were cotransfected with ANO6-GFP/LRRC8A or ANO6/LRRC8A-GFP. Cell lysates (NP-40 lysis buffer containing 1X protease inhibitor cocktail) was pre-cleaned with protein G-agarose at 4 °C for 1 h and incubated with 5 µg primary antibody (Rockland, Gilbertsville, PA 19525) overnight at 4 °C on a rotator. Cell lysates were incubated with protein G-agarose at 4 °C for 3 h, followed by centrifugation at 1000 g for 1 min 3 times. Pellets were collected and resuspended in 1X loading buffer. The supernatant was collected and separated by 10 % SDS-PAGE and transferred to PVDF membrane. The membrane was blocked with 5 % NFM/TBST at RT for 1 h and incubated overnight 4 °C with goat polyclonal anti-GFP AB, rabbit polyclonal anti-ANO6 AB, or rabbit polyclonal anti-LRRC8A AB (AVIVA, San Diego, USA) (1 % NFM/TBST). Subsequently, the membrane was incubated with HRP-conjugated donkey anti-goat IgG at RT for 1 h. Immunoreactive signals were visualized using super signal chemiluminescence substrate detection kit (Pierce Biotechnology, Rockford, USA).

**Measurement of [Ca<sup>2+</sup>]<sub>i</sub>:** The plasma membrane bound calcium sensor has been modified by the addition of a N-terminal signal peptide (20 aa) from Neuromodulin (PI-G-CaMP2). Addition of this peptide results in posttranslational palmitoylation of the protein, which facilitates anchoring of the protein to the plasma membrane. HEK293 cells were transfected on coated glass cover slips with pcDNA31 PI-G-CaMP2, and were mounted in a perfusion chamber 48 hrs after transfection. Cells were perfused with ringer solution at a rate of 8 ml/min at 37°C. Cell fluorescence measurements was measured continuously with an inverted microscope Axiovert S100 (Zeiss) using a x40 objective (Fluar 40x/1.3 Oil, Zeiss) and a high speed polychromator system (VisiChrome, Visitron, Puchheim, Germany). PI-G-CaMP2 was excited at 485 nm and 405 nm. Emission was recorded between 520 and 550 nm using a CCD-camera (CoolSnap HQ, Visitron). Control of experiments, imaging acquisition, and data analysis were done with the software package Meta-Fluor (Universal imaging, New York,

USA). Alternatively cells were loaded with Fura2 and intracellular  $\text{Ca}^{2+}$  concentrations were determined as described earlier (139).

**Flow cytometry and single cell volume measurements:** Cells were washed and re-dissolved in 10 ml isotonic or hypotonic Ringer solution as described for patch clamp experiments. Cells were analyzed at 37 °C / pH 7.4 using a CASY flow cytometer (Roche Diagnostics, Mannheim, Germany). Cells were analyzed at a density of  $10^6$  cells/ml. For single cell volume measurements cells were loaded with 1  $\mu\text{g}$  of calcein-AM (Molecular Probes) and 0.01% pluronic in a standard bath solution (Ringer) for 60 min at 20–22 °C. Fluorescence intensity was measured at an excitation wavelength of 485 nm and an emission wavelength of 520–550 nm. Cell swelling and RVD were observed for 10–15 min after applying hypotonic bath solution.

**Patch Clamping:** Cells were patched on glass cover slips. Lymphocytes were fixed on polylysine-coated coverslips. If not indicated otherwise, patch pipettes were filled with a cytosolic-like solution containing KCl 30, K<sup>-</sup>-gluconate 95,  $\text{NaH}_2\text{PO}_4$  1.2,  $\text{Na}_2\text{HPO}_4$  4.8, EGTA 1, Ca<sup>-</sup>-gluconate 0.758,  $\text{MgCl}_2$  1.03, D - glucose 5, ATP 3, pH 7.2. The  $\text{Ca}^{2+}$  activity was 0.1  $\mu\text{M}$ . Coverslips were mounted in a perfused bath chamber on the stage of an inverted microscope (IM35, Zeiss) and kept at 37 °C. The bath was perfused continuously with Ringer solution at a rate of 8 ml/min. For activation of volume dependent  $\text{Cl}^-$  currents, Ringer bath solution (mM) was first changed to Iso and then to Hypo (c.f. above). Patch clamp experiments were performed in the fast whole cell configuration. Patch pipettes had an input resistance of 2–4  $\text{M}\Omega$  when filled with the cytosolic like (physiological) solution. Currents were corrected for serial resistance. We choose this solution because it enabled swelling/shrinkage behaviour under physiological ion concentrations and allowed for direct comparison of the results from patch clamping and volume measurements. The access conductance was measured continuously and was 60–140 nS. Currents (voltage clamp) and voltages (current clamp) were recorded using a patch clamp amplifier (EPC 7, List Medical Electronics, Darmstadt, Germany), the LIH1600 interface and PULSE software (HEKA, Lambrecht, Germany) as well as Chart software (AD Instruments, Spechbach, Germany). Data were stored continuously on a computer hard disc and analyzed using PULSE software. In regular intervals, membrane voltage ( $V_c$ ) was clamped in steps of 20 mV from -100 to

+100 mV from a holding voltage of -100 mV. Current density was calculated by dividing whole cell currents by cell capacitance.

**Double electrode voltage clamping:** Oocytes were injected with cRNA encoding aquaporin 1 (0.5 ng), Ano6 (5 ng) or both together. Water injected oocytes served as controls. 2 – 4 days after injection, oocytes were impaled with two electrodes (Clark Instruments Ltd, Salisbury, UK), which had a resistances of < 1 MΩ when filled with 2.7 mol/l KCl. Using two bath electrodes and a virtual-ground head stage, the voltage drop across the serial resistance was effectively zero. Membrane currents were measured by voltage clamping (oocyte clamp amplifier, Warner Instruments LLC, Hamden CT) in intervals from -80 to +60 mV, in steps of 20 mV, each 1 s. The bath was continuously perfused at a rate of 5 ml/min. All experiments were conducted at 22 °C.

**Materials and statistical analysis:** All animal experiments were approved by local authorities and were conducted according to the guidelines of the American Physiological Society and the German law for welfare of animals. All compounds used were of highest available grade of purity and were from Sigma or Merck. NS3728 was a generous gift by NeuroSearch (Ballerup, Denmark). Data are reported as mean ± s.e.m. Student's t-test (for paired or unpaired samples as appropriate) or ANOVA were used for statistical analysis. A p-value < 0.05 was accepted as significant difference.

**Ethics statement:** All animal experiments were approved by the local ethics commission of the University of Regensburg and were conducted according to the guidelines of the American Physiological Society and the German law for welfare of animals.

## Results

### ANO6 augments $I_{Cl-swel}$ and volume regulation in HEK293

siRNA-knockdown of ANO6 in HEK293 cells was shown earlier to attenuate  $I_{Cl-swel}$  by about 50 % (96). ANO6 is a ubiquitous protein as comparably high levels of mRNA is found in all cell lines and freshly isolated cells (data not shown). We found that additional expression of exogenous ANO6 is able to augment  $I_{Cl-swel}$  activated by hypotonic bath solutions in HEK293 cells (Hypo; Fig. 1a). Patch pipettes were filled with a buffer solution of

“cytosolic-like” ion composition, which is shown below to be essential for full activation of  $I_{\text{Cl-sw}}_{\text{well}}$ . Hypo activated predominantly  $I_{\text{Cl-sw}}_{\text{well}}$ , as  $\text{K}^+$  channel blockers  $\text{Ba}^{2+}/\text{TEA}^+$  showed little effects on Hypo-activated whole cell currents.  $I_{\text{Cl-sw}}_{\text{well}}$  was inhibited by known blockers of anoctamins, which also inhibit volume activated anion channels (VRAC), such as NPPB, NS3728 or T16<sub>inh</sub>AO1 (Fig. 1a,b) (141-143).

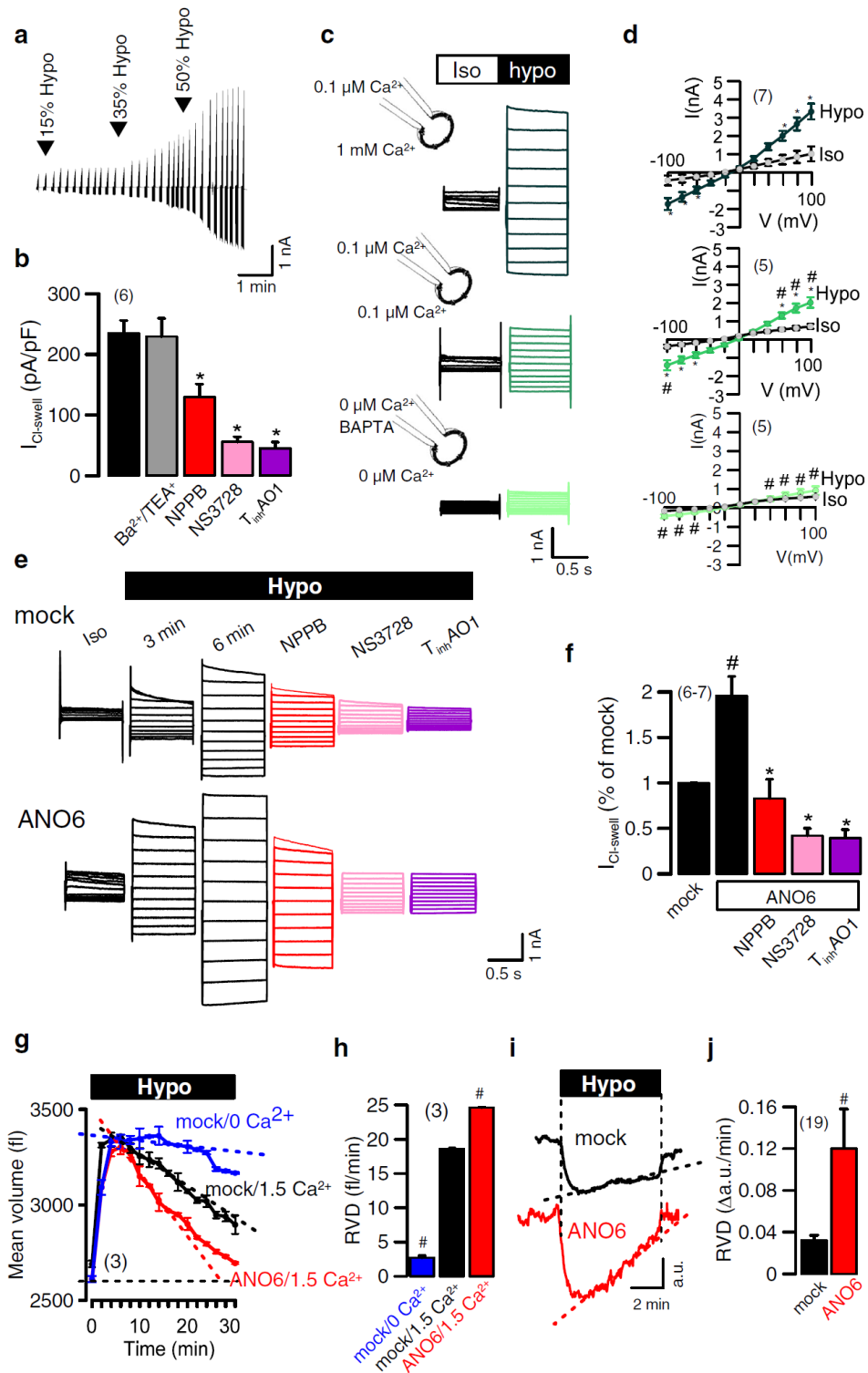


**Fig. 1** Cell swelling activates Anoctamin 6 **(a)** Continuous recording of the whole cell current ( $V_c = \pm 100$  mV in steps of 20 mV) activated in mock transfected HEK293 cells, after exposure to hypotonic bath solution (Hypo; black arrowheads indicate 15, 35 and 50% hypotonicity). **(b)** Summary of Hypo-induced current density in mock transfected HEK293 cells and inhibition by NPPB (50  $\mu$ M), NS3728 (10  $\mu$ M) and T16A<sub>inh</sub>AO1 (10  $\mu$ M). Currents were not inhibited by K<sup>+</sup> channel blockers Ba<sup>2+</sup> (5 mM) and TEA<sup>+</sup> (10  $\mu$ M). **(c)** Inhibition of Hypo-induced whole cell currents by removal of Ca<sup>2+</sup> and additional application of the Ca<sup>2+</sup> chelator BAPTA (50  $\mu$ M). **(d)** Current/voltage (i/v) relationship of the experiments shown in (c). **(e)** Inhibition of Hypo-induced whole cell currents by NPPB (50  $\mu$ M), NS3728 (5  $\mu$ M), or T16A<sub>inh</sub>AO1 (10  $\mu$ M) in mock transfected and ANO6-overexpressing HEK293 cells ( $V_c = \pm 100$  mV in steps of 20 mV). **(f)** Summary of Hypo-induced current densities in mock and ANO6-overexpressing cells and effect of inhibitors. **(g)** Hypo-induced cell swelling and re-shrinkage (RVD) in mock transfected cells in the absence and presence of extracellular Ca<sup>2+</sup>, and in ANO6-expressing cells, as measured by flow cytometry. **(h)** RVD calculated from initial recovery from cell swelling. **(I,j)** RVD in mock transfected and anoctamin-overexpressing cells as assessed by single cell volume measurements using calcein fluorescence. Mean  $\pm$  SEM; \*significant inhibition by NBBP, NS3728, and T<sub>inh</sub>AO1 (paired t-test). #significant difference when compared to high Ca<sup>2+</sup> or mock, respectively (ANOVA). (number of cells or flow cytometry assays).

We found that extra- and intracellular Ca<sup>2+</sup> was required to fully activate  $I_{Cl-swells}$ . Under complete Ca<sup>2+</sup> free conditions, i.e. Ca<sup>2+</sup> free solution and preincubation with the Ca<sup>2+</sup> chelator BAPTA-AM,  $I_{Cl-swells}$  was essentially eliminated (Fig. 1c,d). Overexpression of ANO6 augmented  $I_{Cl-swells}$ .  $I_{Cl-swells}$  did not show time dependent inactivation that has been reported to be characteristic for VRAC (15), but was potently blocked by typical Cl<sup>-</sup> channel blockers (Fig. 1e,f). Volume regulation was measured by flow cytometry and in single cells using calcein fluorescence, and was augmented in ANO6-expressing cells (Fig. 1g-j). Notably, the reduced regulatory decrease (RVD) after hypotonic cell swelling was found to be attenuated in the absence of Ca<sup>2+</sup>. These data indicate that proper volume regulation requires Ca<sup>2+</sup>. Similar to  $I_{Cl-swells}$ , also apoptotic currents induced by staurosporine were augmented by overexpression of ANO6 (data not shown). Additional evidence for the role of ANO6 in volume regulation was detected in *Xenopus* oocytes. Hypotonic swelling can be observed in oocytes overexpressing AQP1, but not in non-injected oocytes (142). A small  $I_{Cl-swells}$  was activated in AQP1-expressing oocytes by hypotonic bath solution that was, however, significantly enhanced in ANO6-coexpressing cells (Supplementary Fig. 1).

## $\text{Ca}^{2+}$ influx and dilution of intracellular $\text{Cl}^-$ during hypotonic swelling is essential for activation of $I_{\text{Cl-sw}}/\text{ANO6}$

We examined whether plasma membrane (PM) localized ANO6 (Supplementary Fig. 2a) is activated by  $\text{Ca}^{2+}$  entering the cell during cell swelling through transient receptor potential (TRP) channels. In the presence of the TRP channel inhibitor SK&F96365 (145) activation of  $I_{\text{Cl-sw}}$  was largely attenuated, and the remaining  $I_{\text{Cl-sw}}$  showed VRAC-typical time dependent inactivation (Fig. 2a,b). ACA, a TRP channel inhibitor and potent blocker of  $\text{PLA}_2$  (146) completely abolished activation of  $I_{\text{Cl-sw}}$ , suggesting a role of  $\text{PLA}_2$  for activation of ANO6. In contrast, the TRPM7 inhibitor NS8593 (10  $\mu\text{M}$ ) or the activator of TRPM7, naltriben (50  $\mu\text{M}$ ) had no inhibitory or activatory effects, respectively (data not shown).

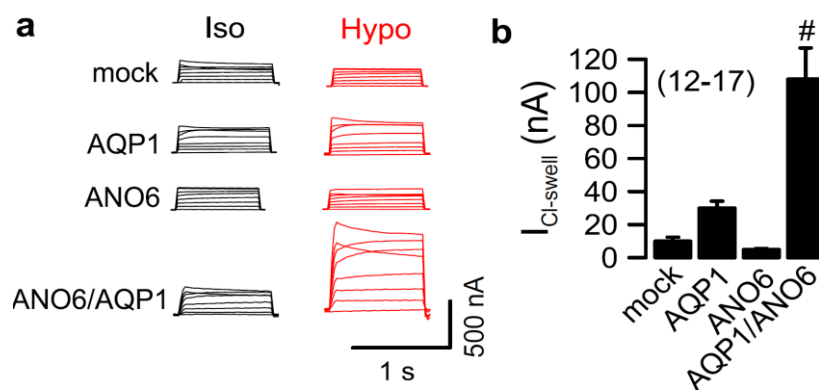


**Fig. S1**  $I_{\text{Cl-sw}}$  in *Xenopus* oocytes expressing ANO6. a) Whole cell currents measured in water injected control oocytes, and oocytes expressing AQP1, ANO6 or coexpressing AQP1/ANO6. Hypotonic bath solution (50% hypotonicity; 101 mosmol/l) activated a small but significant whole cell current only in cells coexpressing AQP1/ANO6. b) Summary of Hypo-induced whole cell currents (at clamp voltage  $V_c = +40$  mV). Mean  $\pm$  SEM. #significantly different when compared to AQP1 (unpaired t-test). (number of oocytes).

Notably,  $I_{\text{Cl-sw}}$  was largely reduced when experiments were performed in the presence of CsCl instead of physiological buffer solutions, and a typical time dependent inactivation was observed (Fig. 2a). Membrane voltages were depolarized in the presence of CsCl, which probably interferes with  $\text{Ca}^{2+}$  influx and activation of ANO6 (147) (data not shown). Thus the contribution of ANO6 to  $I_{\text{Cl-sw}}$  cannot be properly assessed in the presence of CsCl (130).

Perfusion of the cell with high intracellular Cl<sup>-</sup> concentrations in the patch pipette may also interfere with activation of ANO6. We therefore examined whole cell currents in ANO6-expressing cells with either low (5 mM) or high (125 mM) Cl<sup>-</sup> in the patch pipette. In the presence of low cytosolic Cl<sup>-</sup> we observed large whole cell currents under isotonic conditions (no cell swelling), which were strongly reduced when extracellular (bath) Cl<sup>-</sup> was replaced by impermeable gluconate (5Cl<sup>-</sup>) (Fig. 2c,d left panels). Current activation by 5Cl<sup>-</sup> was not blocked by inhibition of TRP channels with SK&F (data not shown). In contrast, whole cell currents were low in the presence of high intracellular Cl<sup>-</sup> (Fig. 2c,d right panels). Similar was observed when  $I_{Cl\text{-}swell}$  was activated in the presence of low or high pipette Cl<sup>-</sup>: Hypo-induced currents were large with low cytosolic Cl<sup>-</sup> but small with high cytosolic Cl<sup>-</sup> (Fig. 2e). We propose that dilution of the cytosolic Cl<sup>-</sup> concentration during hypotonic cell swelling may activate ANO6.

Activation of  $I_{Cl\text{-}swell}$  was largely reduced by the TRP channel inhibitor SK&F, suggesting swelling induced Ca<sup>2+</sup> influx that activates ANO6 (Fig. 2a,b). Apart from TRPM7, which does not seem to contribute to activation of  $I_{Cl\text{-}swell}$ , TRPC1 was found to be expressed in HEK293 cells (Fig. 2f). Using the Ca<sup>2+</sup> sensor Fura2, we detected a variable and transient increase in intracellular Ca<sup>2+</sup> within  $39.9 \pm 1.5$  s after applying Hypo (Fig. 2g,h). Intracellular Ca<sup>2+</sup> was measured near the junctional zone, using the PM-targeted Ca<sup>2+</sup> sensor PI-G-CaMP2 (148) (Supplementary Fig. 2). The delayed and transient Ca<sup>2+</sup> increase caused by hypotonic cell swelling was not inhibited by SK&F96365, but was potently blocked by dantrolene, an inhibitor of ryanodine receptors Fig. 2i). Both Ca<sup>2+</sup> dependent cPLA<sub>2</sub> and Ca<sup>2+</sup> independent iPLA<sub>2</sub> are expressed in HEK293 cells (Supplementary Fig. 2c,d). Nonselective PLA<sub>2</sub>-inhibitors (ACA, aristolochic acid), pyrrophenone (inhibition of cPLA<sub>2</sub>), and BEL (inhibition of iPLA<sub>2</sub>) largely inhibited Ca<sup>2+</sup> increase (Fig. 2 i). In contrast, inhibition of metabolic pathways downstream of PLA<sub>2</sub> (epoxygenase (EG), lipoxygenase (LG), cyclooxygenase (CG)) by an inhibitory cocktail neither blocked Ca<sup>2+</sup> increase nor activation of ANO6, and are therefore not relevant (Fig. 2i, Supplementary Fig. 2e) (149). Thus cell swelling activates iPLA<sub>2</sub> and cPLA<sub>2</sub> and releases Ca<sup>2+</sup> from ryanodine- and IP<sub>3</sub>-sensitive Ca<sup>2+</sup> stores into the junctional zone (Ca<sup>2+</sup> nanodomain) (150-153).

## Cell swelling activates ANO6 primarily through $\text{PLA}_2$ and accumulation of membrane lysophospholipids

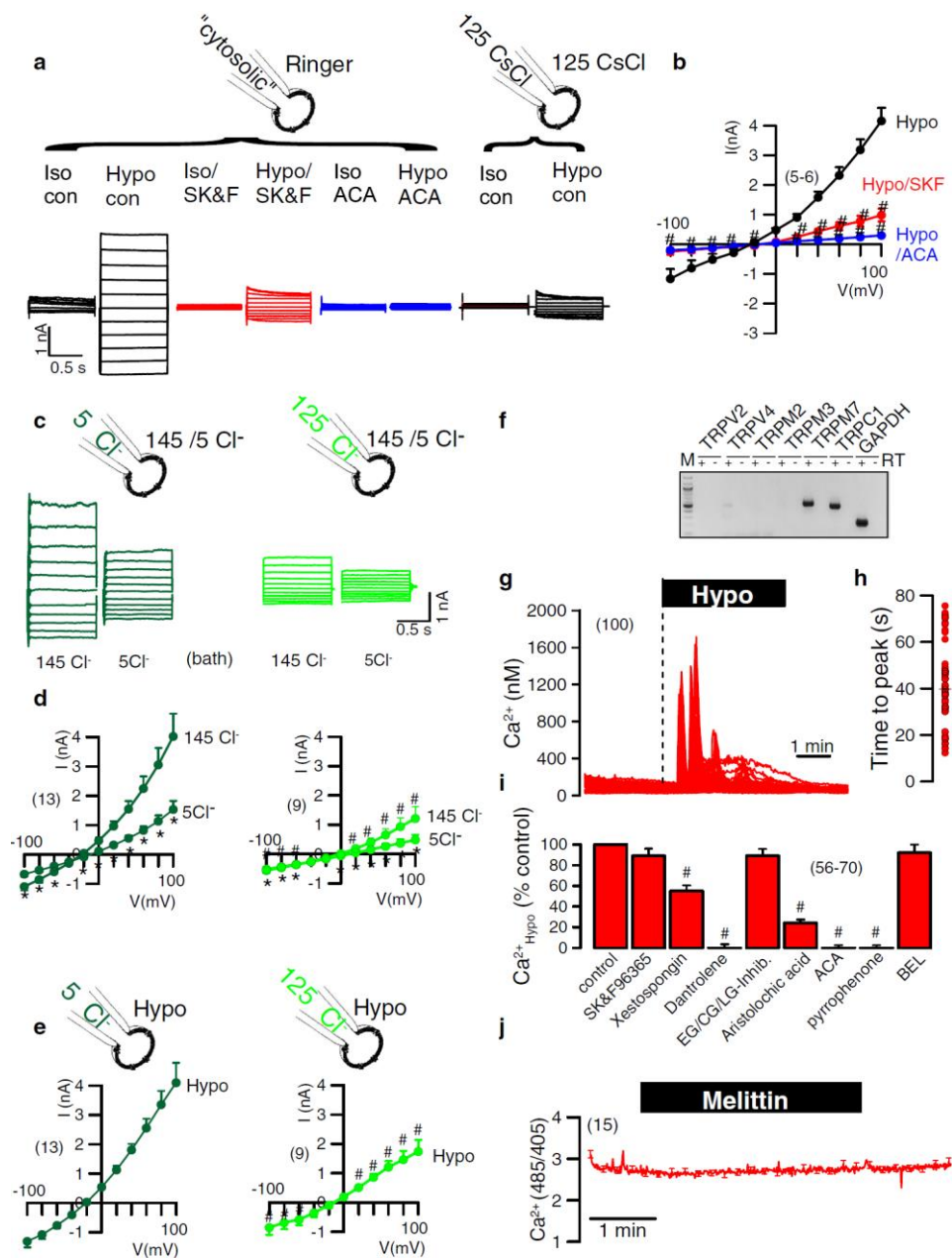


**Fig. 2** ANO6 is activated by hypo-induced  $\text{Ca}^{2+}$  increase. **(a)** Swelling induced (Hypo) whole cell currents in ANO6-overexpressing HEK293 cells, which was inhibited by TRP channel blocker SK&F96365 (20  $\mu\text{M}$ ), the TRP/ $\text{PLA}_2$  blocker ACA (20  $\mu\text{M}$ ), and the presence of CsCl in bath and pipette. **(b)** Corresponding  $i/v$  curves. **(c)** Whole cell currents in ANO6-expressing HEK293 cells with 5 or 125 mmol/l  $\text{Cl}^-$  in the patch pipette. **(d)** Corresponding  $i/v$  curves. **(e)**  $i/v$  curves for Hypo-induced whole cell currents in ANO6-expressing HEK293 cells with 5 or 125 mmol/l  $\text{Cl}^-$  in the patch pipette. **(f)** RT-PCR analysis of volume/mechanosensitive TRP channels in HEK293 cells. RT = reverse transcriptase. **(g)** Delayed  $\text{Ca}^{2+}$  increase induced by hypotonic bath solution as measured in Fura2 loaded

HEK293 cells. **(h)** Time to maximal (peak) Ca<sup>2+</sup> increase upon exposure to hypotonic bath solution measured in 100 individual cells. **(i)** Summary of Ca<sup>2+</sup> increase near ER/plasma membrane junctional zone in HEK293 cells, using plasma membrane localized Ca<sup>2+</sup> sensor PI-G-CaMP2. Effects of TRP channel inhibitor SK&F96365 (20 μM), IP3R inhibitor xestospongine C (10 μM), RyrR inhibitor dantrolene (10 μM), cocktail of inhibitors of epoxygenase (EG; 100 μM), lipoxygenase (LG; 5 μM), and cyclooxygenase (CG; 10 μM), broad PLA<sub>2</sub> inhibitors aristolochic acid (100 μM) and ACA (20 μM), cPLA<sub>2</sub> inhibitor pyrrophenone (50 nM), and iPLA<sub>2</sub> inhibitor BEL (30 μM). **(j)** Continuous recording of intracellular Ca<sup>2+</sup> concentration (detected as 485/405 nm fluorescence ratio) indicating lack of effects of melittin (200 nM) on intracellular Ca<sup>2+</sup>. Mean ± SEM. #significantly different from Hypo, 5Cl<sup>-</sup> in patch pipette or control, respectively (ANOVA). (number of cells).

Melittin, an activator of PLA<sub>2</sub> did not increase intracellular Ca<sup>2+</sup>, but strongly activated ANO6 (Fig. 2j, 3a,b). Activation of ANO6 by melittin was completely suppressed by inhibiting iPLA<sub>2</sub> with BEL, which also largely attenuated RVD (Fig. 3c,d). Direct activation of ANO6 by PLA<sub>2</sub> through melittin did not require Ca<sup>2+</sup> influx through TRP channels, as SK&F96365 did not block activation (Fig. 3e). PLA<sub>2</sub>-activated ANO6 whole cell currents were blocked by the anoctamin inhibitor AO1 (Supplementary Fig. 2f). Notably, membrane currents activated by melittin in inside/out excised membrane patches from ANO6-expressing HEK293 cells were blocked by tannic acid (Supplementary Fig. 2g). The data indicate that ANO6 currents can be activated by PLA<sub>2</sub> without influx of Ca<sup>2+</sup>. In contrast complete removal of Ca<sup>2+</sup> from bath and patch pipette and chelation of Ca<sup>2+</sup> by 100 μM almost completely eliminated the effect of melittin (data not shown). Vice versa, activation of ANO6 by ionomycin was partially blocked by inhibition of PLA<sub>2</sub> with ACA (Fig. 3f).

We speculated that ANO6 is activated by PLA<sub>2</sub> through depletion of fatty acids, such as arachidonic acid (ArA), and generation of membrane lysophospholipids (LPL). The immediate downstream product of LPL, lysophosphatidic acid (LPA), does not appear to be relevant since activation of ANO6 was not compromised in the presence of the Pan-LPA-receptor inhibitor BrP-LPA (data not shown). Accumulation of LPL within the plasma membrane is known to cause membrane tension (154), which could open ANO6. This process should be reversed by simultaneous application of fatty acids like ArA. Strikingly, activation of ANO6 by PLA<sub>2</sub> was much reduced in the presence of ArA (Fig. 3g,h). Moreover, as cell swelling leads to activation of PLA<sub>2</sub> and generation of LPL, thereby activating ANO6, *I<sub>Cl-swelling</sub>*



were filled with “cytosoliclike” buffer solution. Activation of patch currents by 100 nM melittin and inhibition by the anoctamin inhibitor tannic acid (TA; 10  $\mu\text{M}$ ). Mean  $\pm$  SEM. \* significant current increase by melittin and inhibition by TA (paired t-test). #significantly different from AO1 (unpaired t-test). Bath: NaCl 145,  $\text{KH}_2\text{PO}_4$  0.4,  $\text{K}_2\text{HPO}_4$  1.6, D - glucose 5,  $\text{MgCl}_2$  1, Ca-gluconate 1.3, pH 7.4. Patch pipette: KCl 30, K-gluconate 95,  $\text{NaH}_2\text{PO}_4$  1.2,  $\text{Na}_2\text{HPO}_4$  4.8, EGTA 1, Ca-gluconate 0.758,  $\text{MgCl}_2$  1.03, D -glucose 5, ATP 3 (all mM),  $[\text{Ca}^{2+}]_i$  10<sup>-7</sup> M, pH 7.2.

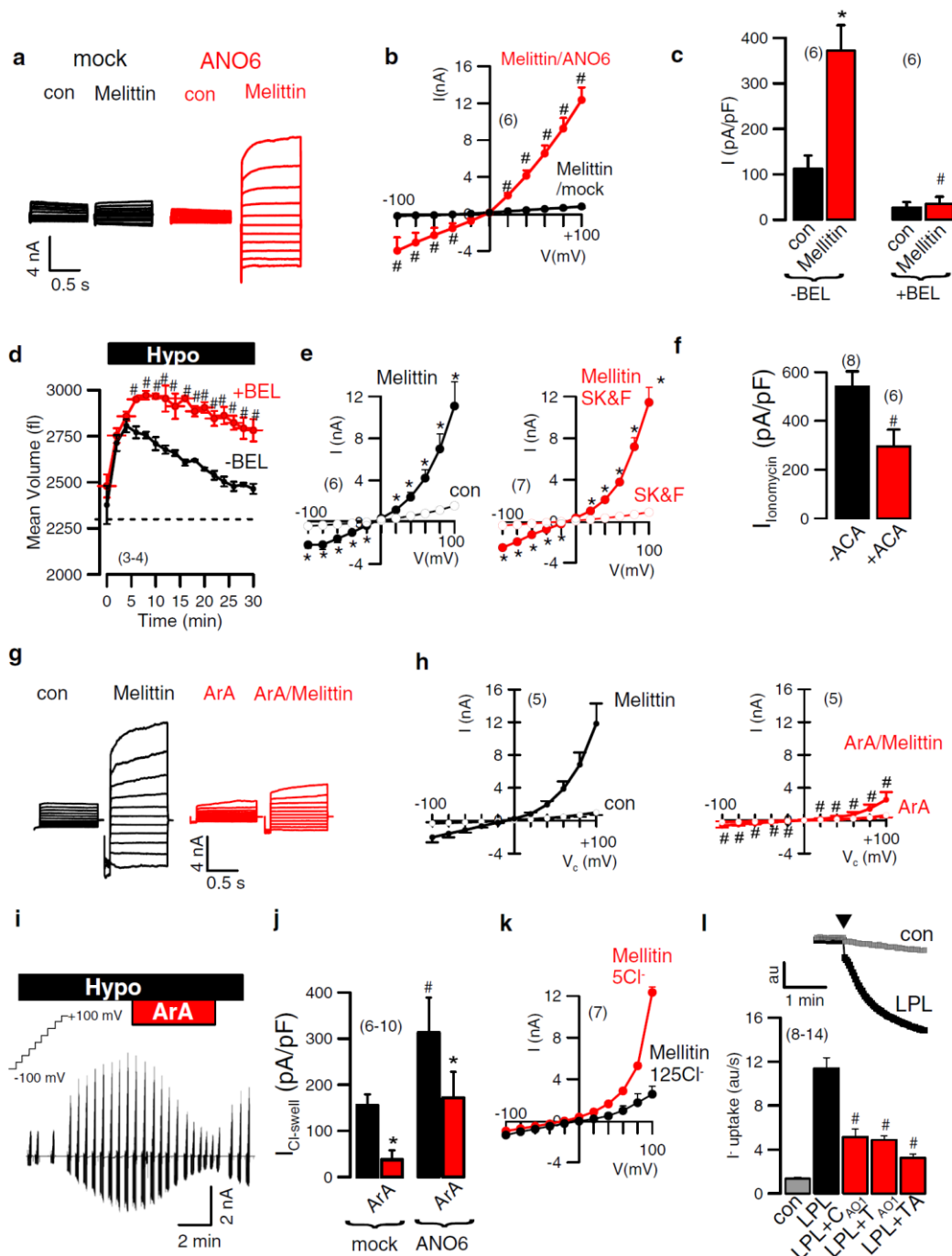


**Fig. 3** Cell swelling activates ANO6 through PLA<sub>2</sub>-generated lysophospholipids. **(a,b)** Activation of whole cell currents by PLA<sub>2</sub>-activator melittin (200 nM) in ANO6-expressing but not mock transfected cells, and corresponding i/v curves. **(c)** Summary of whole cell

currents activated by melittin and inhibition by the iPLA<sub>2</sub>-inhibitor BEL (30 μM). **(d)** Volume regulation measured in ANO6-expressing HEK293 cells in the absence or presence of BEL. **(e)** I/V relationship of whole cell currents activated by melittin (200 nM) in the absence or presence of SK&F (20 μM). **(f)** Summary of ionomycin (1 μM) activated whole cell currents in ANO6-overexpressing HEK293 cells and inhibition by the PLA<sub>2</sub>-inhibitor ACA (20 μM). **(g)** Activation of whole cell currents in ANO6-overexpressing HEK293 cells by PLA<sub>2</sub>-activator melittin and inhibition by arachidonic acid (ArA; 50 μM). **(h)** Corresponding i/v curves. **(i)** Continuous recording of Hypo-induced whole cell currents and reversible inhibition of activated currents by ArA. **(j)** Summary of Hypo-induced current densities in mock transfected and ANO6 overexpressing HEK293 cells, and inhibition by ArA. **(k)** Activation of whole cell currents by melittin in the presence of low (5 mM) pipette Cl<sup>-</sup>, which was largely reduced in the presence of high (125 mM) pipette Cl<sup>-</sup>. **(l)** Activation of I<sup>-</sup> influx in YFP fluorescence quenching assays indicating activation of an anion conductance by LPL (20 μM). The effect of LPL was suppressed by CaCC<sub>inh</sub>AO1 (10 μM), T16A<sub>inh</sub>AO1 (10 μM), and tannic acid (10 μM). Mean ± SEM; \*significant activation by melittin and inhibition by ArA, respectively (paired t-test). #significantly different from mock and absence of inhibitors BEL and ACA, respectively (ANOVA). (number of cells).

### **ANO6 controls I<sub>Cl-swell</sub> and RVD in normal B lymphocytes but not in lymphocytes from a patient with Scott disease**

We examined activation of ANO6 by PLA<sub>2</sub> in B-lymphocytes from a patient with Scott disease. Scott disease is a rare inherited bleeding disorder, which is caused by a defect in ANO6 function (70;84). Cell swelling (Hypo) activated whole cell currents in normal (wt) lymphocytes, which were inhibited by the Cl<sup>-</sup> channel blocker NPPB (Fig. 4a,b). Like in ANO6-overexpressing HEK293 cells, activation of I<sub>Cl-swell</sub> and volume regulation (RVD) was inhibited at low (10<sup>-7</sup> mol/l) extracellular Ca<sup>2+</sup> (Fig. 4b,c). Scott lymphocytes do not express ANO6 and demonstrated reduced I<sub>Cl-swell</sub> and defective volume regulation (Fig. 4d-f). Activation of currents was not affected by BrP-LPA, but was abolished by ACA (Fig. 4g). Lymphocytes show a PLA<sub>2</sub> expression pattern similar to that identified in HEK293 cells (Fig. 4h,j). Remarkably, only normal (wt) but not Scott lymphocytes activated whole cell currents during activation of PLA<sub>2</sub> by melittin (Fig. 4j-l). Moreover, Ca<sup>2+</sup>-dependent activation ANO6 by ionomycin was also strongly attenuated by ACA (Fig. 4m). These results clearly show that also endogenous ANO6 expressed in B-lymphocytes is controlled by PLA<sub>2</sub>, which is activated during cell swelling.

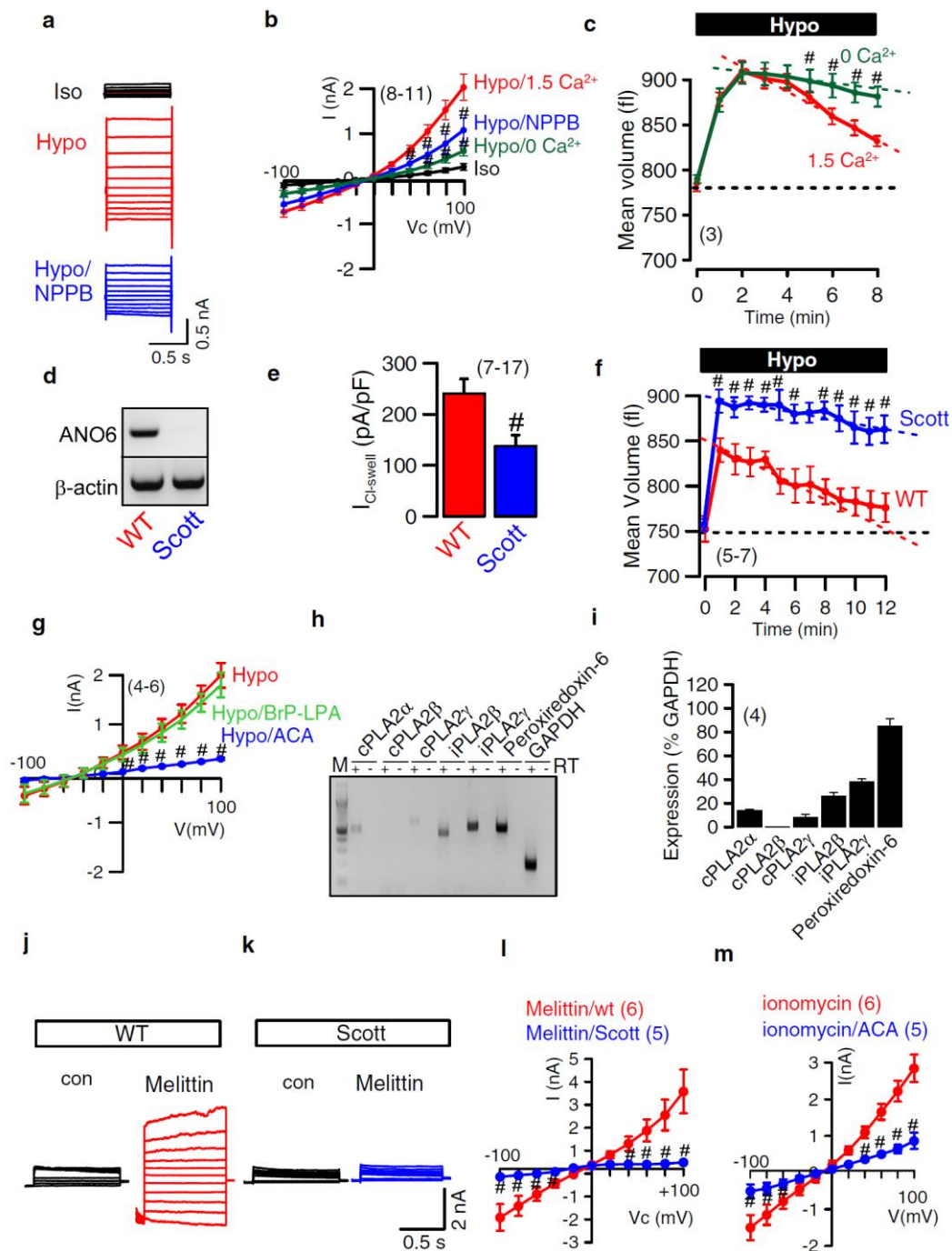


**Fig. 4** ANO6 is necessary for  $I_{Cl\text{-}swell}$  and RVD in human lymphocytes. **(a)** Hypo (50%) induced whole currents in human normal (wt) lymphocytes and inhibition by NPPB (50  $\mu$ M). **(b)** Corresponding  $i/v$  curves, also showing the inhibitory effect of Ca<sup>2+</sup> removal from the bath solution. **(c)** Hypo-induced cell swelling and re-shrinkage (RVD) of normal lymphocytes as measured by flow cytometry in the absence or presence (1.5 mM) extracellular Ca<sup>2+</sup>. **(d)** Western blot indicating expression of endogenous AnO6 in normal (wt) but not in Scott lymphocytes. **(e)** Hypo-induced whole cell currents in wt and Scott lymphocytes. **(f)** Hypo-induced cell swelling and RVD in normal and Scott lymphocytes. Mean  $\pm$  SEM; # significant difference when compared to Hypo, wt, and 0 Ca<sup>2+</sup>, respectively (ANOVA). (number of cells or flow cytometry assays). **(g)** Hypo induced whole currents in wt lymphocytes were inhibited

by ACA (20  $\mu$ M), but not by the Pan-LPA inhibitor BrP-LPA (5  $\mu$ M). (h,i) RT-PCR analysis of PLA<sub>2</sub> isoforms in human B-lymphocytes. RT = reverse transcriptase. (j,l) Activation of endogenous ANO6 in wt lymphocytes, but not in Scott lymphocytes lacking expression of ANO6. (m) Inhibition of Ca<sup>2+</sup> activated whole cell currents by ACA in wt lymphocytes. Mean  $\pm$  SEM; # significant difference when compared to Hypo or wt, respectively (ANOVA). (number of cells).

### Intestinal epithelial cells from *Ano6*<sup>-/-</sup> mice show reduced whole cell currents and defective volume regulation

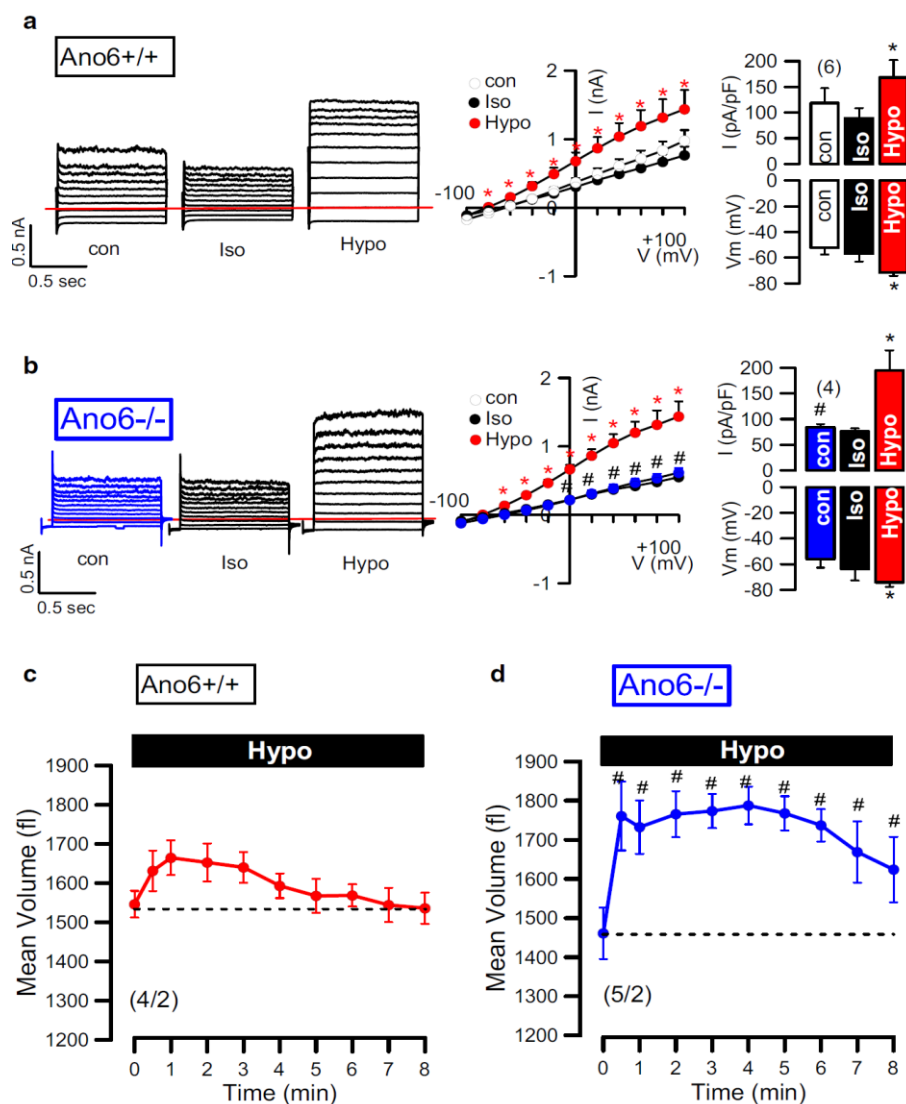


**Fig. 5** ANO6 controls cell volume in freshly isolated intestinal epithelial cells. (a) Whole cell currents in isolated intestinal epithelial cells from *Ano6*<sup>+/+</sup> mice before and after hypotonic (35 %) cell swelling. Corresponding i/v relationships, current densities, and membrane voltages indicating activation of K<sup>+</sup> currents by Hypo. (b) Whole cell currents in isolated intestinal epithelial cells from *Ano6*<sup>-/-</sup> mice before and after hypotonic (33 %) cell swelling.

Corresponding *i/v* relationships, current densities, and membrane voltages. Whole cell currents are reduced under control conditions, suggesting absence of Ano6 currents which are normally active under control conditions. (c) Volume regulation (RVD) in intestinal epithelial cells from *Ano6*<sup>+/+</sup> and *Ano6*<sup>-/-</sup> animals, indicating rapid recovery from hypotonic cell swelling in *Ano6*<sup>+/+</sup> but not *Ano6*<sup>-/-</sup> cells. Enhanced increase in the cell volume and largely delayed recovery from hypotonic cell swelling in *Ano6*<sup>-/-</sup> cells. Mean ± SEM; #significant difference when compared to *Ano6*<sup>+/+</sup> (unpaired t-test). (number of cells or flow cytometry assays).

We isolated small intestinal (jejunal) epithelial cells from *Ano6*<sup>+/+</sup> and *Ano6*<sup>-/-</sup> mice. In these cells hypotonic bath solution activated predominantly K<sup>+</sup> currents in both *Ano6*<sup>+/+</sup> and *Ano6*<sup>-/-</sup> cells, as indicated by hyperpolarization of the membrane voltage (Fig. 5a,b). Swelling activated K<sup>+</sup> currents in intestinal cells have been observed earlier (155). Although swelling activated K<sup>+</sup> currents were identical in *Ano6*<sup>+/+</sup> and *Ano6*<sup>-/-</sup> cells, baseline currents under control conditions were reduced in *Ano6*<sup>-/-</sup> cells, suggesting a missing Cl<sup>-</sup> current in *Ano6*<sup>-/-</sup> cells. Noteworthy, volume activated Cl<sup>-</sup> currents were found to be partially active under isotonic conditions (15).

Moreover, we reported earlier that ANO6 is partially active under control conditions (50). Despite relatively small current changes in *Ano6*<sup>-/-</sup> cells, volume regulation was strongly attenuated in cells from *Ano6* knockout animals: Hypotonic cell swelling was largely enhanced and RVD was strongly delayed in *Ano6*<sup>-/-</sup> cells (Fig. 5c,d). We therefore conclude that ANO6 is a volume regulated anion channel that participates in cellular volume regulation. ANO6 is activated through cell swelling induced Ca<sup>2+</sup> influx, activation of PLA<sub>2</sub> and a drop in Cl<sup>-</sup> concentration within the junctional zone (Fig. 6). We propose that activation of ANO6 occurs by accumulation of membrane lysophospholipids generating tension within the plasma membrane bilayer (154), thereby opening the channel pore possibly by improving accessibility for Ca<sup>2+</sup> ions (138). Alternatively, exposure of phospholipids like phosphatidylserine (PS) by the phospholipid scrambling property of ANO6 may lead to a conformational change allowing Cl<sup>-</sup> transport by ANO6 or may lead to exocytosis of submembraneous channel pools (Fig. 6).

## Discussion

### Activation of ANO6 by $\text{Ca}^{2+}$

The present data demonstrate that volume dependent activation of ANO6 requires  $\text{Ca}^{2+}$ , a result that corresponds well to earlier findings (86). We found that inhibition of  $\text{Ca}^{2+}$  influx through TRP channels activated by cell swelling strongly attenuated  $I_{\text{Cl}^- \text{swell}}$  and left behind a much smaller time dependent whole cell current (Fig. 2a). Although there is an ongoing dispute regarding the role of  $\text{Ca}^{2+}$  for volume regulated anion channels, the role of TRP channels and intracellular  $\text{Ca}^{2+}$  for cellular volume regulation received better acceptance (reviewed in (132;156;157)). Agreement exists concerning a local permissive (threshold)  $\text{Ca}^{2+}$  concentration of around 50 nM that is required to activate  $\text{Cl}^-$  channels during cell swelling (reviewed in (15;156)).  $\text{Ca}^{2+}$  influx through TRP channels appears essential to activate ANO6 during cell swelling. The data suggest  $\text{Ca}^{2+}$  induced  $\text{Ca}^{2+}$  release from dantrolene and  $\text{IP}_3$ -sensitive stores caused by cell swelling.  $\text{Ca}^{2+}$  signaling may happen in a narrow compartmentalized space called the junctional zone (153). The concept that  $\text{Ca}^{2+}$  modulates VRAC in functional nanodomains, via colocalized store-operated  $\text{Ca}^{2+}$  influx channels has been proposed earlier (152;158;159).

### Activation of ANO6 by $\text{PLA}_2$

$\text{Ca}^{2+}$ -induced  $\text{Ca}^{2+}$  release was observed during cell swelling. It was paralleled by  $\text{Ca}^{2+}$  release from  $\text{IP}_3$ -sensitive  $\text{Ca}^{2+}$  stores, probably through autocrine release of ATP and purinergic receptor signaling (96). However, ANO6 can be activated by  $\text{PLA}_2$  without any increase in intracellular  $\text{Ca}^{2+}$  and  $\text{iPLA}_2$  appears to be most important in this regard (Fig. 3). It is unlikely that  $\text{PLA}_2$  and lysophospholipids (LPL) act via opening of TRP channels and  $\text{Ca}^{2+}$  influx, since i) activation of  $\text{PLA}_2$  by melittin, which activates ANO6, does not trigger any  $\text{Ca}^{2+}$  signals, and ii) activation of ANO6 by  $\text{PLA}_2$  was not suppressed by a TRP channel inhibitors (Fig. 3e). Notably, regulation of VRAC and RVD by cell swelling-activated  $\text{PLA}_2$  is well recognized (132;160).

Strong activation of ANO6 through  $\text{PLA}_2$  depolarized the membrane voltage suggesting activation of cation currents, as reported earlier (50;51;71;83;13). Our earlier work suggested a loss of selectivity for ANO6 currents at very large intracellular  $\text{Ca}^{2+}$  concentrations and with

ongoing stimulation (50;139) which was also supported by another report (85). Notwithstanding, the current activated by PLA<sub>2</sub> should be through ANO6 because i) melittin activated a current only in ANO6 expressing cells, ii) ACA inhibited swelling activated ANO6 currents, ACA inhibited melittin activated currents and ACA inhibited Ca<sup>2+</sup> activated ANO6 currents. iii) melittin activated currents are inhibited by the ANO-inhibitors CaCC<sub>inh</sub>AO1 and tannic acid, iv) melittin activated currents in ANO6-expressing wt lymphocytes, but not in Scott lymphocytes, v) melittin did not activate currents in the presence of high intracellular Cl<sup>-</sup> concentration which inhibits ANO6. vi) Currents activated by ionomycin and PLA<sub>2</sub> are not additive

PLA<sub>2</sub>-dependent release of Ca<sup>2+</sup> from internal Ca<sup>2+</sup> stores was also observed in the present study. Lambert, Hoffmann and coworkers have analyzed in detail activation and cellular redistribution of PLA<sub>2</sub> during hypotonic cell swelling (161-163). iPLA<sub>2</sub> and particularly cytosolic cPLA<sub>2</sub> may participate in Ca<sup>2+</sup> store release and activation of ANO6 (162). Notably, iPLA<sub>2</sub> are characterized as being Ca<sup>2+</sup> independent *in vitro*, but in fact were found to be regulated by Ca<sup>2+</sup> when studied *in vivo* (164).

### **ANO6, an osmosensor?**

We observed large Cl<sup>-</sup> currents in ANO6-expressing cells, when the cytosolic Cl<sup>-</sup> concentration was low (Fig. 2c-e). These currents did not require activation by Ca<sup>2+</sup> or hypotonic cell swelling. In contrast, high cytosolic Cl<sup>-</sup> inhibited both baseline and swelling-activated Cl<sup>-</sup> currents. This has also been observed earlier for Ca<sup>2+</sup> dependent activation of ANO6 by the Ca<sup>2+</sup> ionophore ionomycin (50). We therefore propose that ANO6 is regulated by the intracellular Cl<sup>-</sup> concentration and may therefore operate as a kind of osmosensor. The concept of regulation of I<sub>Cl-swelling</sub> by intracellular osmotic strength has been observed earlier (165;166). Osmosensing by TRP channels (167) is unlikely to explain the present findings, as Cl<sup>-</sup> regulation of ANO6 currents is also observed in the presence of TRP channel inhibitors (data not shown). We were unable to identify a chloride binding site as described for e.g. Na<sup>+</sup>/Cl<sup>-</sup> dependent transporters (168). It will be interesting to determine whether chloride sensitive WNK (with no lysine [K]) kinase is controlling ANO6 activity. In fact a role of WNK3 on intracellular chloride concentration and volume regulation in HEK293 cells has been suggested earlier (169).

## ANO6 and VRAC

The present data suggest that  $I_{\text{Cl-swelling}}$  produced by ANO6, and the “classical” VRAC are functionally related. In fact there is no discernible difference between  $I_{\text{Cl-swelling}}$  described here and VRAC, except of the pronounced difference in time dependence. In our experiments VRAC-typical time-dependent inactivation was preferentially observed when  $\text{Ca}^{2+}$ -access was limited, either by removal of extracellular  $\text{Ca}^{2+}$ , inhibition of  $\text{Ca}^{2+}$  influx by TRP channel blockers, or strong depolarization of the membrane voltage. The present study does not address the contribution of LRRC8A, the essential component of VRAC identified recently (134;135).

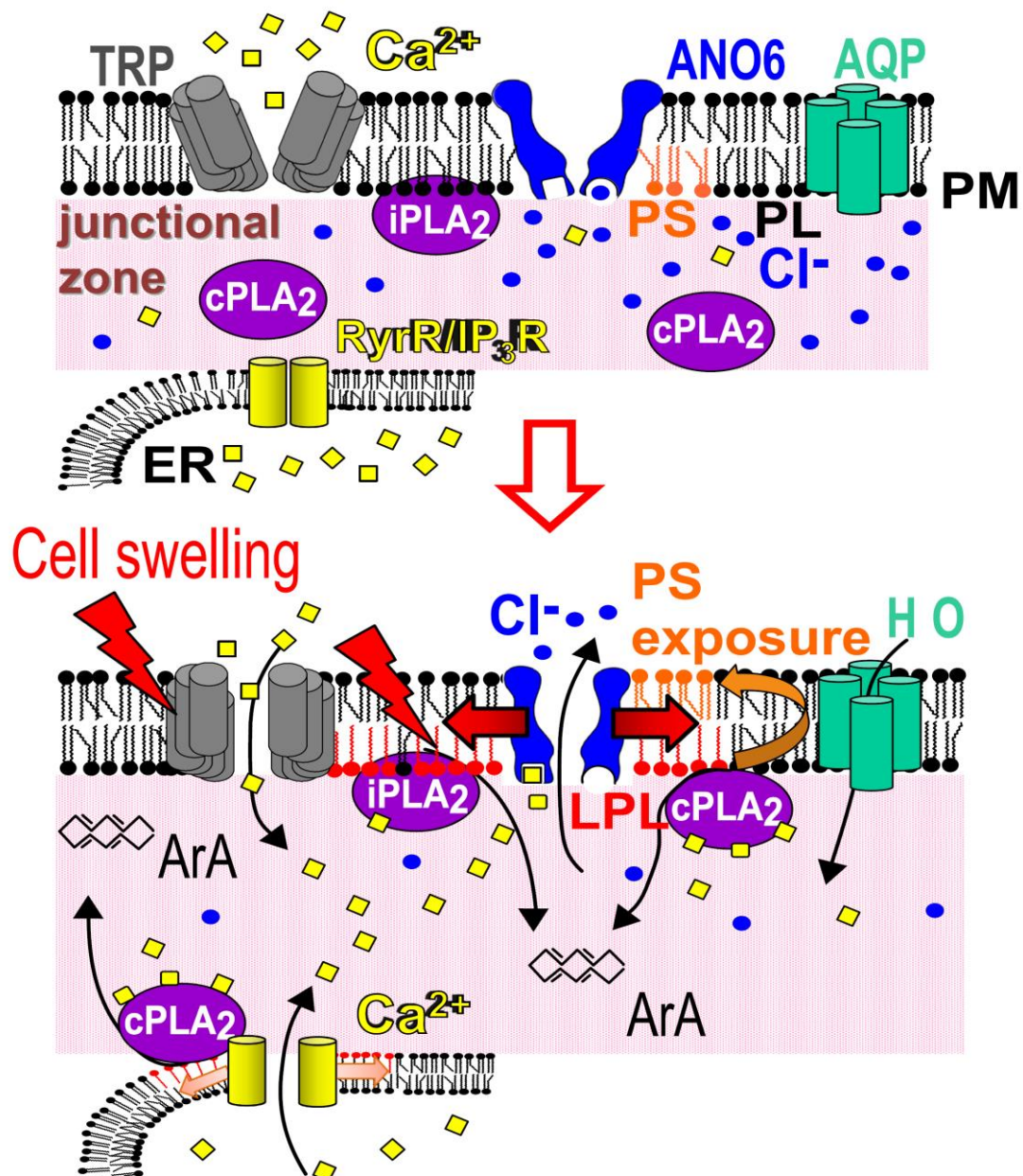


**Fig. 6** Activation of ANO6 by Hypotonic Cell Swelling. Possible mechanisms of hypotonic activation of ANO6. During cell swelling water enters the cell through AQP water channels and reduces osmolarity and Cl<sup>-</sup> concentration within the junctional zone, thereby releasing ANO6 from Cl<sup>-</sup> inhibition. Cell swelling activates mechanosensitive TRP channels such as TRPC1 through Ca<sup>2+</sup> insensitive, stretch activated iPLA<sub>2</sub>, which releases fatty acids, like arachidonic acid (ArA), from plasma membrane phospholipids (PL). Accumulation of lysophospholipids (LPL) causes membrane tension and, together with local increase of Ca<sup>2+</sup> in the junctional zone, activates ANO6. Increase in intracellular Ca<sup>2+</sup> further recruits Ca<sup>2+</sup> dependent cytosolic cPLA<sub>2</sub> to ER membranes and induces a transient ER store release of Ca<sup>2+</sup>. Exposure of phosphatidylserine (PS) by the phospholipid scrambling property of ANO6 may lead to a conformational change allowing Cl<sup>-</sup> transport by ANO6 or may lead to exocytosis of submembraneous channel pools.

The present data identify ANO6 as a cell swelling activated anion channel and uncover a new mechanism of activation through membrane depletion of unsaturated sn-2 fatty acids and accumulation of lysophospholipids. The recently provided structure of TMEM16 from the fungus *Nectria haematococca* suggests poor accessibility of Ca<sup>2+</sup> to the Ca<sup>2+</sup>-binding site (138). Membrane tension induced by accumulation of lysophospholipids could induce a conformational change and thereby improve accessibility for Ca<sup>2+</sup> ions.

The *Ano6* null animals show a largely reduced survival rate. About 70% die before or briefly after birth, due to internal bleedings and massive malformations or asphyxia, respectively. Interestingly, the 30% survivals show expression of a splice variant of ANO6. We generated this splice variant *in vitro*, which produced normal Ca<sup>2+</sup> activated whole cell currents when expressed in HEK293 cells (data not shown). The surviving animals demonstrate bone mineralization defects (82), enhanced bleeding time (170) and macrophage defects (139). Thus ANO6 is protein essential for survival and proper organ function

### Acknowledgments

Supported by DFG SFB699-A7/A12, DFG KU756/12-1, Sander-Stiftung 2013.031.1 and Volkswagenstiftung AZ 87 499. We thank Dr. Johan Heemskerk and Dr. Eduard Bevers for supplying the lymphocyte cell lines. The excellent technical assistance by Mss. B. Wild, P. Seeberger, E. Tartler, Inês Cabrita and Mr. Simon Höllerer is gratefully acknowledged.

## Chapter 4

### Anoctamin 6 mediates Effects essential for Innate Immunity downstream of P2X<sub>7</sub>-Receptors in Macrophages

#### Abstract

Purinergetic P2X<sub>7</sub> receptors (P2X<sub>7</sub>R) are fundamental to innate immune response. In macrophages transient stimulation of P2X<sub>7</sub>R activates several transport mechanisms and induces scrambling of phospholipids with subsequent membrane blebbing and apoptosis. These processes support phagocytosis and subsequent killing of phagocytosed bacteria. Here we demonstrate that stimulation of P2X<sub>7</sub> receptors activates anoctamin 6 (ANO6, TMEM16F), a protein that functions as Ca<sup>2+</sup> dependent phospholipid scramblase and Ca<sup>2+</sup> activated Cl<sup>-</sup> channel. Inhibition or knockdown of ANO6 attenuates ATP-induced cell shrinkage, cell migration and phospholipid scrambling. In mouse macrophages Ano6 produces large ion currents by stimulation of P2X<sub>7</sub> receptors and contributes to ATP-induced membrane blebbing and apoptosis, which is largely reduced in macrophages from *Ano6*<sup>-/-</sup> mice. ANO6 supports bacterial phagocytosis and killing by mouse and human THP-1 macrophages. Our data demonstrate that anoctamin 6 is an essential component of the immune defense by macrophages.

**Key words:** Macrophage, ion channel, purinergetic signaling, Ca<sup>2+</sup> activated Cl<sup>-</sup> currents, Ano6, Anoctamin 6, TMEM16F, apoptosis, phagocytosis, phospholipid scrambling, bacterial killing, P2X<sub>7</sub> receptor, P2X<sub>7</sub> pore, blebbing, apoptosis

**Published in:** Jiraporn Ousingsawat, Podchanart Wanitchakool, Arthur Kmit, Ana Romao, Walailak Jantarajit, Rainer Schreiber, and Karl Kunzelmann. Anoctamin 6 mediates Effects essential for Innate Immunity downstream of P2X<sub>7</sub>-Receptors in Macrophages. Nat Commun. 2015 Feb 5;6:6245.

**Own experimental contribution:** Most western blot, COIP, Migration, Flow cytometry experiment performed in cell lines and animals.

**Own written contribution:** Methods, Results, Parts of Introduction and Discussion.

**Other contributions:** Designed experiments and analyzed data.

## Introduction

P2X<sub>7</sub> receptors (P2X<sub>7</sub>R) are ligand gated non-selective cation channels that are activated by high concentrations of extracellular nucleotides, which may be released during inflammation, tissue injury and T-cell activation (171;172). P2X<sub>7</sub>R has a unique large C-terminus, which may couple to multiple intracellular signaling pathways (173;174). Activation of P2X<sub>7</sub>R not only leads to an instantaneous inward cationic current, but also to formation of a non-selective pore, permeable to molecules up to 900 Da, which eventually leads to cell lysis (175;176). In fact distinct pores for P2X<sub>7</sub>R-activated uptake of cationic and anionic fluorescent dyes have been proposed (177;178), while a contribution of the hemichannel pannexin 1 is discussed controversially (173;179-183). It remains currently unclear whether the concept of pore dilation of P2X<sub>7</sub>R (183) is sufficient to explain the large conductance associated with P2X<sub>7</sub>R, and to what extent other ion channels may contribute.

ANO6 (anoctamin 6, TMEM16F) is a Ca<sup>2+</sup> dependent phospholipid scramblase (70;85;137) and a putative Ca<sup>2+</sup> activated Cl<sup>-</sup> and nonselective cation channel (50;83;85;130) that is activated during apoptotic cell death (86;87;185). ANO6 facilitates apoptotic cell shrinkage and is a component of the ubiquitous outwardly rectifying Cl<sup>-</sup> channel that has been identified in many cell types (86;87). This scramblase/channel is activated by high intracellular Ca<sup>2+</sup> concentrations, as they occur during activation of P2X<sub>7</sub> (70;185;186). We therefore asked whether stimulation of P2X<sub>7</sub>R activates ANO6, and whether both Ca<sup>2+</sup> and the large C-terminus of P2X<sub>7</sub> contribute to activation of ANO6.

P2X<sub>7</sub> receptors show highest expression in macrophages, where they are important for innate immunity during infectious diseases (187;188), while ANO6 was found to be expressed in spleen, osteoclasts and immune cells (70;82;84;87), suggesting overlapping expression. A cascade of cellular events is triggered through stimulation of P2X<sub>7</sub>R, with initial activation of nonselective cation currents and a subsequent pore conductance. This is followed by sequential cell shrinkage/swelling, phospholipid scrambling, membrane blebbing and finally cell death (172;189-191). The aim of the present study was therefore, to examine whether ANO6 and P2X<sub>7</sub>R are coexpressed in macrophages and whether ANO6 mediates some of the cellular effects downstream of P2X<sub>7</sub>R. These questions were tackled by analyzing

activation of ANO6 through stimulation of P2X<sub>7</sub>R in overexpressing *Xenopus* oocytes and HEK293 cells, and in human and mouse macrophages from *wild type* and *Ano6* knockout mice.

## Materials and Methods

**Anoctamin 6 knockout mice, cell culture and cDNA:** Generation of *Anoctamin 6* (*TMEM16F*) knockout mice (C57Bl6, 6-12 weeks, male or female) has been described earlier (80). These mice were kindly provided by Prof. Dr. A. Vortkamp (Department of Developmental Biology, University of Essen, Germany). Procedures were performed in compliance with the guidelines for the welfare of experimental animals issued by the Federal Government of Germany, and were approved by the local board. Human embryonic kidney (HEK293; ATCC) cells were grown in Dulbecco's modified Eagle's medium supplemented with 10% FBS. Cells were incubated in 5 % CO<sub>2</sub> at 37 °C. The vectors pcDNA3.1-hP2X<sub>7</sub>, the oocyte expression vectors pNKS4-hP2X<sub>7</sub>-C-terminal truncated (436aa), pNKS4-hP2X<sub>7</sub> and pNKS4-hP2X<sub>7</sub>-His tagged were kindly provided by Prof Schmalzing and Michaela Stoll (Inst. für Pharmakologie & Toxikologie, Universitätsklinikum der RWTH Aachen, Germany). The vectors pcDNA3.1-hP2X<sub>7</sub>/E496A, pNKS4-hP2X<sub>7</sub>/E496A-His were produced by PCR-based site-directed mutagenesis. pcDNA3.1-hP2X<sub>7</sub>-C-terminal truncated and pcDNA3.1-cmyc /hP2X<sub>7</sub> were generated by subcloning using PCR techniques. Human ANO6 cDNA was amplified from total RNA of 16HBE cells by RT-PCR, as recently described (Schreiber et al, JBC 2011). All sequences were verified by sequencing. Expression of human ANO6 was suppressed by two to three sets of siRNA. Duplexes of 25 nucleotides of Stealth RNAi™ siRNA were designed and synthesized by Invitrogen (Supplementary Table 2). Plasmids or siRNA were transfected into HEK293 cells using standard methods (Lipofectamine, Invitrogen). Cells were examined 48 or 72 h after transfection.

**Patch clamp:** Cells grown on cover slips were mounted in a perfused bath on the stage of an inverted microscope (IM35, Zeiss) and kept at 37° C. The bath was perfused continuously with Ringer solution (mM: NaCl 145, KH<sub>2</sub>PO<sub>4</sub> 0.4, K<sub>2</sub>HPO<sub>4</sub> 1.6, D-glucose 6, MgCl<sub>2</sub> 1, Ca-gluconate 1.3, pH 7.4) at about 10 ml/min. Patch-clamp experiments were performed in the

fast whole-cell configuration. Patch pipettes had an input resistance of 3-4 M $\Omega$ , when filled with an intracellular like solution containing (mM) KCl 30, K-gluconate 95, NaH<sub>2</sub>PO<sub>4</sub> 1.2, Na<sub>2</sub>HPO<sub>4</sub> 4.8, EGTA 1, Ca-gluconate 0.758, MgCl<sub>2</sub> 1.034, D-glucose 5, ATP 3. pH was 7.2, the Ca<sup>2+</sup> activity was 0.1  $\mu$ M. The access conductance was measured continuously and was 90-140 nS (EPC 9 amplifier, List Medical Electronics, Darmstadt, Germany). In regular intervals, membrane voltages ( $V_c$ ) were clamped in steps of 20 mV from -100 to +100 mV and the membrane conductance  $G_m$  was calculated from the measured current ( $I$ ) and  $V_c$  values according to Ohm's law.

**Two electrode voltage clamp:** Oocytes were harvested from *Xenopus laevis* according to German regulations governing animal experiments. Oocytes were defolliculated for 1 h at 18°C with 1.5 mg/ml collagenase type V (Sigma) in OR2 solution (in mmol/l): 82.5 NaCl, 2 KCl, 1 MgCl<sub>2</sub>, and 5 HEPES pH 7.55. Oocytes were injected with 10 ng (47 nl double-distilled water) of cRNA encoding P2X7, P2X7-E496 or P2X7-C-terminal truncated. cRNA was transcribed *in vitro* after linearization, using the appropriate promoter and RNA-polymerase (T3, T7, or SP6). Oocytes were maintained in ND97 solution (in mmol/l): 96 NaCl, 2 KCl, 1.8 CaCl<sub>2</sub>, 1 MgCl<sub>2</sub>, 5 HEPES, 2.5 Na-pyruvate, 0.5 theophylline, and 0.01 mg/ml gentamycin, pH 7.55 at 18°C. 2-4 days after injection, membrane currents were measured by impaling two electrodes (Harvard Apparatus, UK) filled with 3 mol/l KCl, which had a resistance of less than 1 M $\Omega$ . The bath was continuously perfused at a rate of 5 ml/min with ND96 solution (in mmol/l): 96 NaCl, 2 KCl, 1.8 CaCl<sub>2</sub>, 1 MgCl<sub>2</sub>, 5 HEPES and 2.5 Na-pyruvate, pH 7.55. The voltage drop across the serial resistance was optimized to zero using two bath electrodes and a virtual ground head stage. Oocytes were continuously voltage clamped between -60 and +40 mV (oocyte clamp amplifier, Warner Instruments, USA) in steps of 10 mV, each 1 s. All experiments were conducted at room temperature.

**Reverse Transcriptase PCR and Real time PCR:** Total RNA was isolated from human B-lymphocytes, macrophages or from *Xenopus laevis* oocytes using RNeasy Mini-Kit (Qiagen; Hilden, Germany). 2  $\mu$ g of total RNA was reverse-transcribed in 50  $\mu$ l for 1 h at 40 °C using random primer and reverse transcriptase (RT). 30 cycles of RT-PCR was performed using standard procedures (GoTaq DNA Polymerase, Promega), 1  $\mu$ l RT and primers for P2X7 and anoctamins (0.5  $\mu$ M, Supplementary Table 1). For semi-quantitative comparison GAPDH was

amplified. Products were analyzed on ethidium bromide-stained 2% agarose gels. The real time PCR was performed in 10  $\mu$ l of mixture (5  $\mu$ l of 2x SYBR Green I master mix, 0.5  $\mu$ M of each forward and reverse primer (LightCycler<sup>®</sup>, Roche, Germany) (Supplementary Table 1). The cycle threshold value was accessed by LightCycler<sup>®</sup> 480 Software. The cycle threshold values of the human ANO6 and  $\beta$ -actin mRNAs were calculated from the equations and standard curves. Samples were analyzed in triplicate of each and human ANO6 levels were normalized to the corresponding  $\beta$ -actin.

**Western blotting and Immunocytochemistry:** Protein was isolated from transfected HEK293 cells using lysis buffer (50 mM Tris, 150 mM NaCl, 1 mM EDTA, 1% NP-40, 100 mM DTT and 1% proteinase inhibitor cocktail) and protein concentration was measured by Bradford. Samples were run on SDS-PAGE gel and transferred to polyvinylidene difluoride membrane (GE Healthcare Europe GmbH, Germany) using wet transfer (BioRad, Germany). Membranes were incubated with 1:1000 anti-GFP rabbit antibody (# A11122; Invitrogen, Germany), 1:500 rabbit anti-ANO6 antibody (ARP44761; Aviva System Bio, USA), 1:500 rabbit anti-P2X7 antibody (APR-008; Alomone Labs, Israel) and 1:500 mouse anti- $\beta$ -actin antibody (sc-47778; Santa Cruz, Germany) overnight at 4°C. Proteins were visualized using anti-rabbit horseradish peroxidase (HRP)-conjugated antibody (Acris, Germany) or anti-mouse horseradish peroxidase (HRP)-conjugated antibody (Santa Cruz, Germany) and chemiluminescent substrate (Pierce, Thermo Scientific). For detection of expression of anoctamin 6 and P2X<sub>7</sub>, macrophages were collected as described below. After isolation of protein and separation on SDS-PAGE, proteins were detected using 1:500 rabbit anti-ANO6 (ARP44761; Aviva System Bio, USA) and 1:500 rabbit anti-P2X7 antibody (APR-008; Alomone Labs, Israel). For immunocytochemistry, transfected HEK293 cells were grown on glass cover slips and fixed for 10 min with 4% (w/v) paraformaldehyde at room temperature. Cells were incubated for 5 min with 0.1% SDS in PBS. After washing, cells were permeabilized and blocked with 2% (w/v, PBS) bovine serum albumin and 0.04% (v/v, PBS) Triton X-100 and incubated for 1 h with primary anti-P2X7 rabbit antibody (1:500) at 37 °C. Binding of the primary antibody was visualized by incubation with a secondary antibody conjugated with Alexa 568. Green GFP fluorescence was used to indicate ANO6-GFP expression. Nuclei were stained with Hoe33342 (0.1  $\mu$ g/ml PBS, Aplichem, Darmstadt,

Germany). Cells were mounted on glass slides with fluorescent mounting medium (DAKO Cytomation, Hamburg, Germany) and examined with an ApoTome Axiovert 200 M fluorescence microscope (Zeiss, Göttingen, Germany).

**Annexin V binding and dye uptake assays:** HEK293 cells grown on glass cover slips were treated with ATP with or without tannic acid (TA; 10  $\mu$ M). After 5 min, cells were incubated with annexin V-FITC (BD Pharmingen™, Germany) for 15 min at 20 °C. Cells were subsequently analyzed using ApoTome Axiovert 200M fluorescence microscope (Zeiss, Germany) and SlideBook Digital Microscopy Software (Coronado, USA). Membrane permeabilization observed during apoptosis was assayed using the positively charged carbocyanine nucleic acid dye YO-Pro-1 (Life Technologies). Cells grown and transfected in 96 well plates were washed and resuspended in ringer solution. YO-Pro-1 was added at the final concentration of 1  $\mu$ M. Cells were incubated with 3 mM ATP with and without the P2X<sub>7</sub>-inhibitors AZ11645373 (25 nM) and 5-(N, N-hexamethylene)amiloride (40  $\mu$ M), or the anoctamin Cl<sup>-</sup> channel inhibitors NPPB (100  $\mu$ M NPPB), niflumic acid (10  $\mu$ M) or AO1 (20  $\mu$ M). YO-Pro-1 fluorescence (excitation 480 nm/ emission 520 nm) was measured every minute for 3 hrs at 37<sup>0</sup> C using the plate reader NOVOstar (BMG LABTECH, Germany). HEK293 cells grown in 96-well plates were treated with 3 mM ATP for 6 h at 37 °C in the presence and absence of tannic acid. Luminogenic caspase-3/7 substrate (Promega, Germany) was added into each well and mixed at room temperature. The luminescence was measured using the plate reader NOVOstar (BMG LABTECH, Germany). Apoptosis in primary peritoneal macrophages was assessed by NucView™ 488 Caspase-3 assay kit (Biotum, Germany). Briefly, macrophages were incubated with DEVD-NucView488 substrate and apoptotic cells were analyzed using the plate reader NOVOstar before and after treatment with 3 mM ATP. Photos were taken by an Axiovert 200M fluorescence microscope with ApoTome (Zeiss, Germany).

**Intracellular Ca<sup>2+</sup> concentrations and cell volume changes:** HEK293 cells were seeded on glass cover slips and loaded with 2  $\mu$ M Fura-2/AM and 0.02 % Pluronic F-127 (Life technologies, Germany) in ringer solution (mmol/l: NaCl 145; KH<sub>2</sub>PO<sub>4</sub> 0,4; K<sub>2</sub>HPO<sub>4</sub> 1,6; Glucose 5; MgCl<sub>2</sub> 1; Ca<sup>2+</sup>-Gluconat 1,3) for 1h at room temperature. Fluorescence was detected in cells perfused with Ringer's solution at 37 °C using an inverted microscope

(Axiovert S100, Zeiss, Germany) and a high speed polychromator system (VisiChrome, Germany). Fura-2 was excited at 340/380 nm, and emission was recorded between 470 and 550 nm using a CoolSnap camera (CoolSnap HQ, Visitron). For volume measurements macrophages were cultured on glass covers for 2 days and loaded with 1  $\mu$ M calcein-AM (Life technologies, Germany) and 0.01 % Pluronic F-127 (Life technologies, Germany) in ringer solution for 1h at room temperature. Calcein was excited at 490 nm, and the emission was recorded between 520 and 550 nm. Control of experiment, imaging acquisition, and data analysis were done with the software package Meta-Fluor (Universal imaging, USA) and Origin (OriginLab Corporation, USA).

**Isolation and culture of primary peritoneal macrophages:** Mice were anaesthetized by CO<sub>2</sub> and sacrificed via cervical delocation. Intraperitoneal lavage was performed by delivering 10 ml of cold PBS into the abdomen with a 19-gage needle. The cells were collected with a 24-gage needle, plated in 12 well plates (500  $\mu$ l/well) and incubated at 37°C. After 1h the nonadherent cells were removed by washing 5 times with PBS. The adherent cells were cultured in RPMI media supplemented with 10% FBS, 1% PS and Glutamine 200 nM in 5% CO<sub>2</sub> at 37°C (Life technologies, Germany).

**Phagocytosis Assay:** Macrophages were seeded on 18 mm glass coverslips. After 5 min incubation with 3 mM ATP, cells were incubated with the inhibitors tannic acid (TA; 10  $\mu$ M) or AZ11645373 (50 nM) in RPMI media for 5 hours. To measure phagocytosis macrophages were incubated with 0.4 mg pHrodo *E. coli* bioparticles conjugate (Life technologies, Germany) in 1 ml ringer solution for 1h at 37°C. After washing cellular fluorescence was measured using an ApoTome Axiovert 200M fluorescence microscope and the software AxioVision (Zeiss, Germany). To calibrate the fluorescence intensity to pH, cells were incubated in MES buffer at pH 7.5 and 4 in the presence of 5  $\mu$ M nigericin.

***E. coli* viability assay:** Macrophages were infected with *E. coli* XL1 Blue MRF' (Agilent Technologies) for 1 h at 37 °C. After 5 min incubation with 3 mM ATP, cells were incubated with the inhibitors tannic acid (10  $\mu$ M) or AZ11645373 (50 nM) in ringer solution for 0, 3 and 6 hr. After washing, cells were lysed in LB media with 0.4% saponin at 37°C for 2 hr. Number of viable *E. coli* was accessed by determination of CFU on tetracycline containing agar plates.

**Boyden chamber assay:** Migration of macrophages was measured using the Cell Biolabs CytoSelect™ 96-well Cell Migration Assay Kit (Cell Biolabs, USA). In brief, macrophages were seeded on polycarbonate membrane with 5 µm pore size for 1 h. Medium of the upper chamber was replaced by serum free RPMI medium containing tannic acid (10 µM), AZ11645373 (50 nM), 100 µM NPPB, 10 µM niflumic acid or 20 µM AO1. To the lower chamber RPMI with MCP-1 (10 nM) as chemoattractant was added. After 4 h incubation at 37 °C migrated macrophages were lysed and incubated with CyQuant® GR dye solution at 20 °C for 20 min. Fluorescence (excitation 480 nm/ emission 520 nm) was measured using the plate reader NOVOstar (BMG LABTECH, Germany).

**Materials and statistical analysis:** All animal experiments were approved by local authorities and were conducted according to the guidelines of the American Physiological Society and the German law for welfare of animals. All compounds used were of highest available grade of purity and were from Sigma or Merck. All cell culture reagents were from Invitrogen. Experiments were repeated 4 – 30 times, exact numbers are reported in the figures. Data are reported as mean ± SEM. Student's t-test (for paired or unpaired samples as appropriate), Fisher's exact tests and ANOVA were used for statistical analysis. P<0.05 was accepted as significant difference.

## Results

### P2X<sub>7</sub>R activates a large conductance in *Xenopus* oocytes

Pore formation by stimulation of P2X<sub>7</sub>R expressed in *Xenopus* oocytes has been proposed earlier (192). We expressed hP2X<sub>7</sub>R in *Xenopus* oocytes and observed very large delayed activated currents upon continuous stimulation by 1 mM ATP (Fig. 1a,b). These pore currents were not observed in water injected oocytes, and were not due to activation of endogenous Ca<sup>2+</sup> activated Cl<sup>-</sup> currents (xANO), since whole cell currents activated by the Ca<sup>2+</sup> ionophore ionomycin were negligible when compared to P2X<sub>7</sub>R pore currents (Fig. 1c, Supplementary Fig. 1a). Activation of large currents was inhibited by blockers of P2X<sub>7</sub>R, such as HMA (5-(N,N-hexamethylene)-amiloride) and AZ11645373 (Supplementary Fig. 1b). *Xenopus* oocytes express endogenous xAno6, as demonstrated by RT-PCR (Fig. 1d). Because

a substantial portion of delayed P2X<sub>7</sub>R-activated currents was inhibited by blockers of An<sub>o</sub>6, like niflumic acid (NFA), NPPB (5-nitro-2-(3-phenylpropylamino) benzoic acid), and tannic acid (TA) (193), a contribution of xAn<sub>o</sub>6 to the large current was suggested (Fig. 1f). Notably, NFA blocked activation of a large pore current in *Xenopus* oocytes also in a previous study (194). The inhibitors had no significant effects on immediate P2X<sub>7</sub>R currents activated within 1 s of ATP-application but blocked delayed (after 3 min) currents, suggesting inhibition of xAn<sub>o</sub>6 but not a direct inhibition of P2X<sub>7</sub>R by these blockers (Fig. 1e,f). Moreover, we injected sense or antisense-DNA for xAn<sub>o</sub>6 into oocytes three days before injecting cRNA for P2X<sub>7</sub>R, and 6 days before performing the DEVC experiments. We found that the whole cell current activated by ATP was significantly reduced by about 45% in oocytes injected with antisense-DNA (n = 28), when compared with oocytes injected with sense-DNA (n = 30) (Supplementary Fig. 1c).

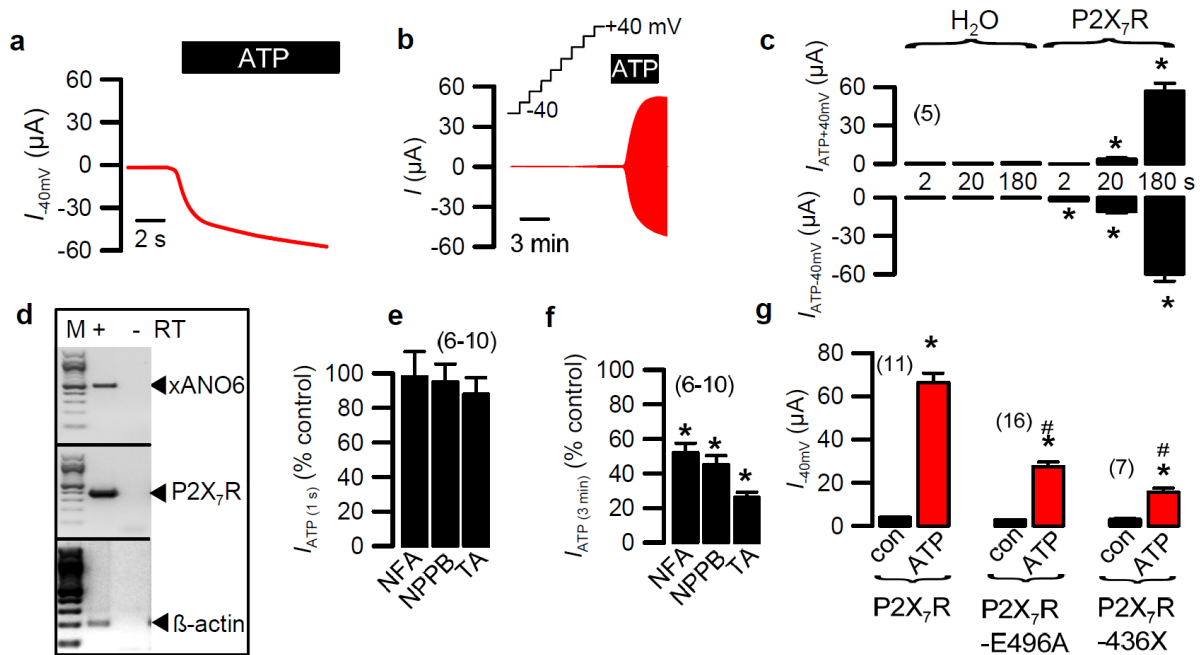


**Fig. 1 Stimulation of P2X<sub>7</sub>R activates a pore current in *Xenopus* oocytes that is inhibited by inhibitors of An<sub>o</sub>6.** **a)** Whole cell currents (holding voltage = -40 mV) activated by 1 mM ATP in a *Xenopus* oocyte expressing P2X<sub>7</sub>R. **b)** Continuous recording of whole cell currents (clamp voltage +/- 40 mV in steps of 10 mV) activated by ATP in a P2X<sub>7</sub>R-expressing oocyte. **c)** Summary of whole cell currents in water injected control or P2X<sub>7</sub>R- expressing oocytes measured 2 s, 20 s, and 180 s, respectively, after application of ATP. **d)** RT-PCR

analysis of endogenous *xAno6*, overexpressed P2X<sub>7</sub>R, and  $\beta$ -actin. M = marker, +/- reverse transcriptase (RT). **e,f**) Inhibition of whole cell currents (%) by niflumic acid (NFA; 10  $\mu$ M), 5-nitro-2-(3-phenylpropylamino) benzoic acid (NPPB; 100  $\mu$ M), and tannic acid (TA; 20  $\mu$ M), when measured 1 s (**e**) or 3 min (**f**) after application of ATP. **g**) Summary of whole cell currents before and after stimulation with ATP of oocytes expressing P2X<sub>7</sub>R (wt), P2X<sub>7</sub>R-E496A, and P2X<sub>7</sub>R-436X, respectively. All experiments were measured using double electrode voltage clamp techniques. Mean  $\pm$  SEM, n = number of cells. #significant difference to P2X<sub>7</sub>R ( $p < 0.05$ ; ANOVA). \*significant activation by ATP or inhibition by channel blockers ( $p < 0.05$ ; paired t-test).

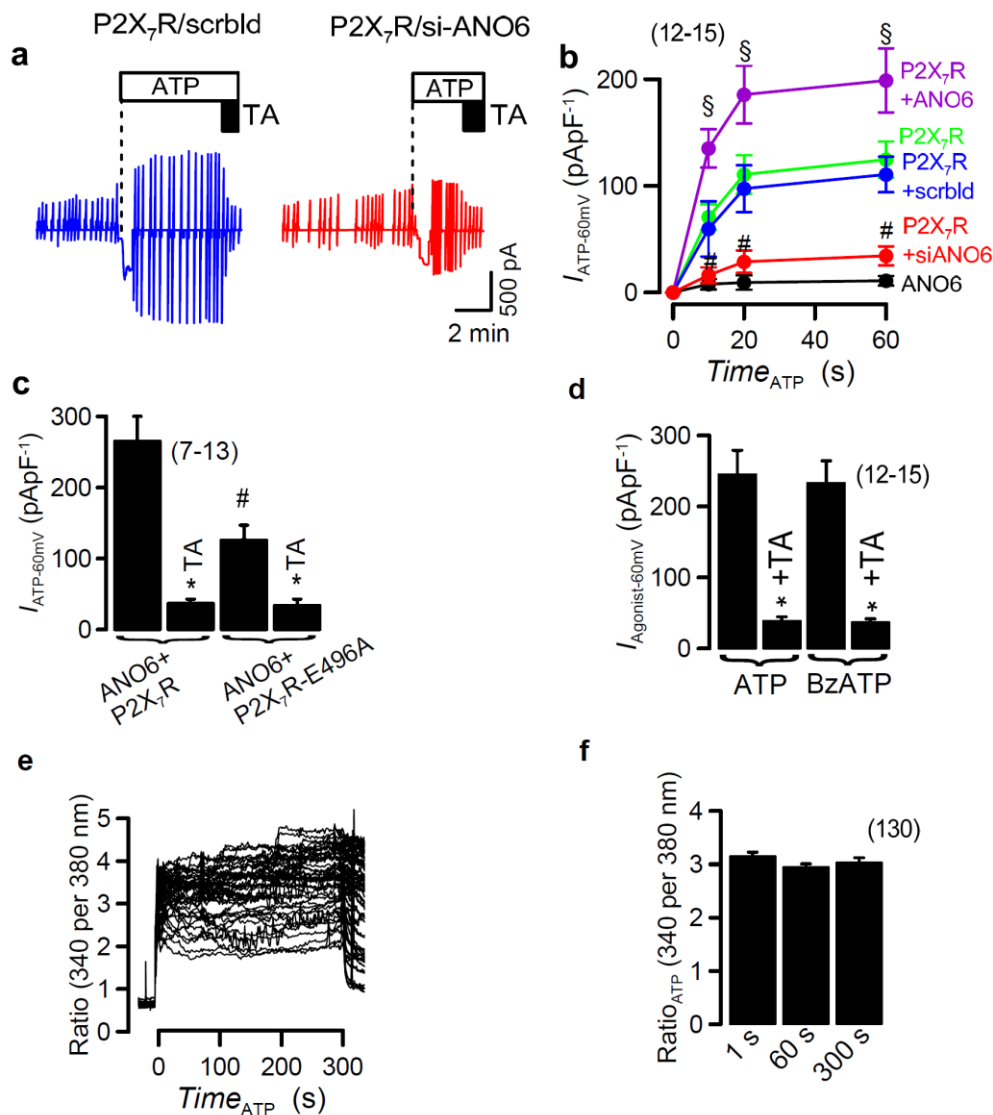


**Fig. 2 ANO6 is activated through stimulation of P2X<sub>7</sub> receptors.** **a**) Whole cell currents activated by 3 mM ATP in HEK293 cells expressing P2X<sub>7</sub>R. Cells were treated with

scrambled RNA (scrbl; left) or siRNA-ANO6 (si-ANO6; right). Cells were continuously voltage clamped between  $\pm 100$  mV; ATP was applied at a holding voltage of -60 mV. Tannic acid (TA, 20  $\mu$ M) was applied at the end of the recording to indicate activation of  $\text{Cl}^-$  currents. **b)** Time dependent activation of whole cell currents by ATP in HEK293 cells expressing P2X<sub>7</sub>R, ANO6, or both, and treated with scrbl RNA or siRNA-ANO6. **d)** Summary of whole cell currents activated by ATP (3 mM) or BzATP (100  $\mu$ M), and inhibition of the activated current by TA (20  $\mu$ M). **e)** Original recordings demonstrating strong increase in free intracellular  $\text{Ca}^{2+}$  concentrations (Fura-2; 340/380 nm) by ATP (3 mM) in cells coexpressing ANO6/P2X<sub>7</sub>R. **f)** Summary of Fura2 340/380 nm ratios indicating continuous high levels of cytosolic  $[\text{Ca}^{2+}]$  during 30 min stimulation with ATP. Current data were obtained in fast whole cell patch clamp experiments. Mean  $\pm$  SEM, n = number of cells. #§significant difference from P2X<sub>7</sub>R (p < 0.05; ANOVA). \*significant inhibition by TA (p < 0.05; paired t-test).

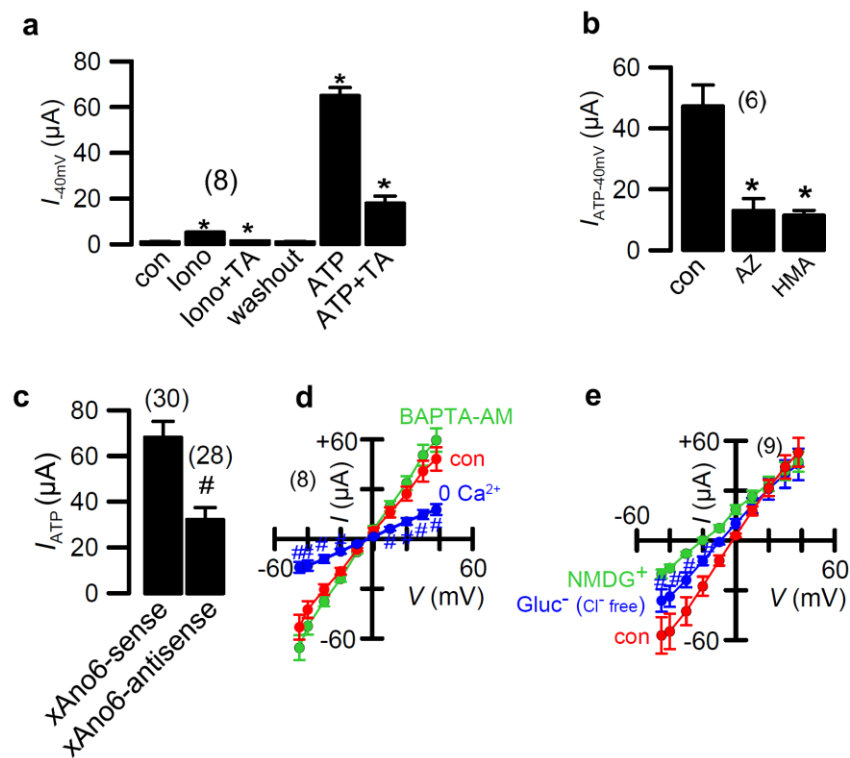


**Fig. S1** Activation of pore currents by stimulation of P2X<sub>7</sub> receptors in *Xenopus oocytes*. (a) Summary of the activation of largenpore currents by ATP (1 mM) but not by ionomycin (5  $\mu$ M) in oocytes expressing P2X<sub>7</sub>R, and inhibition by 20  $\mu$ M TA. (b) Summary of ATP-activated whole cell currents and inhibition by AZ (100 nM) and HMA (40  $\mu$ M). \*significant activation and inhibition, respectively (paired t-tests). (c) Summary of ATP-activated whole cell currents in oocytes injected with sense-DNA or with antisense-DNA for endogenous *Xenopus* xAno6. (d) I/V curves of whole cell currents activated in the presence of BAPTA and  $\text{Ca}^{2+}$ -free extracellular bath solution (0  $\text{Ca}^{2+}$  added +1 mmol/l EGTA), respectively. Efficient chelation of intracellular  $\text{Ca}^{2+}$  by BAPTA-AM was verified by a lack of activation of xANO with 10  $\mu$ mol/l ATP in P2Y<sub>2</sub>-expressing oocytes (not shown). (e) I/V curves of whole cell currents activated in the presence of ND96 control Ringer(con), extracellular  $\text{Na}^+$ -free (NMDG) or extracellular  $\text{Cl}^-$ -free (Gluconate) solution, respectively. Mean $\pm$  SEM; n=

number of cells. #significantly different from control or sense-DNA, respectively (unpaired t-test).

Activation of currents was largely reduced but not completely inhibited by removal of extracellular  $\text{Ca}^{2+}$ , suggesting  $\text{Ca}^{2+}$  dependent and  $\text{Ca}^{2+}$  independent components of the large whole cell conductance(178) (Supplementary Fig. 1d). In contrast chelation of intracellular  $\text{Ca}^{2+}$  by preincubation of the oocytes with 1,2-Bis(2-amino-5-methylphenoxy)ethane-N,N,N',N'-tetraacetic acid tetrakis (acetoxymethyl) ester (BAPTA-AM; 0.1-1 mM) had no effects on activation of currents (Supplementary Fig. 1d). The current was also attenuated by mutating (hP2X<sub>7</sub>R-E496A) or truncating (hP2X<sub>7</sub>R-436X) the C-terminus of P2X<sub>7</sub>R, suggesting requirement of both  $\text{Ca}^{2+}$  influx and the C-terminus of P2X<sub>7</sub>R for activation of the large currents (Fig. 1g). Notably, removal of extracellular  $\text{Cl}^-$  inhibited the inward current rather than the outward current, a phenomenon that was observed earlier for P2X<sub>7</sub>R expressed in HEK293 cells (195). However, replacement of extracellular  $\text{Na}^+$  by NMDG<sup>+</sup> only partially inhibited ATP-activated whole cell currents, suggesting a permeability for large cations like NMDG<sup>+</sup>, as observed earlier (192) (Supplementary Fig. 1e).

### **P2X<sub>7</sub> receptors and $\text{Ca}^{2+}$ activate ANO6 currents**

When expressed in HEK293 cells, ANO6 localized to the cell membrane and produced a whole cell current at high intracellular  $\text{Ca}^{2+}$  concentrations, or when stimulated with the  $\text{Ca}^{2+}$  ionophore ionomycin (Supplementary Fig. 2a-c). Some currents were also activated in mock transfected cells probably due to activation of endogenous ANO6 (Supplementary Fig. 2b) (50). ANO6 whole cell currents remained outwardly rectifying in an extracellular  $\text{Na}^+$ -free bath solution, but changed from outwardly rectifying to more linear currents when  $\text{Na}^+$  was present in the bath solution, suggesting delayed activation of nonselective ANO6 currents (Supplementary Fig. 2d) (85). ANO6 currents were partially inhibited by  $\text{Cl}^-$  removal and were blocked by NFA, DIDS (4,4-diidothiocyano-2,2-stilbenedisulphonate), NPPB, and TA (Supplementary Fig. 2e). The current exhibited an Eisenman type 1 anion selectivity sequence (Supplementary Fig. 2f) (85).

In HEK293 cells overexpressing P2X<sub>7</sub>R, high extracellular ATP (3 mM) activated an immediate inward current that was followed by a somewhat delayed more linear current(182) (Fig. 2a). No currents were activated in the absence of P2X<sub>7</sub>R (Fig. 2b). Linear currents were

significantly reduced by knockdown of ANO6, using two different siRNAs (Fig. 2a,b, Supplementary Fig. 3a). ANO6-knockdown was also verified by real-time RT-PCR, which indicated a knockdown by  $76.4 \pm 3.7\%$  (siRNA1; n = 3) and  $66.5 \pm 1.7\%$  (siRNA2; n = 3). The immediate P2X<sub>7</sub>R inward current was not affected by siRNA-ANO6, suggesting that the observed whole cell current is the sum of P2X<sub>7</sub> and ANO6 currents (Fig. 2a).

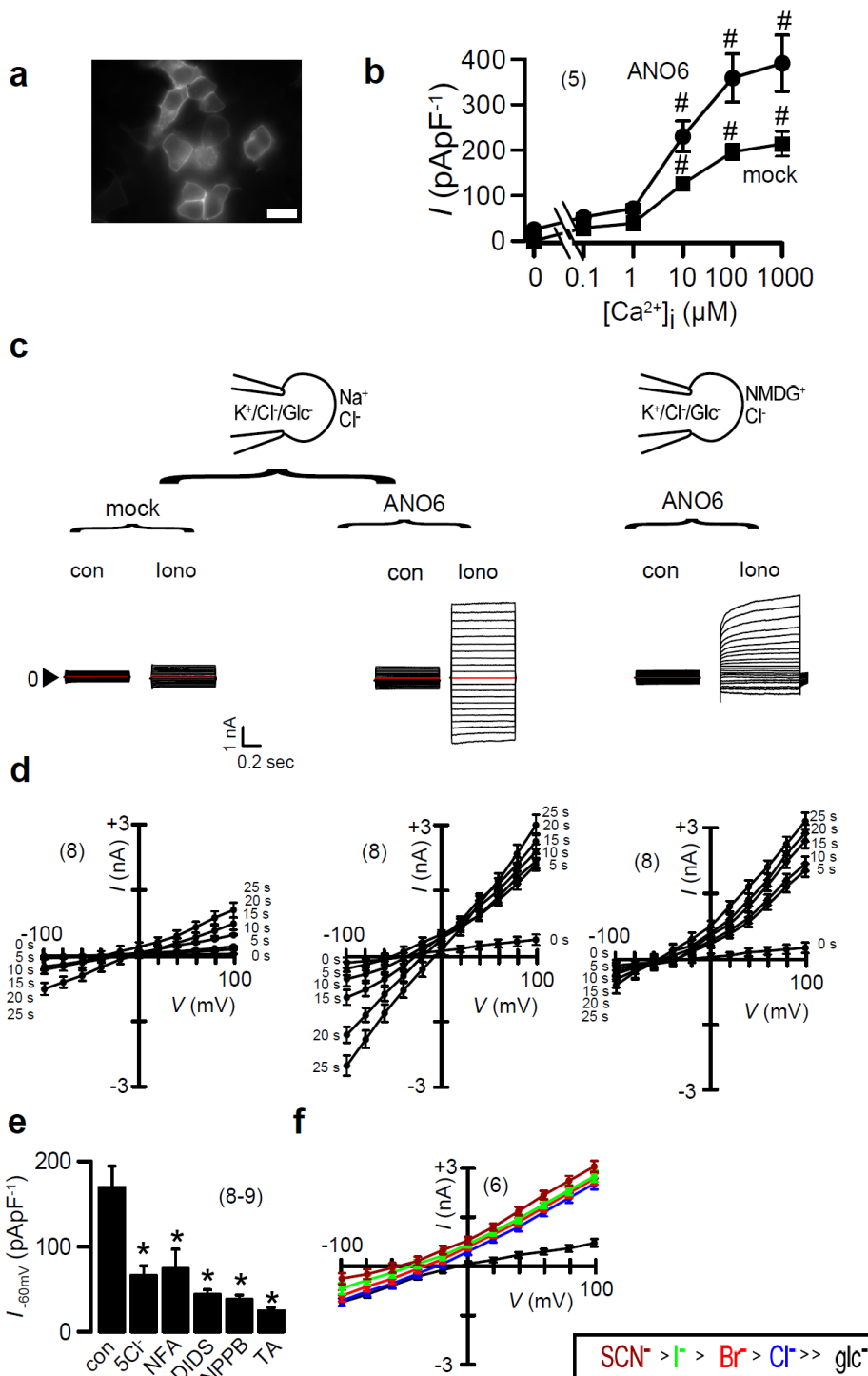


**Fig. S2** ANO6 produces  $\text{Ca}^{2+}$ -activated whole cell currents (a) Membrane Expression of ANO6-GFP in HEK 293 cells. (b) Concentration-dependent activation of whole cell currents by cytosolic  $\text{Ca}^{2+}$  in mock and ANO6-transfected cells. (c) Overlay currents activated by ionomycin (1  $\mu\text{M}$ ) in ANO6-expressing HEK293 cells in the absence or presence of extracellular  $\text{Na}^+$ . (d) I/V curves of time-dependent activation of whole cell currents by ionomycin. (e) Inhibition of ANO6 currents by replacement of extracellular  $\text{Cl}^-$  ( $5\text{Cl}^-$ ), and  $\text{Cl}^-$  channel blockers NFA (10  $\mu\text{M}$ ), DIDS (100  $\mu\text{M}$ ), NPPB (100  $\mu\text{M}$ ), TA (100  $\mu\text{M}$ ). (f) I/V curves  $\text{Ca}^{2+}$ -activated ANO6 currents with different anions present in the bath solution. Insert: Halide permeability sequence for ANO6-related currents. Mean  $\pm$  SEM; n = number of cells. \*significant inhibition (paired t-test), #significant difference to mock (ANOVA). Bar = 20  $\mu\text{m}$ .

Although our experiments cannot definitely separate between pure P2X<sub>7</sub>R currents and  $\text{Ca}^{2+}$  activated ANO6 currents, we found that the ANO6 blocker tannic acid inhibited delayed activated currents (3 min after application of ATP), but not instantaneous currents (1 s after ATP) (Fig. 2d, Supplementary Fig. 4a). Moreover, coexpression of P2X<sub>7</sub>R and ANO6 further augmented ATP-activated currents, while coexpression of ANO6 with P2X<sub>7</sub>R-E496A showed reduced current activation (Fig. 2b,c). No currents were activated by ATP in the absence of P2X<sub>7</sub>R. Fura2-measurements indicated a strong and sustained increase in intracellular  $[\text{Ca}^{2+}]$  by ATP in P2X<sub>7</sub>R expressing cells (Fig. 2e,f). These experiments demonstrate activation of ANO6 by P2X<sub>7</sub>R in HEK293 cells. Together with the results obtained in *Xenopus* oocytes (Fig. 1g), we may suggest a role of the P2X<sub>7</sub>R C-terminus for current activation (194). Evidence for a possible direct interaction of P2X<sub>7</sub>R with ANO6 was detected coimmunoprecipitation of both proteins overexpressed in HEK293 cells (Supplementary Fig. 4b).

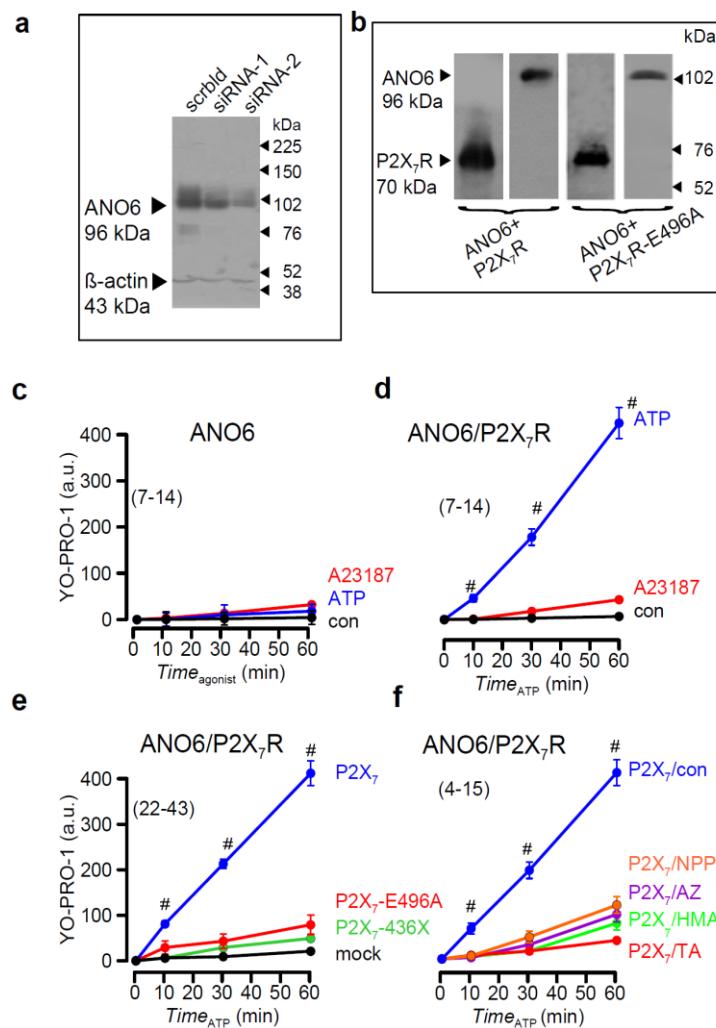


**Fig. S3** Activation of whole cell currents and pore conductance by stimulation of P2X<sub>7</sub> receptors (a) Western blot indicating successful Ano6-knockdown in HEK293 cells by two different siRNAs. (b) Western blot indicating expression of Ano6, P2X<sub>7</sub>R and P2X<sub>7</sub>R-E496A in HEK293 cells. (c,d) Uptake of YO-PRO-1 after stimulation with A23187 (1 μM) or ATP (3 μM) in HEK293 cells expressing Ano6 or coexpressing Ano6/P2X<sub>7</sub>R. (e) Attenuated YO-PRO-1 uptake in cell expressing P2X<sub>7</sub>R-E496A and P2X<sub>7</sub>R-436X, respectively. (f) Inhibition of YO-PRO-1 uptake by Cl<sup>-</sup> channel inhibitors NPPB (100 μM) and TA (20 μM), and the P2X<sub>7</sub>R-blockers AZ (50 nM) and HMA (40 μM). Mean±SEM; n = number of cells and assays, respectively. # significantly different from mutated P2X<sub>7</sub>R or inhibitors, respectively.

### Ano6 causes cellular effects downstream of P2X<sub>7</sub> receptors

Phosphatidylserine (PS) exposure upon stimulation of P2X<sub>7</sub> has been reported earlier (197), while ANO6 was shown to operate as a Ca<sup>2+</sup> dependent phospholipid scramblase (70). We found that activation of P2X<sub>7</sub>R induced exposure of PS to the outer membrane leaflet, when measured by annexin V binding. PS exposure was partially inhibited TA but was abolished after siRNA-knockdown of ANO6-expression (Fig. 3a,b). Stimulation of P2X<sub>7</sub>R by ATP induced massive membrane blebbing, which was depending on the function of ANO6 and the presence of functional P2X<sub>7</sub>R (Fig. 3c,d). Moreover, ATP induced cell shrinkage preceding membrane blebbing was detected by a transient fluorescence increase in calcein loaded cells. Cell shrinkage leads to concentration of the calcein dye and thereby increases fluorescence, while cell swelling leads to decrease in fluorescence (87).

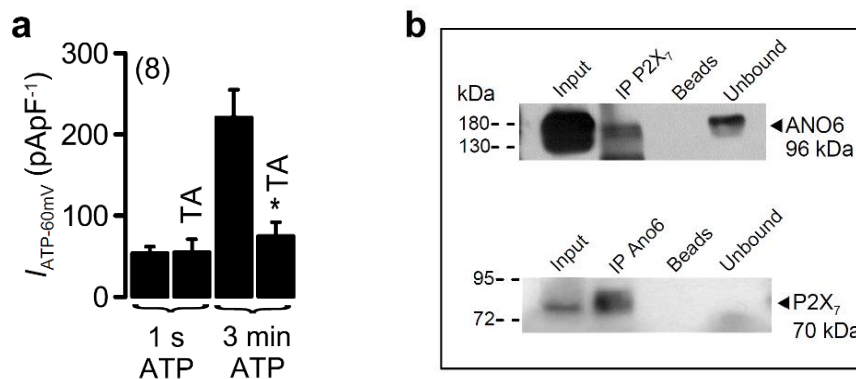


**Fig. S4** Activation of ANO6 by stimulation of P2X<sub>7</sub> receptors (a) Summary of current densities at  $V_c = -60$  mV in HEK293 cells activated by stimulation of P2X<sub>7</sub>R. Whole cell currents activated within 1 s of stimulation by ATP (3 mM) are not inhibited by tannic acid (TA; 20  $\mu$ M), while currents activated with a delay of 3 min are significantly reduced by ANO6 blocker TA (\*paired t-test). (b) Coimmunoprecipitation of Ano6 and P2X<sub>7</sub>R coexpressed in HEK293 cells. Upper panel: ANO6-GFP was detected by GFP-antibody (AB). ANO6 was coimmunoprecipitated by P2X<sub>7</sub>-AB. Lower panel: P2X<sub>7</sub> was coimmunoprecipitated by GFP-AB. Beads indicates IP with beadsonly. Cells were lysed with 1%CHAPs. Rabbit anti-P2X<sub>7</sub> 1:1000 in 1%BSA/PBST. Goat anti-GFP in 1%NFM/PBST. For input 50  $\mu$ g protein were loaded. Other lanes were loaded with each 80  $\mu$ l; experiments performed in triplicates. Mean $\pm$ SEM; (n) = number of cells.

Subsequent to brief shrinkage, the cells appeared swollen and gradually lost their calcein signal, a phenomenon that had been observed earlier in lymphocytes (191). Initial shrinkage relied on the presence and function of ANO6 (Fig. 3e,f). These data demonstrate that ANO6 is central to the deleterious cellular effects downstream of P2X<sub>7</sub>R. Similar effects of ANO6 on cellular volume have been observed earlier(94) and are described below for macrophages (Fig. 4f,g, Supplemental Fig. 6e,f).

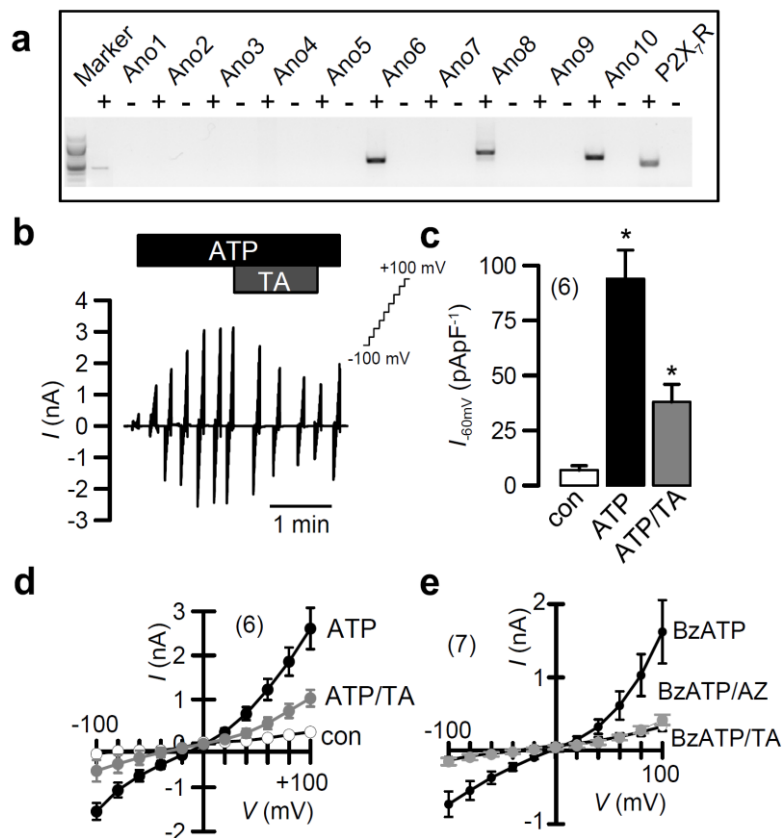


**Fig. S5** ATP induced currents in mouse macrophages (a) RT-PCR-analysis of expression of anoctamins and P2X<sub>7</sub>R in mouse peritoneal macrophages. (b) Whole cell current activated by ATP (3 mM) and inhibition by TA (20  $\mu$ M). (c) Current densities in macrophages stimulated by ATP. (d) I/V curves of ATP-induced whole cell currents and inhibitory effects of TA. (e) I/V curves of Bz-ATP (100  $\mu$ M) induced whole cell currents and inhibition by TA or AZ11645373 (100 nM). Mean $\pm$ SEM; n= number of cells. \*significant activation by ATP and subsequent inhibition by TA (paired t-test).

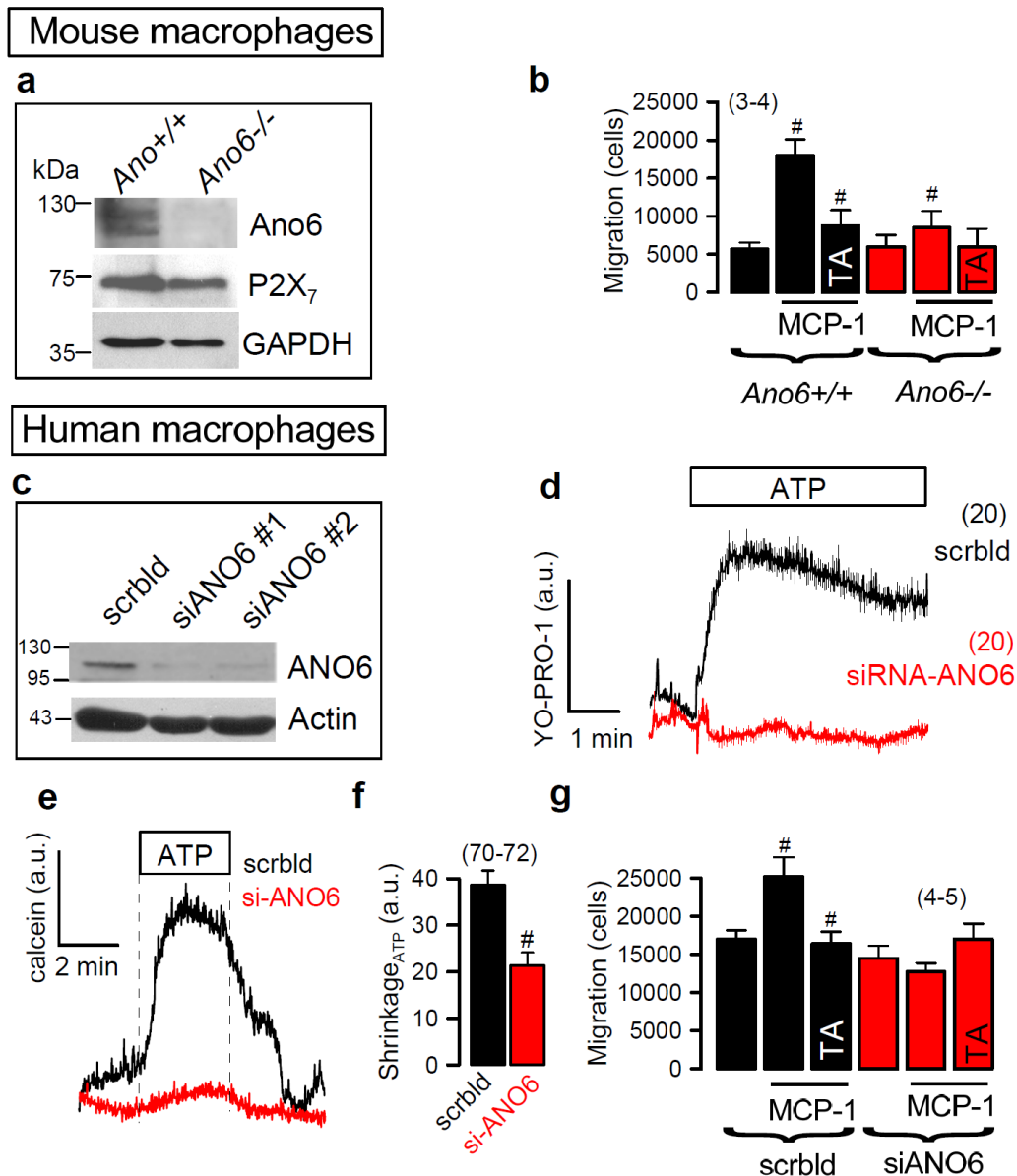


**Fig. S6** Anoctamin 6-dependent YO-PRO-1 uptake, shrinkage and migration of macrophages. (a) Western blot analysis indicating lack of expression of Ano6 but unchanged expression of P2X<sub>7</sub> receptors in macrophages of *Ano6*<sup>-/-</sup> animals. (b) Migration of macrophages from *Ano6*<sup>+/+</sup> and *Ano6*<sup>-/-</sup> animals. Stimulation of migration by the monocyte chemoattractant protein-1 (MCP-1; 100 ng/ml) was also abolished in *Ano6*<sup>-/-</sup> macrophages and the inhibitory effect of TA (20 μM) was largely reduced. Macrophages were isolated from 4 *Ano6*<sup>+/+</sup> and 4 *Ano6*<sup>-/-</sup> animals. (c) Western blot analysis indicating inhibition of Ano6 expression in human THP-1 macrophages by two different siRNAs. (d) YO-PRO-1 uptake in single macrophages. Summary curve of n = 20 cells. Cells were treated with PMA (100 nM), TNFα (10 ng/ml), and INFγ (1000 U/ml). The uptake of YO-PRO-1 was largely inhibited by siRNA knockdown of Ano6. (e,f) ATP-induced cell shrinkage measured by calcein fluorescence. Cell shrinkage was inhibited by siRNA-knockdown of Ano6. (g) Migration of THP-1 cells treated with scrambled RNA or siRNA for Ano6. Mean±SEM; n= number of cells. # significant effects of MCP-1, *Ano6*<sup>-/-</sup>, siAno6, and inhibition by TA (unpaired t-tests).

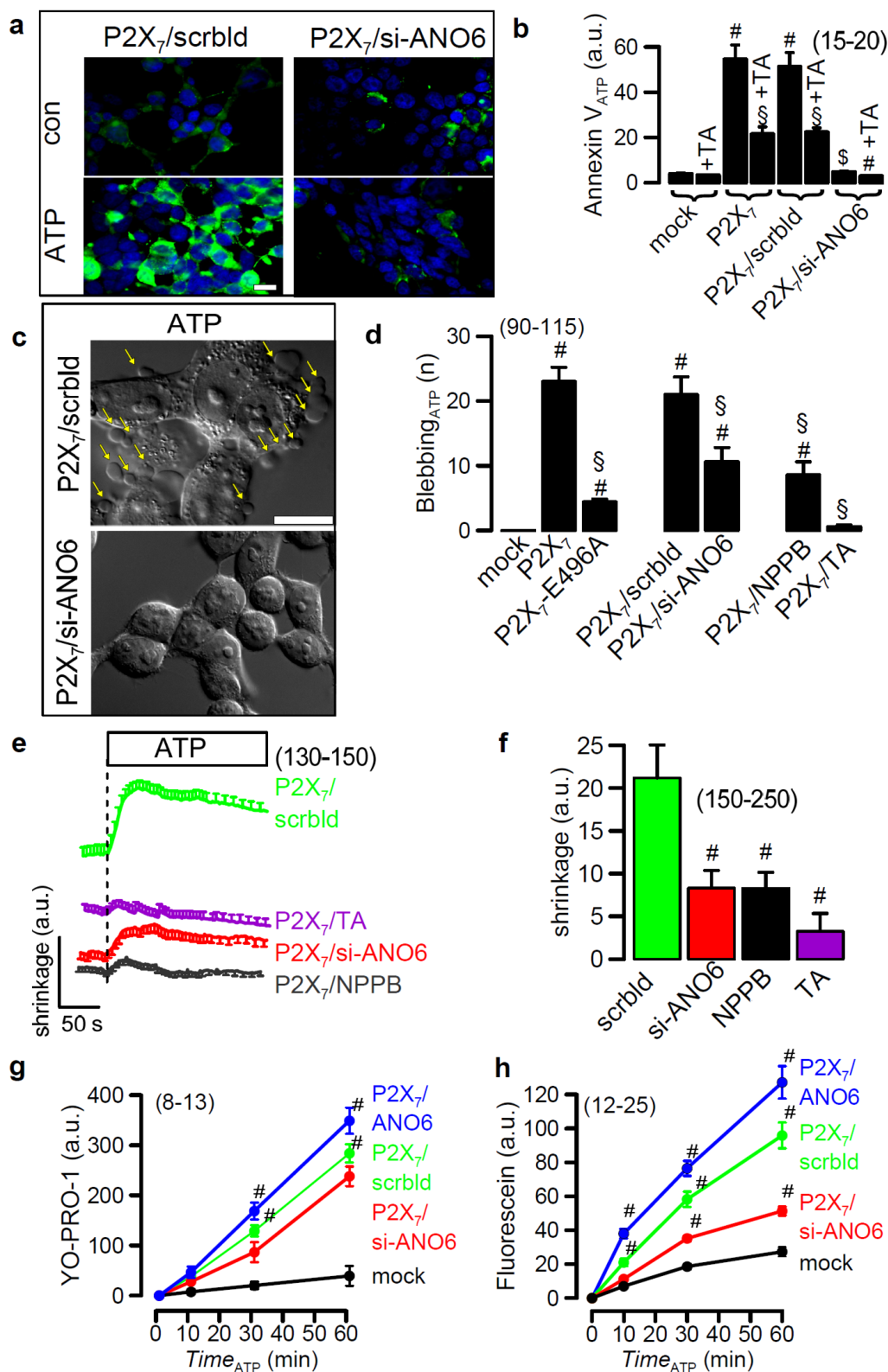


**Fig. 3 ANO6 is part of the P2X<sub>7</sub>R pore conductance and responsible for cellular downstream effects.** a) ATP-induced annexin V binding in P2X<sub>7</sub>R-expressing HEK293 cells and effects of treatment with siRNA-ANO6 or scrambled RNA. Phospholipid scrambling and binding of annexin V (green fluorescence) was abolished after knockdown of ANO6. b) Summary of annexin V binding in mock transfected and P2X<sub>7</sub>R-expressing HEK293 cells,

and effects of the ANO6 blocker TA (10  $\mu$ M). **c)** Effect of ANO6-knockdown on ATP-induced membrane blebbing. Yellow arrows indicate multiple blebs in P2X<sub>7</sub>R-expressing HEK293 cells after application of ATP, which were absent after knockdown of ANO6. **d)** Effects of P2X<sub>7</sub>R-E496A mutation, ANO6-knockdown, and ANO6 blockers NPPB (100  $\mu$ M) and TA (20  $\mu$ M) on ATP-induced membrane blebbing. **e,f)** Effects of ANO6-knockdown and ANO6 blockers on ATP-induced cell shrinkage. **g)** Effects of expression or si-RNA knockdown of ANO6 and P2X<sub>7</sub>R on ATP-induced YO-PRO-1 uptake. YO-PRO-1 uptake was assessed by increase in fluorescence intensity. **h)** Effects of expression or si-RNA knockdown of ANO6 and P2X<sub>7</sub>R on ATP-induced fluorescein uptake. Mean  $\pm$  SEM, n = number of cells and assays, respectively. <sup>#</sup>significant difference when compared to mock or scrambled (p < 0.05; ANOVA). <sup>§</sup>significant inhibition by TA or various treatments (p < 0.05; ANOVA). <sup>\*</sup>significant inhibition by TA (p < 0.05; paired t-test). Scale bars = 20  $\mu$ m.

### Pore formation is ANO6 dependent

Numerous reports demonstrate formation of a large pore conductance by activation of P2X<sub>7</sub>R that is permeable for fluorescent dyes such as YO-PRO-1, fluorescein or calcein (177;178;198;199). We therefore analyzed whether ANO6 also contributes to P2X<sub>7</sub>R pore formation. In the absence of P2X<sub>7</sub>R (mock), ATP or the Ca<sup>2+</sup> ionophore A23187 were unable to induce uptake of YO-PRO-1 into HEK293 (Fig. 3g, Supplementary Fig. 3c,d). In contrast YO-PRO-1 uptake was detected after ATP-stimulation of P2X<sub>7</sub>R-overexpressing cells, which was only slightly attenuated by knockdown of ANO6 (Fig. 3g), but strongly inhibited by blockers of ANO6 such as NPPB and TA (Supplementary Fig. 3f). Blockers of P2X<sub>7</sub>R (HMA, AZ) and mutations within P2X<sub>7</sub>R (P2X<sub>7</sub>-E496A or P2X<sub>7</sub>-436X) also inhibited YO-PRO-1 uptake (Supplementary Fig. 3e,f). YO-PRO-1 uptake was relatively slow in HEK293 cells probably due to low rate (40 %) of transfection of P2X<sub>7</sub>R or low endogenous levels of ANO6. We therefore measured ATP-induced YO-PRO-1 uptake also in single human THP-1 macrophages. YO-PRO-1 uptake was strongly inhibited by siRNA knockdown of ANO6 by two different siRNAs (Supplementary Fig. 6c,d). Moreover, uptake of the negatively charged dye fluorescein was inhibited by siRNA-knockdown of endogenous ANO6, but was augmented by overexpression of exogenous ANO6, respectively (Fig. 3h). This suggests that both P2X<sub>7</sub>R containing an intact C-terminus, as well as ANO6 are required for dye uptake and large conductance.

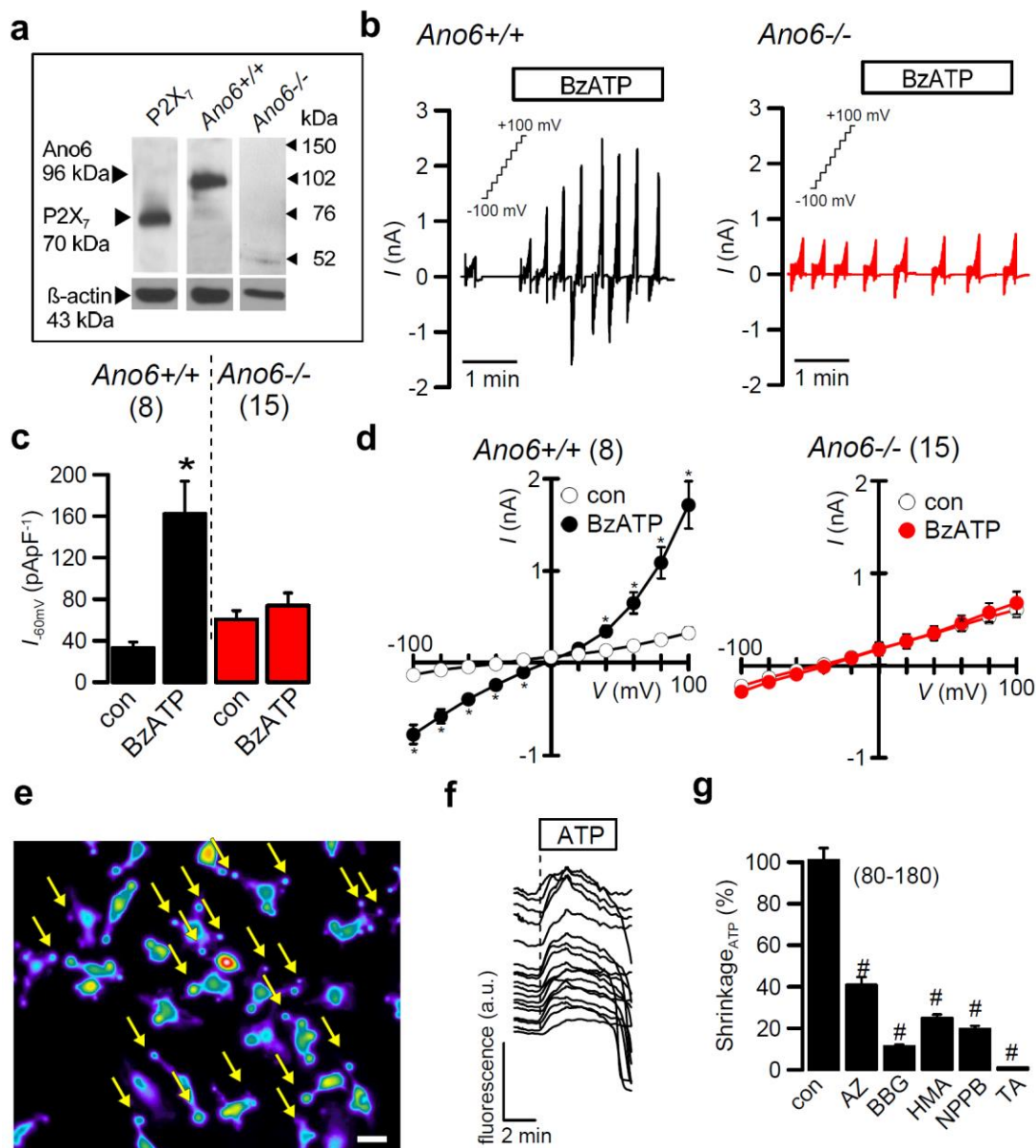


**Fig. 4 Stimulation of P2X<sub>7</sub>R in macrophages activates Anoctamin 6 and changes cell volume.** **a)** Western blot demonstrating expression of P2X<sub>7</sub>R and Anoctamin 6 in mouse *Ano6<sup>+/+</sup>* and lack of expression of Anoctamin 6 in *Ano6<sup>-/-</sup>* macrophages. **b)** Activation of whole cell currents by 100  $\mu$ M BzATP in macrophages from *Ano6<sup>+/+</sup>* mice and lack of activation in macrophages from *Ano6<sup>-/-</sup>* mice. **c)** Summary of current densities measured in *wt* and *Ano6-KO* macrophages. **d)** Current/voltage relationships of ATP-induced whole cell currents from *wt* and *Ano6-KO* macrophages. **e)** Membrane blebbing in mouse macrophages exposed to 3 mM ATP. Macrophages have been loaded with calcein. **f)** Initial shrinkage and subsequent swelling with loss of fluorescence in *Ano6<sup>+/+</sup>* macrophages exposed to ATP. Volume changes were assessed by change in calcein fluorescence. **g)** ATP-induced initial shrinkage (%) and attenuation of shrinkage by inhibition of P2X<sub>7</sub>R (100 nM AZ11645373; 10  $\mu$ M Brilliant blue G; 40  $\mu$ M 5-(N,N-hexamethylene)amiloride) or blocking of Anoctamin 6 (100  $\mu$ M NPPB, 10  $\mu$ M

TA). Mean  $\pm$  SEM, n = number of cells. # significant difference when compared to control ( $p < 0.05$ ; ANOVA). \*significant activation by BzATP ( $p < 0.05$ ; paired t-test). Scale bar = 20  $\mu$ m.

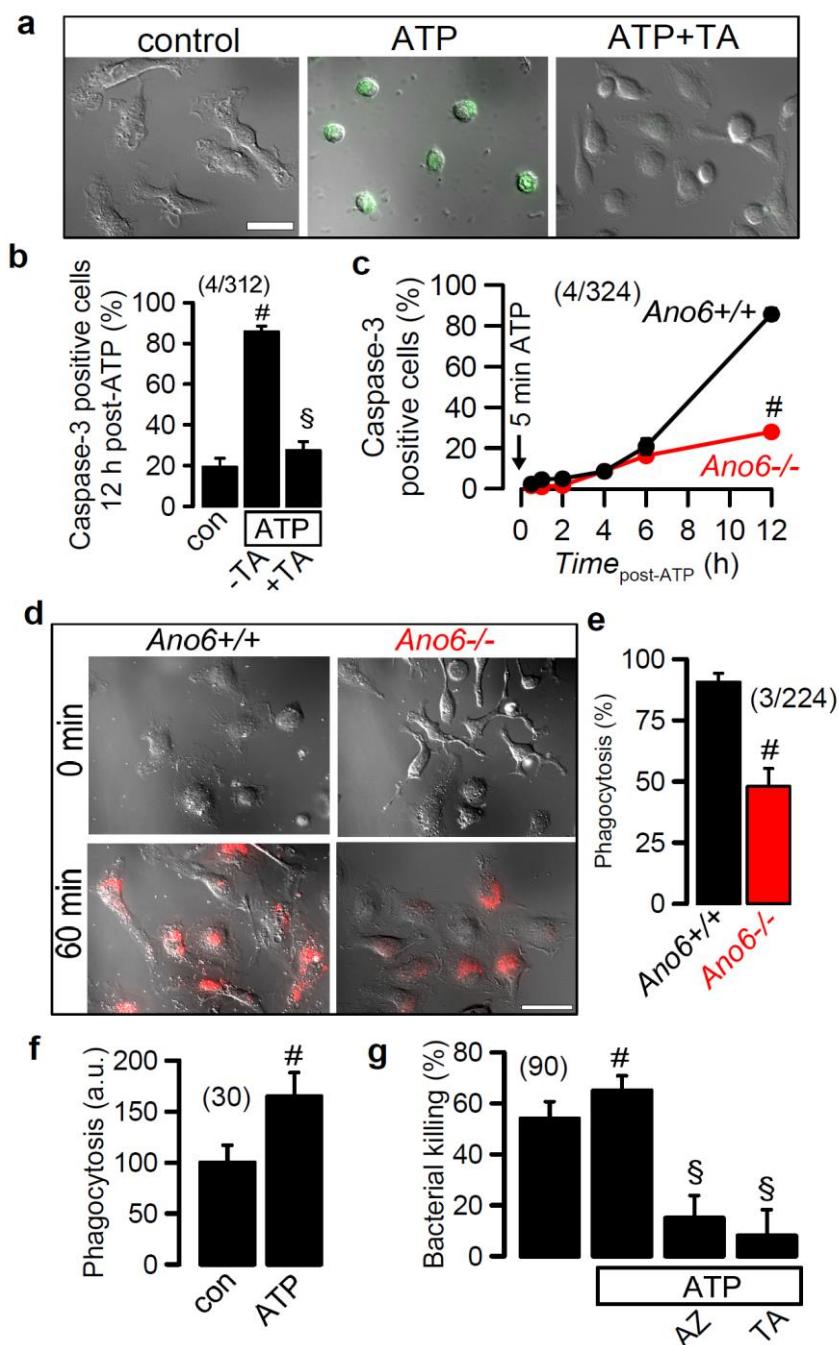


**Fig. 5 Effects of P2X<sub>7</sub>R on macrophage functions is controlled by Anoct6.** **a)** Activation of caspase-3 in mouse macrophages by 3 mM ATP and inhibition by 20  $\mu$ M TA. **b)** Percentage of caspase-3 positive cells 12 hrs after exposure (5 min) to 3 mM ATP and inhibition by TA. **c)** Time course for caspase-3 positive macrophages from *wt* and *Ano6*<sup>-/-</sup> animals. **d)** Phagocytosis (1 hour) of fluorescent bioparticles by macrophages from *wt* and *Ano6*<sup>-/-</sup> animals. **e)** Percentage of phagocytosis-positive *wt* and *Ano6*<sup>-/-</sup> macrophages after 1 hour exposure to bioparticles. **f)** Fluorescence intensity after one hour of phagocytosis and effects of initial 5 min exposure to 3 mM ATP. **g)** Effect of initial exposure to 3 mM ATP on

bacterial killing, and inhibition of killing by 100 nM AZ11645373 and 20  $\mu$ M TA. Mean  $\pm$  SEM, n = number of cells and assays, respectively. #significant difference when compared to control or to *Ano6*<sup>+/+</sup> (p < 0.05; ANOVA). §significant inhibition by blockers (p < 0.05; ANOVA). Scale bars = 20  $\mu$ m.

### **P2X<sub>7</sub> activates Ano6 in macrophages**

Macrophages express high levels of P2X<sub>7</sub>R (Supplementary Fig. 6). Numerous studies report a role of P2X<sub>7</sub>R during inflammation, immune defense and host-pathogen response (for review see (171;188)). We detected expression of both mRNA and protein of P2X<sub>7</sub>R and Ano6 in mouse and human macrophages using RT-PCR and Western blotting (Fig. 4a, Supplementary Fig. 5a, 6a,c). Large whole cell currents were activated in Ano6-expressing *wt* macrophages by either ATP or BzATP, and activation was inhibited by TA (Fig. 4b-d, Supplementary Fig. 5b-e). In contrast no whole cell currents were activated in macrophages of *Ano6*<sup>-/-</sup> mice, apart from a small negative current (Fig. 4b-d). This result indicates an essential contribution of Ano6 to P2X<sub>7</sub>R induced whole cell currents in macrophages. Interestingly, when *Ano6*<sup>-/-</sup> macrophages were stimulated with ATP (3 mM) instead of BzATP, an inward current ( $\Delta I_{100mV} = 169 \pm 28$  pA/pF; n=5) was activated, similar to that obtained in *Ano6*<sup>+/+</sup> animals ( $\Delta I_{100mV} = 189 \pm 36$  pA/pF; n=4). Thus additional purinergic receptors in macrophages (P2X<sub>4</sub>, P2Y<sub>2</sub>) may be stimulated by ATP, leading to activation of other anoctamins such as ANO1, or coupling of Ano6/P2X<sub>7</sub> may not be mandatory for stimulation by ATP.

*Ano6*<sup>+/+</sup> macrophages demonstrated pronounced membrane blebbing when exposed to ATP (Fig. 4e, Supplementary Fig. 7). Blebbing followed brief cell shrinkage (measured as increase in calcein fluorescence) and loss of calcein fluorescence ensued blebbing. Shrinkage and loss of fluorescence were inhibited by blockers of P2X<sub>7</sub>R (Brilliant blue G, HMA, AZ116453739) and inhibitors of Ano6 (NPPB and TA) (Fig. 4g). In macrophages from two *Ano6*<sup>-/-</sup> animals we did not observe ATP-induced cell shrinkage or cell rupture. Moreover, ANO6-knockdown in human THP-1 macrophages significantly reduced ATP-induced shrinkage (Supplementary Fig. 6e,f). This suggests that ATP-induced volume changes in macrophages and membrane blebbing is ANO6-dependent.

Changes in cell volume are intimately related to the ability of cells to migrate, which is also an important function of macrophages (58;200). Monocyte chemoattractant protein-1 (MCP-1) is one of the key chemokines that regulate migration and infiltration of macrophages and other immune cells (201). Notably, a role of anoctamins for cell migration has been identified earlier (78;202). We found that in mouse macrophages MCP-1-induced migration through Boyden chambers was inhibited by the Ano6-blocker TA, suggesting a role of Ano6 for migration of mouse macrophages (Supplementary Fig. 6a,b). More importantly, MCP-1 induced migration was absent in macrophages from *Ano6*<sup>-/-</sup> animals, and inhibition of migration by TA was abolished (Supplementary Fig. 6b). While expression of Ano6 was absent in *Ano6*<sup>-/-</sup> macrophages, expression of P2X<sub>7</sub>R remained unchanged (Supplementary Fig. 6a). We further confirmed the role of ANO6 for migration by downregulation of Ano6 expression in human THP-1 macrophages using two different siRNAs: ANO6-knockdown abolished the effects of MCP-1 and TA (Supplementary Fig. 6c,g).

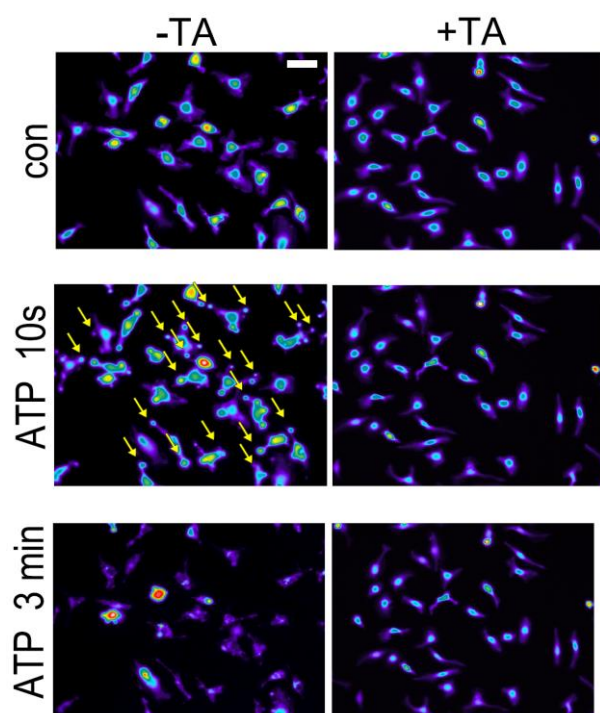


**Fig. S7** Effects of ATP on mouse peritoneal macrophages. Exposure of mouse macrophages to ATP (3 mM) in the absence or presence of tannic acid (TA; 20  $\mu$ M). Macrophages have been loaded with calcein. Exposure to ATP leads to sudden shrinkage of the cells and massive blebbing of the cell membrane which is indicated by yellow arrows. 2-3 min after application of ATP, the fluorescence suddenly disappears, suggesting loss of calcein by formation of pores. Cell shrinkage, membrane blebbing and pore formation is completely suppressed by 10  $\mu$ M tannic acid. Bar = 20  $\mu$ m.

### Activation of Anoctamin 6 is essential for macrophage function.

We examined whether activation of Anoctamin 6 is essential for further cellular effects downstream of P2X<sub>7</sub>R. Apoptosis is one of the key events that take place after stimulation of P2X<sub>7</sub>R. *In vivo* macrophages may be exposed to high extracellular ATP probably only for

short periods of time, during tissue damage or inflammation (200). We therefore exposed mouse peritoneal macrophages to 3 mM ATP for only 5 min, and measured activation of caspase-3 during the following 12 hrs. ATP was applied without previous priming by lipopolysaccharide (LPS), which exerted an immediate pro-apoptotic effect (Supplementary Fig. 8a). Transient exposure to ATP induced delayed activation of caspase-3, which was completely suppressed by tannic acid (Fig. 5a,b, Supplementary Fig. 8c,d). Moreover, activation of caspase 3 was significantly reduced in macrophages from Ano6 null mice (Fig. 5c) or after knockdown of Ano6-expression in macrophages from wt animals (Supplementary Fig. 8b,c).

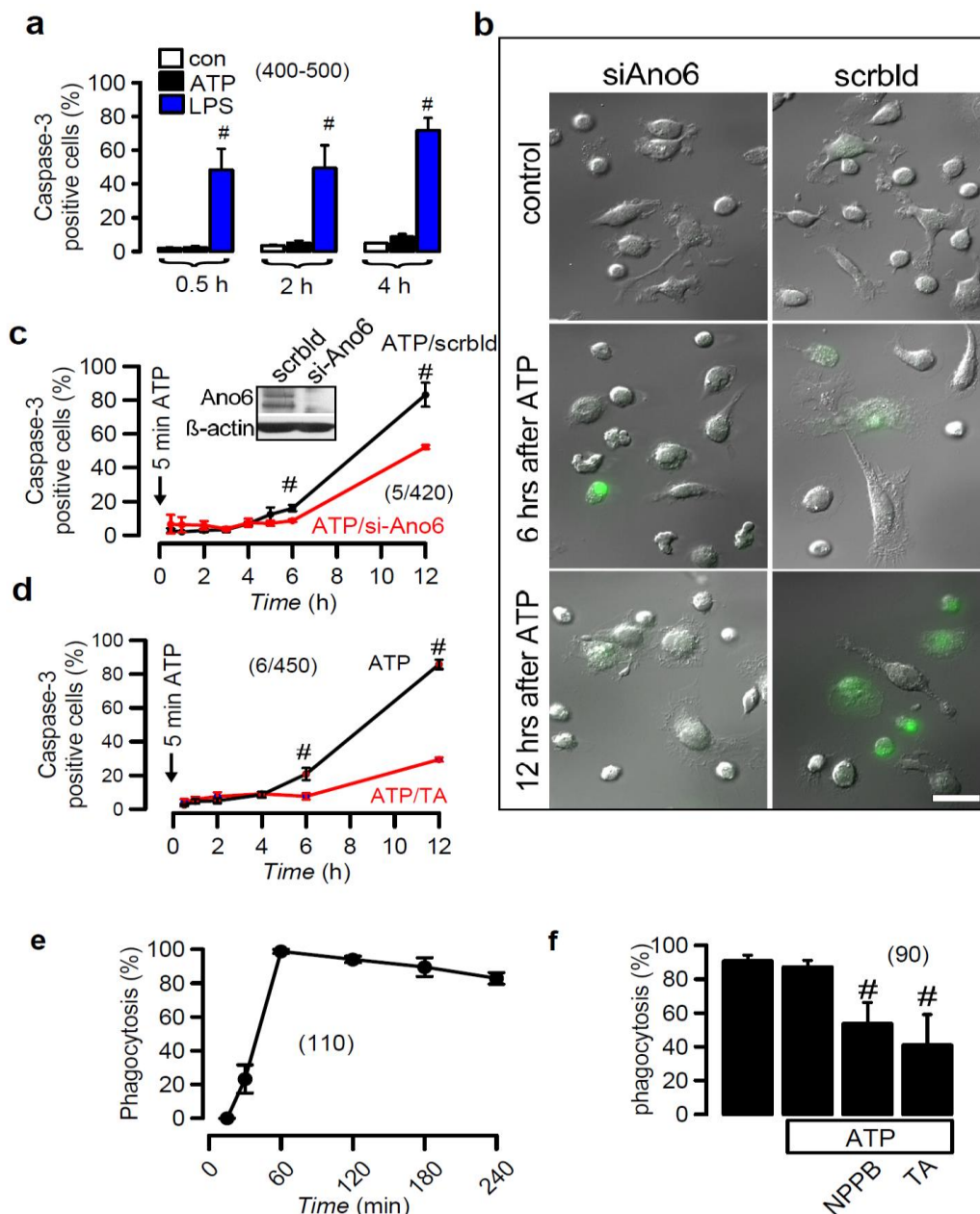


**Fig. S8** ATP activates caspase and phagocytosis in mouse peritoneal macrophages (a) Short term incubation by lipopolysaccharide (LPS; 1  $\mu\text{g}/\text{ml}$ ), but not ATP (3 mM) activated caspase in mouse macrophages. Caspase activity was assessed by NucView<sup>TM</sup> Caspase-3 assay (Biotum, Germany). (b) Caspase activation 12 hours after short term exposure (5 min) to ATP (3 mM), and inhibition of activation of caspase by siRNA knockdown of Ano6. (c,d) Time course for caspase activation after 5 min exposure to ATP (3 min) and inhibition of caspase by siRNA-Ano6 and TA (20  $\mu\text{M}$ ). Inset knockdown of Ano6 expression by siRNA as demonstrated by western blotting. (e) Time course for phagocytosis by macrophages. Phagocytosis was assessed by fluorescent pHrodo E.coli bioparticals conjugates /Life technologies, Germany). (f) Effect of ATP (3 mM), NPPB (100  $\mu\text{M}$ ) and TA (20  $\mu\text{M}$ ) on phagocytic activity of macrophages. Mean $\pm$ -SEM; n = number of cells or assays, respectively. \*significantly different when compared to control, siAno6 and TA, respectively (unpaired t-test). Bar = 20  $\mu\text{m}$ .

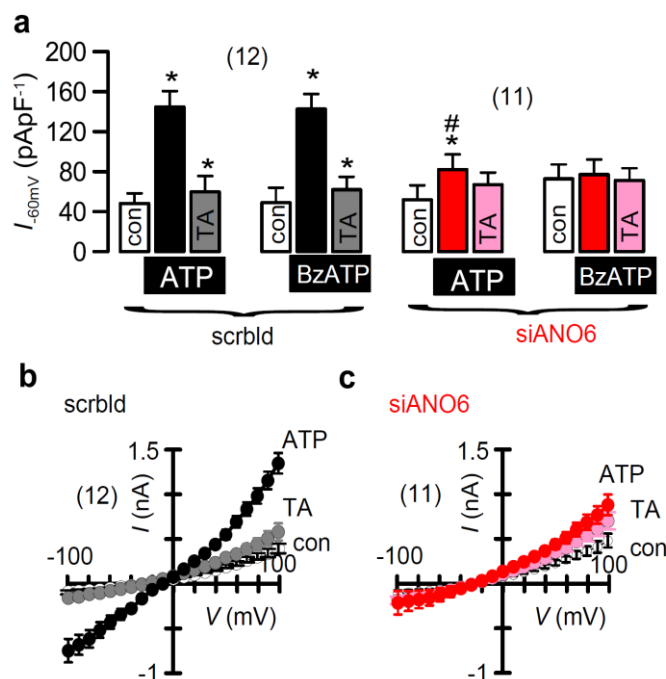


**Fig. S9** Activation of Ano6 by stimulation of P2X7 receptors in T-lymphocytes (a) Summary of current densities ( $V_c = -60 \text{ mV}$ ) in Jurkat T-Lymphocytes treated with scrambled RNA or after siRNA-knockdown of Ano6. Effects of stimulation of P2X<sub>7</sub>R by ATP (3 mM) and BzATP (100  $\mu\text{M}$ ) and inhibition of Ano6 by tannic acid (TA; 20  $\mu\text{M}$ ). Experiments were performed in the presence of 10 nM apamin to block endogenous Ca<sup>2+</sup> dependent K<sup>+</sup> channels. (b,c) I/V relationships for the activated whole cell currents. Mean $\pm$ -SEM; n = number of cells. \* significant effect of ATP or BzATP and inhibition by TA (paired t-test). #significantly difference when compared to scrambled RNA (unpaired t-test).

Mouse macrophages showed strong spontaneous phagocytic activity even without addition of ATP, as demonstrated by phagocytosis of fluorescence-conjugated bioparticles (Fig. 5d, Supplementary Fig. 8e,f). All cells showed phagocytosed bioparticles after 60 min of exposure, as indicated by visual red fluorescence. However, phagocytosis was significantly inhibited by NPPB and TA (Supplementary Fig.8f). The amount of phagocytosis (as measured by fluorescence intensity) was further augmented by short term application (5 min)

of ATP (Fig. 5f). Notably macrophages from *Ano6*<sup>-/-</sup> mice demonstrated reduced spontaneous phagocytosis, when compared to *wt* animals (Fig. 5d,e). We finally tested in an *E. coli* viability assay the ability of macrophages to destroy phagocytosed bacteria. Bacterial killing by macrophages was observed without additional ATP, but was further enhanced by short ATP-exposure. In contrast, killing was largely inhibited by AZ and TA (Fig. 5g). This result suggests a release of ATP by bacterial contact, as demonstrated previously (203). Released ATP binds to purinergic receptors thereby allowing chemotactic navigation via P2Y<sub>2</sub> and P2Y<sub>12</sub> (200). Macrophage responses to bacterial infection are augmented via P2X<sub>7</sub>R signaling, as shown here and in an earlier study (180), leading to augmented bacterial killing (204;205). Taken together, the present data suggest a crucial role of Ano6 for the cellular effects downstream of P2X<sub>7</sub>R, and for the innate immunity function of macrophages (Fig. 6).

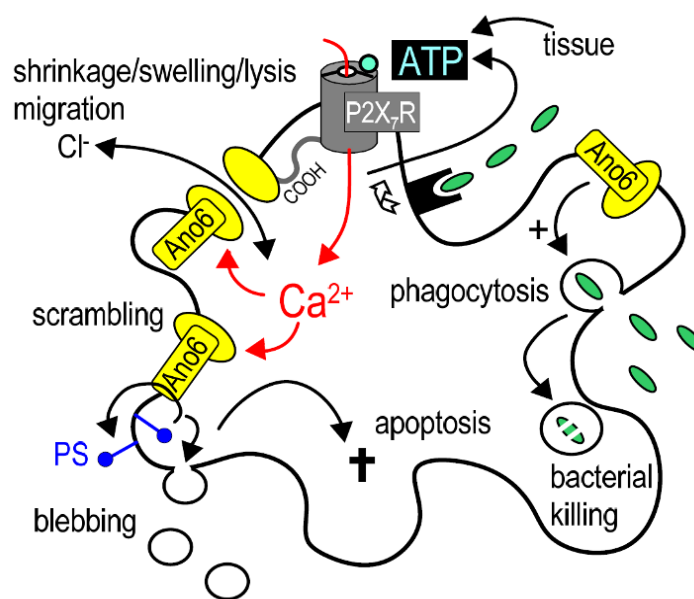


**Fig. 6** Model for the role of ANO6 in macrophages. Lectin-type binding of bacteria to the macrophage membrane induces ATP release by unknown mechanisms. Autocrine ATP - binding activates P2X<sub>7</sub>R, increases intracellular Ca<sup>2+</sup> and activates Cl<sup>-</sup> currents, leading to immediate cell shrinkage. Ano6 induces phospholipid scrambling, which leads to subsequent plasma membrane blebbing and apoptosis. Activation of Ano6 whole cell currents also supports migration of macrophages, thereby enhancing the chance for phagocytosis and subsequent killing of phagocytosed bacteria.

## Discussion

The present results show that opening of P2X<sub>7</sub>R channels causes immediate influx of Ca<sup>2+</sup> that activates a large whole cell current with a delay of only seconds to two minutes, depending on the cell type. This whole cell conductance allows permeation of the fluorescent molecules YO-PRO-1, fluorescein, and calcein and thus relates to the large P2X<sub>7</sub>R “pore” conductance (175;198;199;206). Whether P2X<sub>7</sub>R channels dilate to a dye-permeable pore upon continuous binding of ATP (207;208) or whether dyes use one or several independent permeation pathways(177-179;198;199), is still a matter of debate. These pathways may be activated through increase in intracellular Ca<sup>2+</sup> and/or via a signaling complex located at the C-terminus of P2X<sub>7</sub>R. In either event, the present data show that ANO6 i) is activated by the P2X<sub>7</sub>R-mediated increase in intracellular Ca<sup>2+</sup> and ii) is in part responsible for delayed pore conductance and dye uptake. Previous work (50;84;85;130) and present results indicate that ANO6 requires high intracellular [Ca<sup>2+</sup>]<sub>i</sub> to be activated, corresponding to the high [Ca<sup>2+</sup>]<sub>i</sub> levels provided by activation of P2X<sub>7</sub>R. Moreover, recent data from mouse and human ANO6 and the reconstituted ANO6 homologue from *Aspergillus fumigatus* suggest a rather large pore size for ANO6 (50;83;137). Because we could coimmunoprecipitate ANO6 and P2X<sub>7</sub>R, we speculate that ANO6 is part of a macromolecular complex containing P2X<sub>7</sub>R and possibly different diffusion pathways for cations and anions (174;177). In this regard, the unique extended C-terminus of P2X<sub>7</sub>R appears essential for pore formation and subsequent cell death, as suggested earlier (206;209).

We show that ANO6 participates in many of the essential cellular responses downstream of P2X<sub>7</sub>R like i) Initial cell shrinkage, ii) membrane blebbing, iii) membrane phospholipid scrambling and iv) apoptosis. (Fig. 6). These findings support the general concept of cell shrinkage being an early and essential step, triggering the cell death machinery (210). Notably, evidence for cell shrinkage due to activation of ANO6 has been shown previously, and ANO6 currents were activated by pro-apoptotic stimuli (84;86;87;96). Sequential shrinkage/swelling and translocation of phosphatidylserine upon P2X<sub>7</sub>R-stimulation have also been reported for lymphocytes (191). Our own data indicate that stimulation of P2X<sub>7</sub>R activates ANO6 in *Xenopus* oocytes, HEK293 cells, macrophages and Jurkat T-lymphocytes

(Supplementary Fig. 9). The importance of Cl<sup>-</sup> ions for P2X<sub>7</sub>R-induced cell shrinkage and subsequent cell death has been also suggested in previous studies (195;211). ANO6 does not produce classical volume regulated Cl<sup>-</sup> currents ( $I_{Cl, \text{swell}}$ ) with typical time dependent inactivation (9). It is nevertheless activated by apoptotic stimuli and cell swelling, and thus forms the Ca<sup>2+</sup> dependent component of volume regulated Cl<sup>-</sup> currents (86;87;96). Phospholipid scrambling induced by stimulation of P2X<sub>7</sub>R is probably due to strong [Ca<sup>2+</sup>]<sub>i</sub> increase, inducing the scramblase activity of ANO6(70;84), and may also support membrane blebbing, two intimately related cellular events (210;212).

Activation of ANO6 by stimulation of P2X<sub>7</sub>R affects essential macrophage functions such as i) migration, ii) phagocytosis of bacteria, and iii) bacterial killing (Fig. 6). Autocrine purinergic signaling has been shown recently to control chemotaxis and migration of macrophages (200). Both ANO1 and ANO6 contribute to migration also in other cell types, which has large implications for tumor metastasis (58;78;79;202). The present report now establishes a role of ANO6 for migration of macrophages, which has an impact on phagocytic activity and subsequent bacterial killing. In situ macrophages are probably only transiently exposed to high extracellular ATP concentrations (180;200). The present data show that only 5 min exposure to 3 mM ATP enhances phagocytosis and bacterial killing, and induces delayed apoptosis, corresponding to the delayed ATP-induced apoptosis observed in an earlier report (180). A role of P2X<sub>7</sub>R-signaling in macrophages for killing of mycobacteria (204;213) and other pathogens (188) has been demonstrated earlier. We may speculate that P2X<sub>7</sub>R-induced phagolysosomal fusion (188;214) is supported by ANO6 after engulfment of bacteria. Notably, ANO6 was shown recently to support endosomal acidification and renal tubular protein reabsorption (215). Taken together, we demonstrate that ANO6 is central to cellular effects downstream of the P2X<sub>7</sub> receptor. It therefore reflects a potential pharmacological target to interfere with immunological processes and cellular apoptosis.

### **Acknowledgments**

This study was supported by DFG KU756/12-1 and SFB699 Project A7. We gratefully acknowledge the P2X<sub>7</sub>R cDNA provided by Prof. Dr. G. Schmalzing (Department of Molecular Pharmacology, University of Aachen, Aachen, Germany), and *Ano6*<sup>-/-</sup> mice

provided by Prof. Dr. A. Vortkamp (Department of developmental biology, Universität Duisburg-Essen, Essen, Germany). The technical assistance by Walailak Jantarajit, Ana Marta Romao, Brigitte Wild and Ernestine Tartler is gratefully acknowledged.

## Chapter 5

### A coding variant of *ANO10*, affecting volume regulation of macrophages, is associated with *Borrelia* seropositivity

#### Abstract

In a first genome-wide association study (GWAS) approach to anti-*Borrelia* seropositivity, we identified two significant single nucleotide polymorphisms (SNP) (rs17850869,  $P=4.17E-09$ ; rs41289586,  $P=7.18E-08$ ). Both markers, located on chromosomes 16 and 3, respectively, are within or close to genes previously connected to spinocerebellar ataxia. The risk SNP rs41289586 represents a missense variant (R263H) of anoctamin10 (*ANO10*), a member of a protein family encoding  $Cl^-$  channels and phospholipid scramblases. *ANO10* augments volume regulated  $Cl^-$  currents ( $I_{Hypo}$ ) in *Xenopus* oocytes, HEK293 cells, lymphocytes and macrophages and controls volume regulation by enhancing regulatory volume decrease (RVD). *ANO10* supports migration of macrophages, and phagocytosis of spirochetes. The R263H variant is inhibitory on  $I_{Hypo}$ , RVD and intracellular  $Ca^{2+}$  signals, which may delay spirochete clearance, thereby sensitizing adaptive immunity. Our data demonstrate for the first time that *ANO10* has a central role in innate immune defense against *Borrelia* infection.

**Key words:** Genome-wide Association Study, Lyme Borreliosis, Spinocerebellar Ataxia, Anoctamin10, TMEM16K, Macrophages, Phagocytosis, LRRC8A

**Published in:** Christian Hammer<sup>1</sup>, Podchanart Wanitchakool<sup>2</sup>, Lalida Sirianant<sup>2</sup>, Sergi Papiol<sup>1</sup>, Mathieu Monnheim<sup>1</sup>, Diana Faria<sup>2</sup>, Jiraporn Ousingsawat<sup>2</sup>, Natalie Schramek<sup>3</sup>, Corinna Schmitt<sup>4</sup>, Gabriele Margos<sup>5</sup>, Angelika Michel<sup>6</sup>, Peter Kraiczy<sup>7</sup>, Michael Pawlita<sup>6</sup>, Rainer Schreiber<sup>2</sup>, Thomas F. Schulz<sup>4</sup>, Volker Fingerle<sup>5</sup>, Hayrettin Tumani<sup>3</sup>, Hannelore Ehrenreich<sup>1,8\*</sup>, and Karl Kunzelmann<sup>2\*</sup>. A coding variant of *ANO10*, affecting volume regulation of macrophages, is associated with *Borrelia* seropositivity. Mol Med. 2015 Feb 23;21:26-37.

**Own experimental contribution:** Most western blot, COIP, Flow cytometry and cell migration experiment performed in cell lines.

**Own written contribution:** Methods, Results, Parts of Introduction and Discussion.

**Other contributions:** Designed experiments and analyzed data.

## Introduction

Lyme borreliosis, caused by bacteria mainly transmitted by ticks of the species *Ixodes*, is the most common tick-borne disease in Europe and the United States (216). It involves many organs, predominantly skin, musculoskeletal system, heart, and nervous system (217). Central nervous system manifestations can imitate a broad range of neuropsychiatric syndromes (218), in rare cases even be indistinguishable from acute schizophrenia (219). Borreliosis is caused by a variety of species of *Borrelia burgdorferi* sensu lato complex, some of which show distinct differences in their pathogenic properties in the human host (220). *Borrelia* species have a highly complex genomic structure, and genetic variation may account for a large proportion of the variability of pathogenicity (221). However, pathogens are not only depending on their own fitness for a successful establishment of infection, but also on the genetic makeup of their hosts. The recent years have witnessed a wealth of studies elucidating the important role of human genomic variation in host defense mechanisms, both for viral and bacterial infections (222). Given the immense phenotypic variation of *Borrelia* disease symptoms, it is likely that part of it is due to differences in human immune response, originating in genomic variation. We therefore set out to (i) identify host genomic variants mediating differential susceptibility to *Borrelia* infection/seropositivity by means of a genome-wide association study (GWAS) and (ii) uncover a possible contribution of *Borrelia* seropositivity to core phenotypes of neuropsychiatric disorders. For advancing these objectives, we employed the Göttingen Research Association for Schizophrenia (GRAS) sample (223;224) comprising 1,271 healthy blood donors and 1,224 patients suffering from neuropsychiatric disease.

## Materials and Methods

**Participants:** All subject data were collected in accordance with ethical guidelines and the Helsinki Declaration. Regarding the discovery sample (total of N=2,495), subject selection was unbiased, i.e. sera collection concluded before specific serological analysis was planned: Schizophrenic patients (N=1,076) were recruited in 2005-2011 at 23 German sites for the

GRAS (Göttingen Research Association for Schizophrenia) data collection. Patients fulfilling DSM-IV criteria for schizophrenia (81.4%) or schizoaffective disorder (18.6%) were included regardless of disease stage (223;225). Healthy GRAS controls were anonymized blood-donors (N=1,271; Transfusion Medicine, Göttingen). Health was ensured by pre-donation screening (questionnaires, interviews, hemoglobin, blood pressure, pulse, temperature). Patients with affective disorders (N=146) were also included (ongoing GRAS extension).

**Exploration sample:** (N=100): In Ulm, a total of 257 patients with documented history of *Borrelia* infection were contacted in written form, resulting in 100 individuals interested to participate. The study included: (a) A comprehensive history on tick bite and borreliosis-specific symptoms; (b) a neurological examination with special emphasis on cerebellar signs and (c) drawing of blood for genetic and serological analyses. Patients were classified in 3 subgroups, based on clinical and serological findings: (i) neuroborreliosis, (ii) systemic borreliosis or (iii) laboratory-based borreliosis without typical clinical signs and symptoms.

**Phenotypical analyses:** Of all schizophrenic (GRAS) patients, extensive phenotypical characterization was conducted as referenced previously (223;225). Age of onset, age at first psychotic episode, positive and negative syndrome scale (PANSS) scores, chlorpromazine equivalents (CPZ), neurological symptoms (CNI; Cambridge Neurological Inventory) including fine motor skills (MacQuarrie dotting/tapping), current cognitive functioning (composite score comprising reasoning, executive function, verbal learning & memory), global assessment of functioning (GAF), Parkinsonism, hard neurological signs, motor coordination, sensory integration, and gait were employed as disease characteristics. Moreover, patient self-rating was performed using the Brief Symptom Inventory (BSI) (226). The Ulm borreliosis patients had a comprehensive clinical neurological, serological and in 81/100 patients also cerebrospinal fluid (CSF) examination. CSF diagnostics included leukocyte and differential cell count, nephelometric determination of total protein, CSF/serum ratios for albumin IgG / IgA / IgM, ELISA for *Borrelia* specific antibodies and oligoclonal IgG analysis in CSF/serum by immunoelectrophoresis.

**Serological analyses:** The presence of antibodies against *Borrelia* was first determined using Enzygnost Lyme link VlsE/IgG, a quantitative immunoenzymatic method based on a mix of native *Borrelia* antigens from *B. afzelii* strain PKo and recombinant VlsE obtained from three

genospecies pathogenic to humans (*B. Burgdorferi* sensu stricto, *B. garinii*, *B. afzelii*) (Siemens Healthcare-Diagnostics GmbH, Eschborn, Germany). Assays were automatically processed on BEP®III (Siemens Healthcare-Diagnostics GmbH), and interpreted (manufacturer's instructions) as positive, negative or borderline. Positive and borderline samples were re-analyzed using the EUROLINE *Borrelia*-RN-AT Immunoblot (Euroimmun, Lübeck, Germany). Only the confirmed were defined seropositive for statistical analysis and contrasted against all others. Titer levels, when mentioned in the manuscript, refer to the ELISA results. To test for specificity of association signals, the following immunoenzymatic assays were conducted: Novagnost Chlamydia pneumoniae IgG, Novagnost Chlamydia trachomatis IgG, Novagnost Mycoplasma pneumoniae IgG, Enzygnost Anti-Helicobacter pylori/IgG (all Siemens Healthcare-Diagnostics GmbH).

**Genetic analyses:** A semi-custom Axiom®myDesign™ genotyping array (Affymetrix, Santa Clara, CA, USA) was used. Array specifications and quality controls have been described in detail before (224). Principal components were generated using GCTA (v1.24) (227) and genetic outliers were excluded based on inspection of the first two principal components. Genomic inflation was calculated using PLINK (v1.07) (228) to ensure minimization of population stratification, excluding SNPs in the complex MHC region (chromosome 6, 29-33MB). PLINK was also used for association testing, using the following exclusion criteria: Hardy-Weinberg  $P < 5E-07$ , minor allele frequency  $< 0.01$ , missingness per marker  $> 0.05$ , and missingness per individual  $> 0.02$ . SNPs on sex chromosomes were excluded from analysis. Variants in high linkage of genome-wide significant SNPs were identified using SNAP Proxy Search (<http://www.broadinstitute.org/mpg/snap/>), using the 1000 Genomes Pilot 1 CEU population panel and a  $r^2$  threshold of 0.8. Patients with confirmed diagnosis of borreliosis (N=100) recruited in Ulm were genotyped using the KASP genotyping system (LGC Genomics, Berlin, Germany), after DNA isolation from blood using the JETQUICK Blood and Cell Culture Kit (Genomed, Loehe, Germany).

**Cell culture, animals, cDNAs, site-directed mutagenesis, and transfection:** Human *ANO10* cDNA (NM\_018075.2) was purchased from OriGene (SC113757, Rockville, MD, USA), and cloned in pcDNA3.1 with a C-terminal His-Tag (Life Technologies, Darmstadt, Germany). R263H-ANO10, L510R-ANO10, L384fs-ANO10, LRRC8A and AQP1 were

mutated and cloned, respectively, using standard PCR-techniques. All cDNAs were verified by sequencing. Culturing of HEK293 cells, THP-1 cells and lymphocytes, and isolation of mouse macrophages has been described earlier (139). Site-directed mutagenesis, transfection methods, and other used constructs have been described previously (96).

**Fluorescent *Borrelia*:** Red fluorescent *B. garinii* PRJS1009-Cherry were used to infect macrophages. In some experiments cells were exposed to TNF $\alpha$  (100ng/ml) for 2–6h. THP-1 monocytes were differentiated into macrophages by incubation with 100nM phorbol 12-myristate 13-acetate (PMA) (Sigma, Munich, Germany) for 48h.

**Patch clamping:** Cells grown on cover slips were mounted in a perfused bath on the stage of an inverted microscope (IM35, Zeiss, Munich, Germany) and kept at 37°C. The bath was perfused continuously with Ringer solution (mM: NaCl 145, KH<sub>2</sub>PO<sub>4</sub> 0.4, K<sub>2</sub>HPO<sub>4</sub> 1.6, D-glucose 6, MgCl<sub>2</sub> 1, Ca-gluconate 1.3, pH7.4) at about 10ml/min. Cell swelling was induced by removing 100mM mannitol from an isotonic (300mosmol/l) modified Ringer solution to achieve a hypotonic bath solution (Hypo, 33%, 200mosmol/l). Patch-clamp experiments were performed in the fast whole-cell configuration as described previously (139).

**Two electrode voltage clamp:** Oocytes were harvested from *Xenopus laevis* according to German regulations governing animal experiments. Oocytes were defolliculated for 1 h at 18°C with 1.5 mg/ml collagenase type V (Sigma). After washing oocytes were injected with cRNA encoding ANO10, R263H-ANO10, and AQP1. Preparation of cRNA and voltage clamping of the oocytes have been described earlier (139).

**Measurement of [Ca<sup>2+</sup>]<sub>i</sub>:** The plasma membrane bound calcium sensor has been modified by the addition of a N-terminal signal peptide (20 aa) from Neuromodulin (PI-G-CaMP2). Addition of this peptide results in posttranslational palmitoylation of the protein, which facilitates anchoring of the protein to the plasma membrane. HEK293 cells were transfected on coated glass cover slips with pcDNA31 PI-G-CaMP2, and were mounted in a perfusion chamber 48 hrs after transfection. Cells were perfused with ringer solution at a rate of 8 ml/min at 37°C. Cell fluorescence measurements was measured continuously with an inverted microscope Axiovert S100 (Zeiss) using a x40 objective (Fluar 40x/1.3 Oil, Zeiss) and a high speed polychromator system (VisiChrome, Visitron, Puchheim, Germany). PI-G-CaMP2 was excited at 485 nm and 405 nm. Emission was recorded between 520 and 550 nm using a

CCD-camera (CoolSnap HQ, Visitron). Control of experiments, imaging acquisition, and data analysis were done with the software package Meta-Fluor (Universal imaging, New York, USA). Alternatively cells were loaded with Fura2 and intracellular  $\text{Ca}^{2+}$  concentrations were determined as described earlier (139).

**Flow cytometry, single cell volume measurements and migration:** Cells were washed and re-dissolved in 10 ml isotonic or hypotonic Ringer solution as described for patch clamp experiments. Cells were analyzed at 37 °C / pH 7.4 using a CASY flow cytometer (Roche Diagnostics, Mannheim, Germany). Cells were analyzed at a density of  $10^6$  cells/ml. For single cell volume measurements cells were loaded with 1  $\mu\text{g}$  of calcein-AM (Molecular Probes) and 0.01% pluronic in a standard bath solution (Ringer) for 60 min at 20-22 °C. Fluorescence intensity was measured at an excitation wavelength of 485 nm and an emission wavelength of 520–550 nm. Cell swelling and RVD were observed for 10–15 min after applying hypotonic bath solution. Cell migration was assessed in Boyden chambers as described previously (139).

**Measurement of TNF $\alpha$  release:** THP-1 cells were grown in 96 well plates and, when mentioned, treated with PMA (100nM) for 2 days. Before sample collection, cells were infected with cherry-labeled *B. garinii* (MOI 1:10) for 4h at 37°C. Following a centrifugation step the supernatant was collected and immediately stored at -20°C. TNF $\alpha$  was measured using Platinum ELISA kit (eBioscience Affymetrix, Vienna, Austria) according to manufacturer's instructions.

**Phagocytosis assay:** THP-1 cells were treated with PMA (100nM) for 2 days. Cells were infected with cherry-labeled *B. garinii* (MOI 1:10) at 37°C. After infection cells were washed with PBS to remove remaining *Borrelia*. Cells were visualized and fluorescence was detected using an Axiovert 200 microscope/AxioVision software (Zeiss) and mean fluorescence intensity was quantified.

**Annexin V binding assay:** THP-1 cells treated with PMA (100nM, 48h) were grown in a 96-well plate. Cells were washed twice with cold PBS and incubated with annexin V-FITC for 15min at room temperature (FITC Annexin V Detection Kit, BD Biosciences, Heidelberg, Germany). Fluorescence intensity was detected using a plate reader (Novostar, BMG Labtech, Ortenberg, Germany). Cells were treated with TNF $\alpha$  (10ng/ml, 4hr) or with cherry-labeled *B.*

*garinii* (MOI 1:10) for 4h, followed by washing with PBS and fluorescence detection, considered as time point zero. For other time points, the cells were washed to remove the remaining *Borrelia*, and kept with fresh media for the following days after infection.

**Western blotting, biotinylation and immunocytochemistry:** Protein was isolated from THP-1 cells grown in the absence or presence of PMA (100nM) and transfected with siRNA-ANO10 (ID# s30237, s30238, Ambion, Life Technologies, Darmstadt, Germany). Cells were lysed using lysis buffer containing 150mM NaCl, 50mM Tris, 1mM EDTA, 100mM DTT, 0,5% NP-40, and 1% protease inhibitor cocktail (Roche, Mannheim Germany). Protein separation, transfer, blotting and detection have been described previously (137). A polyclonal rabbit anti-ANO10 antibody (Aviva Systems Biology, San Diego, USA) was used at a dilution of 1:500. Rabbit anti  $\beta$ -actin antibody (Sigma-Aldrich, Taufkirchen, Germany) was used at a dilution of 1:1000. For biotinylation of plasma membrane proteins EZ-Link Sulfo-NHS-SS-Biotin (#89881, Pierce, Thermo Fisher Scientific, Waltham, USA) was prepared at a concentration of 1mg/ml in ice-cold phosphate-buffered saline (PBS). Biotinylated cells were lysed and 100  $\mu$ l streptavidin beads (Thermo Fisher Scientific, Waltham, USA) were added to the supernatant after centrifugation. After incubation O/N at 4 °C, beads were washed 5 times with cold lysis buffer and biotinylated proteins were eluted by boiling the sample for 5 min at 95°C in SDS sample buffer. For immunocytochemistry of ANO10 the anti-ANO10 antibody was used at a dilution of 1:500.

**Statistics:** Group differences in categorical and continuous variables were assessed using Chi-square or Mann-Whitney U tests. A generalized linear model was employed upon covariate inclusion. At normal distribution of continuous variables, T-tests were performed (paired and unpaired tests, respectively, for experiments in oocytes, HEK293 cells, lymphocytes and macrophages). A basic allelic test, implemented in PLINK was used to test for association between single nucleotide polymorphisms (SNPs) and *Borrelia* serological status. *P*-values<0.05 were considered significant and multiple-testing corrected (Bonferroni) where indicated, but are displayed uncorrected. Data in Figures are expressed as mean $\pm$ SEM, in Tables as mean $\pm$ SD.

## Results

### ***Borrelia* seropositivity in health and neuropsychiatric disease**

We detected anti-*Borrelia* antibodies (AB) in 169 out of 2,495 individuals in total (6.8%) (Table 1). AB prevalence tended to be higher in schizophrenia patients (7.9%,  $P=0.05$ ) and affective disorder patients (11.0%,  $P=0.07$ ), when compared to psychiatrically healthy controls (5.4%).  $P$  values are corrected for sex and age, since male subjects are more likely to be seropositive than females (8.2% vs. 4.3%,  $P=1.96E-04$ ,  $OR=1.98$ , Supplementary Table 1). Furthermore, groups differ significantly in mean age (Supplementary Table 2), which has to be considered because the likelihood of a past *Borrelia* infection and subsequent antibody formation increase with age (Supplementary Figure 1). We did not find a difference in mean titer levels of seropositive subjects between patient groups and controls (Supplementary Table 3). Overall, seropositive and seronegative schizophrenia patients do not show differences with respect to major disease phenotypes of schizophrenia including neurological signs as determined by the Cambridge Neurological Inventory (CNI), which should also cover symptoms of borreliosis (Supplementary Table 4). Interestingly, however, AB carriers score significantly worse throughout all scales of the Brief Symptom Inventory (BSI, corrected for age and sex as a proxy for gender) (226), an instrument based on patients' self-evaluation (Supplementary Figure 2).

### **GWAS on *Borrelia* antibody seropositivity**

In a principal component analysis, 19 subjects showed non-European ancestry, and were consequently excluded from genetic analyses (Supplementary Figure 3). We finally analyzed a total of 2,376 individuals with available complete genotype and serological data, fulfilling all inclusion criteria. Of these, 162 (6.8%) were seropositive, and 2,214 (93.2%) seronegative. Using an allelic model, 580,108 autosomal SNPs were tested, and genomic inflation was low ( $\lambda=1.016$ , Supplementary Figure 4). Two SNPs (rs17850869, rs41289586) exceeded the threshold for genome-wide significance, when correcting for the number of tested SNPs ( $P=8.62E-08$ , Figure 1). A list of 11 SNPs with  $P<1.0E-05$  is provided as Supplementary Table 5, including minor allele frequencies, association statistics, positions, and SNP classifications.

**Table 1** Prevalence of anti-*Borrelia* antibodies

Study Group	Anti- <i>Borrelia</i> AB status - N (%)			P (Pearson`s chi <sup>2</sup> ) (corrected for age & sex)
	Seropositive	Seronegative	Total	
GRAS patients (schizophrenia)	85 (7.9)	991 (92.1)	1,076 (100)	<b>0.05</b>
Affective disorder patients*	16 (10.8)	132 (89.2)	148 (100)	0.07
GRAS controls (healthy subjects)	68 (5.4)	1,203 (94.6)	1,271 (100)	
<b>TOTAL</b>	<b>169 (6.8)</b>	<b>2,326 (93.2)</b>	<b>2,495 (100)</b>	

Cross-sectional prevalence of anti-*Borrelia* antibodies in GRAS (Göttingen Research Association for Schizophrenia) patients, patients with affective disorders (\*included are patients with monopolar or bipolar depression), and healthy GRAS controls. P-values represent results of  $\chi^2$  tests, comparing the respective patient sample with healthy controls. AB, antibodies.

**Supplementary Table S1.** Gender distribution by serostatus.

Gender	<i>Borrelia</i> antibody status - N (%)			P-value (OR, (CI)) chi <sup>2</sup> , d.f. = 1
	Seropositive	Seronegative	Total	
Male	129 (8.2)	1,441 (91.8)	1,570 (100)	1.86-04 (1.98, (1.38 - 2.85))
Female	40 (4.3)	885 (95.7)	925 (100)	
TOTAL	169 (6.8)	2,326 (93.2)	2,495 (100)	

OR, odds ratio; CI, 95% confidence interval.

**Supplementary Table S2.** Mean age of study cohorts by serostatus.

Study group	<i>Borrelia</i> antibody status - Mean age in years (SD)		
	Seropositive	Seronegative	Total
Schizophrenia patients	42.5 (13.3)	39.2 (12.5) *	39.5 (12.6) *
Affective disorder patients	61.3 (15.2) *	48.3 (15.0) *	49.7 (15.5) *
Healthy controls	42.2 (14.1)	37.1 (13.1)	37.4 (13.2)
TOTAL	44.1 (14.8)	38.7 (13.2)	39.0 (13.4)

\* denotes significant difference ( $p \leq 0.05$ ) of patient group versus respective controls. *P* values were calculated using 2-tailed independent samples *t*-tests, equal variances not assumed in case of significant Levene's test. SD, standard deviation.

**Supplementary Table S3.** Anti-borrelia antibody titer distribution.

Study group (seropositives)	Mean	SD	<i>P</i> (GLM), corrected for gender & age
Schizophrenia patients (N=85)	165,998	184,900	0.376
Affective disorder patients (N=16)	118,063	93047	0.339
Healthy controls (N=68)	149,429	166,065	
TOTAL (N=169)	154,793	170,496	

*P* values represent association results, comparing the respective patient sample with healthy controls. SD, standard deviation; GLM, generalized linear model.

**Supplementary Table S4.** Baseline characteristics, according to study group.

Patient and control groups	Total sample	Borrelia-AB +	Borrelia-AB -	P ( $\chi^2$ , Z, T value) <sup>a</sup>
Schizophrenia patients (GRAS)	<i>N</i> =874-1,076 <sup>b</sup>	<i>N</i> =72-85 <sup>b</sup>	<i>N</i> =802-991 <sup>b</sup>	
Age, y, Mean±SD, (range)	39.46±12.59 (17-79)	42.47±13.30 (19-75)	39.21±12.50 (17-79)	<b>0.032</b> (Z=-2.14)
Gender, N male (%)	721 (67.0)	62 (72.9)	659 (66.5)	0.225 ( $\chi^2$ =1.47)
Prodrome, N cases (%)	753 (81.0)	61 (82.4)	692 (80.8)	0.738 ( $\chi^2$ =0.11)
Age at first episode, y, Mean±SD, (range)	26.44±8.89 (5-68)	26.77±8.78 (15-51)	26.41±8.91 (5-68)	0.625 (Z=-0.49)
PANSS positive score, Mean±SD, (range)	13.73±6.25 (7-38)	13.78±6.31 (7-34)	13.72±6.24 (7-38)	0.962 (Z=-0.05)
PANSS negative score, Mean±SD, (range)	18.24±7.93 (7-46)	19.04±7.88 (7-37)	18.17±7.93 (7-46)	0.293 (Z=-1.05)
PANSS general score, Mean±SD, (range)	33.73±11.78 (16-82)	34.88±11.33 (16-75)	33.63±11.81 (16-82)	0.230 (Z=-1.20)
Current chlorpromazine equivalents (CPZ), Mean±SD, (range)	685.38±698.08 (0-7375)	602.90±492.97 (0-2925)	692.36±712.48 (0-7375)	0.620 (Z=-0.50)
Cambridge Neurological Inventory (CNI) <sup>c,d</sup> , Mean±SD, (range)	0.00±1.00 (-2.08-13.80)	0.01±0.86 (-1.82-2.37)	0.00±1.01 (-2.08-13.80)	0.897 (T=-0.13)
MacQuarrie Dotting <sup>e</sup> , Mean±SD, (range)	0.00±1.00 (-3.49-3.51)	0.04±0.98 (-1.83-3.51)	0.00±1.00 (-3.49-3.06)	0.695 (T=-0.39)
MacQuarrie Tapping <sup>e</sup> , Mean±SD, (range)	0.00±1.00 (-4.76-4.03)	0.17±1.00 (-1.69-3.71)	-0.01±1.00 (-4.76-4.03)	0.114 (T=-1.58)
Cognitive Composite score <sup>e</sup> , Mean±SD, (range)	-0.01±0.84 (-2.57-2.98)	-0.09±0.96 (-2.12-1.93)	-0.01±0.83 (-2.57-2.98)	0.390 (T=0.86)
Global Assessment of Functioning (GAF), Mean±SD, (range)	45.76±17.20 (5-90)	44.74±17.23 (8-90)	45.84±17.20 (5-90)	0.490 (Z=-0.69)
Healthy controls (GRAS)	<i>N</i> =1,271	<i>N</i> =68	<i>N</i> =1,203	
Age, y, Mean±SD, (range)	37.42±13.42 (18-69)	42.41±14.14 (19-67)	37.15±13.14 (18-69)	<b>0.003</b> (Z=-3.01)
Gender, N male (%)	779 (61.3)	58 (85.3)	721 (59.9)	<b>&lt;0.001</b> ( $\chi^2$ =17.45)
Affective disorder patients	<i>N</i> =148	<i>N</i> =24	<i>N</i> =124	
Age, y, Mean±SD, (range)	49.68±15.49 (20-92)	61.31±15.16 (44-92)	48.27±14.98 (20-87)	<b>0.004</b> (Z=-2.86)
Gender, N male (%)	70 (47.3)	9 (56.3)	61 (46.2)	0.448 ( $\chi^2$ =0.58)

Abbreviations: AB, antibody; CPZ, chlorpromazine equivalents; GAF, global assessment of functioning; GRAS, Göttingen Research Association for Schizophrenia; PANSS, positive and negative syndrome scale. Bolded values,  $P < 0.05$ . <sup>a</sup>As statistical methods, Mann-Whitney U or  $\chi^2$  tests, and for normally distributed variables,  $t$ -tests were used. <sup>b</sup>Due to missing data, sample sizes vary. <sup>c</sup>Cambridge Neurological Inventory mean value if more than 95 items were available. <sup>d</sup>Corrected for age and CPZ. <sup>e</sup>Corrected for age, PANSS negative score and CPZ.

**Supplementary Table S5.** GWAS hits  $P < 1.0E-05$ .

SNP	Chr.	Mb	Major / minor allele	MAF patients	MAF controls	$P$ (allelic)	OR (95% CI)	Gene (RefSeq, hg19)	Distance (kb)	Class
rs17850869	16	71.9	C/T	0.043	0.008	4.17E-09	5.36 (2.87-10.02)	<i>ZNF821</i>	intragenic	synonymous
rs41289586	3	43.6	C/T	0.071	0.022	7.18E-08	3.38 (2.11-5.39)	<i>ANO10</i>	intragenic	missense
rs4527629	5	163.5	A/G	0.142	0.068	9.95E-07	2.25 (1.61-3.14)	<i>MAT2B</i>	522.4	
rs10267374	7	88.6	C/T	0.247	0.146	1.05E-06	1.92 (1.47-2.51)	<i>ZNF804B</i>	intragenic	intronic
rs10232922	7	88.6	A/G	0.259	0.156	1.29E-06	1.89 (1.46-2.45)	<i>ZNF804B</i>	intragenic	intronic
rs17749281	3	94.2	T/G	0.367	0.249	2.62E-06	1.75 (1.38-2.22)	<i>NSUN3</i>	307.8	
rs2499955	11	5.0	C/T	0.219	0.13	5.33E-06	1.89 (1.43-2.49)	<i>OR51L1</i>	5.6	
rs34796938	10	130.3	C/T	0.103	0.046	5.90E-06	2.38 (1.62-3.51)	<i>PREX2</i>	intragenic	intronic
rs7755387	6	106.2	G/T	0.117	0.056	7.00E-06	2.25 (1.57-3.23)	<i>PRDM1</i>	297.7	
rs4883922	13	73.7	C/T	0.345	0.234	7.30E-06	1.72 (1.36-2.19)	<i>KLF5</i>	2.2	
rs12616914	2	232.0	T/C	0.084	0.035	9.20E-06	2.54 (1.66-3.88)	<i>PSMD1</i>	intragenic	intronic

SNP, single nucleotide polymorphism; Chr., chromosome; Mb, mega base pairs; MAF, minor allele frequency; OR, odds ratio; CI, confidence interval; kb, kilo base pairs.

**Supplementary Table S6.** Association of genome-wide significant hits with other bacterial infections.

Pathogen	rs41289586	rs17850869
	$P$ (allelic) (OR, (95% CI))	$P$ (allelic) (OR, (95% CI))
<i>Borrelia</i>	7.18E-08 (3.38, (2.11-5.39))	4.17E-09 (5.36, (2.87-10.02))
<i>Helicobacter pylori</i>	0.64 (0.90, (0.59-1.39))	0.55 (0.82, (0.42-1.58))
<i>Mycoplasma pneumoniae</i>	0.51 (0.89, (0.62-1.26))	0.59 (1.16, (0.68-1.97))
<i>Chlamydia pneumoniae</i>	0.77 (1.06, (0.71-1.57))	0.81 (0.93, (0.51-1.71))
<i>Chlamydia trachomatis</i>	0.54 (0.87, (0.54-1.38))	0.32 (1.36, (0.74-2.50))
	$P$ (linear regression) (BETA, (95% CI))	$P$ (linear regression) (BETA, (95% CI))
ALL except <i>Borrelia</i> (sum score: 0-4)	0.34 (-0.14, (-0.41-0.14))	0.35 (0.20, (-0.22-0.62))

OR, odds ratio; CI, confidence interval.

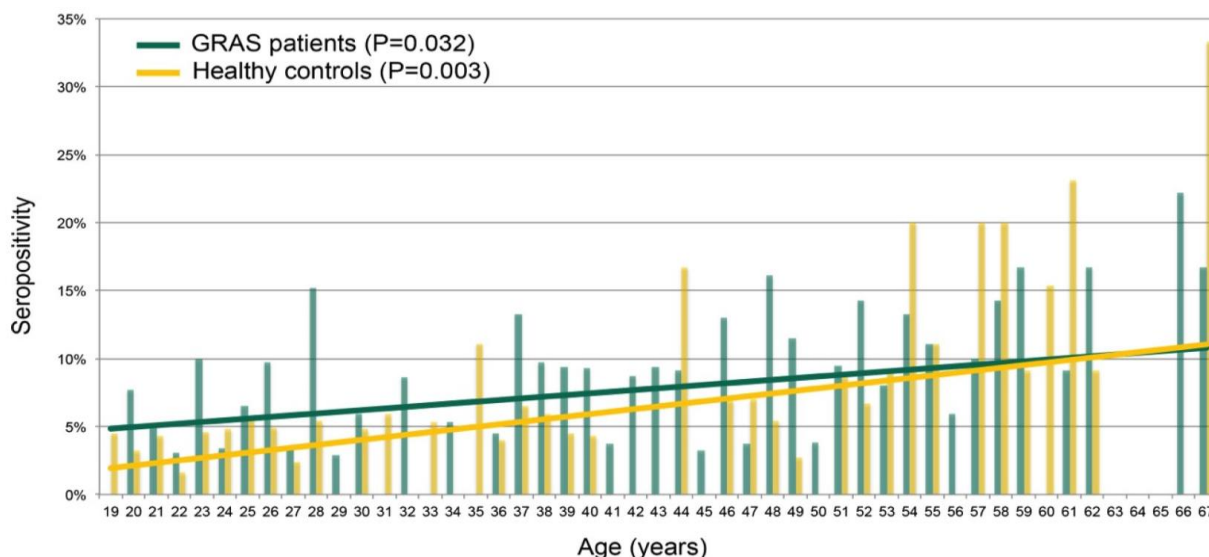


**Fig. S1** Age dependence of seropositivity. Bars represent seroprevalence per year of age, solid lines represent linear trends. Only GRAS patients and healthy controls were included due to the significantly smaller number of affective disorder patients. Patients younger than 19 and older than 67 were not included due to low numbers per year of age. P values are derived from Mann-Whitney-U tests, using seropositivity as grouping variable and age as dependent variable.

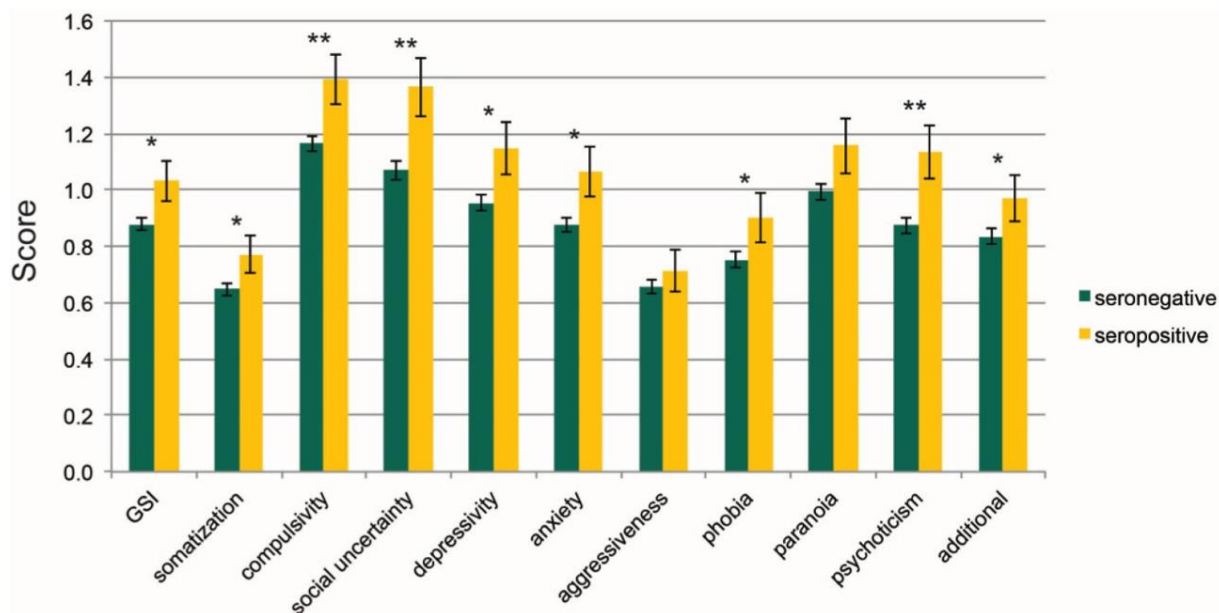


**Fig. S2** Brief symptom inventory (BSI) patient self-assessment GSI, global severity index; \*,  $P < 0.05$ ; \*\*,  $P < 0.005$

Reference: Franke, G.H. *Brief Symptom Inventory*, (Beltz, Göttingen, 2000).

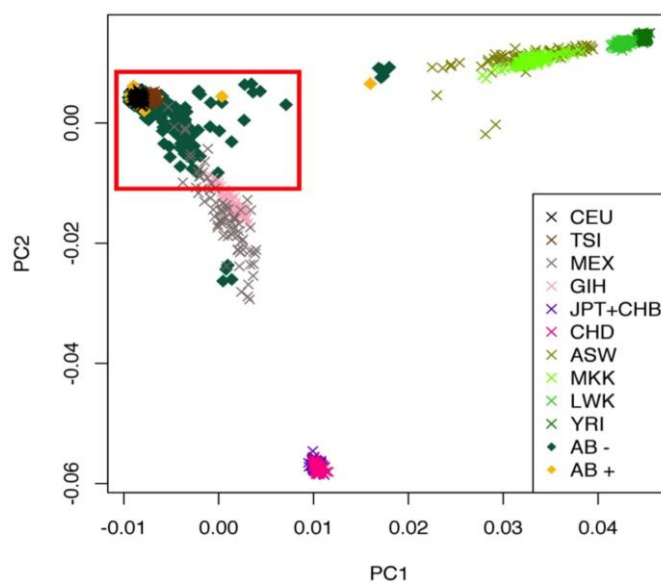


**Fig. S3** Principal component analysis, removal of genetic outliers. Study participants are displayed together with Hapmap version3 r2 samples, according to their first two principal components (PC1, PC2). All subjects clustering outside the red rectangle were excluded from genetic analyses. ASW, African ancestry in Southwest USA; CEU, Utah residents with Northern and Western European ancestry from the CEPH collection; CHB, Han Chinese in Beijing, China; CHD, Chinese in Metropolitan Denver, Colorado; GIH, Gujarati Indians in Houston, Texas; JPT, Japanese in Tokyo, Japan; LWK, Luhya in Webuye, Kenya; MXL, Mexican Ancestry in Los Angeles, California; MKK, Maasai in Kinyawa, Kenya, TSI, Toscani in Italia; YRI, Yoruba in Ibadan, Nigeria; AB -, anti-*Borrelia* negative; AB +, anti-*Borrelia* positive.

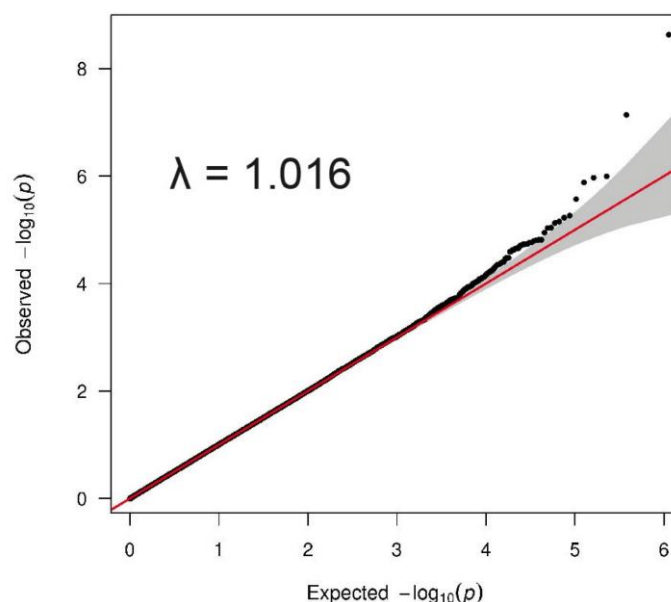


**Fig. S4** Quantile-quantile plot for assessment of population stratification. Quantile-quantile plot of association results. For each tested variant, the  $-\log_{10}$  P-value is plotted against the null distribution (red line, 95% confidence intervals in gray). The highly complex MHC region (chromosome 6, 29-33MB) was removed for assessment of population stratification.  $\lambda$ , genomic inflation factor.

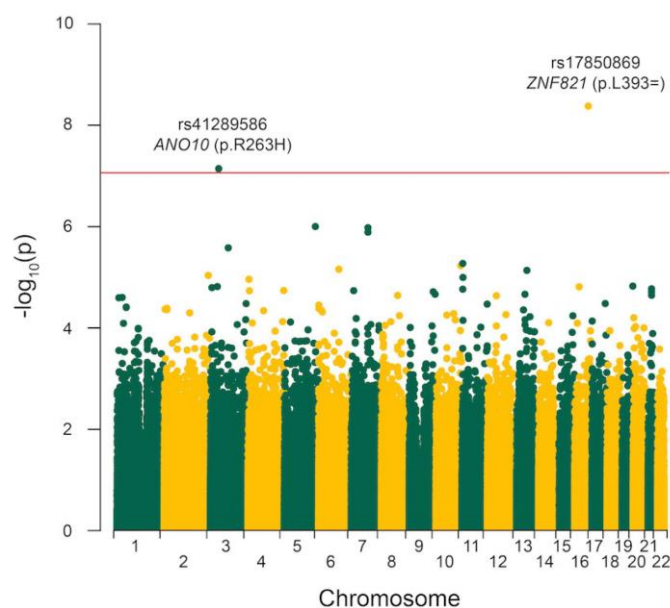


**Fig. 1** Manhattan plot of genome-wide association analysis. The red horizontal line designates the threshold for genome-wide significance, corrected for number of tested SNPs.

### Genome-wide significant hits

Both genome-wide significant SNPs show a low minor allele frequency in seronegative subjects, which is significantly higher in AB carriers (rs17850869: 0.008 versus 0.043; rs41289586: 0.022 versus 0.071, Supplementary Table 5). Genotype distributions are presented in Table 2, where we also display results using additional open-access resources from the 1000 Genomes Project (229) and the Exome Variant Server (NHLBI GO Exome Sequencing Project (ESP), Seattle, WA, URL: <http://evs.gs.washington.edu/EVS/>, access date: July 17, 2014). Overall, these data are highly similar to the distribution in our seronegative population; hence an under-representation of the minor alleles is unlikely to be the source of association. As an exception, the MAF of rs17850869 is higher in the European 1000 Genomes Project study participants (MAF=0.022). This may, however, be a bias of the small number of individuals included there (Table 2).

One of the two genome-wide significant SNPs, rs17850869, is a synonymous coding variant of zinc finger protein 821, encoded by the *ZNF821* gene on chromosome 16 (NP\_001188482.1, p.Leu393), and associated with a P value of  $4.17E-09$  (OR=5.36). It is in complete linkage with only one other SNP, rs74944699, an intronic variant in *PMFBP3*. Of note, the gene upstream of *ZNF821* is *ATXNIL* (ataxin 1-like), a paralog of *ATXN1* (ataxin 1), which is associated with spinocerebellar ataxia type 1 (SCA1) (230).

The other SNP, rs41289586 ( $P=7.18E-08$ , OR=3.38), is a missense variant of anoctamin 10, encoded by the gene *ANO10* (NP\_060545.3, p.R263H) on chromosome 3. It shows

linkage ( $r^2 > 0.8$ ) with two intronic SNPs, rs62250916 in *ANO10*, and rs11926254 in *SNRK*. Using software tools for a prediction of the effect of amino acid substitutions on protein function, the ANO10-R263H variant was predicted to be ‘probably damaging’ (score 1.000) by PolyPhen-2 (<http://genetics.bwh.harvard.edu/pph2/>), ‘deleterious’ (score -4.66) by PROVEAN, and ‘damaging’ (score 0.000) by SIFT (both <http://provean.jcvi.org/>). Notably, also mutations in *ANO10* were reported to be causative for spinocerebellar ataxia (91;93).

We investigated, but did not find an association of either SNP with antibodies against several other bacterial infections (*Helicobacter pylori*, *Mycoplasma pneumoniae*, *Chlamydia pneumoniae*, *Chlamydia trachomatis*). They were also not associated with a sum score including all five serological tests against bacterial infections in a linear regression model (Supplementary Table 6). Both SNPs are not found on commonly used genotyping arrays, and were thus not included previously in GWAS investigating other phenotypes. In our study cohort, they were not associated with the diagnosis of schizophrenia (rs41289586:  $P_{\text{allelic}}=0.11$ , rs17850869:  $P_{\text{allelic}}=0.28$ ).

**Table 2** Genotype and minor allele frequencies of GWAS hits

SNP rsID	Genotypes			MAF	P (allelic test) (OR, [95% CI])
	CC	CT	TT		
<b>rs17850869</b>					
Seropositive	148	14	0	0.043	
Seronegative	2,177	37	0	0.008	4.17E-09 (5.36, [2.87-10.02])
1000g (CEU)	80	5	0	0.029	0.449 (1.49, [0.53-4.21])
1000g (EUR)	362	17	0	0.022	0.061 (1.97, [0.96-4.04])
EVS (EA)	4,148	50	2	0.006	1.50E-13 (6.98, [3.84-12.70])
<b>rs41289586</b>					
Seropositive	140	21	1	0.071	
Seronegative	2,118	96	1	0.022	7.18E-08 (3.38, [2.11-5.39])
1000g (CEU)	80	5	0	0.029	0.058 (2.52, [0.94-6.76])
1000g (EUR)	362	17	0	0.022	1.1E-04 (3.33, [1.75-6.32])
EVS (EA)	4,074	222	4	0.027	2.47E-06 (2.78, [1.78-4.33])

Genotype distribution of GWAS hits in seropositive versus seronegative subjects, as well as in additional control populations. P-values represent results of allelic tests, comparing the respective control sample with the seropositive subjects. rsID, reference SNP ID; MAF, minor allele frequency; OR, odds ratio; CI, confidence interval; 1000g, 1000 genomes project; CEU, Utah Residents (CEPH) with Northern and Western European ancestry panel; EUR, European super population panel; EVS (EA), Exome variant server European American population panel

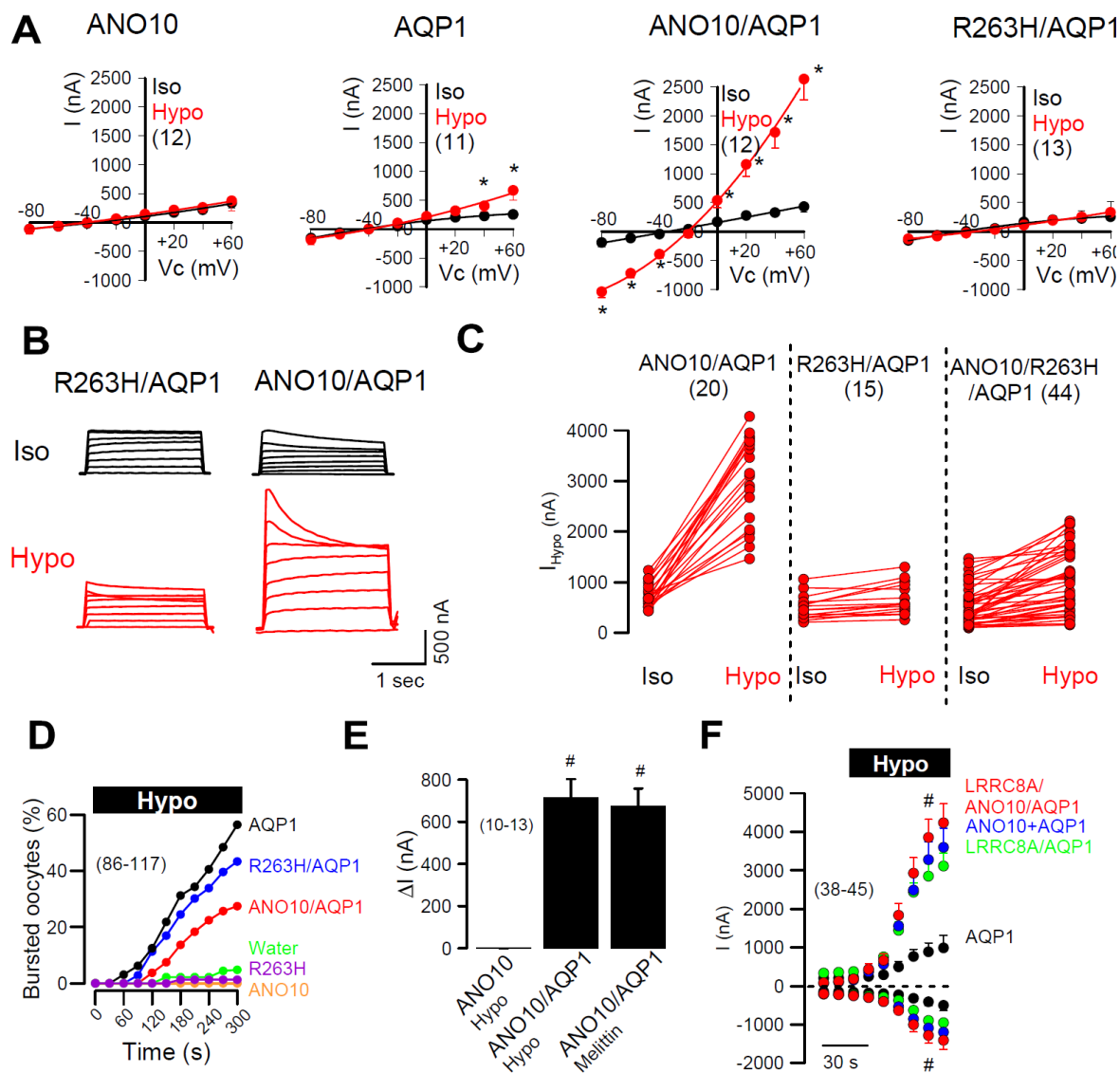


**Fig. 2** ANO10 but not R263H-ANO10 generates volume activated whole cell currents in *Xenopus* oocytes. **A**) Current/voltage relationships of whole cell currents activated by cell swelling ( $I_{\text{Hypo}}$ , 50 % reduced extracellular osmolarity) in *Xenopus* oocytes. R263H-ANO10 does not produce  $I_{\text{Hypo}}$ . **B**) Current overlay ( $V_c = \pm 100$  mV) demonstrates typical time dependent inactivation of  $I_{\text{Hypo}}$ . **C**)  $I_{\text{Hypo}}$  in oocytes expressing AQP1/ANO10, AQP1/ANO10-R263H, and AQP1/ANO10/ANO10-R263H, respectively. Coexpression of ANO10-R263H suppressed currents produced by wt ANO10. **D**) Oocyte bursting after exposure to hypotonic bath solution. Fraction of bursted oocytes was reduced by expression of ANO10. Oocytes survived in the absence of AQP1. **E**) Summary of whole cell currents activated by Hypo and the  $\text{PLA}_2$ -activator melittin (100 nM). **F**) Summary of time dependent activation of whole cell currents in cells expressing ANO10, LRRC8A, or coexpressing both. All oocytes expressed AQP1. Mean  $\pm$  SEM (number of oocytes); \*significant activation by Hypo (paired t-test). # significant difference to ANO10 and ANO10/AQP1, respectively (unpaired t-test).

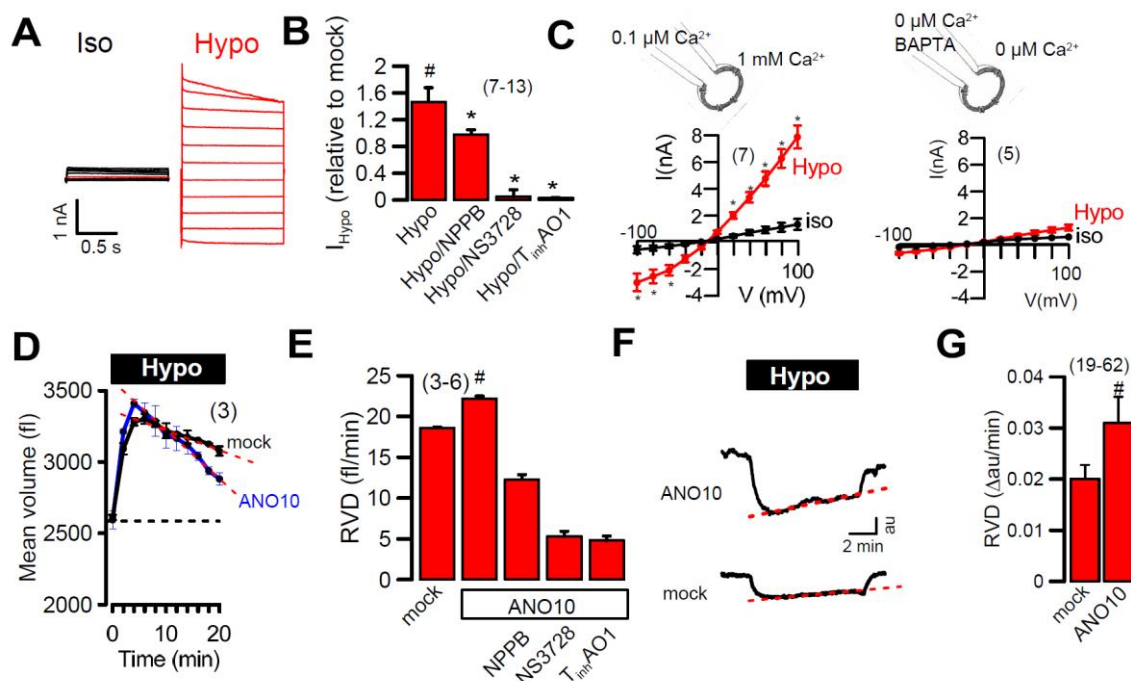


**Fig. 3** ANO10 affects volume activated whole cell currents in HEK293 cells. **A)** Whole cell currents ( $V_c = \pm 100$  mV) activated by cell swelling ( $I_{Hypo}$ , 33% reduced extracellular osmolarity) in ANO10-expressing cells. **B)** Swelling induced currents ( $I_{Hypo}$ ) in ANO10-expressing cells relative to mock transfected cells, and inhibition by NPPB (50  $\mu$ M), NS3728 (5  $\mu$ M), and  $T_{inh}AO1$  (20  $\mu$ M). **C)** I/V curves indicating loss of  $I_{Hypo}$  with complete elimination of  $Ca^{2+}$  and preincubation with BAPTA (50  $\mu$ M, 30 min). **D)** Regulation of cell volume in the presence of Hypo (regulatory volume decrease, RVD) in mock transfected cells or cells overexpressing ANO10 (flow cytometry). **E)** RVD in mock transfected cells or cells overexpressing ANO10, and inhibition by NPPB, NS3728, and  $T_{inh}AO1$ . **F)** Re-shrinkage of cells exposed to hypotonic bath solution (RVD), measured in single cells loaded with calcein. **G)** Comparison of RVD (measured by calcein fluorescence) obtained in mock-transfected and ANO10-overexpressing cells. Mean  $\pm$  SEM (number of cells); \*significant inhibition (paired t-test). #significant difference to mock (unpaired t-test).

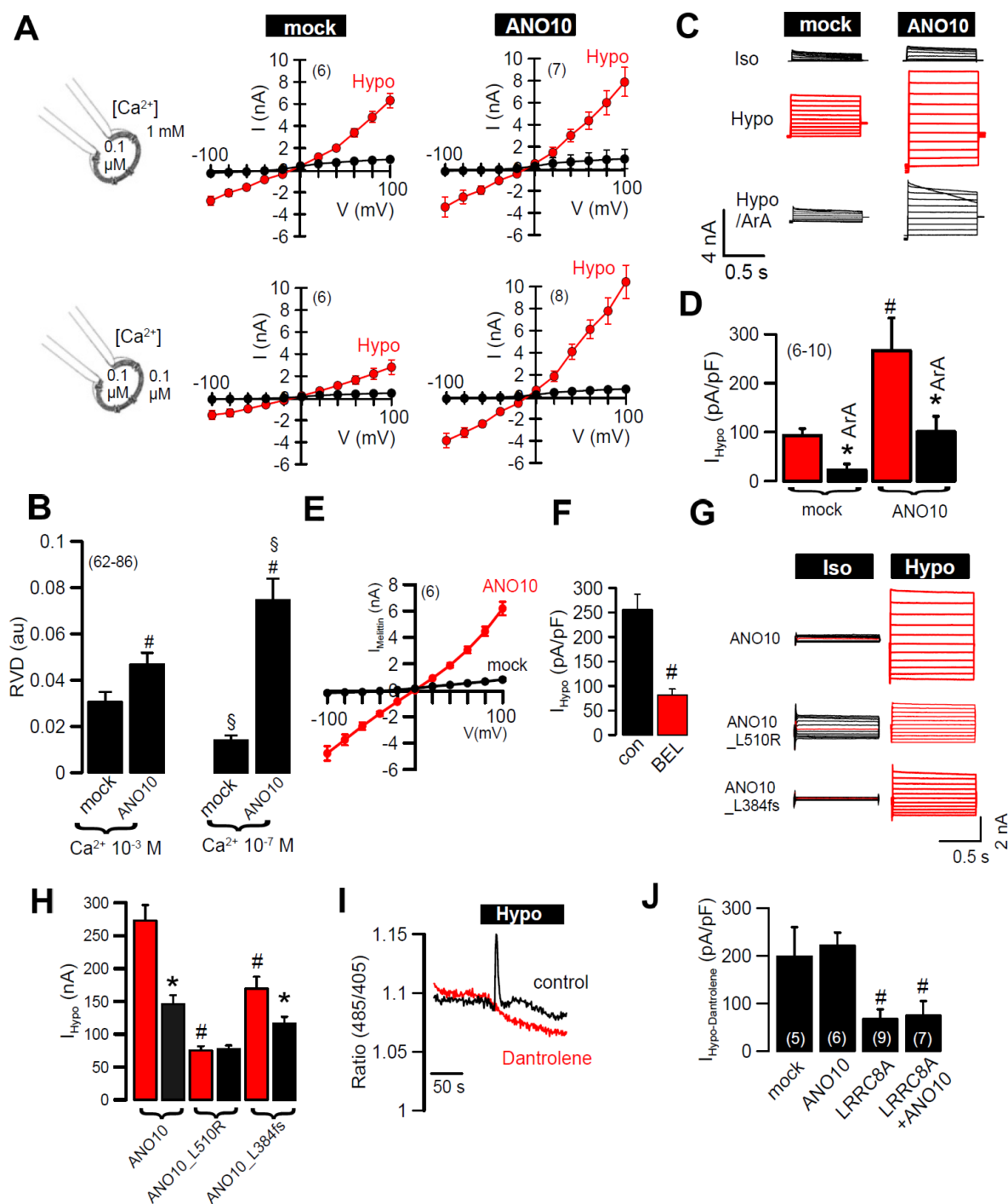


**Fig. S5** ANO10 increases  $I_{Cl\text{-swell}}$  and volume regulation in HEK293 cells **A**) I/V relationship of currents activated by hypotonic bath solution ( $I_{Hypo}$ ) in mock-transfected and ANO10-overexpressing HEK293 cells in the presence of normal ( $10^{-3}$  M) and low ( $10^{-7}$  M) extracellular  $Ca^{2+}$ . Note that ANO10 induces larger  $I_{Hypo}$  when extracellular  $Ca^{2+}$  is low. **B**) Summary of RVD in mock-transfected and ANO10-overexpressing HEK293 cells in the presence of normal ( $10^{-3}$  M) and low ( $10^{-7}$  M) extracellular  $Ca^{2+}$ , as measured in single cell calcein fluorescence assays. **C**) Activation of  $I_{Hypo}$  in mock-transfected and ANO10-overexpressing HEK293 cells and inhibition by arachidonic acid (50  $\mu$ M). **D**) Summary of the current measurements shown in C). **E**) I/V relationship of whole cell currents activated by the  $PLA_2$  activator melittin (100 nM). **F**) Inhibition of  $I_{Hypo}$  by the inhibitor of phospholipase A2,

bromoellactone (BEL; 30  $\mu$ M). **G**) Activation of  $I_{Hypo}$  in HEK293 cells expressing wt ANO10 and two mutants reported in autosomal-recessive cerebellar ataxia. **H**) Summary of the current measurements shown in G). **I**) Intracellular  $Ca^{2+}$  as measured by GCAMP2, showing inhibition of Hypo-induced  $Ca^{2+}$  release with dantrolene (10  $\mu$ M), a blocker of the ryanodine receptor. **J**) Summary of  $I_{Hypo}$  in the presence of dantrolene. Note that i) ANO10 did not increase  $I_{Hypo}$  and ii) LRRC8A inhibited  $I_{Hypo}$  significantly different to mock, ANO10, and con, respectively (unpaired t-test). \*Significant effect of Ara and NPPB, respectively (paired t-test). §significantly different to high  $Ca^{2+}$  (unpaired t-test). (number of cells).

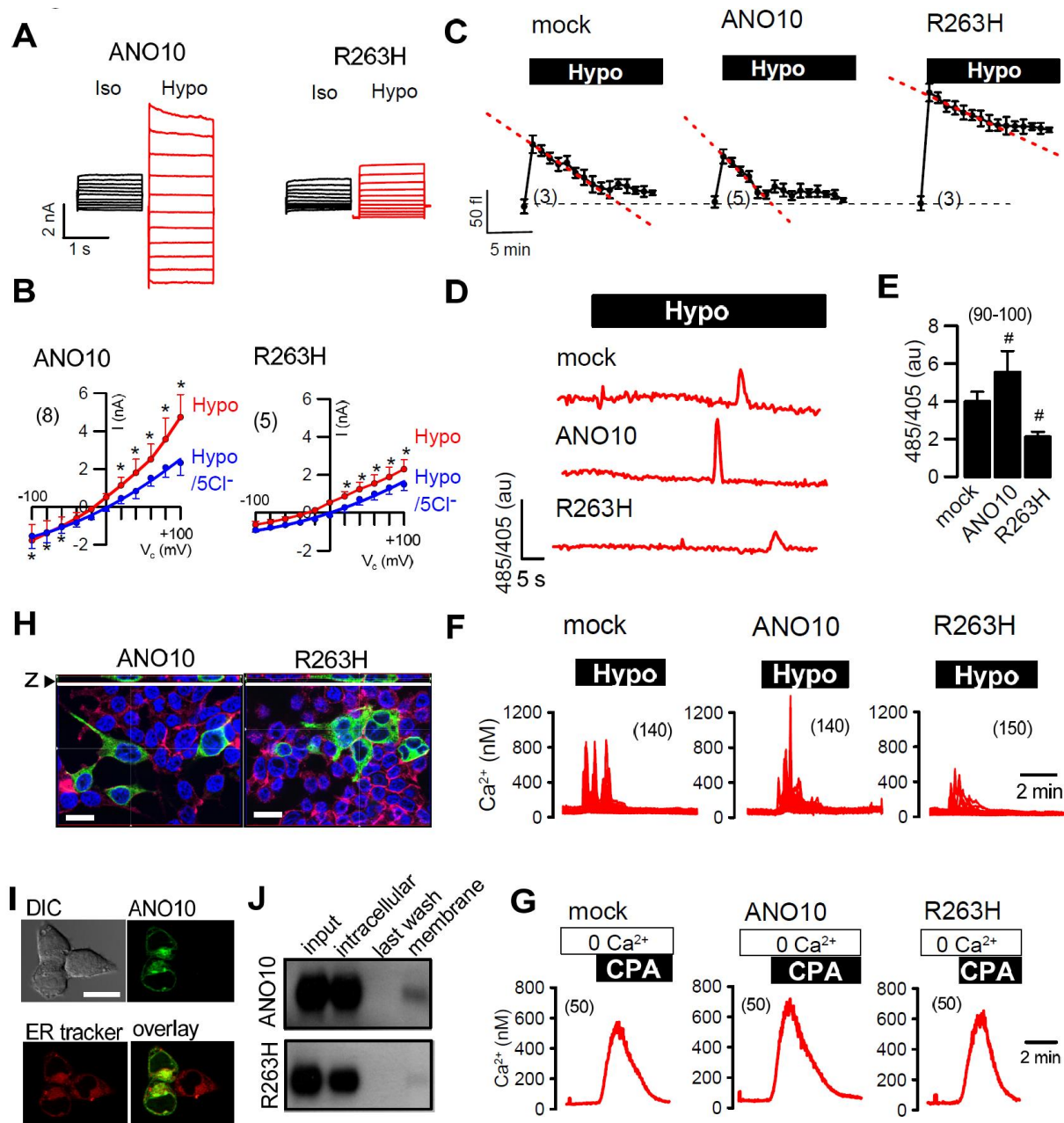


**Fig. 4** R263H inhibits volume regulation,  $I_{Hypo}$ , and intracellular  $Ca^{2+}$  signaling in HEK293 cells. **A**) Whole cell currents ( $V_c = \pm 100$  mV) activated by cell swelling ( $I_{Hypo}$ , 33 % reduced extracellular osmolarity) in cells expressing ANO10 and R263H-ANO10 (R263H). **B**) Current/voltage relationships for  $I_{Hypo}$  and inhibition of  $I_{Hypo}$  by removal of  $Cl^-$  from the

extracellular bath solution (5Cl). **C**) Regulation of cell volume in the presence of Hypo (regulatory volume decrease, RVD) in cells expressing ANO10 or R263H (flow cytometry). **D**) Effect of cell swelling on intracellular  $[Ca^{2+}]_i$  in cells expressing ANO10 or R263H or mock transfected cells, as measured by the  $Ca^{2+}$  sensor GCAMP2. **E**) Summary of the effects of cell swelling on  $[Ca^{2+}]_i$  (485/405 fluorescence emission ratio) in ANO10 and R263H expressing cells. **F**) Collected recordings of the effects of cell swelling on  $[Ca^{2+}]_i$ , measured by Fura2. **G**) Collected recordings of the effects of ER-store emptying by cyclopiazonic acid (CPA; 10  $\mu$ M) on  $[Ca^{2+}]_i$ , measured by Fura2. **H**) Confocal images of cells expressing ANO10 or R263H suggesting weak membrane expression. **I**) Live staining of ANO10-GFP (green) and ER (ER-tracker; red) suggesting ER localization of ANO10. **J**) Membrane biotinylation of cells expressing ANO10 or R263H, suggesting low membrane expression of ANO10, which is even reduced for R263H. Mean  $\pm$  SEM (number of experiments); #significant difference when compared to mock (ANOVA); §significant difference when compared to ANO10 (ANOVA). Bar = 20  $\mu$ m. Numbers are given in the graph in parenthesis.

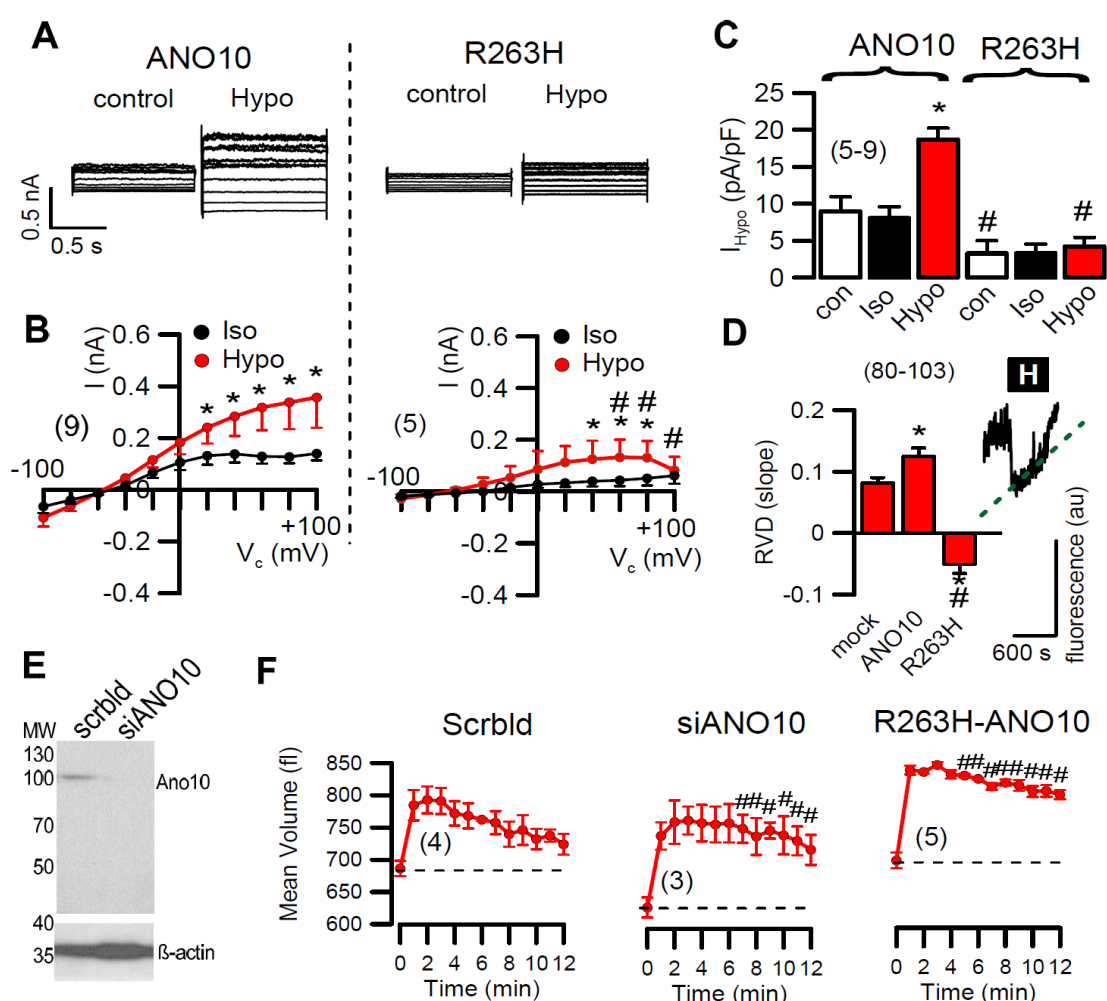


**Fig. S6** R263H eliminates swelling induced currents and RVD in B-lymphocytes **A**) Swelling induced (Hypo; 35% reduced tonicity) currents in human B-lymphocytes expressing ANO10 or ANO10-R263H. **B**) Current/voltage relationships obtained in ANO10 and ANO10-R263H expressing cells. **C**) Summary of  $I_{Hypo}$  densities in ANO10 and ANO10-R263H overexpressing lymphocytes. Note that  $I_{Hypo}$  is absent in ANO10-R263H overexpressing cells. **D**) RVD (regulatory volume decrease) = re-shrinkage from hypotonic swelling. Inset shows original summary trace of the Hypo- induced fluorescence change (arbitrary units, au) in

calcein loaded lymphocytes. Note that RVD was absent in cells expressing ANO10-R263H. Mean  $\pm$  SEM (number of experiments). **E**) Western blot indicating knockdown of ANO10 expression in human B-lymphocytes. **F**) Regulatory volume decrease (RVD) as measured by flow cytometry, indicating delayed RVD after siRNA knockdown of ANO10 in lymphocytes and after overexpression of ANO10-R263H. \*significant activation by Hypo (paired t-test). #significant difference when compared with ANO10, mock, or scrambled, respectively (unpaired t-test). (number of cells).

### **Compromised cellular volume regulation by ANO10-R263H**

ANO10 belongs to a family of 10 proteins which operate as  $\text{Cl}^-$  channels and phospholipid scramblases (70;123;137;231;232). Structural insights into TMEM16/anoctamin proteins were provided recently (138). R263 is located close to the dimer interface and is well conserved within the anoctamin family and between species (Supplementary Fig. 8B,C). Anoctamins have been reported earlier to be relevant for cellular volume regulation (86;87;96), which is essential for cell migration and immune defense (108). Anoctamins may be part of a channel or regulatory complex that produce volume regulated anion currents ( $I_{\text{Hypo}}$ ) activated by hypotonic bath solution (Hypo). An essential component of such a complex has been identified as LRRC8 (134;135). We examined the role of ANO10 for volume regulation by coexpression with aquaporin 1 in *Xenopus* oocytes, which swell and eventually burst when exposed to Hypo (144). Expression of ANO10, but not R263H-ANO10, produced large outwardly rectifying whole cell currents ( $I_{\text{Hypo}}$ ) when oocytes were exposed to Hypo (Fig. 2A,B). Coexpression of R263H-ANO10 together with ANO10 suppressed activation of  $I_{\text{Hypo}}$  (Fig. 2C). Moreover, bursting of oocytes due to Hypo-induced swelling was reduced by ANO10 but not by R263H-ANO10 (Fig. 2D). Noteworthy, activation of phospholipase A2 by melittin, a known activator of  $I_{\text{Hypo}}$ , also activated ANO10. Moreover, coexpression of LRRC8A, which itself induced  $I_{\text{Hypo}}$ , did not further augment  $I_{\text{Hypo}}$  produced by ANO10 (Fig. 2E,F). Taken together, ANO10 but not R263H-ANO10 generates swelling activated whole cell currents in oocytes.

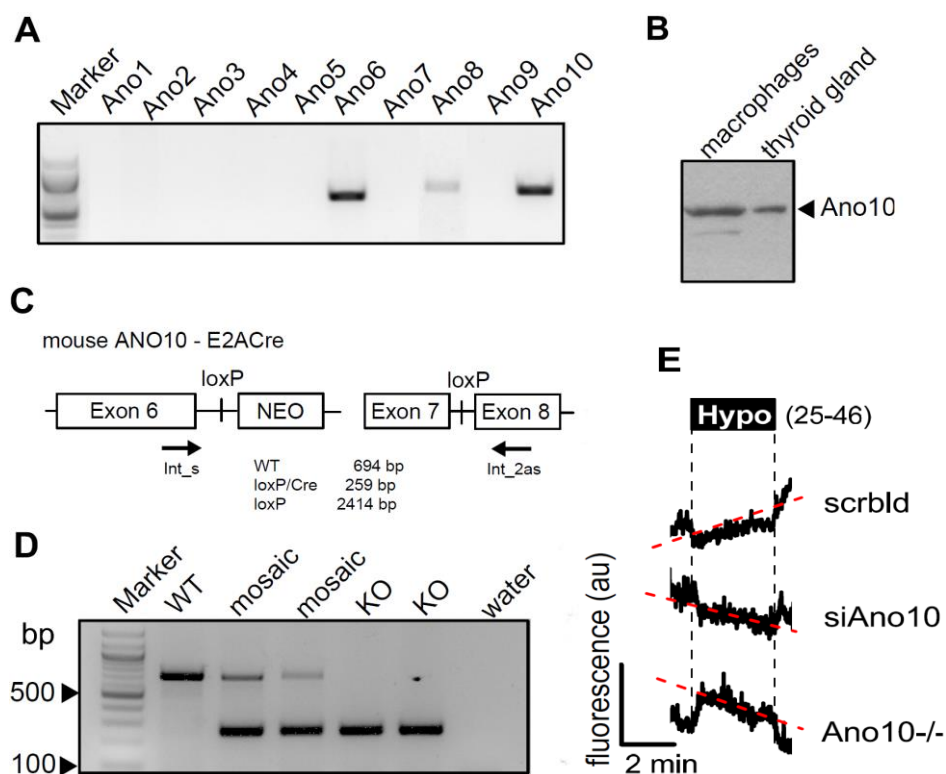


**Fig. S7** Role of ANO10 for volume regulation in mouse macrophages **A**) RT-PCR analysis of anoctamin expression in freshly isolated mouse peritoneal macrophages. **B**) Western blot indicating expression of ANO10 in mouse macrophages and thyroid gland, which is known to express high levels of ANO10. **C**) Generation of ANO10 KO animals by crossbreeding ANO10 loxP/loxP mice with E2A-Cre animals. **D**) Genomic analysis demonstrating ANO10 knockout. **E**) Summary traces of single cell fluorescence in calcein loaded cells (arbitrary units, au). Exposure of macrophages to hypotonic bath solution (Hypo; 33% reduced tonicity) induced cell swelling (loss of fluorescence), from which control cells (treated with scrambled RNA; scrblid) quickly recovered (RVD; regulatory volume decrease). In contrast, siRNA-knockdown of ANO10 or ANO10 knockdown in ANO10 loxP/loxP/E2a-Cre animals abolished RVD. (number of cells).

We also expressed ANO10 in HEK293 cells and found enhanced whole cell currents activated by Hypo, which were inhibited by typical anoctamin blockers such as NPPB, NS3728, and  $T_{inh}A01$  (Fig. 3A,B). Currents could not be activated in the complete absence of  $Ca^{2+}$ , but were augmented, along with an increase in volume regulation (regulatory volume decrease, RVD), when only extracellular  $Ca^{2+}$  was reduced to  $0.1 \mu M$  (Fig. 3C, Supplementary Fig. S5A,B).  $I_{Hypo}$  was inhibited by arachidonic acid, confirming earlier reports (233), and was controlled by phospholipase A2 (Supplementary Fig. S5C-F). Notably,  $I_{Hypo}$  was significantly reduced by expression of two ANO10-mutants that have been reported to cause cerebellar ataxia (93;95) (Supplementary Fig. S5G,H). Expression of ANO10 augmented RVD during exposure to Hypo, when measured by flow cytometry or single cell

imaging of calcein loaded cells (Fig. 3D-G). These data establish a role of ANO10 for volume regulation in mammalian cells.

In contrast to wt ANO10, R263H-ANO10 failed to produce large  $I_{\text{Hypo}}$ , and compromised RVD in HEK293 cells (Fig. 4A-C). Virtually identical results were obtained when ANO10 and R263H-ANO10 were expressed in lymphocytes (Supplementary Fig. 6). Immunocytochemistry and membrane biotinylation showed weak membrane expression of ANO10 and R263H-ANO10 and suggested primarily a location of ANO10 in the endoplasmic reticulum (ER) (Fig. 4H-J). Using the plasma membrane targeted  $\text{Ca}^{2+}$  sensitive protein GCAMP2 (Fig. 4D,E), or conventional Fura2 imaging (Fig. 4F), we found that Hypo induced a delayed transient rise in intracellular  $\text{Ca}^{2+}$  which was augmented by ANO10, but reduced by R263H-ANO10. However, ANO10 does not seem to affect the filling of the ER  $\text{Ca}^{2+}$  store, since the SERCA pump inhibitor CPA induced a similar  $\text{Ca}^{2+}$  increase in the absence or presence of ANO10 (Fig. 4G). Hypo induced store release occurred through dantrolene-sensitive ryanodine receptors (234). In the presence of dantrolene,  $I_{\text{Hypo}}$  was not augmented by ANO10 (Supplementary Fig. 5A,I,J). Taken together R263H-ANO10 may compromise volume regulation by participating in an ion channel complex or by controlling intracellular  $\text{Ca}^{2+}$  signaling (Supplementary Fig. 8A).

### **Compromised macrophage function in the absence of ANO10**

Macrophages are within the first line of defense during infection with *Borrelia* (235). We found that ANO10 is expressed along with ANO6 in human THP-1 macrophages as well as freshly isolated mouse peritoneal macrophages (Fig. 5A,B; Supplementary Fig. 7A,B). In THP-1 macrophages, ANO10 was located mostly intracellularly (Fig. 5C). RVD was examined in single cells by loading macrophages with calcein. Recovery from Hypo-induced cell swelling (RVD) was reduced after siRNA-knockdown of ANO10 (Fig. 5D,E). Similar results were obtained in mouse macrophages in which ANO10 expression was inhibited by siRNA or was knocked down in ANO10<sup>lox/lox</sup>/E2A-cre mice (Supplementary Fig. 7C-E). The results indicate that ANO10 is important for volume regulation also in human and mouse macrophages.

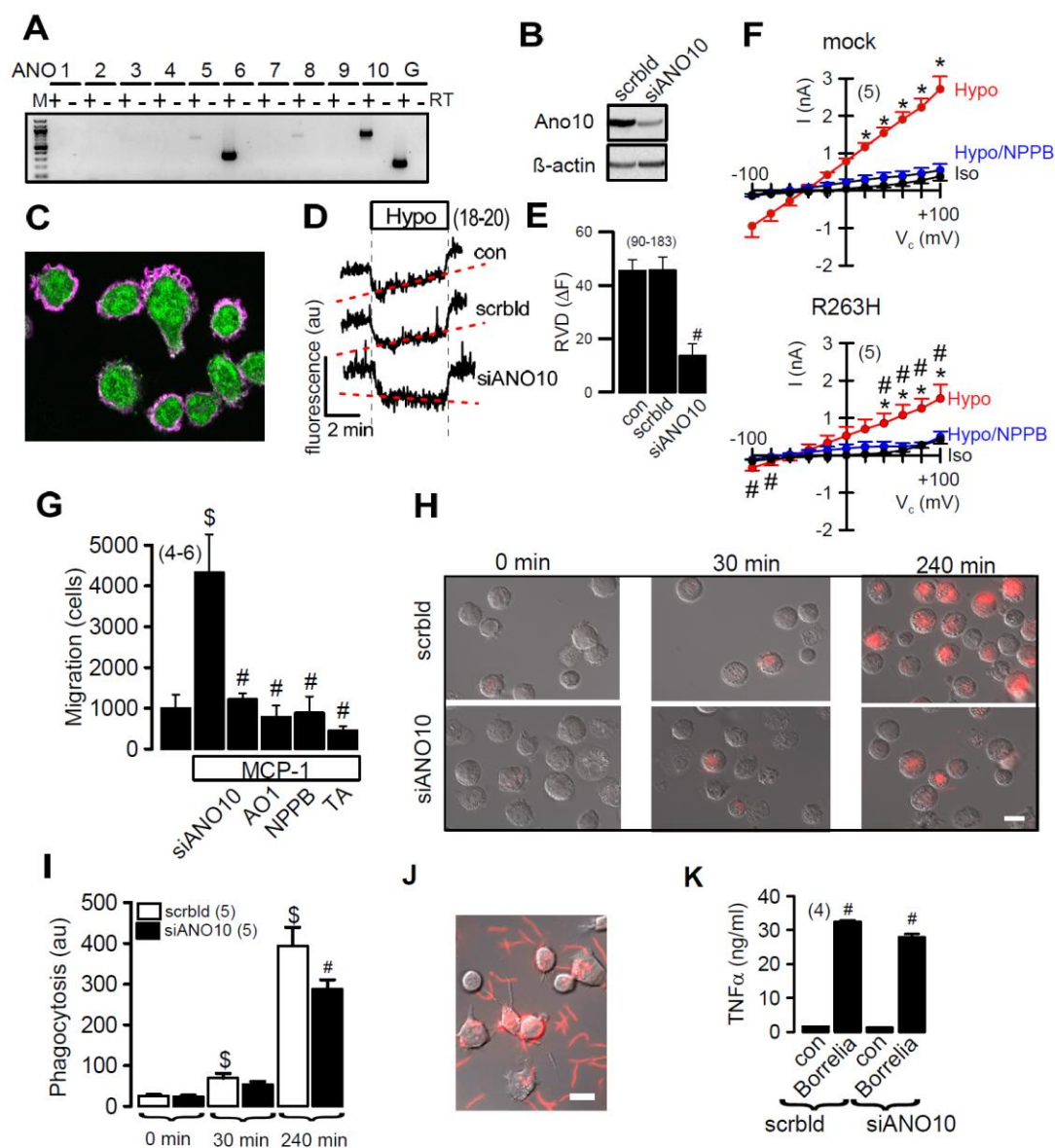


**Fig. 5** Role of ANO10 for volume regulation in macrophages. **A)** RT-PCR analysis of anoctamin expression in THP-1 macrophages. **B)** Western blot indicating knockdown of ANO10-expression by siRNA. **C)** ANO10 (green) and peripheral actin (rhodamin-phalloidin) of THP-1 cells suggesting dominant intracellular location of ANO10. **D)** Summary trace for re-shrinkage of cells exposed to hypotonic bath solution (RVD), measured in single cells loaded with calcein. RVD was abolished after siRNA-knockdown of ANO10. **E)** Summary of RVD measured by absolute fluorescence change. **F)** I/V curves indicating reduced  $I_{Hypo}$  in R263H-expressing cells. **G)** Migration assay in Boyden chambers. MCP-1 induced migration was inhibited by siRNA knockdown of ANO10, and anoctamin inhibitors  $T_{inh}AO1$  (20  $\mu$ M), NPPB (50  $\mu$ M), or tannic acid (TA, 10  $\mu$ M). **H)** THP-1 cells exposed to red-fluorescent cherry-labeled *B. garinii*. Accumulation of cytosolic fluorescence, indicating progressing phagocytosis of *Borrelia* by THP-1 cells. **I)** Increase in fluorescence intensity as a measure of phagocytic activity. **J)** Exposure of THP-1 cells to cherry-labelled *B. garinii*. **K)** Release of  $TNF\alpha$  upon exposure to *B. garinii* was not affected by siRNA-knockdown of ANO10. Mean  $\pm$  SEM (number of cells or assays). # significant difference when compared to scrambled, MCP-1 alone, mock, or con (ANOVA). \$ significant increase in migration and phagocytosis, respectively (unpaired t-test). Bar = 20  $\mu$ m.

Similar to the experiments in oocytes, also in macrophages expression of ANO10-R263H inhibited  $I_{\text{Hypo}}$  (Fig. 5F).  $I_{\text{Hypo}}$  and volume regulation is a prerequisite for cell migration and thus crucial for eradication of spirochetes (108;236). We therefore examined migration of macrophages, which was induced by monocyte chemoattractant protein 1 (MCP-1). Migration was largely reduced by siRNA-knockdown of ANO10, and was inhibited by typical anoctamin blockers (Fig. 5G). Cell viability was not affected by these procedures (data not shown). Because cell migration and phagocytic activity of macrophages will determine the efficacy of spirochete eradication (108;236), we examined phagocytosis of red-fluorescent cherry-labeled *B. garinii* by THP-1 macrophages. Phagocytosis of *B. garinii* was significantly reduced after siRNA-knockdown of ANO10 (Fig. 5H, I). Exposure to *B. garinii* induced a strong release of the major cytokine TNF $\alpha$  by THP-1 cells, which was not affected by knockdown of ANO10 (Fig. 5J, K). No immediate cell death was observed upon exposure and phagocytosis of *B. garinii*, but apoptosis of THP-1 macrophages was reduced 6 days post-exposure to *B. garinii*, which may allow *B. garinii* to circumvent innate defense (data not shown). Taken together, the present results suggest that ANO10 is important for volume regulation of macrophages, and for their role in innate immunity. Eradication of spirochetes may be compromised in carriers of the ANO10 variant R263H.

### Phenotypes in borreliosis patients

In a subsequent exploratory human study, we wondered whether patients with laboratory-confirmed borreliosis, carrying the ANO10-R263H variant would differ in any respect from non-carriers. Specifically, due to the potential association of both identified SNPs with cerebellar ataxia, we searched for a potential overrepresentation of cerebellar ataxia-like symptoms that have also been reported previously in cases of neuroborreliosis (237). To address this question, we recruited prospectively 100 patients with laboratory-confirmed diagnosis of borreliosis. Patients had a mean age of 56.3 years (standard deviation: 16.0 years, range: 15-86 years), 58% were male. Classical clinical correlates of neuroborreliosis (including meningitis, radiculitis, cranial nerve palsy, ataxia, dizziness, encephalitis) were present in 30, of systemic Lyme borreliosis (including erythema migrans, arthralgia, myalgia, headache, malaise, nausea, dizziness) in 20 patients. A total of 50 patients had just a laboratory-based diagnosis without typical clinical signs and symptoms; 4 out of these 100 individuals carried the rs41289586 risk allele (T, ANO10-R263H variant), and 2 of 100 had the rs17850869 risk allele (T); all were heterozygous (CT) for these risk SNPs. Of the 6 (4+2) risk allele carriers, 5 had the diagnosis borreliosis without typical clinical symptoms (only laboratory signs of infection) in contrast to 45 of 94 non-carriers (5/6 versus

45/94: Fisher’s exact  $P=0.20$ ). Moreover, 3/6 had cerebellar symptoms in contrast to 28/94 (3/6 versus 28/94: Fisher’s exact  $P=0.37$ ). Apart from these potentially interesting hints that would need to be consolidated in larger follow-up studies, no prominent clinical differences were detected.

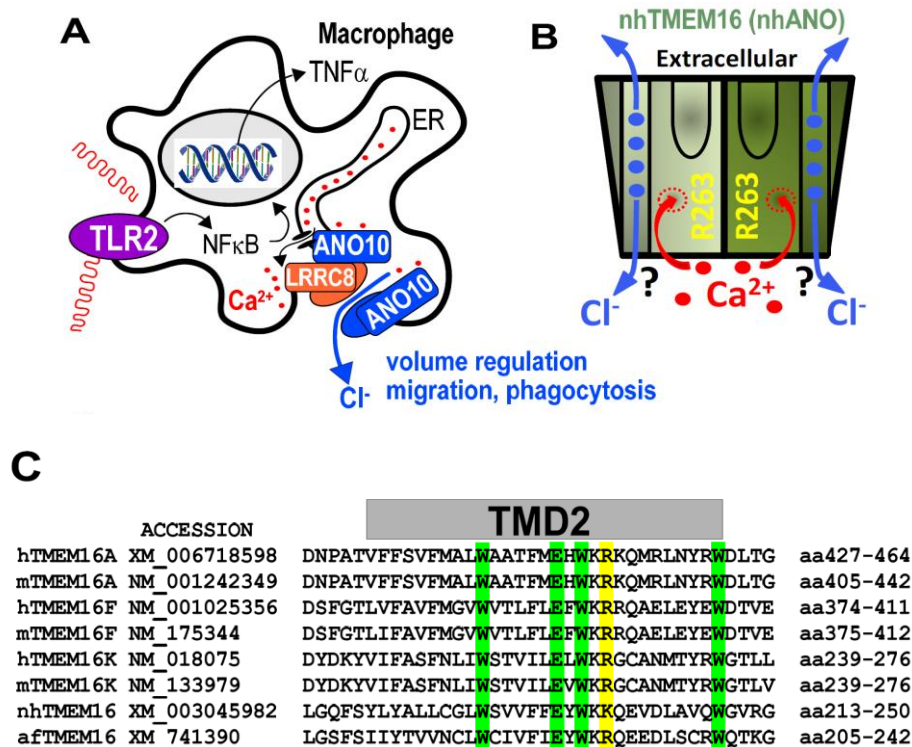


**Fig. S8** ANO10 in macrophages, putative structure and location of R263 **A)** Hypothetical model for the role of ANO10 in immune cells such as macrophages. **B)** Putative structure of nhTMEM16 which exists as a dimer, and location of R263 close to dimerization interface. It is currently unclear whether the two lateral subunit cavities, which serve as conductive pores for polar head groups of phospholipids during phospholipid scrambling, also form Cl<sup>-</sup> conducting channels. Activation by Ca<sup>2+</sup> requires Ca<sup>2+</sup> to move to their binding sites deep in the membrane localized part of nhTMEM16 (Brunner et al.: X-ray structure of a calcium-activated TMEM16 lipid scramblase (2014) Nature). **C)** R263 is located in the putative 2. Transmembrane domain. R263 (related to ANO10) is conserved in ANO1, ANO6, ANO10 and afTMEM16 (highlighted in yellow). In nhTMEM16 R (Arg)263 is replaced by K (Lys) (Higgins et al: Improving the sensitivity of progressive multiple sequence alignment through sequence weighting, positionsspecific gap penalties and weight matrix choice. (1994) Nucleic Acids Research).

## Discussion

In the first GWAS on *Borrelia* antibody serostatus, we identified two host genomic variants mediating differential susceptibility to *Borrelia* seropositivity. Interestingly, both variants, located on chromosomes 3 and 16, happen to be in some context with spinocerebellar

ataxia (93;95). The SNP on chromosome 3, rs41289586, represents the missense variant ANO10-R263H, encoded by the gene *ANO10*. We provide here first evidence of this variant modifying normal host defense. The role of the variant on chromosome 16, rs17850869, a synonymous SNP in *ZNF821* is presently less clear. Addressing the second objective of the present study, i.e. to potentially relate *Borrelia* seropositivity to core phenotypes of neuropsychiatric disorders, we obtained a significantly higher symptom load of seropositive versus seronegative individuals in essentially all items of the BSI (226) self-rating scale.

Macrophage function is essential for eradication of *Borrelia* (235). We recently found a role of anoctamin 6 (ANO6) for immune functions of macrophages (139), while volume regulation by anoctamins has been reported earlier (86;87;96). We therefore analyzed the role of ANO10 for volume regulation and found that  $I_{\text{Hypo}}$  and RVD are depending on ANO10 in oocytes, HEK293 cells, lymphocytes, and macrophages. The properties of ANO10-induced  $I_{\text{Hypo}}$  correspond well to those described for VRAC (reviewed in (15;132;140)). How does ANO10 control  $I_{\text{Hypo}}$  and thereby affect RVD? It could be a binding partner of the essential VRAC component LRRC8A (134;137), although we did not find a potentiation of  $I_{\text{Hypo}}$  by coexpression of ANO10 and LRRC8A in oocytes, and in HEK293 cells exogenous LRRC8A was even inhibitory on  $I_{\text{Hypo}}$ . Interestingly, no  $I_{\text{Hypo}}$  was found when we expressed a LRRC8A mutant lacking the leucine-rich repeat (LRCC8A-D367stop; data not shown), suggesting a role of the LRR-motif for  $I_{\text{Hypo}}$ . Moreover, LRCC8A-D367stop inhibited ionomycin-activation (1  $\mu\text{M}$ ) of endogenous xANO1 currents by  $43 \pm 5.8\%$  ( $n = 27$ ), and abolished  $I_{\text{Hypo}}$  in ANO10 expressing oocytes. This suggests a functional relationship between LRRC8A and anoctamins. ANO10 may also control compartmentalized  $\text{Ca}^{2+}$  signals that have been shown to be important for activation of  $I_{\text{Hypo}}$  (158;234).

R263H-ANO10 had a dominant negative effect on this ANO10 function. Due to the location of R263 close to the dimer interface, the mutation could interfere with dimerization of ANO10 thereby affecting biosynthesis and/or protein function (138) (Supplementary Fig. 8b,C). R263H compromised volume regulation, migration and phagocytosis, thereby reducing spirochete clearance. Interestingly another member of the anoctamin family, ANO9 (*TMEM16J*) is of potential relevance for the defense against *Mycobacteriae*, because polymorphisms in the *PKP3-SIGIRR-TMEM16J* gene region were found to be associated with higher susceptibility to tuberculosis (238).

Notably, mutations in ANO10 were found to cause spinocerebellar ataxia (93;95), which is also a reported phenotype of neuroborreliosis (237). Similar to R263H, also these mutations inhibited  $I_{\text{Hypo}}$  in our present report. We may speculate that ANO10-R263H and putative

further variants convey a genetic predisposition to cerebellar ataxia, possibly requiring an ‘additional hit’ in form of an infection to trigger symptoms. The second associated SNP, rs17850869, is a synonymous variant in *ZNF821*. As mentioned earlier, the gene upstream of *ZNF821* is *ATXNIL* (ataxin 1-like), a paralog of *ATXN1* (ataxin 1), which is associated with spinocerebellar ataxia type 1 (SCA1) (230). In mice, a role of *Atxn1l* in SCA1 pathology was recently demonstrated (239).

Although half of our study participants carry a neuropsychiatric diagnosis, our study design did not allow us to investigate whether *Borrelia* can be (co-)causative of these diseases. Serotyping was performed after neuropsychiatric diagnosis and inclusion of the patients in the GRAS cohort. Thus, the increased seroprevalence in neuropsychiatric patients cannot be interpreted as direct contribution to disease etiology, but rather as disease-related deficits in personal hygiene or increased risk-taking behavior. Furthermore, considering the endemic pattern of *Borrelia* infections (240), the distribution of patient recruitment centers across Germany must also be taken into consideration (223). In contrast to patients, healthy volunteers were mainly from Lower Saxony with a relatively low incidence of borreliosis.

We did not find any evidence for a worse clinical outcome of schizophrenic antibody carriers (independent of genotypes) when compared to seronegative schizophrenia patients with respect to core symptoms of schizophrenia or to neurological deficits, as assessed by trained investigators. However, it is important to remember that antibody seropositivity cannot simply be equated with Lyme disease or neuroborreliosis. Nevertheless, when asked for self-assessment of their overall condition employing the BSI (226) seropositive schizophrenia patients rated more severe symptoms throughout all inventory items including the Global Severity Index (GSI). We cannot provide at this time a reliable interpretation of this data, but their non-specific nature may reflect the reputation of *Borrelia* as the ‘great imitator’ (241), and it is well known that subjective symptoms can persist after disappearance of objective criteria (216).

## Acknowledgments

This work was supported by the Max Planck Society and the Max Planck Förderstiftung as well as by the DFGSFB699A12, DFG KU756/12-1, Volkswagenstiftung AZ 87499 and the Niedersachsen-Research Network on Neuroinfectiology (N-RENNT) of the Ministry of Science and Culture of Lower Saxony. C.H. acknowledges grant support by the Daimler & Benz Foundation as well as the Brain & Behavior Foundation.

## CHAPTER 6

### DISCUSSION

Many physiological processes occurring in mammalian cells such as epithelial transport, hormones and transmitters release, muscular excitability and contraction, cell migration, proliferation and cell death, require proper intracellular ions concentrations. In particular the maintenance of a constant cell volume plays a pivotal role for normal cell function. It is greatly influenced by changes in intracellular and extracellular osmolarity. In fact after an osmotic challenge by reduction of extracellular osmolarity animal cells are able to restore their original volume by activation of  $K^+$  and  $Cl^-$  channel. The water efflux that follows the loss of these ions permits the homeostatic response called regulatory volume decrease (RVD). Moreover volume-regulated chloride currents are involved in a process termed apoptotic volume decrease (AVD) that precedes the apoptotic cell death. The present work demonstrates that anoctamins (TMEM16), particularly ANO6, have a major role in RVD. Apart from their role in volume regulation, anoctamins are expressed in several cell types and implicated in many physiological functions including epithelial chloride transport, maintenance of cellular homeostasis, cell proliferation, migration, neuronal and cardiac excitability and smooth muscle contraction.

#### **Anoctamin1 contributes to cell proliferation and metastasis in cancer.**

Anoctamin 1 (ANO1, TMEM16A) is a  $Ca^{2+}$  activated  $Cl^-$  channel and is located within the 11q13 amplicon, a locus which is frequently amplified in a number of different human cancers which are characterized by poor prognosis. ANO1 is particularly well expressed in gastrointestinal stromal tumors and head and neck squamous cell carcinoma (HNSCC). It has been shown that the 11q13 amplicon harbors several genes related to cell cycle, proliferation and apoptosis (such as cyclin D1, FGF4 and Fas-associated via death domain) (58;74;101). It has been characterized as a potential oncogene. In this study, I investigated the role of ANO1 in head and neck squamous cell carcinoma (HNSCC) and gastrointestinal stromal tumors. I showed that higher ANO1 expression in HNSCC cell lines (CAL33, BHY) was correlated with enhanced cell proliferation. Notably, such an association was not observed in human colonic adenocarcinoma cells (HT<sub>29</sub>). In the same way siRNA-knockdown of ANO1 attenuated cells proliferation in CAL33 and BHY cells, but it did not have an effect on HT<sub>29</sub> cells.

Interestingly, we found an inverse correlation between ANO1 and cell proliferation in mouse distal colon. According to our investigations the inverse correlation between low ANO1 levels and upregulation of mTOR suggests that ANO1 may be inhibitory on the proliferation of mouse intestinal epithelial cells, a notion that would parallel the observations done in HT<sub>29</sub> colonic epithelial cells.

Our observations are also in line with previous studies which demonstrated that ANO1 is coexpressed in the zone of polarizing activity in limb buds during mouse embryogenesis together with proteins of the sonic hedgehog pathway (125). The sonic hedgehog signaling pathway operates together with the Wnt and EGFR signaling pathways (242;243). Also ANO1 has been recently shown to be linked to the RAS-RAF-MEK-ERK1/2 pathway which regulates genes involved in cellular proliferation, such as cyclinD1 (58;112;244). Therefore, our data suggest that ANO1 expression affects cell survival rather than apoptosis in a cell type-dependent manner.

Apart from numerous effects observed during cancer, many studies have shown that uncontrolled growth of cancer is related to alterations of histone modifications (113;245). The level of acetylation in histones is controlled by the concerted action of the histone acetyltransferase (HAT) and the histone deacetylase (HDAC). HAT and HDAC are known to play a crucial role in gene transcription (Fig. 1).

Removal of acetyl groups from histones by HDAC causes chromatin compaction which is known to be involved in growth suppressive genes, thereby promoting cell proliferation (246;247). It has been shown that a loss of function of tumor suppressor adenomatosis (APC) increases HDAC levels in intestinal mucosa (248). Moreover, down-regulation of cyclin D1 and up-regulation of P21<sup>WAF1</sup> by HDAC inhibitors cause reduced proliferation and apoptosis in several cell types (247;249). Interestingly, ANO1 was found to cooperate with cyclin D1 in mouse head and neck tissues (102;250). This study also found that broad-spectrum HDAC inhibitors (valproic and butyric acid) decreased ANO1

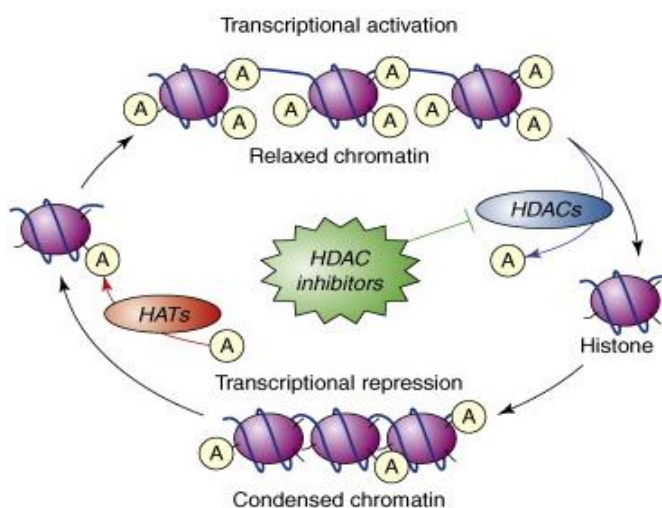


**Fig. 1** The dynamic state of histone acetylation/decetylation by HAT and HDAC enzymes to control gene transcriptions and downstream cellular function (249).

expression in BHY cells, which was accompanied by decreased cell viability. In particular we found that TSA, a selective HDAC class I/II inhibitor, suppressed cell proliferation in UM-SCC cells. Collectively, this data suggest that ANO1 may be an important target gene for HDAC inhibitors in order to inhibit cells proliferation in head and neck cancers.

Moreover cell attachment and migration are also positively influenced by the level of expression of ANO1. In fact we showed that cell attachment and migration were most pronounced in BHY cells, which showed higher amounts of ANO1 expression, when compared to CAL33 and HT<sub>29</sub> cells. In addition cell migration was inhibited under serum-free condition and by the use of ANO1 inhibitors. As mentioned above and according to our hypothesis, ANO1-mediated cell migration depends on growth factors concentrations present in the EGFR pathway. Indeed cell migration, invasion and metastasis in cancer also require the reorganization of the actin cytoskeleton through activation of ezrin-radixin-moesin (ERM) signaling pathway in response to growth factor stimulation (58;72;78). Thus these proteins provide a direct link to the actin cytoskeleton and to the plasma membrane. In addition it has been previously reported by our group that ANO1-mediated Cl<sup>-</sup> currents are regulated by the actin cytoskeleton (75). In accordance to a previous study conducted by Patricia Perez-Cornejo *et al.* (112), ANO1 colocalizes with the ERM complex to the apical side of epithelial cells and modulates the actin cytoskeleton (personal communications).

In-fact the process of migration involves first cell swelling at the leading edge of the cell leading to formation of the lamellipodium. This is followed by cell shrinkage at the rear part of the cells. The increase of intracellular Ca<sup>2+</sup> activates Ca<sup>2+</sup>-dependent K<sup>+</sup> and Cl<sup>-</sup> channels, leading to K<sup>+</sup> and Cl<sup>-</sup> efflux. Our previous study showed that the ATP- induced Ca<sup>2+</sup> activated Cl<sup>-</sup> conductance rapidly reduces cell volume in ANO1-P2Y<sub>2</sub> overexpressing cells (94), and that regulatory volume decrease after hypotonic induced whole-cell swelling occurs very rapidly in BHY cells, which express large levels of ANO1. Taken together this findings point out that ANO1 is involved in cell shape and volume regulation through the interaction with cytoskeletal elements and that this regulation is also involved in cell metastasis during cancer.

### **Ano6 contributes to RVD and phosphatidylserine scrambling.**

The function of anoctamin 6 (ANO6, TMEM16F) has been extensively studied. As shown in our previous report, ANO6 is robustly expressed at the surface of many different cell types (70;83;85), and plays important roles in cell survival (82;139). Along this line, it

has been shown that *Ano6*<sup>-/-</sup> mice have a low survival rate because of various dysfunctions in several organs, such as defective blood coagulation due to malfunction of platelets and defects in bone mineralization (82;83;92).

In this study, we found a reduced RVD and reduced apoptosis in freshly isolated intestinal epithelial cells from *Ano6*<sup>-/-</sup> mice. Many studies have identified a dual function of ANO6, namely that of an essential component of the outwardly rectifying Cl<sup>-</sup> channel ORCC, which can be induced by cell swelling and apoptotic stimuli, and that of a Ca<sup>2+</sup>-dependent phospholipid scramblase (70;71;86;87). In contrast, it has been also reported that ANO6 generates a small Ca<sup>2+</sup>-activated nonselective cation (SCAN) current which is associated with fast phosphatidylserine (PS) translocation (83). According to our results and other studies, ANO6 induced phospholipid scrambling is a key event in apoptosis, limiting the life span of platelets as well as that of white blood cells (WBC) and red blood cells (RBC). Kmit *et al.* (84) also showed that Ca<sup>2+</sup>-dependent whole cell currents, composed of both nonselective cation as well as Cl<sup>-</sup> currents are detectable in wild type B-lymphocytes in parallel with phospholipid scrambling and caspase3 activity.

Earlier studies have shown that ANO6 operates as a Ca<sup>2+</sup>-dependent phospholipid scramblase and that is an important basic mechanism how activation of platelets leads to thrombosis (84;251;252). In fact ANO6 mutations lead to defective function of platelets due to abrogation of Ca<sup>2+</sup>-dependent PS scrambling. This leads to a rare form of bleeding disorder, also known as Scott syndrome. Surprisingly, it has been proposed that ANO6 is necessary for Ca<sup>2+</sup>-dependent PS scrambling but in a Cl<sup>-</sup> current-independent manner (84). In this study, we investigated RVD in WT and Scott B-lymphocytes and found that RVD was not only influenced by the intracellular calcium concentration, but also depending

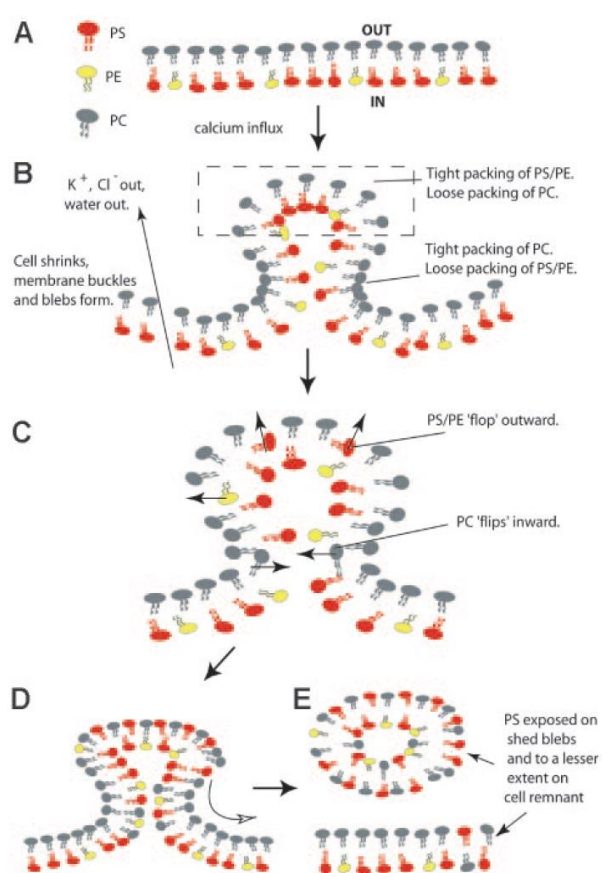


**Fig. 2** Model for Ca<sup>2+</sup>-stimulated PS translocation (253).

on the activation of PLA<sub>2</sub>. According to our hypothesis, hypotonic exposure causes water influx via AQP channels and induces cell swelling. Stretching of the plasma membrane is then followed by activation of Ca<sup>2+</sup> insensitive (iPLA<sub>2</sub>), causing release of arachidonic acid (ArA) and accumulation of lysophospholipids (LPL) within the plasma membrane. This leads to tension changes within the plasma membrane, opening TRP channel and allowing calcium influx. The increased cytosolic Ca<sup>2+</sup> concentration further activates and Ca<sup>2+</sup> sensitive PLA<sub>2</sub> (cPLA<sub>2</sub>), causing release of Ca<sup>2+</sup> out of the ER through IP<sub>3</sub> receptors and dantrolene-sensitive ryanodine receptors. High calcium then activates ANO6 leading to a decrease in cell volume due to Cl<sup>-</sup> loss and water efflux. This is paralleled by ANO6 scramblase activity causing translocation of PS to the outer leaflet of the plasma membrane. All these cellular events lead to cell shrinkage, re-organization of the cytoskeleton, followed by micro-particle shedding (MPs) and cell membrane blebbing (253; Fig. 2). Micro-particle shedding and cell membrane blebbing have been shown to be characteristic of early apoptotic cell death and to be important for innate immune response.

### **Ano6 is essential for innate immunity during bacterial infection.**

To date several studies have demonstrated differential functions of P2X<sub>7</sub> receptors (P2X<sub>7</sub>R) for cell proliferation as well as cell death. P2X<sub>7</sub>R is an ionotropic receptor which is expressed in a number of cell types, particularly in immune cells (macrophages, dendritic cells and microglial cells) (171;254;255). Macrophages are rather motile cells that support immune surveillance and normal tissue development by secreting cytokines, synthesis of growth and angiogenesis factors and engulfment of apoptotic cells. High concentrations of extracellular ATP activate P2X<sub>7</sub>R causing a transient opening of the channel that is permeable for small cations (Na<sup>+</sup>, Ca<sup>2+</sup> and K<sup>+</sup>), whereas a continuing stimulation induces the formation of a pore that allows large molecules to pass across the membrane. It was soon evident that P2X<sub>7</sub>R expressed in *Xenopus* oocytes is able to form a pore and generates inward currents after application of ATP, corresponding to an increase in Ca<sup>2+</sup> influx (194). It was suggested that pore formation of P2X<sub>7</sub>R could involve the C-terminus of the receptor, according to the data obtained in *Xenopus* oocytes and in HEK293 cells. We also found that after stimulation with ATP, a large delayed inward current occurred in hP2X<sub>7</sub>R overexpressing *Xenopus* oocytes. Similar whole cell currents were observed in hP2X<sub>7</sub>R overexpressing HEK293 cells, along with an increase in the intracellular calcium concentration. Furthermore, the extended C-terminus of P2X<sub>7</sub>R was demonstrated to be important for pore formation. Influx of Ca<sup>2+</sup>

through P2X<sub>7</sub> is providing the high intracellular Ca<sup>2+</sup> concentration that leads to activation of ANO6, which participates in pore formation. Moreover, we showed that P2X<sub>7</sub>R coimmunoprecipitated with ANO6. Collectively, these data suggest that ANO6 participates in P2X<sub>7</sub>R-induced apoptotic cell death.

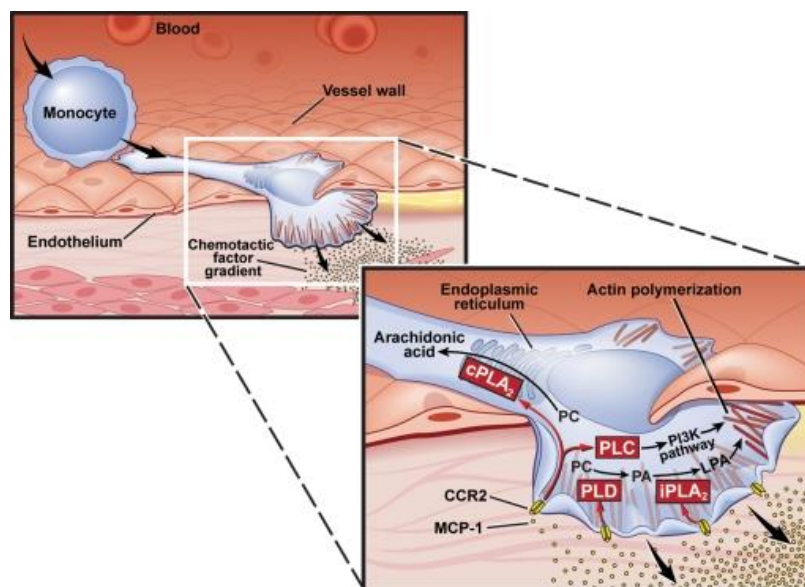


**Fig. 3** Circulating blood monocytes adhere to activated endothelium at sites of disease or injury. The monocyte becomes polarized and forms a pseudopod in response to chemotactic factor production like MCP-1, and follows the increasing concentration of the chemotactic factor into the tissue. Recognition of MCP-1 by CCR2 activates parallel signaling pathways mediated by iPLA<sub>2</sub>β and cPLA<sub>2</sub>α. iPLA<sub>2</sub>β at the leading edge regulates actin polymerization and the protrusion pseudopod. cPLA<sub>2</sub> translocates to the endoplasmic reticulum posterior to the nucleus (263).

Our studies showed that increase in the intracellular calcium concentration by activation of P2X<sub>7</sub>R is required for ANO6 mediated PS exposure, cell shrinkage and cell blebbing initiating apoptosis. Previously it has been suggested that P2X<sub>7</sub>R operates with Cl<sup>-</sup> channels in macrophages (207;256). In our study we found that ANO6 and P2X<sub>7</sub>R were indeed highly expressed in macrophages. We therefore investigated the role of P2X<sub>7</sub>R and ANO6 in macrophages. Endotoxin exposure activates an ATP release in macrophages which was shown to be crucial for their activation. Similarly, only short exposure to ATP induced delayed cell death. Cellular ATP release was observed during infection with pathogens and during tissue damage. In our study we found activation of whole cell currents in *Ano6*<sup>+/+</sup> (wild type) macrophages, even by only short exposure to ATP. The experiments demonstrated that autocrine or paracrine ATP release activated P2X<sub>7</sub>R, which induced cell shrinkage and massive cell blebbing (257;258). Remarkably, ATP-induced whole cell Cl<sup>-</sup> currents and cell

shrinkage were abolished in *Ano6*<sup>-/-</sup> macrophages. Correspondingly, we also demonstrated delayed caspase3 activation in *Ano6*<sup>-/-</sup> macrophages. Moreover, the activation by lipopolysaccharide (LPS) (priming) has been shown to augment the P2X<sub>7</sub>-stimulated IL-1 $\beta$  release and micro-vesicular shedding from the plasma membrane (259-261). This mechanism is particularly important to reduce inflammation during pathogenic infection. Also LPS priming was found to be reduced in *Ano6*<sup>-/-</sup> macrophages. Taken together, the data suggest that ATP-induced cell shrinkage, membrane blebbing and many other P2X<sub>7</sub>R dependent events in macrophages are ANO6-dependent.

Changes in cell volume due to ions fluxes have been reported to be involved in migration of macrophages (45;262). Several publications showed that the intracellular Cl<sup>-</sup> concentration is reduced in chemoattractant-stimulated macrophages which is associated with increased intracellular calcium concentrations (through Ca<sup>2+</sup> influx and/or release from the intracellular stores), actin assembling and cell shrinkage. The monocytes chemoattractant protein-1 (MCP-1) is a ligand for monocyte chemotaxis important to recruit monocytes to the site of inflammation. It has been shown that MCP-1 is recognized by chemokine receptor 2 (CCR2), which activates the signaling pathway mediated by iPLA<sub>2</sub> $\beta$  and cPLA<sub>2</sub> $\alpha$  (263; Fig. 3). These two enzymes regulate actin polymerization during migration of macrophages (264;265). Corresponding to this results, we found the migration in macrophages activated by MCP-1 was inhibited by Cl<sup>-</sup> channel blocker and siRNA-knockdown ANO6 in both *Ano6*<sup>+/+</sup> and *Ano6*<sup>-/-</sup> macrophages. In addition we found that cell migration in mouse and human macrophages was accompanied by RVD and cell shrinkage. In conclusion we believe that ANO6 is involved in migration triggered by stretch-activated PLA<sub>2</sub>, which is essential for the motility signaling pathway in macrophages.

During phagocytosis, killing of pathogens by macrophages is a crucial process which happens through fusion of pathogens-containing phagosomes and lysosomes. Several publications showed that the activation of P2X<sub>7</sub>R induces killing of mycobacteria and parasites in macrophages by phagolysosomal fusion (36;266). In our study, we found ATP-enhanced phagocytosis and *E. coli* killing in *Ano6*<sup>+/+</sup> macrophages, although the macrophages were incubated with ATP only for short periods of time. Remarkably, *E. coli* killing also occurred in the absence of ATP, which is probably due to immediate response of macrophages to chemokines released from bacteria. Furthermore, we showed that phagocytosis was suppressed by Cl<sup>-</sup> blockers as well as in *Ano6*<sup>-/-</sup> macrophages. Taken together these data indicate that ANO6 is essential for the downstream signaling pathway of P2X<sub>7</sub>R and the

innate immune function of macrophages.

### **ANO10 contributes to RVD and innate immune response during spirochete infection.**

ANO10, just like the other members of the anoctamin family, consists of ten transmembrane domains with a so called DUF590 domain of unknown function. According to a previous report by the team of Luis Galletta (267), it has been shown that ANO10 shares 20-30% sequence homology with ANO1. Our group showed that these two anoctamins are associated with volume regulation, cancer and the immune function realized by macrophages. In our study, we analyzed the impact of ANO10 on RVD in two different models overexpressing ANO10 and AQP1, by overexpressing ANO10 in *Xenopus* oocytes and HEK293 cells, respectively. ANO10 generated RVD in these models, requiring the activity of PLA<sub>2</sub> and an increase in the intracellular calcium concentration, similar to what had been outlined for ANO6. The rise in intracellular calcium was mainly due to dantrolene-sensitive ryanodine receptors, which were activated after hypotonic challenging. Based on the structure of nhTMEM16, a crystalized fungal homologue of mammalian ANO6 and ANO10, we speculate that the critical residue R263H is closely located to the lateral interface of the two anoctamin subunits forming the functional dimeric protein. This structure is likely to contribute to formation of the Ca<sup>2+</sup>-activated Cl<sup>-</sup> channel and the channel that allows phospholipid scrambling. When investigating the role of the additional ANO10 mutations R263H, L510R and L384fs, which are associated with cerebellar ataxia (93), we observed that these mutations attenuated RVD and intracellular calcium increase. Furthermore, we showed that ANO10 and mutant ANO10-R263H was localized in an intracellular compartment. Thus ANO10 may control intracellular Ca<sup>2+</sup> signaling rather than participating in an ion channel complex, thereby regulating cell volume and other macrophage functions.

Neuroborreliosis has been reported to be a disease transmitted by ticks, and caused by the spirochete *B. burgdorferi*. Characteristic symptoms are cerebellar ataxia-like symptoms, such as meningitis, ataxia, dizziness and encephalitis (221;241). *Borrelia* adopts different strategies for its survival inside the host tissues. It seems to have developed a long-term survival strategy in the host's defense mechanisms. Therefore, the host's innate and adaptive immune responses are thought to be the major pathways for *borrelia* killing (268;269). We found that ANO10 was expressed in both mouse and human macrophages, similarly to ANO6. Thus we became interested to examine in detail the impact of ANO10 on macrophage function and

response following infection by *B.burgdorferi*.

Again cellular volume regulation (RVD) was compromised in macrophages after siRNA-knockdown of ANO10, as well as in ANO10<sup>lox/lox</sup>/E2A-cre (ANO10<sup>-/-</sup>) mice. Similarly, after exposure to *B. burgdorferi*, migration and phagocytic activity were suppressed in ANO10-knockdown macrophages. We found that the TNF $\alpha$  levels were strongly increased after *B.burgdorferi* exposure and this was not changed by knockdown of ANO10. From these and other experiments we conclude that cell death of macrophages after exposure and phagocytosis of *B. burgdorferi* is reduced, even 6 days after spirochete exposure, and that this is part of the survival strategy of *B. burgdorferi*. Attenuation of cells death in macrophages expressing the R263H variant, might be responsible for longer survival of *B. burgdorferi* in the infected person and thus the enhanced antibody levels observed in these patients.

These results also corroborate previous reports that lipoproteins of spirochetes activate the production of TNF $\alpha$ , which is important for proliferation, differentiation and apoptosis of macrophages. In fact lipoproteins can interact with Toll-like receptors (TLRs), which trigger several downstream signaling pathways (such as NF- $\kappa$ B and MAPK) and induce transcription of cytokines (269-271) that recruit other immune cells to the site of infection (Fig. 4). Our findings suggest that ANO10 is important for volume regulation in macrophages and that it plays a role in innate and adaptive immune response. We suggest compromised spirochete killing in macrophages obtained from patients carrying the ANO10-R263H variation. According to ANO10 variants associated with cerebellar ataxia, in this study, we analyzed the potential association of SNPs and cerebellar ataxia in patients with laboratory-confirmed diagnosis of *Borrelia*, using GWAS analysis. Patients without typical clinical signs and symptoms associated with two variants (SNPs) which were located on chromosome 3 and 16.

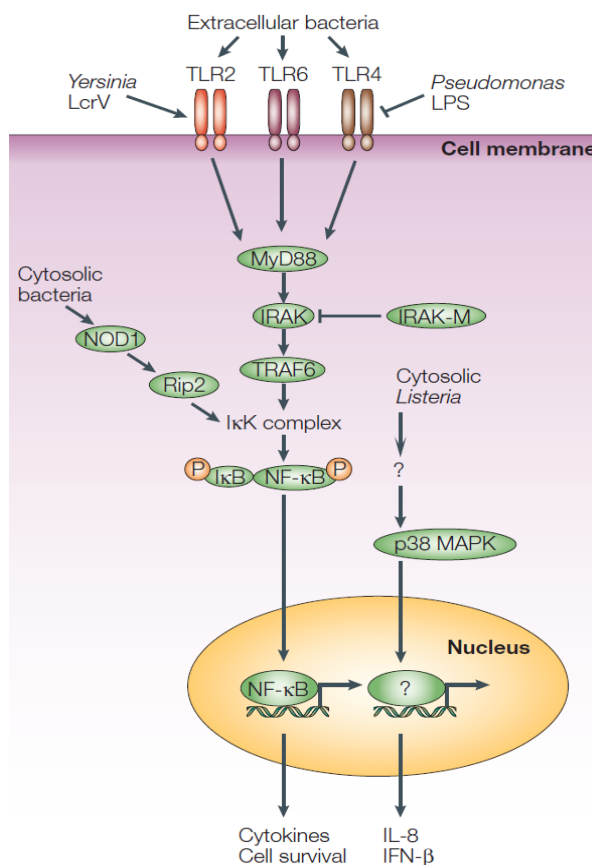


**Figure 4.** Macrophage surveillance systems to detect pathogens

The SNP on chromosome 3, rs41289536, was a missense ANO10-R263H variant. The other one was ZNF821 variant (rs71850869) on chromosome 16. More specifically, we found that the antibody titration against *Borrelia* infection tended to be higher in schizophrenic patients who carried ANO10-R263H variant which did not show the association with other infections as shown in our results. These findings correlate with previous reports in which human genomic variation mediate susceptibility to pathogenic diseases. We conclude that ANO10 is important for the success of the host's defense mechanism towards spirochetes infection.

## CONCLUSION

The present work demonstrates that anoctamins have a fundamental role in cell volume regulation and for other mechanisms of tissue homeostasis, like cell proliferation, differentiation and cell death. All cells express anoctamins, with a basic equipment of ANO6, -8, -9 and -10. Different tissues express additional “specific” anoctamins. This, along with the results described in this thesis, indicate that anoctamins have housekeeper functions as well as cell specific functions, like those observed in secretory epithelial cells, neuronal or muscle cells. Thus mutations in anoctamins abrogate basic cellular functions as well as highly specific cellular functions. The present thesis describes general cell biological functions of ANO1, 6 and 10. Given the fact that functions like proliferation cell volume,  $\text{Ca}^{2+}$  signaling, cell death and many more are controlled by anoctamins, it is not surprising that these proteins have been reported in the context of very different diseases. Therefore in cancer, cancer metastasis, the susceptibility towards infections with borrelia or mycobacteria, hypersecretion during diarrhea, abrogated intestinal peristalsis and digestive problems, and many more diseases and malfunctions, anoctamins are central players. It will be interesting to learn in subsequent studies more about the molecular details and how anoctamins control all these functions. In future, better pharmacological tools with higher specificity for individual anoctamins may allow interfering with anoctamin-dependent cellular processes and may even turn out as novel treatment for cancer and immune defects.

**REFERENCES**

1. Hubner, C. A., Jentsch, T. J. (2002) Ion channel diseases. *Hum.Mol.Genet.*2002 *Oct.1.;11.(20.):2435.-45.* 11, 2435-2445
2. Jentsch, T. J. (1996) Chloride channels: a molecular perspective. *Curr.Opin.Neurobiol.* 6, 303-310
3. Jentsch, T. J., Stein, V., Weinreich, F., Zdebik, A. A. (2002) Molecular structure and physiological function of chloride channels. *Physiol Rev.* 82, 503-568
4. Duran, C., Thompson, C. H., Xiao, Q., Hartzell, H. C. (2010) Chloride channels: often enigmatic, rarely predictable. *Annu.Rev.Physiol* 72, 95-121
5. Jentsch, T. J., Stein, V., Weinreich, F., Zdebik, A. A. (2002) Molecular structure and physiological function of chloride channels. *Physiol Rev.* 82, 503-568
6. Planells-Cases, R., Jentsch, T. J. (2009) Chloride channelopathies. *Biochim.Biophys.Acta.*
7. Jentsch, T. J. (2001) Chloride channels are different. *Nature* 415, 276-277
8. Jentsch, T. J., Friedrich, T., Schriever, A., Yamada, H. (1999) The CLC chloride channel family. *Pflügers Arch* 437, 783-795
9. Nilius, B., Eggermont, J., Voets, T., Droogmans, G. (1996) Volume-activated Cl<sup>-</sup> channels. *Gen.Pharmacol.* 27, 1131-1140
10. Lang, F., Hoffmann, E. K. (2012) Role of ion transport in control of apoptotic cell death. *Compr.Physiol.* 2, 2037-2061
11. Hoffmann, E. K., Simonsen, L. O., Lambert, I. H. (1984) Volume-induced increase of K<sup>+</sup> and Cl<sup>-</sup> permeabilities in Ehrlich ascites tumor cells. Role of internal Ca<sup>2+</sup>. *J Membr.Biol.* 78, 211-222
12. Stutzin, A., Hoffmann, E. K. (2006) Swelling-activated ion channels: functional regulation in cell-swelling, proliferation and apoptosis. *Acta Physiol (Oxf).* 187, 27-42

13. Hoffmann, E. K. (2000) Intracellular signalling involved in volume regulatory decrease. *Cell Physiol Biochem.* 10, 273-288
14. Eggermont, J., Trouet, D., Carton, I., Nilius, B. (2001) Cellular function and control of volume-regulated anion channels. *Cell Biochem Biophys.* 35, 263-274
15. Nilius, B., Eggermont, J., Voets, T., Buyse, G., Manolopoulos, V., Droogmans, G. (1997) Properties of volume-regulated anion channels in mammalian cells. *Prog.Biophys Mol.Biol.* 68, 69-119
16. Bortner, C. D., Cidlowski, J. A. (2004) The role of apoptotic volume decrease and ionic homeostasis in the activation and repression of apoptosis. *Pflugers Arch.* 448, 313-318
17. Chen, L., Wang, L., Zhu, L., Nie, S., Zhang, J., Zhong, P., Cai, B., Luo, H., Jacob, T. J. (2002) Cell cycle-dependent expression of volume-activated chloride currents in nasopharyngeal carcinoma cells. *Am.J Physiol.Cell Physiol.* 2002 Oct.;283(4.):C1313.-23. 283, C1313-C1323
18. Barros, L. F., Castro, J., Bittner, C. X. (2002) Ion movements in cell death: from protection to execution. *Biol Res.* 35, 209-214
19. Okada, Y., Maeno, E., Shimizu, T., Dezaki, K., Wang, J., Morishima, S. (2001) Receptor-mediated control of regulatory volume decrease (RVD) and apoptotic volume decrease (AVD). *J Physiol.* 532, 3-16
20. Maeno, E., Ishizaki, Y., Kanaseki, T., Hazama, A., Okada, Y. (2000) Normotonic cell shrinkage because of disordered volume regulation is an early prerequisite to apoptosis. *Proc.Natl.Acad.Sci.U.S.A.* 97, 9487-9492
21. Tan, C. P., Lu, Y. Y., Ji, L. N., Mao, Z. W. (2014) Metallomics insights into the programmed cell death induced by metal-based anticancer compounds. *Metallomics.* 6, 978-995
22. Cohen, J. J., Duke, R. C., Fadok, V. A., Sellins, K. S. (1992) Apoptosis and programmed cell death in immunity. *Annu.Rev.Immunol.* 10, 267-293
23. Elmore, S. (2007) Apoptosis: a review of programmed cell death. *Toxicol.Pathol.* 35,

495-516

24. Henriquez, M., Armisen, R., Stutzin, A., Quest, A. F. (2008) Cell death by necrosis, a regulated way to go. *Curr.Mol.Med.* 8, 187-206
25. Kroemer, G., Galluzzi, L., Vandenabeele, P., Abrams, J., Alnemri, E. S., Baehrecke, E. H., Blagosklonny, M. V., El-Deiry, W. S., Golstein, P., Green, D. R., Hengartner, M., Knight, R. A., Kumar, S., Lipton, S. A., Malorni, W., Nuñez, G., Peter, M. E., Tschopp, J., Yuan, J., Piacentini, M., Zhivotovsky, B., Melino, G. (2009) Classification of cell death. *Cell Death Differ.* 16, 3-11
26. Vandenabeele, P., Galluzzi, L., Vanden Berghe, T., Kroemer, G. (2010) Molecular mechanisms of necroptosis: an ordered cellular explosion. *Nat.Rev.Mol.Cell Biol.* 11, 700-714
27. Galluzzi, L., Kepp, O., Kroemer, G. (2014) MLKL regulates necrotic plasma membrane permeabilization. *Cell Res.* 24, 139-140
28. Segawa, K., Suzuki, J., Nagata, S. (2014) Flippases and scramblases in the plasma membrane. *Cell Cycle.* 13, 2990-2991
29. Kroemer, G., Galluzzi, L., Brenner, C. (2007) Mitochondrial membrane permeabilization in cell death. *Physiol Rev.* 87, 99-163
30. Ashkenazi, A., Dixit, V. M. (1998) Death receptors: signaling and modulation. *Science.* 281, 1305-1308
31. Nagata, S. (1997) Apoptosis by death factor. *Cell.* 88, 355-365
32. Gulbins, E., Jekle, A., Ferlinz, K., Grassme, H., Lang, F. (2000) Physiology of apoptosis. *Am.J Physiol Renal Physiol* 279, F605-F615
33. de Almagro, M. C., Vucic, D. (2012) The inhibitor of apoptosis (IAP) proteins are critical regulators of signaling pathways and targets for anti-cancer therapy. *Exp.Oncol.* 34, 200-211
34. Kroemer, G., Reed, J. C. (2000) Mitochondrial control of cell death. *Nat.Med.* 6, 513-519

35. Brown, G. C., Neher, J. J. (2012) Eaten alive! Cell death by primary phagocytosis: 'phagoptosis'. *Trends Biochem.Sci.* 37, 325-332
36. Soehnlein, O., Lindbom, L. (2010) Phagocyte partnership during the onset and resolution of inflammation. *Nat.Rev.Immunol.* 10, 427-439
37. Nagata, S., Hanayama, R., Kawane, K. (2010) Autoimmunity and the clearance of dead cells. *Cell.* 140, 619-630
38. Segawa, K., Kurata, S., Yanagihashi, Y., Brummelkamp, T. R., Matsuda, F., Nagata, S. (2014) Caspase-mediated cleavage of phospholipid flippase for apoptotic phosphatidylserine exposure. *Science.* 344, 1164-1168
39. Brown, G. C., Neher, J. J. (2012) Eaten alive! Cell death by primary phagocytosis: 'phagoptosis'. *Trends Biochem.Sci.* 37, 325-332
40. Segawa, K., Suzuki, J., Nagata, S. (2011) Constitutive exposure of phosphatidylserine on viable cells. *Proc.Natl.Acad.Sci.U.S.A.* 108, 19246-19251
41. Suzuki, J., Nagata, S. (2014) Phospholipid scrambling on the plasma membrane. *Methods Enzymol.* 544, 381-393
42. Bevers, E. M., Williamson, P. L. (2010) Phospholipid scramblase: an update. *FEBS Lett.* 584, 2724-2730
43. Asokanathan, N., Graham, P. T., Fink, J., Knight, D. A., Bakker, A. J., McWilliam, A. S., Thompson, P. J., Stewart, G. A. (2002) Activation of protease-activated receptor (PAR)-1, PAR-2, and PAR-4 stimulates IL-6, IL-8, and prostaglandin E2 release from human respiratory epithelial cells. *J Immunol.* 168, 3577-3585
44. Aderem, A., Ulevitch, R. J. (2000) Toll-like receptors in the induction of the innate immune response. *Nature* 406, 782-787
45. Burow, P., Klapperstuck, M., Markwardt, F. (2014) Activation of ATP secretion via volume-regulated anion channels by sphingosine-1-phosphate in RAW macrophages. *Pflugers Arch.*
46. Ratner, D., Mueller, C. (2012) Immune responses in cystic fibrosis: are they

- intrinsically defective? *Am.J.Respir.Cell Mol.Biol.* 46, 715-722
47. Brunner, J. D., Lim, N. K., Schenck, S., Duerst, A., Dutzler, R. (2014) X-ray structure of a calcium-activated TMEM16 lipid scramblase. *Nature.* 516, 207-212
  48. Whitlock, J. M., Hartzell, H. C. (2016) A Pore Idea: the ion conduction pathway of TMEM16/ANO proteins is composed partly of lipid. *Pflugers Arch.* 468, 455-473
  49. Hartzell, H. C., Yu, K., Xiao, Q., Chien, L. T., Qu, Z. (2008) Anoctamin / TMEM16 family members are Ca<sup>2+</sup>-activated Cl<sup>-</sup> channels. *J Physiol.* 587, 2127-2139
  50. Tian, Y., Schreiber, R., Kunzelmann, K. (2012) Anoctamins are a family of Ca<sup>2+</sup> activated Cl<sup>-</sup> channels. *J Cell Sci* 125, 4991-4998
  51. Kunzelmann, K., Tian, Y., Martins, J. R., Faria, D., Kongsuphol, P., Ousingsawat, J., Thevenod, F., Roussa, E., Rock, J. R., Schreiber, R. (2011) Anoctamins. *Pflugers Arch.* 462, 195-208
  52. Duran, C., Qu, Z., Osunkoya, A. O., Cui, Y., Hartzell, H. C. (2011) ANOs 3-7 in the anoctamin/tmem16 Cl<sup>-</sup> channel family are intracellular proteins. *Am J Physiol Cell Physiol.*
  53. Duran, C., Hartzell, H. C. (2011) Physiological roles and diseases of Tmem16/Anoctamin proteins: are they all chloride channels? *Acta Pharmacol.Sin.* 32, 685-692
  54. Kunzelmann, K., Schreiber, R., Kmit, A., Jantarajit, W., Martins, J. R., Faria, D., Kongsuphol, P., Ousingsawat, J., Tian, Y. (2012) Expression and function of epithelial anoctamins. *Exp.Physiol.* 97, 184-192
  55. Duvvuri, U., Shiwariski, D. J., Xiao, D., Bertrand, C., Huang, X., Edinger, R. S., Rock, J. R., Harfe, B. D., Henson, B. J., Kunzelmann, K., Schreiber, R., Seethala, R. R., Egloff, A. M., Chen, X., Lui, V. W., Grandis, J. R., Gollin, S. M. (2012) TMEM16A, induces MAPK and contributes directly to tumorigenesis and cancer progression. *Cancer Res.* 72, 3270-3281
  56. Wielders, S. J., Broers, J., ten Cate, H., Collins, P. W., Bevers, E. M., Lindhout, T. (2009) Absence of platelet-dependent fibrin formation in a patient with Scott

- syndrome. *Thromb.Haemost.* 102, 76-82
57. Sauter, D. R., Novak, I., Pedersen, S. F., Larsen, E. H., Hoffmann, E. K. (2014) ANO1 (TMEM16A) in pancreatic ductal adenocarcinoma (PDAC). *Pflugers Arch.*
58. Ayoub, C., Wasylyk, C., Li, Y., Thomas, E., Marisa, L., Robe, A., Roux, M., Abecassis, J., de Reynies, A., Wasylyk, B. (2010) ANO1 amplification and expression in HNSCC with a high propensity for future distant metastasis and its functions in HNSCC cell lines. *Br.J Cancer.* 103, 715-726
59. Gomez-Pinilla, P. J., Gibbons, S. J., Bardsley, M. R., Lorincz, A., Pozo, M. J., Pasricha, P. J., van de, R. M., West, R. B., Sarr, M. G., Kendrick, M. L., Cima, R. R., Dozois, E. J., Larson, D. W., Ordog, T., Farrugia, G. (2009) ANO is a selective marker of interstitial cells of Cajal in the human and mouse gastrointestinal tract. *Am J Physiol Gastrointest.Liver Physiol.* 296, G1370-G1381
60. Ardeleanu, C., Arsene, D., Hinescu, M., Andrei, F., Gutu, D., Luca, L., Popescu, L. M. (2009) Pancreatic Expression of DOG1: A Novel Gastrointestinal Stromal Tumor (GIST) Biomarker. *Appl.Immunohistochem.Mol.Morphol.* 17, 413-418
61. Manoury, B., Tamuleviciute, A., Tammaro, P. (2010) TMEM16A/Anoctamin1 protein mediates calcium-activated chloride currents in pulmonary arterial smooth muscle cells. *J Physiol.* 588, 2305-2314
62. Berglund, E., Akcakaya, P., Berglund, D., Karlsson, F., Vukojevic, V., Lee, L., Bogdanovic, D., Lui, W. O., Larsson, C., Zedenius, J., Frobom, R., Branstrom, R. (2014) Functional role of the Ca-activated Cl channel DOG1/TMEM16A in gastrointestinal stromal tumor cells. *Exp.Cell Res.* 326, 315-325
63. Brett, T. J. (2015) CLCA1 and TMEM16A: the link towards a potential cure for airway diseases. *Expert.Rev.Respir.Med.* 1-4
64. Catalan, M. A., Kondo, Y., Pena-Munzenmayer, G., Jaramillo, Y., Liu, F., Choi, S., Crandall, E., Borok, Z., Flodby, P., Shull, G. E., Melvin, J. E. (2015) A fluid secretion pathway unmasked by acinar-specific Tmem16A gene ablation in the adult mouse salivary gland. *Proc.Natl.Acad.Sci U.S A.* 201415739

65. Davis, A. J., Forrest, A. S., Jepps, T. A., Valencik, M. L., Wiwchar, M., Singer, C. A., Sones, W. R., Greenwood, I. A., Leblanc, N. (2010) Expression profile and protein translation of TMEM16A in murine smooth muscle. *Am J Physiol Cell Physiol.* 299, C948-C959
66. Sanders, K. M., O'Driscoll, K., Leblanc, N. (2014) Pharmacological Properties of Native CaCCs and TMEM16A. *Channels (Austin).* 0
67. Thomas-Gatewood, C., Neeb, Z. P., Bulley, S., Adebisi, A., Bannister, J. P., Leo, M. D., Jaggar, J. H. (2011) TMEM16A channels generate  $Ca^{2+}$ -activated  $Cl^-$  currents in cerebral artery smooth muscle cells. *Am J Physiol Heart Circ.Physiol.* 301, H1819-H1827
68. Wang, M., Yang, H., Zheng, L. Y., Zhang, Z., Tang, Y. B., Wang, G. L., Du, Y. H., Lv, X. F., Liu, J., Zhou, J. G., Guan, Y. Y. (2012) Downregulation of TMEM16A Calcium-Activated Chloride Channel Contributes to Cerebrovascular Remodeling during Hypertension through Promoting Basilar Smooth Muscle Cell Proliferation. *Circulation.* 125, 697-707
69. Ousingsawat, J., Martins, J. R., Schreiber, R., Rock, J. R., Harfe, B. D., Kunzelmann, K. (2009) Loss of TMEM16A causes a defect in epithelial  $Ca^{2+}$  dependent chloride transport. *J Biol Chem* 284, 28698-28703
70. Suzuki, J., Umeda, M., Sims, P. J., Nagata, S. (2010) Calcium-dependent phospholipid scrambling by TMEM16F. *Nature* 468, 834-838
71. Yu, K., Whitlock, J. M., Lee, K., Ortlund, E. A., Yuan, C. Y., Hartzell, H. C. (2015) Identification of a lipid scrambling domain in ANO6/TMEM16F. *Elife.* 4. doi, 10
72. Liu, W., Lu, M., Liu, B., Huang, Y., Wang, K. (2012) Inhibition of  $Ca^{2+}$ -activated  $Cl^-$  channel ANO1/TMEM16A expression suppresses tumor growth and invasiveness in human prostate carcinoma. *Cancer Lett.* 326, 41-51
73. Mazzone, A., Eisenman, S. T., Strege, P. R., Yao, Z., Ordog, T., Gibbons, S. J., Farrugia, G. (2012) Inhibition of Cell Proliferation by a Selective Inhibitor of the  $Ca^{2+}$ -activated  $Cl^-$  Channel, ANO. *Biochem.Biophys Res.Commun.* 427, 248-253

74. Stanich, J. E., Gibbons, S. J., Eisenman, S. T., Bardsley, M. R., Rock, J. R., Harfe, B. D., Ordog, T., Farrugia, G. (2011) ANO1 AS A REGULATOR OF PROLIFERATION. *Am J Physiol Gastrointest.Liver Physiol.* 301, G1044-G1051
75. Tian, Y., Kongsuphol, P., Hug, M. J., Ousingsawat, J., Witzgall, R., Schreiber, R., Kunzelmann, K. (2011) Calmodulin-dependent activation of the epithelial calcium-dependent chloride channel TMEM16A. *FASEB J* 25, 1058-1068
76. Cramer, L. P. (2010) Forming the cell rear first: breaking cell symmetry to trigger directed cell migration. *Nat.Cell Biol.* 12, 628-632
77. Gutjahr, M. C., Rossy, J., Niggli, V. (2005) Role of Rho, Rac, and Rho-kinase in phosphorylation of myosin light chain, development of polarity, and spontaneous migration of Walker 256 carcinosarcoma cells. *Exp.Cell Res.* 308, 422-438
78. Jacobsen, K. S., Zeeberg, K., Poulsen, K. A., Hoffmann, E. K., Schwab, A. (2013) The role of TMEM16A (ANO1) and TMEM16F (ANO6) in cell migration. *Pflugers Arch* 465, 1753-1762
79. Ruiz, C., Martins, J. R., Rudin, F., Schneider, S., Dietsche, T., Fischer, C. A., Tornillo, L., Terracciano, L. M., Schreiber, R., Bubendorf, L., Kunzelmann, K. (2012) Enhanced Expression of ANO1 in Head and Neck Squamous Cell Carcinoma Causes Cell Migration and Correlates with Poor Prognosis. *PLoS.ONE.* 7, e43265
80. Schreiber, R., Uliyakina, I., Kongsuphol, P., Warth, R., Mirza, M., Martins, J. R., Kunzelmann, K. (2010) Expression and Function of Epithelial Anoctamins. *J.Biol.Chem.* 285, 7838-7845
81. Sztejn, K., Schmid, E., Nurbaeva, M. K., Yang, W., Munzer, P., Kunzelmann, K., Lang, F., Shumilina, E. (2012) Expression and Functional Significance of the Ca<sup>2+</sup> Activated Cl<sup>-</sup> Channel ANO6 in Dendritic Cells. *Cell Physiol Biochem.* 30, 1319-1332
82. Ehlen, H. W., Chinenkova, M., Moser, M., Munter, H. M., Krause, Y., Gross, S., Brachvogel, B., Wuelling, M., Kornak, U., Vortkamp, A. (2012) Inactivation of Anoctamin-6/Tmem16f, a regulator of phosphatidylserine scrambling in osteoblasts, leads to decreased mineral deposition in skeletal tissues. *J Bone Miner.Res.* 28, 246-

259

83. Yang, H., Kim, A., David, T., Palmer, D., Jin, T., Tien, J., Huang, F., Cheng, T., Coughlin, S. R., Jan, Y. N., Jan, L. Y. (2012) TMEM16F Forms a  $\text{Ca}^{2+}$ -Activated Cation Channel Required for Lipid Scrambling in Platelets during Blood Coagulation. *Cell*. 151, 111-122
84. Kmit, A., van Kruchten, R., Ousingsawat, J., Mattheij, N. J., Senden-Gijsbers, B., Heemskerk, J. W., Bevers, E. M., Kunzelmann, K. (2013) Calcium-activated and apoptotic phospholipid scrambling induced by Ano6 can occur independently of Ano6 ion currents. *Cell death and disease* 25, 4:e611
85. Grubb, S., Poulsen, K. A., Juul, C. A., Kyed, T., Klausen, T. K., Larsen, E. H., Hoffmann, E. K. (2013) TMEM16F (Anoctamin 6), an anion channel of delayed  $\text{Ca}^{2+}$  activation. *J Gen.Physiol.* 141, 585-600
86. Juul, C. A., Grubb, S., Poulsen, K. A., Kyed, T., Hashem, N., Lambert, I. H., Larsen, E. H., Hoffmann, E. K. (2014) Anoctamin 6 differs from VRAC and VSOAC but is involved in apoptosis and supports volume regulation in the presence of  $\text{Ca}^{2+}$ . *Pflugers Arch* 466, 1899-1910
87. Martins, J. R., Faria, D., Kongsuphol, P., Reisch, B., Schreiber, R., Kunzelmann, K. (2011) Anoctamin 6 is an essential component of the outwardly rectifying chloride channel. *Proc.Natl.Acad.Sci.U.S.A.* 108, 18168-18172
88. Dekkers, D. W., Comfurius, P., Bevers, E. M., Zwaal, R. F. (2002) Comparison between  $\text{Ca}^{2+}$ -induced scrambling of various fluorescently labelled lipid analogues in red blood cells. *Biochem J.* 362, 741-747
89. Bevers, E. M., Wiedmer, T., Comfurius, P., Shattil, S. J., Weiss, H. J., Zwaal, R. F., Sims, P. J. (1992) Defective  $\text{Ca}^{2+}$ -induced microvesiculation and deficient expression of procoagulant activity in erythrocytes from a patient with a bleeding disorder: a study of the red blood cells of Scott syndrome. *Blood.* 79, 380-388
90. Heemskerk, J. W., Bevers, E. M., Lindhout, T. (2002) Platelet activation and blood coagulation. *Thromb.Haemost.* 88, 186-193

91. Williamson, P., Christie, A., Kohlin, T., Schlegel, R. A., Comfurius, P., Harmsma, M., Zwaal, R. F., Bevers, E. M. (2001) Phospholipid scramblase activation pathways in lymphocytes. *Biochemistry*. 40, 8065-8072
92. Ousingsawat, J., Wanitchakool, P., Schreiber, R., Wuelling, M., Vortkamp, A., Kunzelmann, K. (2015) Anoctamin 6 controls bone mineralization by activating the calcium transporter NCX1. *J Biol Chem*. 290, 6270-6280
93. Vermeer, S., Hoischen, A., Meijer, R. P., Gilissen, C., Neveling, K., Wieskamp, N., de Brouwer, A., Koenig, M., Anheim, M., Assoum, M., Drouot, N., Todorovic, S., Milic-Rasic, V., Lochmuller, H., Stevanin, G., Goizet, C., David, A., Durr, A., Brice, A., Kremer, B., van de Warrenburg, B. P., Schijvenaars, M. M., Heister, A., Kwint, M., Arts, P., van der, W. J., Veltman, J., Kamsteeg, E. J., Scheffer, H., Knoers, N. (2010) Targeted next-generation sequencing of a 12.5 Mb homozygous region reveals ANO10 mutations in patients with autosomal-recessive cerebellar ataxia. *Am J Hum. Genet*. 87, 813-819
94. Duran, C., Thompson, C. H., Xiao, Q., Hartzell, H. C. (2010) Chloride Channels: Often Enigmatic, Rarely Predictable. *Annu. Rev. Physiol*. 72, 95-121
95. Chamova, T., Florez, L., Guergueltcheva, V., Raycheva, M., Kaneva, R., Lochmuller, H., Kalaydjieva, L., Tournev, I. (2012) ANO10 c.1150\_1151del is a founder mutation causing autosomal recessive cerebellar ataxia in Roma/Gypsies. *J Neurol*. 259, 906-911
96. Almaca, J., Tian, Y., AlDehni, F., Ousingsawat, J., Kongsuphol, P., Rock, J. R., Harfe, B. D., Schreiber, R., Kunzelmann, K. (2009) TMEM16 proteins produce volume regulated chloride currents that are reduced in mice lacking TMEM16A. *J Biol Chem* 284, 28571-28578
97. Bolduc, V., Marlow, G., Boycott, K. M., Saleki, K., Inoue, H., Kroon, J., Itakura, M., Robitaille, Y., Parent, L., Baas, F., Mizuta, K., Kamata, N., Richard, I., Linssen, W. H., Mahjneh, I., de Visser, M., Bashir, R., Brais, B. (2010) Recessive mutations in the putative calcium-activated chloride channel Anoctamin 5 cause proximal LGMD2L and distal MMD3 muscular dystrophies. *Am. J Hum. Genet*. 86, 213-221
98. Das, S., Hahn, Y., Nagata, S., Willingham, M. C., Bera, T. K., Lee, B., Pastan, I.

- (2007) NGEF, a prostate-specific plasma membrane protein that promotes the association of LNCaP cells. *Cancer Res.* 67, 1594-1601
99. Li, C., Cai, S., Wang, X., Jiang, Z. (2015) Identification and characterization of ANO9 in stage II and III colorectal carcinoma. *Oncotarget.*
100. Schraml, P., Kononen, J., Bubendorf, L., Moch, H., Bissig, H., Nocito, A., Mihatsch, M. J., Kallioniemi, O. P., Sauter, G. (1999) Tissue microarrays for gene amplification surveys in many different tumor types. *Clin.Cancer Res.* 5, 1966-1975
101. Huang, X., Godfrey, T. E., Gooding, W. E., McCarty, K. S., Jr., Gollin, S. M. (2006) Comprehensive genome and transcriptome analysis of the 11q13 amplicon in human oral cancer and synteny to the 7F5 amplicon in murine oral carcinoma. *Genes Chromosomes.Cancer.* 45, 1058-1069
102. Ormandy, C. J., Musgrove, E. A., Hui, R., Daly, R. J., Sutherland, R. L. (2003) Cyclin D1, EMS1 and 11q13 amplification in breast cancer. *Breast Cancer Res.Treat.* 78, 323-335
103. Shiu, K. K., Natrajan, R., Geyer, F. C., Ashworth, A., Reis-Filho, J. S. (2010) DNA amplifications in breast cancer: genotypic-phenotypic correlations. *Future.Oncol.* 6, 967-984
104. Carles, A., Millon, R., Cromer, A., Ganguli, G., Lemaire, F., Young, J., Wasyluk, C., Muller, D., Schultz, I., Rabouel, Y., Dembele, D., Zhao, C., Marchal, P., Ducray, C., Bracco, L., Abecassis, J., Poch, O., Wasyluk, B. (2006) Head and neck squamous cell carcinoma transcriptome analysis by comprehensive validated differential display. *Oncogene.* 25, 1821-1831
105. Spitzner, M., Martins, J. R., Barro Soria, R., Ousingsawat, J., Scheidt, K., Schreiber, R., Kunzelmann, K. (2008) Eag1 and Bestrophin 1 are upregulated in fast growing colonic cancer cells. *J Biol Chem* 283, 7421-7428
106. Davies, A. R., Belsey, M. J., Kozlowski, R. Z. (2004) Volume-sensitive organic osmolyte/anion channels in cancer: novel approaches to studying channel modulation employing proteomics technologies. *Ann.N.Y.Acad.Sci.* 1028, 38-55

107. Kunzelmann, K. (2005) Ion channels and cancer. *J Membr.Biol* 205, 159-173
108. Schwab, A., Fabian, A., Hanley, P. J., Stock, C. (2012) Role of ion channels and transporters in cell migration. *Physiol Rev.* 92, 1865-1913
109. Sontheimer, H. (2008) An unexpected role for ion channels in brain tumor metastasis. *Exp.Biol Med.(Maywood.)*. 233, 779-791
110. Cuddapah, V. A., Sontheimer, H. (2011) Ion channels and transporters in cancer. 2. Ion channels and the control of cancer cell migration. *Am.J Physiol Cell Physiol.* 301, C541-C549
111. Le Clainche, C., Carlier, M. F. (2008) Regulation of actin assembly associated with protrusion and adhesion in cell migration. *Physiol Rev.* 88, 489-513
112. Perez-Cornejo, P., Gokhale, A., Duran, C., Cui, Y., Xiao, Q., Hartzell, H. C., Faundez, V. (2012) Anoctamin 1 (Tmem16A)  $Ca^{2+}$ -activated chloride channel stoichiometrically interacts with an ezrin-radixin-moesin network. *Proc.Natl.Acad.Sci.U.S.A.* 109, 10376-10381
113. Berger, S. L. (2002) Histone modifications in transcriptional regulation. *Curr.Opin.Genet.Dev.* 12, 142-148
114. Jenuwein, T., Allis, C. D. (2001) Translating the histone code. *Science.* 293, 1074-1080
115. Erlich, R. B., Kherrouche, Z., Rickwood, D., Endo-Munoz, L., Cameron, S., Dahler, A., Hazar-Rethinam, M., de Long, L. M., Wooley, K., Guminski, A., Saunders, N. A. (2012) Preclinical evaluation of dual PI3K-mTOR inhibitors and histone deacetylase inhibitors in head and neck squamous cell carcinoma. *Br.J Cancer.* 106, 107-115
116. Gammoh, N., Lam, D., Puente, C., Ganley, I., Marks, P. A., Jiang, X. (2012) Role of autophagy in histone deacetylase inhibitor-induced apoptotic and nonapoptotic cell death. *Proc.Natl.Acad.Sci U.S.A.* 109, 6561-6565
117. Rock, J. R., Lopez, M. C., Baker, H. V., Harfe, B. D. (2007) Identification of genes expressed in the mouse limb using a novel ZPA microarray approach. *Gene Expr.Patterns.* 8, 19-26

118. Chung, C. H., Dignam, J. J., Hammond, M. E., Klimowicz, A. C., Petrillo, S. K., Magliocco, A., Jordan, R., Trotti, A., Spencer, S., Cooper, J. S., Le, Q. T., Ang, K. K. (2011) Glioma-associated oncogene family zinc finger 1 expression and metastasis in patients with head and neck squamous cell carcinoma treated with radiation therapy (RTOG 9003). *J Clin Oncol.* 29, 1326-1334
119. Pelczar, P., Zibat, A., van Dop, W. A., Heijmans, J., Bleckmann, A., Gruber, W., Nitzki, F., Uhmman, A., Guijarro, M. V., Hernando, E., Dittmann, K., Wienands, J., Dressel, R., Wojnowski, L., Binder, C., Taguchi, T., Beissbarth, T., Hogendoorn, P. C., Antonescu, C. R., Rubin, B. P., Schulz-Schaeffer, W., Aberger, F., van den Brink, G. R., Hahn, H. (2013) Inactivation of patched1 in mice leads to development of gastrointestinal stromal-like tumors that express pdgfralpha but not kit. *Gastroenterology.* 144, 134-144
120. Berman, D. M., Karhadkar, S. S., Maitra, A., Montes, D. O., Gerstenblith, M. R., Briggs, K., Parker, A. R., Shimada, Y., Eshleman, J. R., Watkins, D. N., Beachy, P. A. (2003) Widespread requirement for Hedgehog ligand stimulation in growth of digestive tract tumours. *Nature.* 425, 846-851
121. Qualtrough, D., Buda, A., Gaffield, W., Williams, A. C., Paraskeva, C. (2004) Hedgehog signalling in colorectal tumour cells: induction of apoptosis with cyclopamine treatment. *Int.J Cancer.* 110, 831-837
122. Chenevert, J., Duvvuri, U., Chiosea, S., Dacic, S., Cieply, K., Kim, J., Shiwarski, D., Seethala, R. R. (2012) DOG1: a novel marker of salivary acinar and intercalated duct differentiation. *Mod.Pathol.* 25, 919-929
123. Schroeder, B. C., Cheng, T., Jan, Y. N., Jan, L. Y. (2008) Expression cloning of TMEM16A as a calcium-activated chloride channel subunit. *Cell.* 134, 1019-1029
124. Rose, D. P., Davis, T. E. (1981) Plasma thyronine levels in carcinoma of the breast and colon. *Arch Intern.Med.* 141, 1161-1164
125. Rock, J. R., Harfe, B. D. (2008) Expression of TMEM16 paralogs during murine embryogenesis. *Dev.Dyn.* 237, 2566-2574
126. Bera, T. K., Das, S., Maeda, H., Beers, R., Wolfgang, C. D., Kumar, V., Hahn, Y., Lee,

- B., Pastan, I. (2004) NGEF, a gene encoding a membrane protein detected only in prostate cancer and normal prostate. *Proc.Natl.Acad.Sci.U.S.A.* 101, 3059-3064
127. Dutertre, M., Lacroix-Triki, M., Driouch, K., de la, G. P., Gratadou, L., Beck, S., Millevoi, S., Tazi, J., Lidereau, R., Vagner, S., Auboeuf, D. (2010) Exon-based clustering of murine breast tumor transcriptomes reveals alternative exons whose expression is associated with metastasis. *Cancer Res.* 70, 896-905
128. Poulsen, K. A., Andersen, E. C., Hansen, C. F., Klausen, T. K., Hougaard, C., Lambert, I. H., Hoffmann, E. K. (2010) Deregulation of apoptotic volume decrease and ionic movements in multidrug-resistant tumor cells: role of chloride channels. *Am J Physiol Cell Physiol.* 298, C14-C25
129. Suzuki, J., Fujii, T., Imao, T., Ishihara, K., Kuba, H., Nagata, S. (2013) Calcium-dependent Phospholipid Scramblase Activity of TMEM16 Family Members. *J Biol Chem.* 288, 13305-13316
130. Shimizu, T., Iehara, T., Sato, K., Fujii, T., Sakai, H., Okada, Y. (2013) TMEM16F is a component of a  $Ca^{2+}$ -activated  $Cl^{-}$  channel but not a volume-sensitive outwardly rectifying  $Cl^{-}$  channel. *Am.J Physiol Cell Physiol.* 304, C748-C759
131. Dauner, K., Mobus, C., Frings, S., Mohrlen, F. (2013) Targeted expression of anoctamin calcium-activated chloride channels in rod photoreceptor terminals of the rodent retina. *Invest Ophthalmol.Vis.Sci.* iovs-11711v1
132. Hoffmann, E. K., Lambert, I. H., Pedersen, S. F. (2009) Physiology of cell volume regulation in vertebrates. *Physiol Rev.* 89, 193-277
133. Okada, Y. (2006) Cell volume-sensitive chloride channels: phenotypic properties and molecular identity. *Contrib.Nephrol.* 152, 9-24
134. Voss, F. K., Ullrich, F., Munch, J., Lazarow, K., Lutter, D., Mah, N., Andrade-Navarro, M. A., von Kries, J. P., Stauber, T., Jentsch, T. J. (2014) Identification of LRRC8 Heteromers as an Essential Component of the Volume-Regulated Anion Channel VRAC. *Science.* 344, 634-638
135. Qiu, Z., Dubin, A. E., Mathur, J., Tu, B., Reddy, K., Miraglia, L. J., Reinhardt, J., Orth,

- A. P., Patapoutian, A. (2014) SWELL1, a Plasma Membrane Protein, Is an Essential Component of Volume-Regulated Anion Channel. *Cell*. 157, 447-458
136. Pedemonte, N., Galletta, L. J. (2014) Structure and Function of TMEM16 Proteins (Anoctamins). *Physiol Rev*. 94, 419-459
137. Malvezzi, M., Chalal, M., Janjusevic, R., Picollo, A., Terashima, H., Menon, A. K., Accardi, A. (2013) Ca<sup>2+</sup>-dependent phospholipid scrambling by a reconstituted TMEM16 ion channel. *Nat. Commun*. 4, 2367
138. Brunner, J. D., Lim, N. K., Schenck, S., Duerst, A., Dutzler, R. (2014) X-ray structure of a calcium-activated TMEM16 lipid scramblase. *Nature*. 516, 207-212
139. Ousingsawat, J., Wanitchakool, P., Kmit, A., Romao, A. M., Jantarajit, W., Schreiber, S., Kunzelmann, K. (2015) Anoctamin 6 mediates effects essential for innate immunity downstream of P2X7-receptors in macrophages. *Nat. Commun*. 6, 6245
140. Strange, K., Emma, F., Jackson, P. S. (1996) Cellular and molecular physiology of volume-sensitive anion channels. *Am J Physiol*. 270, C711-C730
141. Helix, N., Strobaek, D., Dahl, B. H., Christophersen, P. (2003) Inhibition of the endogenous volume-regulated anion channel (VRAC) in HEK293 cells by acidic diaryl-ureas. *J Membr. Biol*. 196, 83-94
142. Klausen, T. K., Bergdahl, A., Hougaard, C., Christophersen, P., Pedersen, S. F., Hoffmann, E. K. (2007) Cell cycle-dependent activity of the volume- and Ca<sup>2+</sup>-activated anion currents in Ehrlich lettre ascites cells. *J Cell Physiol*. 210, 831-842
143. Namkung, W., Phuan, P. W., Verkman, A. S. (2011) TMEM16A inhibitors reveal TMEM16A as a minor component of CaCC conductance in airway and intestinal epithelial cells. *J Biol. Chem*. 286, 2365-2374
144. Preston, G. M., Carroll, T. P., Guggino, W. B., Agre, P. (1992) Appearance of water channels in *Xenopus* oocytes expressing red cell CHIP28 protein. *Science* 256, 385-387
145. Harteneck, C., Gollasch, M. (2011) Pharmacological modulation of diacylglycerol-sensitive TRPC3/6/7 channels. *Curr. Pharm. Biotechnol*. 12, 35-41

146. Harteneck, C., Frenzel, H., Kraft, R. (2007) N-(p-aminocinnamoyl)anthranilic acid (ACA): a phospholipase A2 inhibitor and TRP channel blocker. *Cardiovasc. Drug Rev.* 25, 61-75
147. Fischer, K. G., Leipziger, J., Rubini-Illes, P., Nitschke, R., Greger, R. (1996) Attenuation of stimulated  $\text{Ca}^{2+}$  influx in colonic epithelial (HT<sub>29</sub>) cells by cAMP. *Pflugers Arch.* 432, 735-740
148. Lee, M. Y., Song, H., Nakai, J., Ohkura, M., Kotlikoff, M. I., Kinsey, S. P., Golovina, V. A., Blaustein, M. P. (2006) Local subplasma membrane  $\text{Ca}^{2+}$  signals detected by a tethered  $\text{Ca}^{2+}$  sensor. *Proc. Natl. Acad. Sci. U.S.A.* 103, 13232-13237
149. Nilius, B., Oike, M., Zahradnik, I., Droogmans, G. (1994) Activation of a  $\text{Cl}^-$  current by hypotonic volume increase in human endothelial cells. *J. Gen. Physiol.* 103, 787-805
150. Ishii, T., Hashimoto, T., Ohmori, H. (1996) Hypotonic stimulation induced  $\text{Ca}^{2+}$  release from IP<sub>3</sub>-sensitive internal stores in a green monkey kidney cell line. *J. Physiol.* 493, 371-384
151. Mohanty, M. J., Ye, M., Li, X., Rossi, N. F. (2001) Hypotonic swelling-induced  $\text{Ca}^{2+}$  release by an IP<sub>3</sub>-insensitive  $\text{Ca}^{2+}$  store. *Am. J. Physiol. Cell Physiol.* 281, C555-C562
152. Akita, T., Okada, Y. (2011) Regulation of bradykinin-induced activation of volume-sensitive outwardly rectifying anion channels by  $\text{Ca}^{2+}$  nanodomains in mouse astrocytes. *J. Physiol.* 589, 3909-3927
153. Berridge, M. J. (2004) Conformational coupling: a physiological calcium entry mechanism. *Sci STKE.* 2004, e33
154. Yoo, J., Cui, Q. (2009) Curvature generation and pressure profile modulation in membrane by lysolipids: insights from coarse-grained simulations. *Biophys. J.* 97, 2267-2276
155. Dawson, D. C., Van Driessche, W., Helman, S. I. (1988) Osmotically induced basolateral  $\text{K}^+$  conductance in turtle colon: lidocaine-induced  $\text{K}^+$  channel noise. *Am J Physiol.* 254, C165-C174
156. McCarty, N. A., O'Neil, R. G. (1992) Calcium signalling in volume regulation.

- Physiol.Rev.* 72, 1037-1061
157. Pedersen, S. F., Nilius, B. (2007) Transient receptor potential channels in mechanosensing and cell volume regulation. *Methods Enzymol.* 428, 183-207
  158. Lemonnier, L., Prevarskaya, N., Shuba, Y., Vanden Abeele, F., Nilius, B., Mazurier, J., Skryma, R. (2002) Ca<sup>2+</sup> modulation of volume-regulated anion channels: evidence for colocalization with store-operated channels. *FASEB J.* 16, 222-224
  159. Zholos, A., Beck, B., Sydorenko, V., Lemonnier, L., Bordat, P., Prevarskaya, N., Skryma, R. (2005) Ca<sup>2+</sup>- and volume-sensitive chloride currents are differentially regulated by agonists and store-operated Ca<sup>2+</sup> entry. *J.Gen.Physiol.* 125, 197-211
  160. Lehtonen, J. Y., Kinnunen, P. K. (1995) Phospholipase A2 as a mechanosensor. *Biophys.J.* 68, 1888-1894
  161. Pedersen, S. F., Poulsen, K. A., Lambert, I. H. (2006) Roles of phospholipase A2 isoforms in swelling- and melittin-induced arachidonic acid release and taurine efflux in NIH3T3 fibroblasts. *Am.J.Physiol Cell Physiol.* 291, C1286-C1296
  162. Pedersen, S., Lambert, I. H., Thoroed, S. M., Hoffmann, E. K. (2000) Hypotonic cell swelling induces translocation of the alpha isoform of cytosolic phospholipase A2 but not the gamma isoform in Ehrlich ascites tumor cells. *Eur.J.Biochem.* 267, 5531-5539
  163. Thoroed, S. M., Lauritzen, L., Lambert, I. H., Hansen, H. S., Hoffmann, E. K. (1997) Cell swelling activates phospholipase A2 in Ehrlich ascites tumor cells. *J.Membr.Biol.* 160, 47-58
  164. Murakami, M., Kudo, I. (2002) Phospholipase A2. *J Biochem.* 131, 285-292
  165. Voets, T., Droogmans, G., Raskin, G., Eggermont, J., Nilius, B. (1999) Reduced intracellular ionic strength as the initial trigger for activation of endothelial volume-regulated anion channels. *Proc.Natl.Acad.Sci U.S A.* 96, 5298-5303
  166. Sabirov, R. Z., Prenen, J., Tomita, T., Droogmans, G., Nilius, B. (2000) Reduction of ionic strength activates single volume-regulated anion channels (VRAC) in endothelial cells. *Pflugers Arch.* 439, 315-320

167. Bessac, B. F., Fleig, A. (2007) TRPM7 channel is sensitive to osmotic gradients in human kidney cells. *J Physiol.* 582, 1073-1086
168. Forrest, L. R., Tavoulari, S., Zhang, Y. W., Rudnick, G., Honig, B. (2007) Identification of a chloride ion binding site in Na<sup>+</sup>/Cl<sup>-</sup>-dependent transporters. *Proc.Natl.Acad.Sci U.S.A.* 104, 12761-12766
169. Cruz-Rangel, S., Gamba, G., Ramos-Mandujano, G., Pasantes-Morales, H. (2012) Influence of WNK3 on intracellular chloride concentration and volume regulation in HEK293 cells. *Pflugers Arch.* 464, 317-330
170. Schreiber, R., Faria, D., Skryabin, B. V., Rock, J. R., Kunzelmann, K. (2014) Anoctamins support calcium-dependent chloride secretion by facilitating calcium signaling in adult mouse intestine. *Pflügers Arch* 467, 1203-1213
171. Wiley, J. S., Sluyter, R., Gu, B. J., Stokes, L., Fuller, S. J. (2011) The human P2X7 receptor and its role in innate immunity. *Tissue Antigens.* 78, 321-332
172. Elliott, J. I., Surprenant, A., Marelli-Berg, F. M., Cooper, J. C., Cassady-Cain, R. L., Wooding, C., Linton, K., Alexander, D. R., Higgins, C. F. (2005) Membrane phosphatidylserine distribution as a non-apoptotic signalling mechanism in lymphocytes. *Nat.Cell Biol.* 7, 808-816
173. Smart, M. L., Gu, B., Panchal, R. G., Wiley, J., Cromer, B., Williams, D. A., Petrou, S. (2003) P2X7 receptor cell surface expression and cytolytic pore formation are regulated by a distal C-terminal region. *J Biol Chem.* 278, 8853-8860
174. Kim, M., Jiang, L. H., Wilson, H. L., North, R. A., Surprenant, A. (2001) Proteomic and functional evidence for a P2X7 receptor signalling complex. *EMBO J.* 20, 6347-6358
175. Surprenant, A., Rassendren, F., Kawashima, E., North, R. A., Buell, G. (1996) The cytolytic P2Z receptor for extracellular ATP identified as a P2X receptor (P2X7). *Science.* 272, 735-738
176. Coddou, C., Yan, Z., Obsil, T., Huidobro-Toro, J. P., Stojilkovic, S. S. (2011) Activation and regulation of purinergic P2X receptor channels. *Pharmacol.Rev.* 63,

- 641-683
177. Schachter, J., Motta, A. P., de Souza, Z. A., Silva-Souza, H. A., Guimaraes, M. Z., Persechini, P. M. (2008) ATP-induced P2X7-associated uptake of large molecules involves distinct mechanisms for cations and anions in macrophages. *J Cell Sci.* 121, 3261-3270
  178. Cankurtaran-Sayar, S., Sayar, K., Ugur, M. (2009) P2X7 receptor activates multiple selective dye-permeation pathways in RAW 264.7 and human embryonic kidney 293 cells. *Mol.Pharmacol.* 76, 1323-1332
  179. Pelegrin, P., Surprenant, A. (2006) Pannexin-1 mediates large pore formation and interleukin-1beta release by the ATP-gated P2X7 receptor. *EMBO J.* 25, 5071-5082
  180. Hanley, P. J., Kronlage, M., Kirschning, C., Del Rey, A., Di Virgilio, F., Leipziger, J., Chessell, I. P., Sargin, S., Filippov, M. A., Lindemann, O., Mohr, S., Koenigs, V., Schillers, H., Baehler, M., Schwab, A. (2012) Transient P2X7 receptor activation triggers macrophage death independent of TLR2/4, Casp1 and Panx1. *J Biol Chem.*
  181. Locovei, S., Scemes, E., Qiu, F., Spray, D. C., Dahl, G. (2007) Pannexin1 is part of the pore forming unit of the P2X7 receptor death complex. *FEBS Lett.* 581, 483-488
  182. Worthington, R. A., Smart, M. L., Gu, B. J., Williams, D. A., Petrou, S., Wiley, J. S., Barden, J. A. (2002) Point mutations confer loss of ATP-induced human P2X7 receptor function. *FEBS Lett.* 512, 43-46
  183. Gulbransen, B. D., Bashashati, M., Hirota, S. A., Gui, X., Roberts, J. A., Macdonald, J. A., Muruve, D. A., McKay, D. M., Beck, P. L., Mawe, G. M., Thompson, R. J., Sharkey, K. A. (2012) Activation of neuronal P2X7 receptor-pannexin-1 mediates death of enteric neurons during colitis. *Nat.Med.* 10
  184. Yan, Z., Khadra, A., Li, S., Tomic, M., Sherman, A., Stojilkovic, S. S. (2010) Experimental characterization and mathematical modeling of P2X7 receptor channel gating. *J Neurosci.* 30, 14213-14224
  185. Shimizu, T., Numata, T., Okada, Y. (2004) A role of reactive oxygen species in apoptotic activation of volume-sensitive Cl<sup>-</sup> channel. *Proc.Natl.Acad.Sci.U.S.A.* 101,

6770-6773

186. Kunzelmann, K., Nilius, B., Owsianik, G., Schreiber, R., Ousingsawat, J., Sirianant, L., Wanitchakool, P., Bevers, E. M., Heemskerk, J. W. (2014) Molecular functions of anoctamin 6 (TMEM16F): A chloride channel, cation channel or phospholipid scramblase? *Pflügers Arch* 466, 407-414
187. Gu, B. J., Zhang, W. Y., Bendall, L. J., Chessell, I. P., Buell, G. N., Wiley, J. S. (2000) Expression of P2X7 purinoceptors on human lymphocytes and monocytes: evidence for nonfunctional P2X7 receptors. *Am.J.Physiol Cell Physiol.* 279, C1189-C1197
188. Miller, C. M., Boulter, N. R., Fuller, S. J., Zakrzewski, A. M., Lees, M. P., Saunders, B. M., Wiley, J. S., Smith, N. C. (2011) The role of the P2X7 receptor in infectious diseases. *PLoS.Pathog.* 7, e1002212
189. Pelegrin, P. (2011) The many ways for P2X7 receptor pore dilatation. *Br.J Pharmacol.* 10-5381
190. Morelli, A., Chiozzi, P., Chiesa, A., Ferrari, D., Sanz, J. M., Falzoni, S., Pinton, P., Rizzuto, R., Olson, M. F., Di Virgilio, F. (2003) Extracellular ATP causes ROCK I-dependent bleb formation in P2X7-transfected HEK293 cells. *Mol.Biol Cell.* 14, 2655-2664
191. Taylor, S. R., Gonzalez-Begne, M., Dewhurst, S., Chimini, G., Higgins, C. F., Melvin, J. E., Elliott, J. I. (2008) Sequential shrinkage and swelling underlie P2X7-stimulated lymphocyte phosphatidylserine exposure and death. *J.Immunol.* 180, 300-308
192. Paukert, M., Hidayat, S., Grunder, S. (2002) The P2X7 receptor from *Xenopus laevis*: formation of a large pore in *Xenopus* oocytes. *FEBS Lett.* 513, 253-258
193. Namkung, W., Thiagarajah, J. R., Phuan, P. W., Verkman, A. S. (2010) Inhibition of Ca<sup>2+</sup>-activated Cl<sup>-</sup> channels by gallotannins as a possible molecular basis for health benefits of red wine and green tea. *FASEB J.* 24, 4178-4186
194. Klapperstuck, M., Buttner, C., Bohm, T., Schmalzing, G., Markwardt, F. (2000) Characteristics of P2X7 receptors from human B lymphocytes expressed in *Xenopus* oocytes. *Biochim.Biophys.Acta.* 1467, 444-456

195. Li, Q., Luo, X., Muallem, S. (2005) Regulation of the P2X7 receptor permeability to large molecules by extracellular Cl<sup>-</sup> and Na<sup>+</sup>. *J Biol Chem.* 280, 26922-26927
196. Gu, B. J., Zhang, W., Worthington, R. A., Sluyter, R., Dao-Ung, P., Petrou, S., Barden, J. A., Wiley, J. S. (2001) A Glu-496 to Ala polymorphism leads to loss of function of the human P2X7 receptor. *J Biol.Chem.* 276, 11135-11142
197. Courageot, M. P., Lepine, S., Hours, M., Giraud, F., Sulpice, J. C. (2004) Involvement of sodium in early phosphatidylserine exposure and phospholipid scrambling induced by P2X7 purinoceptor activation in thymocytes. *J Biol Chem.* 279, 21815-21823
198. Faria, R. X., Reis, R. A., Casabulho, C. M., Alberto, A. V., de Farias, F. P., Henriques-Pons, A., Alves, L. A. (2009) Pharmacological properties of a pore induced by raising intracellular Ca<sup>2+</sup>. *Am J Physiol Cell Physiol.* 297, C28-C42
199. Faria, R. X., Defarias, F. P., Alves, L. A. (2005) Are second messengers crucial for opening the pore associated with P2X7 receptor? *Am J Physiol Cell Physiol.* 288, C260-C271
200. Kronlage, M., Song, J., Sorokin, L., Isfort, K., Schwerdtle, T., Leipziger, J., Robaye, B., Conley, P. B., Kim, H. C., Sargin, S., Schon, P., Schwab, A., Hanley, P. J. (2010) Autocrine purinergic receptor signaling is essential for macrophage chemotaxis. *Sci.Signal.* 3, ra55
201. Carr, M. W., Roth, S. J., Luther, E., Rose, S. S., Springer, T. A. (1994) Monocyte chemoattractant protein 1 acts as a T-lymphocyte chemoattractant. *Proc.Natl.Acad.Sci.U.S.A.* 91, 3652-3656
202. Wanitchakool, P., Wolf, L., Koehl, G., Sirianant, L., Gaumann, A., Schreiber, R., Duvvuri, U., Kunzelmann, K. (2014) Role of Anoctamins in Cancer and Apoptosis. *Philos Trans R Soc Lond B Biol Sci* 369, 20130096
203. McNamara, N., Khong, A., McKemy, D., Caterina, M., Boyer, J., Julius, D., Basbaum, C. B. (2001) ATP transduces signals from ASGM1, a glycolipid that functions as a bacterial receptor. *Proc.Natl.Acad Sci U.S A.* 98, 9086-9091
204. Lammas, D. A., Stober, C., Harvey, C. J., Kendrick, N., Panchalingam, S.,

- Kumararatne, D. S. (1997) ATP-induced killing of mycobacteria by human macrophages is mediated by purinergic P2Z(P2X7) receptors. *Immunity*. 7, 433-444
205. Coutinho-Silva, R., Ojcius, D. M. (2012) Role of extracellular nucleotides in the immune response against intracellular bacteria and protozoan parasites. *Microbes.Infect.* 14, 1271-1277
206. Virginio, C., Mackenzie, A., Rassendren, F. A., North, R. A., Surprenant, A. (1999) Pore dilation of neuronal P2X receptor channels. *Nat.Neurosci.* 2, 315-321
207. Yan, Z., Li, S., Liang, Z., Tomic, M., Stojilkovic, S. S. (2008) The P2X7 receptor channel pore dilates under physiological ion conditions. *J Gen.Physiol.* 132, 563-573
208. Browne, L. E., Compan, V., Bragg, L., North, R. A. (2013) P2X7 receptor channels allow direct permeation of nanometer-sized dyes. *J Neurosci.* 33, 3557-3566
209. North, R. A. (2002) Molecular physiology of P2X receptors. *Physiol Rev.* 82, 1013-1067
210. Lang, F., Hoffmann, E. K. (2013) CrossTalk proposal: Cell volume changes are an essential step in the cell death machinery. *J Physiol.* 591, 6119-6121
211. Tsukimoto, M., Harada, H., Ikari, A., Takagi, K. (2005) Involvement of chloride in apoptotic cell death induced by activation of ATP-sensitive P2X7 purinoceptor. *J Biol Chem.* 280, 2653-2658
212. Tepper, A. D., Ruurs, P., Wiedmer, T., Sims, P. J., Borst, J., van Blitterswijk, W. J. (2000) Sphingomyelin hydrolysis to ceramide during the execution phase of apoptosis results from phospholipid scrambling and alters cell-surface morphology. *J Cell Biol.* 150, 155-164
213. Molloy, A., Laochumroonvorapong, P., Kaplan, G. (1994) Apoptosis, but not necrosis, of infected monocytes is coupled with killing of intracellular bacillus Calmette-Guerin. *J Exp.Med.* 180, 1499-1509
214. Fairbairn, I. P., Stober, C. B., Kumararatne, D. S., Lammas, D. A. (2001) ATP-mediated killing of intracellular mycobacteria by macrophages is a P2X7-dependent process inducing bacterial death by phagosome-lysosome fusion. *J.Immunol.* 167,

3300-3307

215. Faria, D., Schlatter, E., Witzgall, R., Grahammer, F., Bandulik, S., Schweda, F., Bierer, S., Rock, J. R., Heitzmann, D., Kunzelmann, K., Schreiber, R. (2014) The calcium activated chloride channel Anoctamin 1 contributes to the regulation of renal function. *Kidney Int.* 85, 1369-1381
216. Shapiro, E. D. (2014) Clinical practice. Lyme disease. *N.Engl.J Med.* 370, 1724-1731
217. Stanek, G., Wormser, G. P., Gray, J., Strle, F. (2012) Lyme borreliosis. *Lancet.* 379, 461-473
218. Fallon, B. A., Nields, J. A. (1994) Lyme disease: a neuropsychiatric illness. *Am J Psychiatry.* 151, 1571-1583
219. Hess, A., Buchmann, J., Zettl, U. K., Henschel, S., Schlaefke, D., Grau, G., Benecke, R. (1999) *Borrelia burgdorferi* central nervous system infection presenting as an organic schizophrenialike disorder. *Biol Psychiatry.* 45, 795
220. Hanincova, K., Mukherjee, P., Ogden, N. H., Margos, G., Wormser, G. P., Reed, K. D., Meece, J. K., Vandermause, M. F., Schwartz, I. (2013) Multilocus sequence typing of *Borrelia burgdorferi* suggests existence of lineages with differential pathogenic properties in humans. *PLoS.ONE.* 8, e73066
221. Casjens, S. R., Mongodin, E. F., Qiu, W. G., Luft, B. J., Schutzer, S. E., Gilcrease, E. B., Huang, W. M., Vujadinovic, M., Aron, J. K., Vargas, L. C., Freeman, S., Radune, D., Weidman, J. F., Dimitrov, G. I., Khouri, H. M., Sosa, J. E., Halpin, R. A., Dunn, J. J., Fraser, C. M. (2012) Genome stability of Lyme disease spirochetes: comparative genomics of *Borrelia burgdorferi* plasmids. *PLoS.ONE.* 7, e33280
222. Chapman, S. J., Hill, A. V. (2012) Human genetic susceptibility to infectious disease. *Nat.Rev.Genet.* 13, 175-188
223. Ribbe, K., Friedrichs, H., Begemann, M., Grube, S., Papiol, S., Kastner, A., Gerchen, M. F., Ackermann, V., Tarami, A., Treitz, A., Flogel, M., Adler, L., Aldenhoff, J. B., Becker-Emner, M., Becker, T., Czernik, A., Dose, M., Folkerts, H., Freese, R., Gunther, R., Herpertz, S., Hesse, D., Kruse, G., Kunze, H., Franz, M., Lohrer, F.,

- Maier, W., Mielke, A., Muller-Isberner, R., Oestereich, C., Pajonk, F. G., Pollmacher, T., Schneider, U., Schwarz, H. J., Kroner-Herwig, B., Havemann-Reinecke, U., Frahm, J., Stuhmer, W., Falkai, P., Brose, N., Nave, K. A., Ehrenreich, H. (2010) The cross-sectional GRAS sample: a comprehensive phenotypical data collection of schizophrenic patients. *BMC.Psychiatry*. 10, 91-10
224. Hammer, C., Stepniak, B., Schneider, A., Papiol, S., Tantra, M., Begemann, M., Siren, A. L., Pardo, L. A., Sperling, S., Mohd, J. S., Gurvich, A., Jensen, N., Ostmeier, K., Luhder, F., Probst, C., Martens, H., Gillis, M., Saher, G., Assogna, F., Spalletta, G., Stocker, W., Schulz, T. F., Nave, K. A., Ehrenreich, H. (2014) Neuropsychiatric disease relevance of circulating anti-NMDA receptor autoantibodies depends on blood-brain barrier integrity. *Mol.Psychiatry*. 19, 1143-1149
225. Begemann, M., Grube, S., Papiol, S., Malzahn, D., Krampe, H., Ribbe, K., Friedrichs, H., Radyushkin, K. A., El Kordi, A., Benseler, F., Hannke, K., Sperling, S., Schwerdtfeger, D., Thanhauser, I., Gerchen, M. F., Ghorbani, M., Gutwinski, S., Hilmes, C., Leppert, R., Ronnenberg, A., Sowislo, J., Stawicki, S., Stodtke, M., Szuszi, C., Reim, K., Riggert, J., Eckstein, F., Falkai, P., Bickeboller, H., Nave, K. A., Brose, N., Ehrenreich, H. (2010) Modification of cognitive performance in schizophrenia by complexin 2 gene polymorphisms. *Arch Gen.Psychiatry*. 67, 879-888
226. Franke, G. H. (2000) Brief Symptom Inventory. Göttingen. *Beltz*
227. Yang, J., Lee, S. H., Goddard, M. E., Visscher, P. M. (2011) GCTA: a tool for genome-wide complex trait analysis. *Am J Hum.Genet*. 88, 76-82
228. Purcell, S., Neale, B., Todd-Brown, K., Thomas, L., Ferreira, M. A., Bender, D., Maller, J., Sklar, P., de Bakker, P. I., Daly, M. J., Sham, P. C. (2007) PLINK: a tool set for whole-genome association and population-based linkage analyses. *Am J Hum.Genet*. 81, 559-575
229. Abecasis, G. R., Auton, A., Brooks, L. D., DePristo, M. A., Durbin, R. M., Handsaker, R. E., Kang, H. M., Marth, G. T., McVean, G. A. (2012) An integrated map of genetic variation from 1,092 human genomes. *Nature*. 491, 56-65
230. Zoghbi, H. Y., Orr, H. T. (2009) Pathogenic mechanisms of a polyglutamine-mediated neurodegenerative disease, spinocerebellar ataxia type 1. *J Biol Chem*. 284, 7425-7429

231. Yang, Y. D., Cho, H., Koo, J. Y., Tak, M. H., Cho, Y., Shim, W. S., Park, S. P., Lee, J., Lee, B., Kim, B. M., Raouf, R., Shin, Y. K., Oh, U. (2008) TMEM16A confers receptor-activated calcium-dependent chloride conductance. *Nature*. 455, 1210-1215
232. Caputo, A., Caci, E., Ferrera, L., Pedemonte, N., Barsanti, C., Sondo, E., Pfeiffer, U., Ravazzolo, R., Zegarra-Moran, O., Galletta, L. J. (2008) TMEM16A, A Membrane Protein Associated With Calcium-Dependent Chloride Channel Activity. *Science*. 322, 590-594
233. Gosling, M., Poyner, D. R., Smith, J. W. (1996) Effects of arachidonic acid upon the volume-sensitive chloride current in rat osteoblast-like (ROS 17/2.8) cells. *J.Physiol.* 493, 613-623
234. Wu, X., Yang, H., Iserovich, P., Fischbarg, J., Reinach, P. S. (1997) Regulatory volume decrease by SV40-transformed rabbit corneal epithelial cells requires ryanodine-sensitive  $Ca^{2+}$ -induced  $Ca^{2+}$  release. *J Membr.Biol.* 158, 127-136
235. Berende, A., Oosting, M., Kullberg, B. J., Netea, M. G., Joosten, L. A. (2010) Activation of innate host defense mechanisms by *Borrelia*. *Eur.Cytokine Netw.* 21, 7-18
236. Steere, A. C., Coburn, J., Glickstein, L. (2004) The emergence of Lyme disease. *J Clin.Invest.* 113, 1093-1101
237. Arav-Boger, R., Crawford, T., Steere, A. C., Halsey, N. A. (2002) Cerebellar ataxia as the presenting manifestation of Lyme disease. *Pediatr.Infect.Dis.J.* 21, 353-356
238. Horne, D. J., Randhawa, A. K., Chau, T. T., Bang, N. D., Yen, N. T., Farrar, J. J., Dunstan, S. J., Hawn, T. R. (2012) Common polymorphisms in the PKP3-SIGIRR-TMEM16J gene region are associated with susceptibility to tuberculosis. *J Infect.Dis.* 205, 586-594
239. Bowman, A. B., Lam, Y. C., Jafar-Nejad, P., Chen, H. K., Richman, R., Samaco, R. C., Fryer, J. D., Kahle, J. J., Orr, H. T., Zoghbi, H. Y. (2007) Duplication of *Atxn11* suppresses SCA1 neuropathology by decreasing incorporation of polyglutamine-expanded ataxin-1 into native complexes. *Nat.Genet.* 39, 373-379

240. Dehnert, M., Fingerle, V., Klier, C., Talaska, T., Schlaud, M., Krause, G., Wilking, H., Poggensee, G. (2012) Seropositivity of Lyme borreliosis and associated risk factors: a population-based study in Children and Adolescents in Germany (KiGGS). *PLoS.ONE*. 7, e41321
241. Pachner, A. R. (1988) *Borrelia burgdorferi* in the nervous system: the new "great imitator". *Ann.N.Y.Acad.Sci.* 539, 56-64
242. Schreiber, R. (2005)  $Ca^{2+}$  signaling, intracellular pH and cell volume in cell proliferation. *J Membr.Biol.* 205, 129-137
243. Ji, J., Zheng, P. S. (2010) Activation of mTOR signaling pathway contributes to survival of cervical cancer cells. *Gynecol.Oncol.* 117, 103-108
244. Mroz, M. S., Keely, S. J. (2012) Epidermal Growth Factor Chronically Upregulates  $Ca^{2+}$ -Dependent  $Cl^-$  Conductance and TMEM16A Expression in Intestinal Epithelial Cells. *J.Physiol.*
245. Wolffe, A. P. (1996) Histone deacetylase: a regulator of transcription. *Science.* 272, 371-372
246. Gottlicher, M., Minucci, S., Zhu, P., Kramer, O. H., Schimpf, A., Giavara, S., Sleeman, J. P., Lo, C. F., Nervi, C., Pelicci, P. G., Heinzl, T. (2001) Valproic acid defines a novel class of HDAC inhibitors inducing differentiation of transformed cells. *EMBO J.* 20, 6969-6978
247. Mariadason, J. M. (2008) HDACs and HDAC inhibitors in colon cancer. *Epigenetics.* 3, 28-37
248. Zhu, P., Martin, E., Mengwasser, J., Schlag, P., Janssen, K. P., Gottlicher, M. (2004) Induction of HDAC2 expression upon loss of APC in colorectal tumorigenesis. *Cancer Cell.* 5, 455-463
249. Chuang, D. M., Leng, Y., Marinova, Z., Kim, H. J., Chiu, C. T. (2009) Multiple roles of HDAC inhibition in neurodegenerative conditions. *Trends Neurosci.* 32, 591-601
250. Nimeus, E., Baldetorp, B., Bendahl, P. O., Rennstam, K., Wennerberg, J., Akervall, J., Ferno, M. (2004) Amplification of the cyclin D1 gene is associated with tumour

- subsite, DNA non-diploidy and high S-phase fraction in squamous cell carcinoma of the head and neck. *Oral Oncol.* 40, 624-629
251. Kim, H. J., Jun, I., Yoon, J. S., Jung, J., Kim, Y. K., Kim, W. K., Kim, B. J., Song, J., Kim, S. J., Nam, J. H., Lee, M. G. (2015) Selective serotonin reuptake inhibitors facilitate ANO6 (TMEM16F) current activation and phosphatidylserine exposure. *Pflugers Arch.*
252. Scudieri, P., Caci, E., Venturini, A., Sondo, E., Pianigiani, G., Marchetti, C., Ravazzolo, R., Pagani, F., Galletta, L. J. (2015) Ion channel and lipid scramblase activity associated with expression of tmem16F/ANO6 isoforms. *J Physiol.(in press)*
253. Elliott, J. I., Sardini, A., Cooper, J. C., Alexander, D. R., Davanture, S., Chimini, G., Higgins, C. F. (2006) Phosphatidylserine exposure in B lymphocytes: a role for lipid packing. *Blood* 108, 1611-1617
254. Alberto, A. V., Faria, R. X., Couto, C. G., Ferreira, L. G., Souza, C. A., Teixeira, P. C., Froes, M. M., Alves, L. A. (2013) Is pannexin the pore associated with the P2X7 receptor? *Naunyn Schmiedebergs Arch Pharmacol.* 386, 775-787
255. Collo, G., Neidhart, S., Kawashima, E., Kosco-Vilbois, M., North, R. A., Buell, G. (1997) Tissue distribution of the P2X7 receptor. *Neuropharmacology.* 36, 1277-1283
256. Gabriel, S. E., Makhlina, M., Martsen, E., Thomas, E. J., Lethem, M. I., Boucher, R. C. (2000) Permeabilization via the P<sub>2X7</sub> purinoreceptor reveals the presence of a Ca<sup>2+</sup>-activated Cl<sup>-</sup> conductance in the apical membrane of CF and normal tracheal epithelial cells. *J Biol Chem* 275, 35028-35033
257. Mackenzie, A. B., Young, M. T., Adinolfi, E., Surprenant, A. (2005) Pseudoapoptosis induced by brief activation of ATP-gated P2X7 receptors. *J Biol Chem.* 280, 33968-33976
258. Schulze-Lohoff, E., Hugo, C., Rost, S., Arnold, S., Gruber, A., Brune, B., Sterzel, R. B. (1998) Extracellular ATP causes apoptosis and necrosis of cultured mesangial cells via P2Z/P2X7 receptors. *Am J Physiol.* 275, F962-F971
259. Chen, Q., Jin, Y., Zhang, K., Li, H., Chen, W., Meng, G., Fang, X. (2014) Alarmin

- HNP-1 promotes pyroptosis and IL-1 $\beta$  release through different roles of NLRP3 inflammasome via P2X7 in LPS-primed macrophages. *Innate.Immun.* 20, 290-300
260. Hu, Z., Murakami, T., Suzuki, K., Tamura, H., Kuwahara-Arai, K., Iba, T., Nagaoka, I. (2014) Antimicrobial cathelicidin peptide LL-37 inhibits the LPS/ATP-induced pyroptosis of macrophages by dual mechanism. *PLoS.ONE.* 9, e85765
261. Xaus, J., Comalada, M., Valledor, A. F., Lloberas, J., Lopez-Soriano, F., Argiles, J. M., Bogdan, C., Celada, A. (2000) LPS induces apoptosis in macrophages mostly through the autocrine production of TNF- $\alpha$ . *Blood.* 95, 3823-3831
262. Lang, F., Gulbins, E., Szabo, I., Lepple-Wienhues, A., Huber, S. M., Duranton, C., Lang, K. S., Lang, P. A., Wieder, T. (2004) Cell volume and the regulation of apoptotic cell death. *J Mol.Recognit.* 17, 473-480
263. Cathcart, M. K. (2009) Signal-activated phospholipase regulation of leukocyte chemotaxis. *J.Lipid Res.* 50 Suppl, S231-S236
264. Lauber, K., Bohn, E., Krober, S. M., Xiao, Y. J., Blumenthal, S. G., Lindemann, R. K., Marini, P., Wiedig, C., Zobywalski, A., Baksh, S., Xu, Y., Autenrieth, I. B., Schulze-Osthoff, K., Belka, C., Stuhler, G., Wesselborg, S. (2003) Apoptotic cells induce migration of phagocytes via caspase-3-mediated release of a lipid attraction signal. *Cell.* 113, 717-730
265. Hoffman, T., Brando, C., Lizzio, E. F., Lee, C., Hanson, M., Ting, K., Kim, Y. J., Abrahamsen, T., Puri, J., Bonvini, E. (1990) Functional consequences of phospholipase A2 activation in human monocytes. *Adv.Exp Med Biol* 279, 125-136
266. Donnelly, L. E., Barnes, P. J. (2012) Defective phagocytosis in airways disease. *Chest.* 141, 1055-1062
267. Ferrera, L., Caputo, A., Galiotta, L. J. V. (2010) TMEM16A Protein: A New Identity for Ca<sup>2+</sup>-Dependent Cl<sup>-</sup> Channels. *Am J Physiol* 25, 357-363

268. Cervantes, J. L., La Vake, C. J., Weinerman, B., Luu, S., O'Connell, C., Verardi, P. H., Salazar, J. C. (2013) Human TLR8 is activated upon recognition of *Borrelia burgdorferi* RNA in the phagosome of human monocytes. *J Leukoc.Biol.* 94, 1231-1241
269. Cervantes, J. L., Dunham-Ems, S. M., La Vake, C. J., Petzke, M. M., Sahay, B., Sellati, T. J., Radolf, J. D., Salazar, J. C. (2011) Phagosomal signaling by *Borrelia burgdorferi* in human monocytes involves Toll-like receptor (TLR) 2 and TLR8 cooperativity and TLR8-mediated induction of IFN-beta. *Proc.Natl.Acad.Sci.U.S A.* 108, 3683-3688
270. Dennis, V. A., Dixit, S., O'Brien, S. M., Alvarez, X., Pahar, B., Philipp, M. T. (2009) Live *Borrelia burgdorferi* spirochetes elicit inflammatory mediators from human monocytes via the Toll-like receptor signaling pathway. *Infect.Immun.* 77, 1238-1245
271. Rosenberger, C. M., Finlay, B. B. (2003) Phagocyte sabotage: disruption of macrophage signalling by bacterial pathogens. *Nat.Rev.Mol.Cell Biol.* 4, 385-396

## ACKNOWLEDGEMENTS

Firstly, I would like to use this opportunity to express my gratitude and deepest appreciation to my advisor Prof. Dr. Karl Kunzelmann who supported me throughout my Ph.D. study. I am thankful for his guidance, helpful suggestion, motivation, encouragement, immense knowledge, and patience throughout my research and writing of this thesis.

Besides my advisor, I am equally grateful to express my gratitude and deep appreciation to Prof. Dr. Rainer Schreiber for his suggestion, encouragement, and grateful helps. I deeply would like to thanks Dr. Jiraporn Ousingsawat for her kindness. I appreciate all her advices, contributions of time and ideas to make the success of my Ph.D. life.

I would like to thank all our current and former technicians who I had the chance to meet and work with during the past years. A special thank you goes to Brigitte and Tini who helped and supported me to get started in the lab and made my lives easier in every day.

I am especially grateful to my friends particularly Kaem, Inês, and Roberta for talking, having fun, listening to my worries and cheering me up whenever it was necessary.

I would like to show my gratitude to all the grants that support my present work: DFG SFB699-A7/A12, DFG KU756/12-1, Sander-Stiftung 2013.031.1 and Volkswagenstiftung AZ 87 499

Most importantly, I am also very grateful to my parents, who supported me constantly over the past years. Thank you for always believing in me and being interested in what I do.

**ERKLÄRUNGEN****Erklärung:**

Hiermit erkläre ich, gem. § 6 Abs. 2, Nr. 6 der Promotionsordnung der Math.-Nat.-Fachbereiche zur Erlangung des Dr. rer. nat., dass ich die vorliegende Dissertation selbständig verfasst und mich keiner anderen als der angegebenen Hilfsmittel bedient habe.

Regensburg, den 01.09.2016

Podchanart Wanitchakool

## Curriculum Vitae

### Personal information

Date of Birth: June 4<sup>th</sup>, 1984  
Sex: Female  
Place of birth: Bangkok, Thailand  
Nationality: Thai  
Address: Hochweg56A, Room 22, 93049 Regensburg, Germany  
Tel: 17631556070 (mobile)  
Email: podchanart@gmail.com

### Education

2012-present Ph.D., (Physiology) Faculty of Natural Sciences III: Biology and Preclinical medicine, University of Regensburg, Germany  
2008-2011 M.Sc., (Toxicology) Faculty of Science Mahidol University, Thailand  
2004-2007 B.Sc., (Medical Technology) Faculty of Allied Health Science Thammasat University, Thailand

### Publications

1. TMEM16F-Mediated Platelet Membrane Phospholipid Scrambling Is Critical for Hemostasis and Thrombosis but not Thromboinflammation in Mice. Baig AA, Haining EJ, Geuss E, Beck S, Swieringa F, **Wanitchakool P**, Schuhmann MK, Stegner D, Kunzelmann K, Kleinschnitz C, Heemskerk JW, Braun A, Nieswandt B. *Arterioscler Thromb Vasc Biol.* 2016 Sep 15.
2. Ca<sup>2+</sup> signals, cell membrane disintegration, and activation of TMEM16F during necroptosis. Ousingsawat J, Cabrita I, **Wanitchakool P**, Sirianant L, Krautwald S, Linkermann A, Schreiber R, Kunzelmann K. *Cell Mol Life Sci.* 2016 Aug 17.
3. Relationship between TMEM16A/anoctamin 1 and LRRC8A. Benedetto R, Sirianant L, Pankonien I, **Wanitchakool P**, Ousingsawat J, Cabrita I, Schreiber R, Amaral M, Kunzelmann K. *Pflugers Arch.* 2016 Oct;468(10):1751-63.
4. Cl<sup>-</sup> channels in apoptosis. **Wanitchakool P**, Ousingsawat J, Sirianant L, MacAulay N, Schreiber R, Kunzelmann K. *Eur Biophys J.* 2016 Jun 7. Review.
5. Non-essential contribution of LRRC8A to volume regulation. Sirianant L, **Wanitchakool P**, Ousingsawat J, Benedetto R, Zormpa A, Cabrita I, Schreiber R, Kunzelmann K.

- Pflugers Arch. 2016 May;468(5):805-16. doi: 10.1007/s00424-016-1789-6. Epub 2016 Feb 13.
6. Modulating Ca<sup>2+</sup> signals: a common theme for TMEM16, Ist2, and TMC. Kunzelmann K, Cabrita I, **Wanitchakool P**, Ousingsawat J, Sirianant L, Benedetto R, Schreiber R. Pflugers Arch. 2016 Mar;468(3):475-90. doi: 10.1007/s00424-015-1767-4. Epub 2015 Dec 23.
  7. Cellular volume regulation by anoctamin 6: Ca<sub>2+</sub>, phospholipase A2 and osmosensing. Sirianant L, Ousingsawat J, **Wanitchakool P**, Schreiber R, Kunzelmann K. Pflugers Arch. 2015 Oct 6.
  8. Bestrophin 1 is indispensable for volume regulation in human retinal pigment epithelium cells. Milenkovic A, Brandl C, Milenkovic VM, Jendryke T, Sirianant L, **Wanitchakool P**, Zimmermann S, Reiff CM, Horling F, Schrewe H, Schreiber R, Kunzelmann K, Wetzel CH, Weber BH. Proc Natl Acad Sci U S A. 2015 May 19;112(20):E2630-9. doi: 10.1073/pnas.1418840112. Epub 2015 May 4.
  9. A Coding Variant of ANO10, Affecting Volume Regulation of Macrophages, Is Associated with Borrelia Seropositivity. Hammer C, **Wanitchakool P**, Sirianant L, Papiol S, Monnheim M, Faria D, Ousingsawat J, Schramek N, Schmitt C, Margos G, Michel A, Kraiczky P, Pawlita M, Schreiber R, Schulz TF, Fingerle V, Tumani H, Ehrenreich H, Kunzelmann K. Mol Med. 2015 Feb 23;21:26-37. doi: 10.2119/molmed.2014.00219.
  10. Anoctamin 6 mediates effects essential for innate immunity downstream of P2X7 receptors in macrophages. Ousingsawat J, **Wanitchakool P**, Kmit A, Romao AM, Jantarajit W, Schreiber R, Kunzelmann K. Nat Commun. 2015 Feb 5;6:6245. doi: 10.1038/ncomms7245.
  11. Anoctamin-6 controls bone mineralization by activating the calcium transporter NCX1. Ousingsawat J, **Wanitchakool P**, Schreiber R, Wuelling M, Vortkamp A, Kunzelmann K. J Biol Chem. 2015 Mar 6;290(10):6270-80. doi: 10.1074/jbc.M114.602979. Epub 2015 Jan 14.
  12. Anoctamins support calcium-dependent chloride secretion by facilitating calcium signaling in adult mouse intestine. Schreiber R, Faria D, Skryabin BV, **Wanitchakool P**, Rock JR, Kunzelmann K. Pflugers Arch. 2015 Jun;467(6):1203-13. doi: 10.1007/s00424-014-1559-2. Epub 2014 Jul 1.

13. Role of anoctamins in cancer and apoptosis. **Wanitchakool P**, Wolf L, Koehl GE, Sirianant L, Schreiber R, Kulkarni S, Duvvuri U, Kunzelmann K. *Philos Trans R Soc Lond B Biol Sci*. 2014 Feb 3;369(1638):20130096. doi: 10.1098/rstb.2013.0096. Print 2014 Mar 19. Review.
14. Molecular functions of anoctamin 6 (TMEM16F): a chloride channel, cation channel, or phospholipid scramblase? Kunzelmann K, Nilius B, Owsianik G, Schreiber R, Ousingsawat J, Sirianant L, **Wanitchakool P**, Bevers EM, Heemskerk JW. *Pflugers Arch*. 2014 Mar;466(3):407-14. doi: 10.1007/s00424-013-1305-1. Epub 2013 Jun 8. Review.
15. Control of TMEM16A by INO-4995 and other inositolphosphates. Tian Y, Schreiber R, **Wanitchakool P**, Kongsuphol P, Sousa M, Uliyakina I, Palma M, Faria D, Traynor-Kaplan AE, Fragata JI, Amaral MD, Kunzelmann K. *Br J Pharmacol*. 2013 Jan;168(1):253-65. doi: 10.1111/j.1476-5381.2012.02193.x.
16. Cleistanthoside A tetraacetate-induced DNA damage leading to cell cycle arrest and apoptosis with the involvement of p53 in lung cancer cells. **Wanitchakool P**, Jariyawat S, Suksen K, Soorukram D, Tuchinda P, Piyachaturawat P. *Eur J Pharmacol*. 2012 Dec 5;696(1-3):35-42. doi: 10.1016/j.ejphar.2012.09.029. Epub 2012 Oct 3.
17. Induction of apoptosis in murine leukemia by diarylheptanoids from *Curcuma comosa* Roxb. Jariyawat S, Thammaprati T, Suksen K, **Wanitchakool P**, Nateewattana J, Chairoungdua A, Suksamrarn A, Piyachaturawat P. *Cell Biol Toxicol*. 2011 Dec;27(6):413-23. doi: 10.1007/s10565-011-9196-4. Epub 2011 Jul 16.